PhD Thesis

Design and Development of Advanced Porous Organic Polymeric Adsorbents for the Efficient and Selective Removal and Recovery of Phosphate and Arsenate from Water

A dissertation submitted to the
Indian Institute of Technology Guwahati
as partial fulfilment for the Degree of
Doctor of Philosophy in Centre for the Environment

By

Gunanka Hazarika

Centre for the Environment
Indian Institute of Technology Guwahati
Guwahati 781039, Assam, India

To

My Beloved Family

Declaration

17th November 2025

I hereby declare that the thesis entitled **"Design and Development of Advanced Porous Organic Polymeric Adsorbents for the Efficient and Selective Removal and Recovery of Phosphate and Arsenate from Water"** is upshots of research which was carried out by me under the supervision of Prof. Debasis Manna, Centre for the Environment & Department of Chemistry and co-supervision of Dr. Deepmoni Deka, Centre for the Environment, Indian Institute of Technology Guwahati. This thesis has been submitted by me to the Centre for the Environment, Indian Institute of Technology Guwahati, for the award of the degree of Doctor of Philosophy. In keeping with the general practice of reporting scientific observations, due acknowledgements have been made wherever the work described is based on the findings of other investigators.

I further declare that this work has not been submitted anywhere else for any degree, diploma, associateship or membership etc. of any Institute or University to the best of my knowledge.

Gunanka Hazarika

Gunanka Hazarika

Centre for the Environment

IIT Guwahati

Assam - 781039, India

भारतीय प्रौद्योगिकी संस्थान गुवाहाटी
Indian Institute of Technology Guwahati
Prof. Debasis Manna
&
Dr. Depmoni Deka
Centre for the Environment
Indian Institute of Technology Guwahati
Assam – 7 81039, India

17th November 2025

To whom it may concern

This is to certify that the thesis entitled **"Design and Development of Advanced Porous Organic Polymeric Adsorbents for the Efficient and Selective Removal and Recovery of Phosphate and Arsenate from Water"** being submitted by Mr. Gunanka Hazarika (Roll No. 206152003) for the award of PhD degree in Centre for the Environment to the Indian Institute of Technology Guwahati, is a genuinely his own research work which was carried out by him. The information and data reported by him are completely his original findings. He has meticulously carried out the investigations and also followed the guidelines of my laboratory. Neither this thesis nor any part of it has been submitted for the award of any degree/diploma to anywhere before.

Deepmoni Deka

Dr. Deepmoni Deka
Thesis Co-Supervisor
Centre for the Environment
IIT Guwahati
Assam - 781039, India

Debasis Manna

Prof. Debasis Manna
Thesis Supervisor
Centre for the Environment
IIT Guwahati
Assam - 781039, India

Contents

Chapter 2

Guanidine-modified cellulose enhances capturing and recovery of phosphates from wastewater

Acknowledgements

This dissertation is a consequence of endless support and encouragement by numerous well-wishers'. I would like to acknowledge each of them for helping me to reach the milestone in my life.

Prior to all, I would like to convey my sincere gratefulness to my supervising guide, Prof. Debasis Manna who introduced me to the splendid world of Science. His consistent guidance, encouragement and scholarly inputs enrich me a lot for shining in science. I am truly honoured and blessed to have been a part of his research group. Apart from research, his thoughts and ideas about life paved the way to me a better person in future. Thank you, Sir, for being my Mentor.

My sincere and heartfelt thanks to my co-supervisor, Dr. Deepmoni Deka, for her invaluable guidance, support, and encouragement throughout my PhD journey. I am truly grateful for their time, patience, and unwavering commitment, which played a vital role in the successful completion of this work.

I would also like to thank my doctoral committee members Prof. Bishnupada Mandal, Prof. Subrata Kumar Majumder, and Prof. Ranjan Tamuli for their valuable suggestions and consistent evaluation of my research works.

My sincere and heartfelt thanks to Dr. Koushik Dutta (CSIR NEIST, Jorhat), Ms. Tapashi sarmah (Dept. of Chemistry, IITG), Mr. Himangshu Baishya (Centre for Nano Technology, IITG), and Mr. Bikram Mondal (Dept. of Chemistry, IITG) for their constructive support in my research. Thank you, guys, for being a part of my research journey, and you guys will definitely stay in my heart for a lifetime.

I would like to express my gratitude to all the faculty and staff members of Centre for the Environment and Department of Chemistry for their continuous support. Also, I am immensely thankful to Centre for the Environment, Department of Chemistry and CIF (IIT Guwahati) for allowing me to use the sophisticated instrument facility. A special mention in this note of acknowledgement will certainly be of IIT Guwahati for providing me the scholarship.

I would also like to acknowledge all my past and present lab members including Dr. Abhishek Saha, Dr. Nirmalya Pradhan, Dr. Nasim Akhtar, Dr. Oindrila Biswas, Dr. Subhasis Dey, Dr. Sribash Das, Dr. Anjali Patel, Ms. Priyanka Mazumder, Mr. Biswa Mohan Prusty, Ms. Soumya Srimayee, Ms. Nikumoni Das, Mr. Mrinal Kanti Kar, Ms. Rama Karn, Mr. Rahul Kumar, Ms. Suravi Chauhan, Mr. Joydip Pal, and Mr. Pritam Kumar Mohanta for providing me a healthy and friendly atmosphere in the lab.

I extend my sincere thanks to all of my friends, especially Dr. Bhavik M. Patel, Mr. Hemanga Bhattacharyya, Mr. Anirban Basumatary, Mr. Rahul Ranjan Bharti, Mr. Akshay Daydar, Mr. Prangan Duarah, Ms. Debolina Ghosh and Ms. Sumona Koley for their constant support and encouragement.

Last but not the least, my Ph. D. endeavours would not have been accomplished without acknowledging my loving family and parents, Late Mahendra Hazarika and Ms. Dipali Hazarika. Their endless love, continuous support and blessings boost me up to cross the hurdles of my career. Whatever I have achieved so far in my life, all because of their supports and blessings. I am also immensely grateful to my dear sister, Ms. Namita Hazarika, my brother, Dr. Pabitra Pran Hazarika, my brother-in-law, Mr. Krishna Borah, and my beloved nieces, Ms. Abhilasha Junak Borah and Ms. Mukulita Borah. Their endless love, encouragement, and steadfast support have always uplifted me during challenging times and played a crucial role in helping me overcome the hurdles of my career. Their presence in my life has been a constant reminder of the power of family, and I am deeply indebted to each one of them for their love and belief in me.

Thank you all for being a memorable part of my life.

Mr. Gunanka Hazarika

Abstract

The thesis entitled as “Design and Development of Advanced Porous Organic Polymeric Adsorbents for the Efficient and Selective Removal and Recovery of Phosphate and Arsenate from Water”, mainly focuses on the design, synthesis, and application of novel modern polymeric adsorbents for the efficient removal and recovery of environmentally hazardous oxoanions – specifically phosphate and arsenate – from aqueous media. This thesis comprises five distinct chapters, which begins with a thorough review of pertinent literature and is followed by chapters that outline the development and findings of the experimental investigations conducted during the research period.

Chapter 1 represents an in-depth analysis of the present literature on reported adsorbent materials for oxoanion remediation, especially phosphate and arsenic, emphasizing their structural properties and basic adsorption mechanisms.

Chapter 2 presents the development of a Zn(II)-coordinated, 1-aminoguanidine-functionalized cellulose biopolymer (Zn-gCP) with efficient phosphate removal and recovery. Guanidinium groups enabled aqueous exfoliation and imparted broad-spectrum antibacterial activity. The study offers a sustainable route for dual-functional, reusable biopolymer adsorbents.

Chapter 3 describes the synthesis of a pH-responsive 2D covalent organic network (2D ag-CON) incorporating tris-aminoguanidine units. The material enabled rapid, selective phosphate capture and release via pH modulation. Phosphate adsorption induced a morphological change from spherical to sheet-like structures, serving as a distinguishing feature of ag-CON.

Chapter 4 introduces a bis-imidazolium-based covalent organic network (IC-CON) and is intended for the selective extraction of phosphate and arsenate ions. Because of its strong affinity for arsenate as compared to phosphate, IC-CON is useful for removing arsenate from phosphate-rich environments.

Chapter 5 outlines future directions for the rational design of advanced polymeric adsorbents, along with a summary of the major findings from the thesis.

भारतीय प्रौद्योगिकी संस्थान गुवाहाटी
Indian Institute of Technology Guwahati

List of Abbreviation

SDWA	Safe Drinking Water Act
HAB	Harmful algal bloom
U.S.	United States
ATP	Adenosine Triphosphate
SDG	Sustainable Development Goal
DNA	Deoxyribonucleic acid
LDH	Layered double hydroxide
CBB	Cellulose-based biomaterial
AC	Activated carbon
PAAHCl	Poly (allylamine hydrochloride)
MOF	Metal organic framework
POP	Porous organic polymer
PAF	Porous Aromatic Framework
HCP	Hypercrosslinked polymer
CTF	Covalent triazine framework
CMP	Conjugated microporous polymer
COF	Covalent organic framework
iPOP	Ionic porous organic polymer
MF	Microfiltration
UF	Ultrafiltration
NF	Nanofiltration
RO	Reverse osmosis

FO	Forward osmosis
EC	Electrocoagulation
DCM	Dichloromethane
EBPR	Enhanced biological phosphorus removal
DMF	Dimethylformamide
BNR	Biological nutrient removal
DMSO	Dimethyl sulfoxide
PAO	Polyphosphate-accumulating organism
DTT	Dithiothreitol
VFA	Volatile fatty acid
PHA	Poly-β-hydroxyalkanoates
DLS	Dynamic light scattering
DPAO	Denitrifying polyphosphate-accumulating organism
GAO	Glycogen-accumulating organism
AsOB	Arsenite-oxidizing bacterial
WHO	World Health Organization
EtOAc	Ethyl acetate
USEPA	United States Environmental Protection Agency
ag	1-aminoguanidine
gCP	1-aminoguanidine -modified cellulose-based polymer
Zn-gCP	Zn(II)-modified gCP
FESEM	Field emission scanning electron microscopy
FETEM	Field emission transmission electron microscopy

dH	Hydrodynamic diameter
ACN	Acetonitrile
EtOAc	Ethyl acetate
MeOH	Methanol
THF	Tetrahydrofuran
HCl	Hydrochloric acid
NaOH	Sodium hydroxide
IC	Ion chromatography
HRMS	High-resolution mass spectrometry
S. aureus	*Staphylococcus aureus*
E. coli	*Escherichia coli*
AAS	Atomic Absorption Spectrophotometer
ICP-MS	Inductively Coupled Plasma Mass Spectrometer
FT-IR	Fourier-Transform Infrared Spectroscopy
ATR	Attenuated total reflectance
XPS	X-Ray Photoelectron Spectroscopy
TGA	Thermogravimetric analysis
LB	Luria Bertani
SAED	Selected area electron diffraction
PXRD	The Powder X-ray Diffraction
BET	Brunauer-Emmett-Teller
BJH	Barrett–Joyner–Halenda
$CDCl_3$	deuterated chloroform

$AlCl_3$	Aluminium chloride
Et_3N	Trimethylamine
TLC	Thin layer chromatography
$MgCl_2$	Magnesium chloride
NMR	Nuclear Magnetic Resonance
AFM	Atomic Force Microscopy
CON	Covalent organic network
CP-MAS	Cross-polarization magic angle spinning
Al	Aluminium
Fe	Iron
CNT	Carbon nanotube
DTG	Derivative Thermogravimetry
N_2	Nitrogen

For symbols/units

cm	Centimetre
eV	Electron volt
Nm	Nanometre
mm	Millimetre
ξ	Zeta potential
C	Celsius
J	Coupling constant
°	Degree
mV	Millivolt
Hz	Hertz
K	Kelvin
R^2	Correlation coefficient
N	Normality
ppm	Parts-per-million
µM	Micro mole
µg	Micro gram
mL	Millilitre
h	Hour
min	Minute
mg	Milligram
kg	Kilogram
g	Gram
Q_e	Equilibrium adsorption capacity
ppm	Parts per million
%	Percent
Q_m	Maximum adsorption capacity
Sec	Second

MΩ	Megaohm
µL	Microliter
rpm	Revolutions per minute
wt	Weight
α	Alpha
kV	Kilovolt
V	Volume of solution
M	Amount of adsorbent
N	Dilution factor
K_l	Langmuir constant
K_f	Freundlich constant
Q_t	Adsorption capacities at time t
k_1	Adsorption rate constants of the pseudo-first order reaction
k_1	Adsorption rate constants of the pseudo-second order reaction
CFU	Colony Forming Unit
δ	Chemical shift
θ	Theta
P	Equilibrium pressure
P_0	Saturation pressure
π	Pi

Chapter 1

Oxoanion Pollutant Mitigation: Strategic Frameworks, Environmental Relevance, and Emerging Remediation Technologies

This chapter highlights the importance of water in sustaining ecosystems and addresses the growing concerns related to water pollution. It provides a thorough overview of the existing literature on wastewater remediation, focusing on the limitations of current treatment materials and methods concerning selectivity, stability, and regeneration. Additionally, the chapter underscores the necessity of developing advanced materials for the removal and recovery of phosphate and arsenate ions from wastewater.

Water contaminants can be systematically categorized into three main classes: physical, chemical, and biological, which pose different risks to the environment and human health.[1] Because of the extreme solubility, redox properties, and resistance to degradation processes, oxoanionic pollutants – in particular, phosphate and arsenate – present serious problems. Even though they typically have low bioaccumulation, because of their high oxidative stability and chemical resistance, these oxoanions pose serious problems for environmental modeling and remediation processes.[2-4]

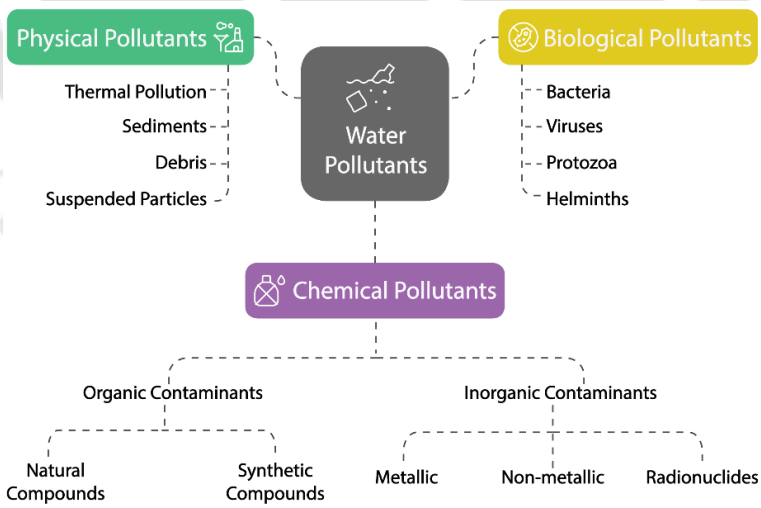

Figure 1.2. Schematic diagram depicting the classification of various water pollutants.

Among the many physicochemical techniques used to treat wastewater, adsorption has gained attention as a particularly selective, efficient, and

environmentally friendly method – especially for removing oxoanions, which are often present in tiny amounts ranging from micrograms to milligrams per liter in waters.[5, 6] In this context, cellulose – based biopolymers (CBBs) and covalent organic frameworks (COFs) have gained prominence as promising adsorbent materials.[7-12] Cellulose, the most abundant natural biopolymer on Earth, offers a renewable, cost-effective, and sustainable option for capturing phosphates. Its structure, rich in hydroxyl groups, makes it highly amenable to chemical modifications that enhance its adsorption capabilities. Modified cellulose materials improve the ability to capture pollutants while keeping their structure and longevity intact – aligning well with the principles of green chemistry and the circular economy. COFs, on the other hand, are perfect for harsh environmental conditions because they are very stable chemically and thermally.[13, 14] They are very selective about which contaminants they target because they can be made with different pore sizes and surface properties. This facilitates the recovery and removal of pollutants.[15] Together, these materials offer powerful tools for tackling wastewater pollutants in a sustainable and effective way.

Figure 1.2. Schematic diagram illustrating commonly used water treatment methods, encompassing physical, chemical, and biological approaches to effectively remove contaminants and improve water quality in various wastewater treatment plants.

Chapter 2

Guanidine-modified cellulose enhances the capturing and recovery of phosphates from wastewater.

The uncontrolled growth in population and cumulative demand for diverse food options has resulted in the widespread use of phosphate-based fertilizers in agriculture. However, the excess phosphate that plants do not utilize leaches from agricultural fields and accumulates in water bodies. Municipalities, food processors, and other industries also contribute to phosphate discharge into waterways. This excess phosphate causes eutrophication, resulting in depleted oxygen levels in lakes and other water bodies, which severely threatens the sustainability of aquatic ecosystems and drinking water supplies. The phenomenon of anthropogenic hyper-eutrophication leads to persistent environmental, public health, and economic consequences for nations worldwide. This issue is expected to escalate with climate change, highlighting the urgent need for sustainable technologies.[2, 16]

In response to these challenges, herein, we demonstrate an efficient strategy to remove and recover phosphates selectively from water to remediate environmental impacts. Chapter 2 presents the design and synthesis of a zinc-coordinated 1-aminoguanidine functionalized cellulose-based biopolymer (Zn-gCP). This material showed a high binding affinity for phosphate ions due to the synergistic interactions between the Zn(II) ion and the guanidine moieties. The Zn-gCP exhibited a maximum adsorption capacity of 310 $mg \cdot g^{-1}$ at neutral pH and maintained stable performance over multiple adsorption–desorption cycles, enabled by simple pH adjustment for regeneration. Despite exhibiting comparatively slower adsorption kinetics, the material outperformed previously published biopolymeric systems in terms of adsorption capacity, reusability, and additional antimicrobial functionality. These combined characteristics demostrate its potential as a multifunctional sorbent for practical and environmentally friendly wastewater treatment applications.

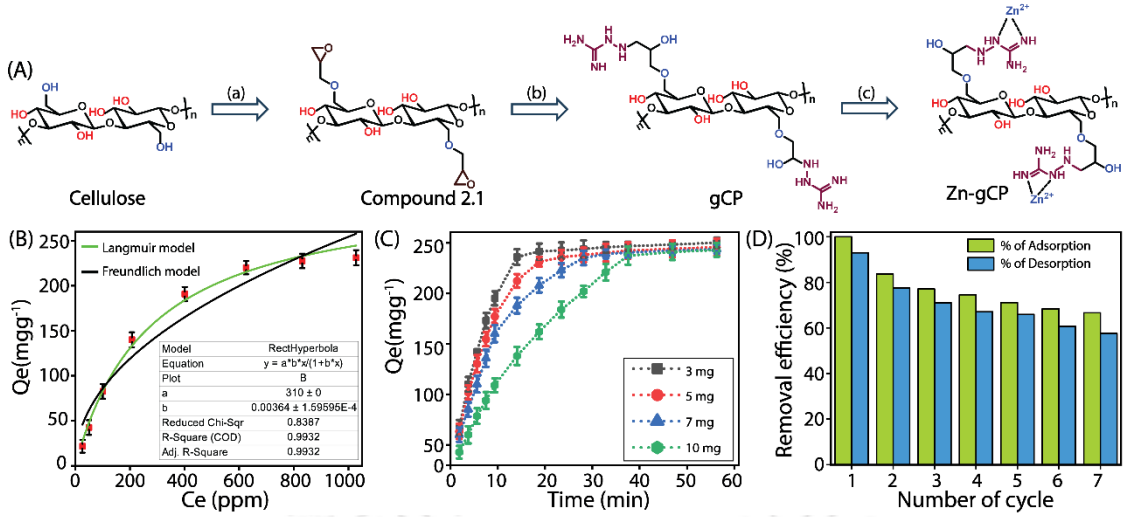

Figure 2.1. Synthetic scheme of the gCP and Zn-gCP polymers (a = epichlorohydrin, NaOH, H_2O, 0 – 60 °C, 3 h; b = 1-aminoguanidine hydrogen carbonate,NaOH, H_2O, rt – 0 – 60 °C, 3 h; c = $ZnCl_2.6H_2O$, H_2O, 60 °C, 12 h) (A). Phosphate anion adsorption isotherm of Zn-gCP (B). Time-dependent adsorption isotherm of phosphate ions by the Zn-gCP polymer (3 – 10 mg) at pH 7.0 at room rt (C). Phosphate ion adsorption and desorption efficiency of the Zn-gCP polymer after different cycles (D).

Chapter 3

A pH-responsive covalent organic network: Morphology change leads to capture and removal of phosphate ions from water

The Zn(II)-coordinated cellulose-based biopolymer (Zn-gCP), presented in Chapter 2, has shown considerable potential for the selective removal and recovery of phosphate from aquatic systems. However, its relatively lower adsorption capacity and slower kinetics than advanced adsorbents like metal-organic frameworks (MOFs) and COFs – which typically offer higher uptake and faster adsorption rates – may limit its large-scale practical application.[17]

To overcome the relatively slow adsorption kinetics of Zn-gCP, Chapter 3 focused on developing a tris-aminoguanidine-functionalized 2D covalent organic framework (ag-CON). This advanced polymer exhibited significantly enhanced adsorption kinetics and a superior phosphate uptake capacity of 719 $mg{\cdot}g^{-1}$ at pH 6, outperforming Zn-gCP in both rate and efficiency. The improved phosphate recognition and removal efficacy of the ag-CON could be due to the presence of

multiple hydrogen-bonding and salt-bridge-forming sites of tris-aminoguanidine moieties. The ag-CON also showed excellent chemical stability across a wide pH range and could be readily regenerated through simple pH adjustments, retaining its performance over multiple adsorption-desorption cycles. Notably, ag-CON exhibited dynamic morphological transitions–shifting between spherical and sheet-like configurations in response to phosphate binding and release, which adds a unique and functional characteristic to the material. These features highlight ag-CON as a promising, high-performance, reusable sorbent for phosphate remediation and recovery, particularly under harsh environmental conditions.

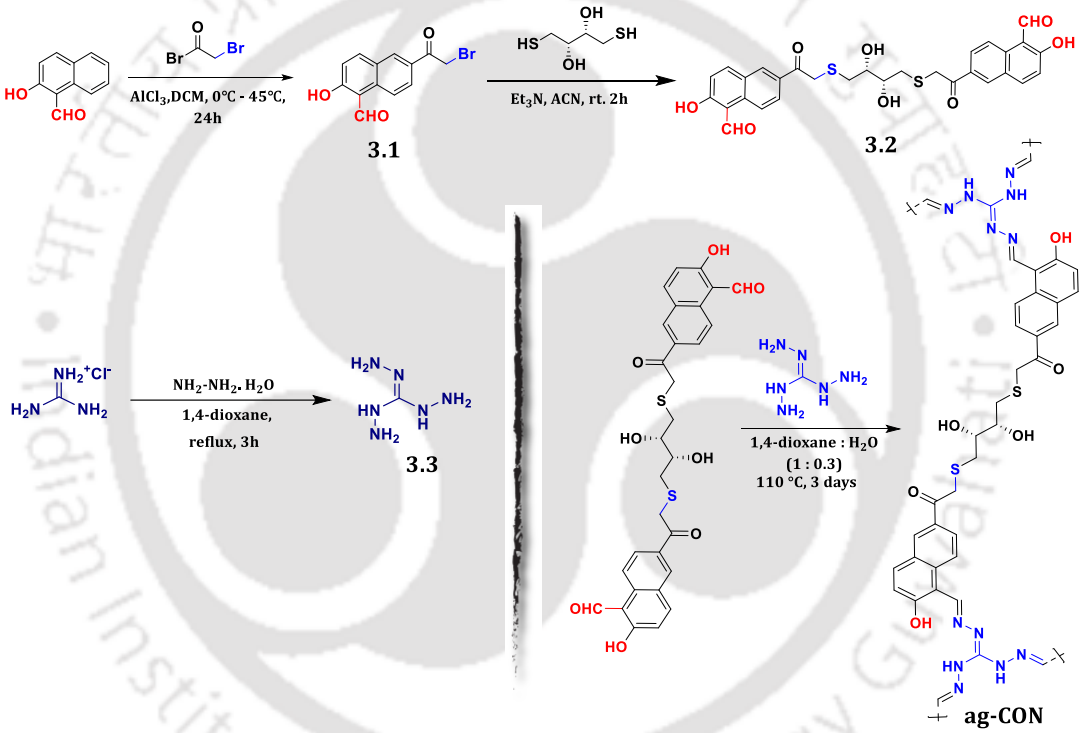

Figure 3.1. Synthetic scheme of ag-CON.

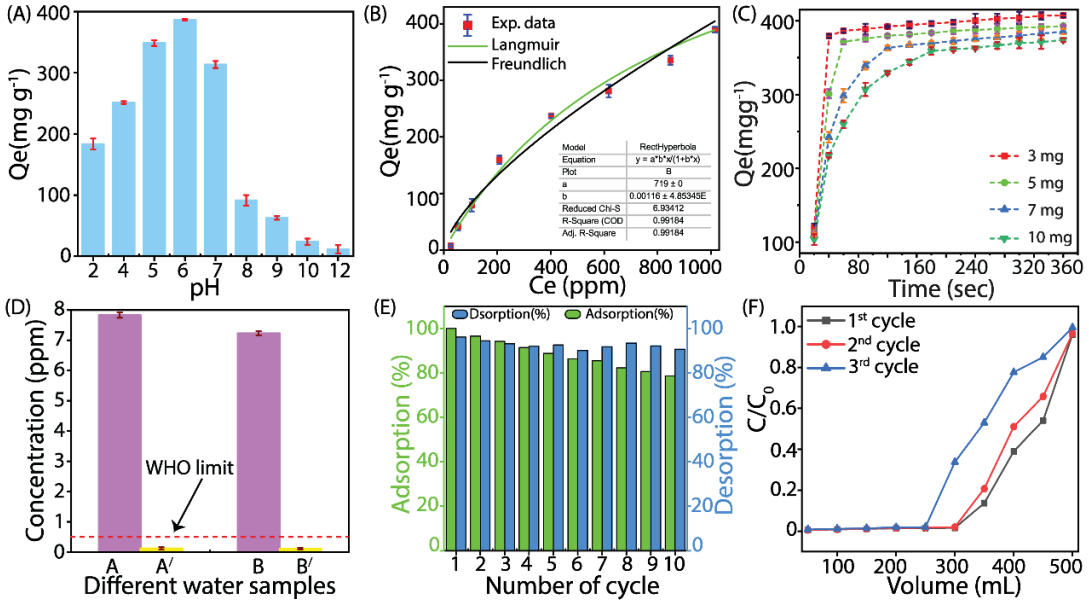

Figure 3.2. The pH-dependent phosphate ion adsorption efficiency of ag-CON (A). Phosphate ion adsorption isotherm of ag-CON (B). Time-dependent adsorption isotherm of phosphate ions by ag-CON (3-10 mg) at pH 6.0 under rt (C). Phosphate adsorption capacity of the ag-CON from the real phosphate-contaminated wastewater (D). Phosphate ions adsorption and desorption efficiency of ag-CON after different cycles (E). Phosphate ions adsorption efficiency of the ag-CON by dynamic adsorption column experiment (C0 = Initial concentration of the phosphate solution and C = Final concentration of the phosphate solution after passing through the column) (F).

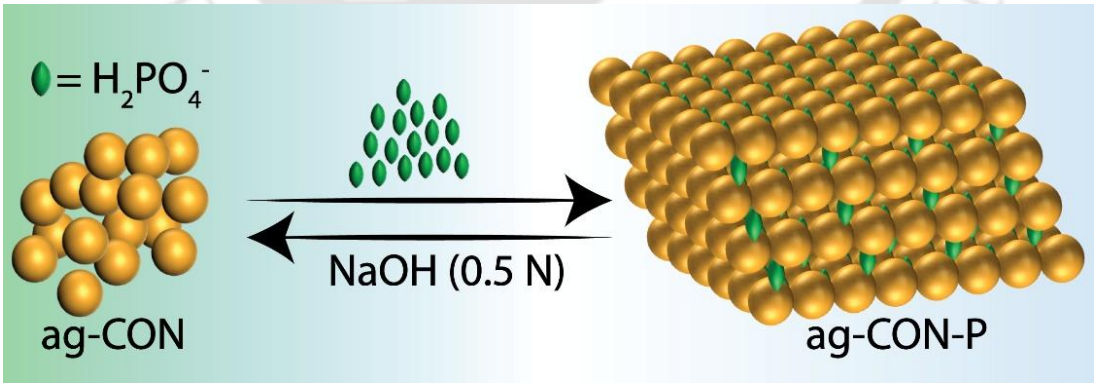

Figure 3.3. The pictorial representation of the transformation from spherical to sheet-like structure of ag-CON polymer after phosphate ions adsorption.

Chapter 4

Bis-imidazolium-linked covalent organic network effectively removes arsenate from water and wastewater containing phosphates

To extend the scope of remediation to arsenate along with phosphate, Chapter 4 presented the synthesis of a bis-imidazolium-based cationic covalent organic framework (IC-CON). This polymer demonstrated high adsorption capacity, rapid kinetics, and strong selectivity for both arsenate and phosphate, with a marked preference for arsenate in equimolar systems. Mechanistic investigations revealed that electrostatic interactions, hydrogen bonding, and anion exchange primarily influenced to the adsorption process. IC – CON exhibited excellent recyclability, maintaining its performance over 15 adsorption – desorption cycles, and could be efficiently regenerated using a mild alkaline salt treatment (0.5 N NaOH followed by 0.1 N NaBr). Furthermore, the polymer showed strong potential for continuous flow applications via column chromatography, making it suitable for scalable water treatment processes. A distinctive feature of IC-CON is its ion-responsive morphological reversibility, particularly during arsenate adsorption, transitioning between spherical and sheet-like structures – a property not observed during phosphate binding. These characteristics position IC-CON as a versatile and robust adsorbent for the selective removal and recovery of hazardous oxoanions from contaminated water sources.[18]

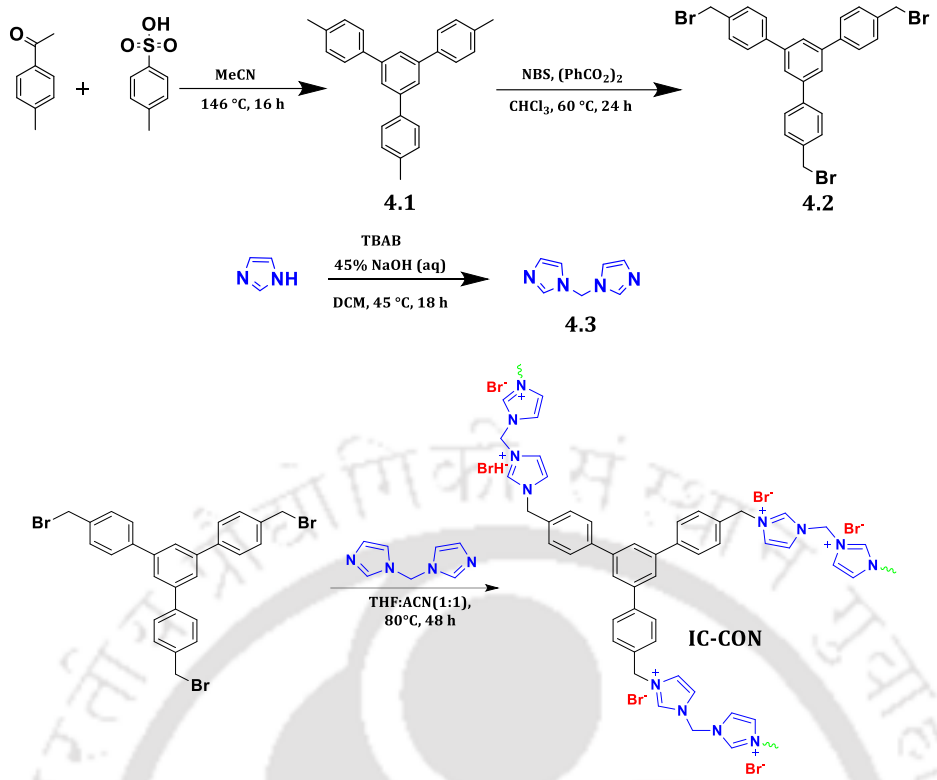

Figure 4.1. Synthetic scheme of IC-CON.

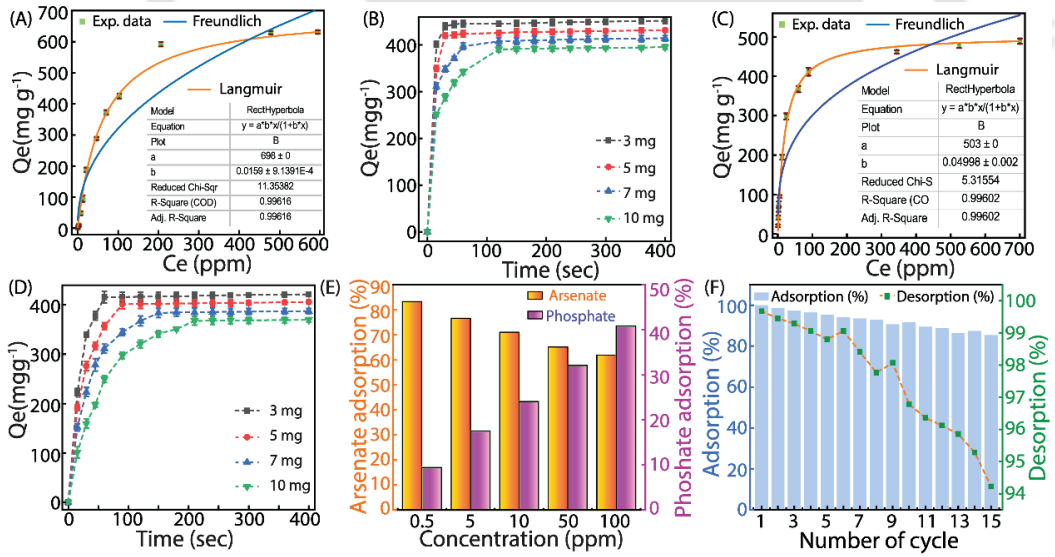

Figure 4.2. Arsenate ion adsorption isotherm of IC-CON (A). Time-dependent adsorption isotherm of arsenate ions by IC-CON (3–10 mg) at pH 7.0 under room temperature (B). Phosphate ion adsorption isotherm of IC-CON (C). Time-dependent adsorption isotherm of phosphate ions by IC-CON (3–10 mg) at pH 7.0 under room temperature (D). Adsorption efficiency of IC-CON from varying concentrations of 1:1 stock solution of arsenate and phosphate ions (E). Arsenate ion adsorption and desorption efficiency of IC-CON after different cycles (F).

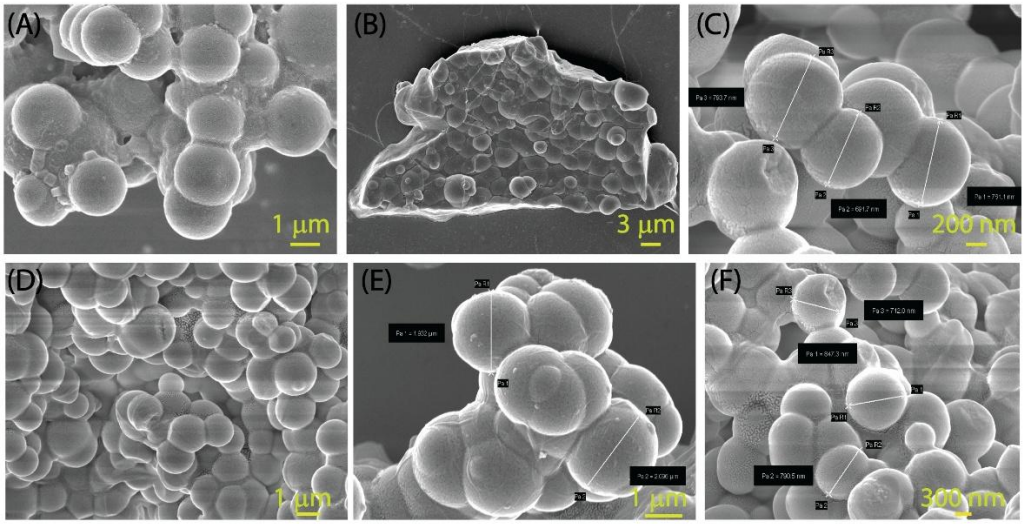

Figure 4.3. FESEM image of IC-CON(A), after arsenate adsorption (B), and after arsenate desorption (C). FESEM images of IC-CON (D), after phosphate adsorption (E), and after phosphate desorption (F).

Conclusion

Overall, by offering insightful analysis of the logical design of multifunctional, robust, and regenerable polymeric adsorbents for environmental remediation, the key findings of this thesis contribute significantly to the field of water purification. All the synthesized materials demonstrated outstanding adsorption performance, high selectivity, excellent reusability, and structural stability under harsh conditions, effectively targeting hazardous and valuable oxoanions such as phosphate and arsenate, outperforming most previously reported adsorbent materials. The research results highlight the practical applications of these polymeric frameworks while establishing a solid basis for advancing next-generation sorbents that feature adjustable structures and improved functionalities. Collectively, this work offers a promising direction toward sustainable remediation technologies and resource recovery strategies for addressing water contamination challenges.

Future prospects

To establish COFs as a next-generation material platform for environmental remediation and water purification, future research must address several critical

directions. A major focus lies in moving beyond batch adsorption systems toward the development of COF-based membranes capable of operating under continuous flow conditions. These membranes, owing to the intrinsic porosity, high water permeability, and chemical tunability of COFs, offer great promise for selective pollutant retention. Innovative fabrication strategies such as mixed-matrix membranes (MMMs), layer-by-layer assemblies, and in situ COF growth on polymeric or ceramic substrates are expected to be key in scaling up their practical application. Moreover, it will be crucial for ensuring sustained operational stability and antifouling effectiveness of COF in real – world water matrices. Techniques for surface modification, such as grafting with hydrophilic or antimicrobial polymers, the incorporation of metal nanoparticles, or the embedding of photoactive sites for visible-light-driven self-cleaning, are expected to improve the durability and reusability of membranes. To maximize the potential of COFs in advanced water treatment applications, it is important to encourage collaboration among diverse fields, including materials science, environmental engineering, and nanotechnology, is essential.

References

1. Sun, D. T.; Peng, L.; Reeder, W. S.; Moosavi, S. M.; Tiana, D.; Britt, D. K.; Oveisi, E.; Queen, W. L., Rapid, selective heavy metal removal from water by a metal–organic framework/polydopamine composite. *ACS Cent. Sci.* **2018,** *4* (3), 349-356.

2. Dey, S.; Das, S.; Patel, A.; Raj, K. V.; Vanka, K.; Manna, D., Antimicrobial two-dimensional covalent organic nanosheets (2D-CONs) for the fast and highly efficient capture and recovery of phosphate ions from water. *J. Mater. Chem. A* **2022,** *10* (9), 4585-4593.

3. Das, S.; Hazarika, G.; Manna, D., Guanidine-functionalized fluorescent sp2 carbon-conjugated covalent organic framework for sensing and capturing Pd (II) and Cr (VI) ions. *Chem. Eur. J.* **2023,** *29* (15), e202203595.

4. Zhao, L.; Liu, Q. X.; Li, C. P., Sequestration of Metal Oxoanions by Covalent Organic Frameworks. *Eur. J. Inorg. Chem.* **2025,** *28* (9), e202400639.

5. Nadagouda, M. N.; Varshney, G.; Varshney, V.; Hejase, C. A., Recent Advances in Technologies for Phosphate Removal and Recovery: A Review. *ACS Environ. Au* **2024,** *4* (6), 271-291.

6. Weerasundara, L.; Ok, Y.-S.; Bundschuh, J., Selective removal of arsenic in water: A critical review. *Environ. Pollut.* **2021,** *268*, 115668.

7. Nguyen, T.; Ngo, H.; Guo, W.; Zhang, J.; Liang, S.; Lee, D.; Nguyen, P.; Bui, X., Modification of agricultural waste/by-products for enhanced phosphate removal and recovery: potential and obstacles. *Bioresour. Technol.* **2014,** *169*, 750-762.

8. Motloung, M. T.; Magagula, S. I.; Kaleni, A.; Sikhosana, T. S.; Lebelo, K.; Mochane, M. J., Recent advances on chemically functionalized cellulose-based materials for arsenic removal in wastewater: a review. *Water* **2023,** *15* (4), 793.

9. Chauhan, K.; Singh, P.; Sen, K.; Singhal, R. K.; Thakur, V. K., Recent Advancements in the Field of Chitosan/Cellulose-Based Nanocomposites for Maximizing Arsenic Removal from Aqueous Environment. *ACS Omega* **2024,** *9* (26), 27766-27788.

10. Dong, S.; Ji, Q.; Wang, Y.; Liu, H.; Qu, J., Enhanced phosphate removal using zirconium hydroxide encapsulated in quaternized cellulose. *J. Environ. Sci.* **2020,** *89*, 102-112.

11. Qiu, H.; Liang, C.; Zhang, X.; Chen, M.; Zhao, Y.; Tao, T.; Xu, Z.; Liu, G., Fabrication of a biomass-based hydrous zirconium oxide nanocomposite for preferable phosphate removal and recovery. *Acs Appl. Mater. Inter.* **2015,** *7* (37), 20835-20844.

12. Nie, G.; Liu, X.; Li, X.; Meng, C.; Wang, W.; Zou, D., Efficient phosphate removal and recovery by using nanosized La (III) oxides anchored on aminated biomass waste. *Sep. Purif. Technol.* **2023,** *305*, 122513.

13. Zhuang, H.; Guo, C.; Huang, J.; Wang, L.; Zheng, Z.; Wang, H. N.; Chen, Y.; Lan, Y. Q., Hydrazone-Linked Covalent Organic Frameworks. *Angew. Chem. Int. Ed.* **2024,** *63* (31), e202404941.

14. Zheng, S.; Bi, S.; Fu, Y.; Wu, Y.; Liu, M.; Xu, Q.; Zeng, G., 3D crown ether covalent organic framework as interphase layer toward high-performance lithium metal batteries. *Adv. Mater.* **2024,** *36* (21), 2313076.

15. Segura, J. L.; Royuela, S.; Ramos, M. M., Post-synthetic modification of covalent organic frameworks. *Chem. Soc. Rev.* **2019,** *48* (14), 3903-3945.

16. Hazarika, G.; Das, S.; Patel, A.; Manna, D., Guanidine-modified cellulose enhances capturing and recovery of phosphates from wastewater. *Environ. Sci.: Water Res. Technol.* **2025,** *11* (3), 691-701.

17. Hazarika, G.; Das, S.; Das, N. M.; Manna, D., A pH-responsive covalent organic network: Morphology change leads to capture and removal of phosphate ions from water. *J. Mater. Chem. A* **2024,** *12* (30), 19559-19566.

18. Hazarika, G.; Manna, D., Bis-imidazolium linked covalent organic network effectively removes arsenate from water and wastewater containing phosphates. *J. Mater. Chem. A* **2025,** *13*, 19695-19704.

Chapter 1

Oxoanion Pollutant Mitigation: Strategic Frameworks, Environmental Relevance, and Emerging Remediation Technologies

1.1. Water: the essence of life and its significance

Water plays a crucial role in all biological, ecological, and industrial systems.[1-3] It significantly influences the ecosystem dynamics, species distribution, and habitat sustainability. Water also plays a crucial role in regulating the climate through interactions between the ocean and atmosphere and carbon sequestration.[4]

Although 71% of the Earth's surface is covered with water, only 2.5% is freshwater, and less than 1% is accessible for human use.[5] The rapid growth of the population, along with industrialization and urbanization, has greatly increased the need for water and the rate of pollution. Untreated industrial and other effluents have caused significant contamination.[6] Therefore, immediate, scientifically supported strategies for pollution reduction and sustainable water management are required to protect this vital resource for future generations.

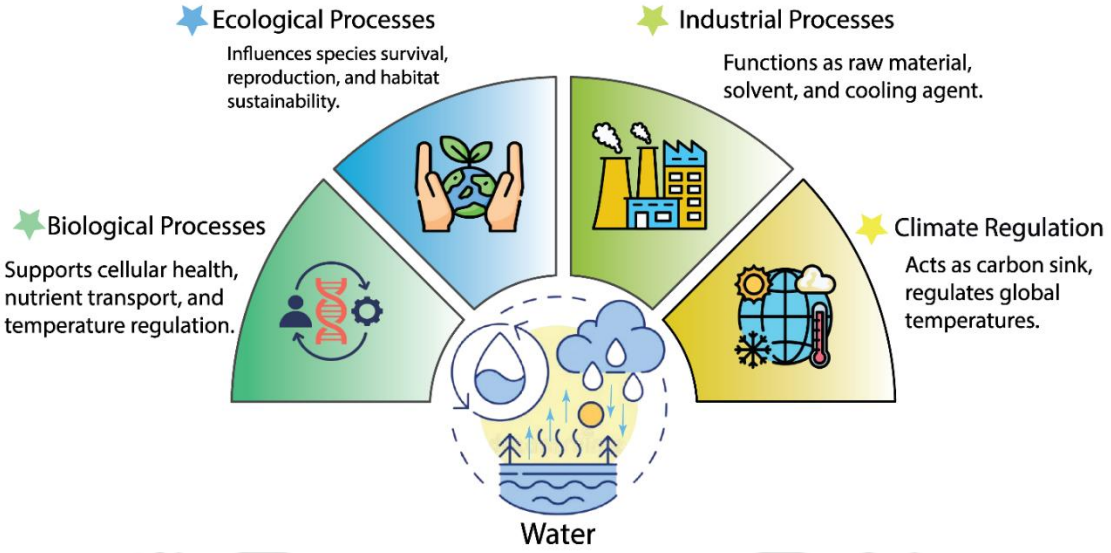

Figure 1.1. Diagrammatic illustration of water consumption for different purposes.

1.2. Water pollution: types and categories

The Safe Drinking Water Act (SDWA) divides water pollutants into three main groups: chemical, biological, and physical. Among these, chemical pollutants are considered to be the most dangerous because they are very toxic, stay in the environment for a long time, and can easily spread through water sources, which can be very harmful for human health and the environment.[7] Inorganic chemical pollutants, particularly oxoanions such as phosphate (PO_4^{3-}), arsenate (AsO_4^{3-}), chromate (CrO_4^{2-}), selenate (SeO_4^{2-}), nitrate (NO_3^-), and others, are highly soluble,

redox-active, and resistant to degradation. Unlike heavy metal cations, oxoanions aren't easily adsorbed to surfaces of adsorbents in neutral to alkaline conditions. This allows them to leach into groundwater and remain in aquatic systems for extended periods. Although bioaccumulation is limited, their ability to exist in different oxidation states and their chemical stability make them difficult to predict and remove from the environment.[6, 8, 9]

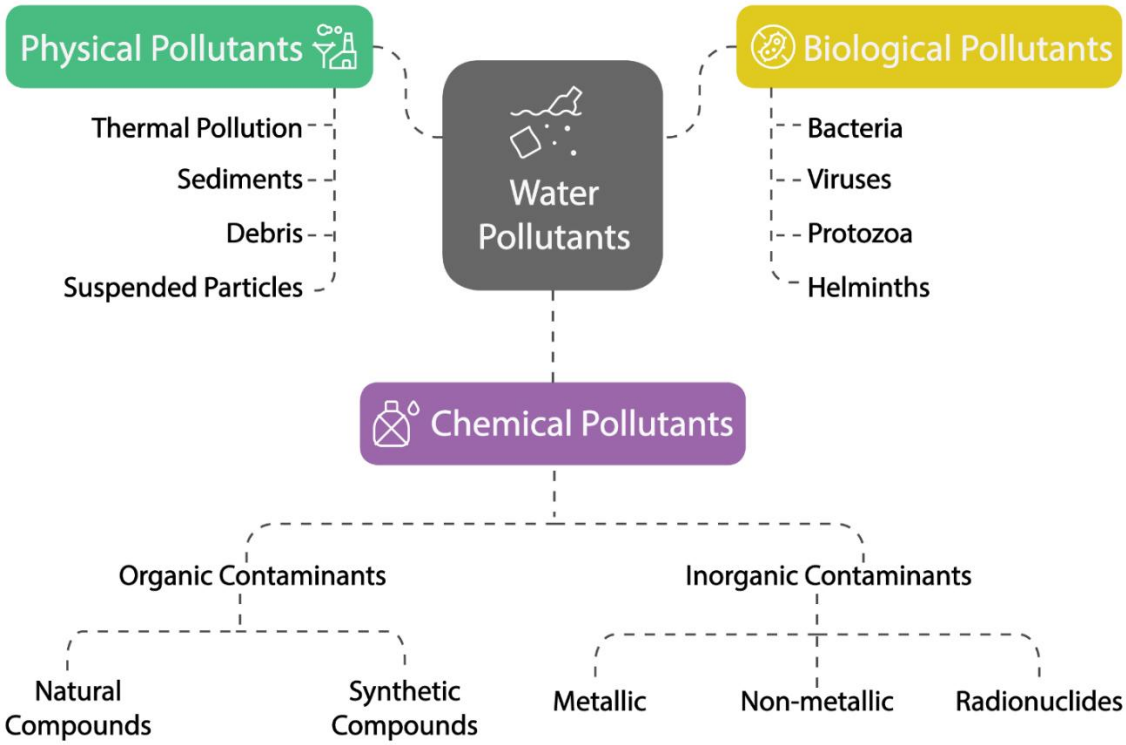

Figure 1.2. Schematic diagram depicting the classification of various water pollutants.

Among various oxoanion contaminants in aquatic environments, phosphates are major contributors to eutrophication – a global issue exacerbated by anthropogenic inputs from agriculture, industry, and wastewater. Elevated phosphate concentrations trigger harmful algal blooms (HABs), causing hypoxia, biodiversity loss, and ecosystem collapse. Cyanotoxins released by blooms further pose severe public health risks. Eutrophication additionally contributes to greenhouse gas emissions, especially methane, which makes climate change more serious.[6] The U.S. alone incurs an estimated annual cost of $2.2 billion for eutrophication mitigation.[10]

Arsenate, another very poisonous oxoanion that is chemically similar to phosphate, replaces phosphate in ATP synthesis, making unstable intermediates that deplete cellular energy. Long-term exposure can cause arsenicosis and raise the risk of cancer, especially in the skin, bladder, lungs, and liver.[11] Arsenate also causes ecological harm through reduced reproduction, growth, and enzymatic activity in aquatic organisms.

Besides phosphate and arsenate, other environmentally relevant oxoanions also pose toxicological threats. Chromate (CrO_4^{2-}), a known carcinogen, induces oxidative stress and DNA damage; nitrate (NO_3^-) causes methemoglobinemia and is linked to thyroid dysfunction; selenium oxyanions (SeO_3^{2-}, SeO_4^{2-}), essential in trace amounts, become toxic at elevated levels, disrupting redox balance and protein function. These contaminants demonstrate high mobility, bioavailability, and environmental persistence.[8]

This study explores the selective removal and recovery of phosphate and arsenate from wastewater, recognizing their complex roles in both environmental harm and agricultural necessity. Phosphate is an especially important nutrient vital for plant growth, energy production (ATP), and genetic processes, extracted from phosphate rock, which is limited and often located in geopolitically sensitive regions, making sustainable management crucial. Complementing circular economy ideas, its recovery from wastewater is essential for environmental sustainability, resource security, and nutrient cycling. Inefficient techniques of using phosphate-based fertilisers in agriculture, combined with runoff and leaching, exacerbate ecological damage. Phosphate recovery from industrial and municipal wastewater reduces reliance on limited mineral resources, improves supply resilience, and reduces nutrient pollution.[6]

Similarly, arsenic contamination – from geogenic sources, industrial effluents, mining, and coal combustion – affects over 140 million people globally. Both arsenate and arsenite are highly toxic forms of arsenic that can easily move through the environment and are bioavailable under varying redox and pH conditions. This makes it especially important to develop effective ways to reduce their presence and impact.[12]

Traditional treatment technologies primarily aim for removal rather than recovery. Thus, developing advanced, cost-effective, and sustainable technologies for removing and recovering phosphate and arsenate is essential for mitigating environmental and health risks. Integrating such technologies into existing wastewater infrastructure supports resource conservation, pollution control, and global water quality objectives stated in the United Nations Sustainable Development Goals (SDGs). A circular economy approach – emphasizing recovery and reuse over disposal – offers a sustainable solution to nutrient management and water security.

1.3. Strategies for removing and recovering oxoanions from aqueous solutions

A range of treatment methods has been utilized to extract and remove harmful oxoanions from wastewater and groundwater sources, which pose considerable threats to environmental and human health. The frequently applied methods of water purification include adsorption, membrane filtration, chemical precipitation, electrocoagulation, and biological processes.[13, 14] Each technology functions via unique physicochemical or biological mechanisms and demonstrates differing levels of efficacy, cost-effectiveness, scalability, and environmental friendliness, contingent upon the specific contamination and the properties of the water matrix. Emphasizing their operational concepts, mechanisms, advantages, constraints, and possibilities for integration into sustainable water purification systems, the following sections thoroughly review these treatment technologies.

1.3.1. Adsorption —

Adsorption represents a mass transfer phenomenon whereby one or more solute species, which may include atoms, ions, or molecules in either the gas or liquid phase, accumulate on the surface of a solid material referred to as the adsorbent. The species referred to as adsorbates adhere to the surface of the adsorbent through various interactions, which can be categorized as either physical interactions, such as electrostatic forces and van der Waals dispersive interactions, or chemical interactions that involve covalent or ionic bonding. An ideal adsorbent must have higher selectivity and adsorption capacity. The requirements for the adsorbent include long-term stability, reusability, cost-effectiveness, and ecological dependability – more specifically, biodegradability and biocompatibility.[14]

13.1.1. Mechanisms:

Based on the type of molecular interactions, the adsorption mechanism can be broadly categorized based on physical or chemical adsorption characteristics, and it is briefly summarized below.

Figure 1.3. Schematic diagram illustrating commonly used water treatment methods, encompassing physical, chemical, and biological approaches to effectively remove contaminants and improve water quality in various wastewater treatment plants.

1.3.1.1.1. Ion exchange:

Ion exchange is a specific molecular process in which a chemically equivalent counterion from the surrounding solution replaces a counterion originally bound to the surface of a solid-phase adsorbent. This exchange maintains the overall electroneutrality of the system by providing that the adsorption of an incoming ion onto the solid surface is accompanied by the concurrent desorption of an ion previously attached to the surface. In essence, ion exchange is a reversible, stoichiometric process driven mainly by electrostatic interactions between the mobile ions in solution and the fixed charges on the resin. Because of their

reversibility, which allows for regeneration and repeated use under suitable thermodynamic conditions, ion-exchange materials are economically viable for various industrial applications. Ion exchange is commonly considered an "outersphere" surface complexation mechanism at the molecular level. Within the framework, the exchanging ions are situated in the second coordination shell of a surface-bound metal complex or charged group, maintaining their complete hydration shells during the exchange process. Ion-exchange materials are generally divided into two main types: cation and anion exchange resins. Cation-exchange resins have negatively charged functional groups – like carboxylic acid, phosphonic acid, or sulfonic acid – that allow them to attract and swap out positively charged ions such as H^+, Na^+, K^+, and Ca^{2+}. Whereas the anion-exchange resins contain positively charged functional groups such as quaternary ammonium or tertiary amine functionalities. These cationic moieties facilitate the exchange of anions such as OH^-, Cl^-, NO_3^-, and SO_4^{2-}. The ion exchange technique remains an essential technique in materials chemistry and separation science because of its high selectivity, reversibility and regulation approach for altering ionic species on the solid-liquid interface.[14, 15]

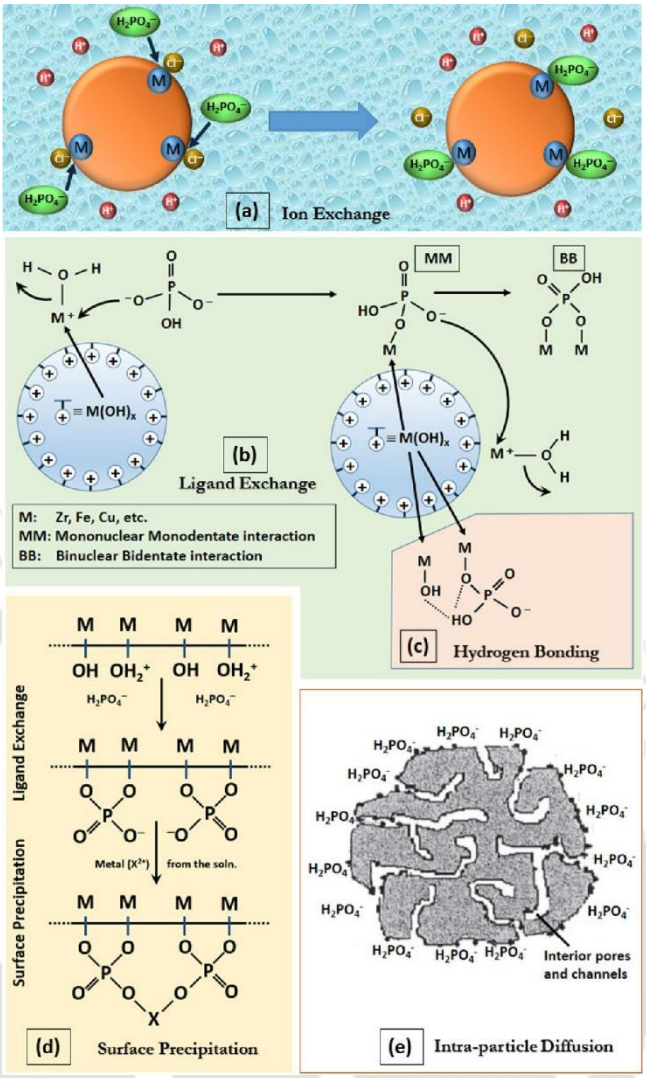

Figure 1.4. Schematic illustration of different adsorption mechanisms. ion-exchange (a); ligand-exchange (b); hydrogen-bonding (c); surface precipitation (d); and diffusion (e). Reproduced from ref. 14 with permission from the American Chemical Society, Copyright2024.

1.3.1.1.2. Ligand exchange:

Ligand exchange is a key surface interaction mechanism wherein an adsorbate, typically an anionic species, forms coordinate covalent bonds with specific surface sites on an adsorbent material. These sites are often composed of metal (hydr)oxides or materials modified with metal centres. In this process, a new ligand replaces an existing one – like a hydroxyl group that's already attached to the surface of a metal atom. This substitution forms an inner-sphere complex, characterized by direct coordination between the incoming ligand and the metal

centre, often accompanied by partial or complete dehydration of the surface. Due to its covalent nature, ligand exchange interactions are typically strong, rapid, and usually irreversible under environmentally relevant conditions.[14, 15]

1.3.1.1.3. Hydrogen bonding:

Hydrogen bonding interactions are the fundamental driving force behind the adsorption of oxoanions from aqueous solutions onto a range of adsorbent materials. Hydrogen bonding usually takes place between proton-donating groups on the surface of the adsorbent, such as -OH, -NH_2, -COOH, or another polar functional group, and the negatively charged oxygen atoms of the oxoanion species, which act as hydrogen bond acceptors. The presence of hydrogen-bond-donating groups on the surface of the adsorbent significantly increases the affinity of oxoanions through specific, directed interactions. Hydrogen bonding becomes a significant and crucial mechanism enabling adsorption, especially in neutral to nearly acidic conditions, where competing ions may lessen or screen the electrostatic attraction between the negatively charged oxoanions and the adsorbent surface.[14, 15]

1.3.1.1.4. Surface precipitation:

When adsorption sites are saturated or oxoanion concentrations are high, surface precipitation is crucial in eliminating oxoanions such as phosphate, arsenate, chromate, and vanadate from water. Initial adsorption, nucleation, and precipitate growth are the three main phases of this process, which are impacted by pH, ionic strength, and competing ions.[14, 15] Examples of the surface precipitation reaction involved in phosphate and arsenate removal are given below.

Phosphate removal on iron oxides

$$FeOOH\ (s) + PO_4^{3-} + Fe^{3+} \longrightarrow FePO_4 . xH_2O\ (s)$$

Arsenate removal on Alumina

$$Al_2O_3\ (s) + AsO_4^{3-} + Al^{3+} \longrightarrow AlAsO_4\ (s)$$

This mechanism enhances oxoanion removal beyond monolayer adsorption, offering a robust solution for water treatment in high-contamination scenarios.

1.3.1.1.5. Diffusion:

The mechanism of diffusion that regulates the removal of oxoanions from aqueous environments consists of multiple mass transfer stages, ultimately leading to the binding or entrapment of oxoanions onto or within a host material, which may

include adsorbents, membranes, or porous frameworks. Oxoanions like nitrate, chromate, arsenate, and phosphate usually exist as hydrated anions in water. Diffusion from the bulk solution to reactive sites is necessary for their efficient removal and adsorption processes; this phenomenon is impacted by interfacial chemistry, hydrodynamic conditions, and material properties.[14, 15]

1.3.1.1.6. Intercalation:

The intercalation mechanism for oxoanion removal from aqueous systems is a host–guest process wherein oxoanion species are incorporated into the interlayer galleries of layered materials through anion exchange or electrostatic stabilization**.** This mechanism is especially important in materials with two-dimensional lamellar structures with exchangeable interlayer anions and positively charged layers, like layered double hydroxides (LDHs), hydrotalcites, clays, and graphene oxide derivatives.[14, 15]

1.3.1.1.7. Lewis's acid/base concept:

Metals such as Al^{3+}, Mg^{2+}, Fe^{3+}, and La^{3+} fall under the category of hard acids and are particularly effective in binding with the hard-base oxyanions such as phosphate and arsenate. Metals with higher valency tend to interact more strongly with phosphate and arsenate species (for example, $La^{3+} > Mg^{2+}$). Smaller ionic radii also form more stable complexes by increasing charge density and reducing repulsive forces.[15]

1.3.1.2. Factors affecting the adsorption process:

Numerous physicochemical factors, such as adsorbent dosage, solution pH, initial adsorbate concentration, contact time, temperature, and the presence of coexisting ions, influence an adsorbent's adsorption performance toward various adsorbate species, such as phosphate or arsenate. Using more adsorbent generally boosts the overall amount of material that gets adsorbed, since there are more active sites available. However, this can sometimes lower the adsorption capacity per gram of adsorbent. That’s because particles may clump together, active sites can overlap, or the solution's pH might shift. pH plays a key role – It affects both the form of the substance being adsorbed and the charge on the adsorbent’s surface, which in turn impacts how well they attract and bind to each other. Selectivity and material robustness are crucial because the presence of competing ions in multi-component

systems can decrease adsorption efficiency through site competition. Contact time determines adsorption kinetics, which is usually examined using pseudo-first-order and pseudo-second-order models to differentiate between chemisorption and physisorption processes. Adsorption capacity increases with initial adsorbate concentration due to a stronger concentration gradient, although removal efficiency may decline as binding sites become saturated. Temperature impacts the spontaneity and nature of the adsorption process; endothermic systems exhibit increased adsorption with rising temperature, while exothermic systems show the opposite. Thermodynamic parameters – ΔG°, ΔH°, and ΔS° – offer valuable inputs about the adsorption pattern. They help to assess the process (spontaneous or non – spontaneous), reveal whether it is driven by physical or chemical interactions, and show the level of entropy changes at the interface between the solid and liquid phases. Understanding these factors is key to choosing the right materials and improving the efficiency of the process. A comprehensive understanding of these interrelated factors is essential for optimizing adsorbent design and operational conditions in environmental remediation applications.[14]

1.3.1.3. Comparative overview of adsorbent materials for phosphate and arsenate removal:

Numerous adsorbents have been extensively studied for removing phosphate and arsenate from aqueous environments. Below is a scientific overview of the principal classes of phosphate and arsenate adsorbents, highlighting recent advancements in their design and application:

1.3.1.3.1. Activated carbon-based adsorbents:

Activated carbon (AC) is widely employed in water treatment due to its high surface area, porosity, cost-effectiveness, and availability. Modification of ACs via impregnation with metal oxides of Fe(III), Mn(II, III, IV), La(III), Zr(IV) and others demonstrates significant improvement in adsorption capacities for phosphate and arsenate, making them more effective in water treatment applications. In addition to modifying commercially available activated carbon, researchers have also synthesized activated carbon from various natural carbon sources such as sewage sludge, lignin, pinecones, banana waste, etc. Overall, activated carbon is widely employed in water treatment applications for the adsorption of anionic

contaminants such as phosphate and arsenate. Although commercial AC exhibits general efficacy, its performance in removing these oxyanions can be considerably enhanced by surface modification or incorporation of metal additives, thereby tailoring its surface chemistry for improved affinity and capacity.[16-21]

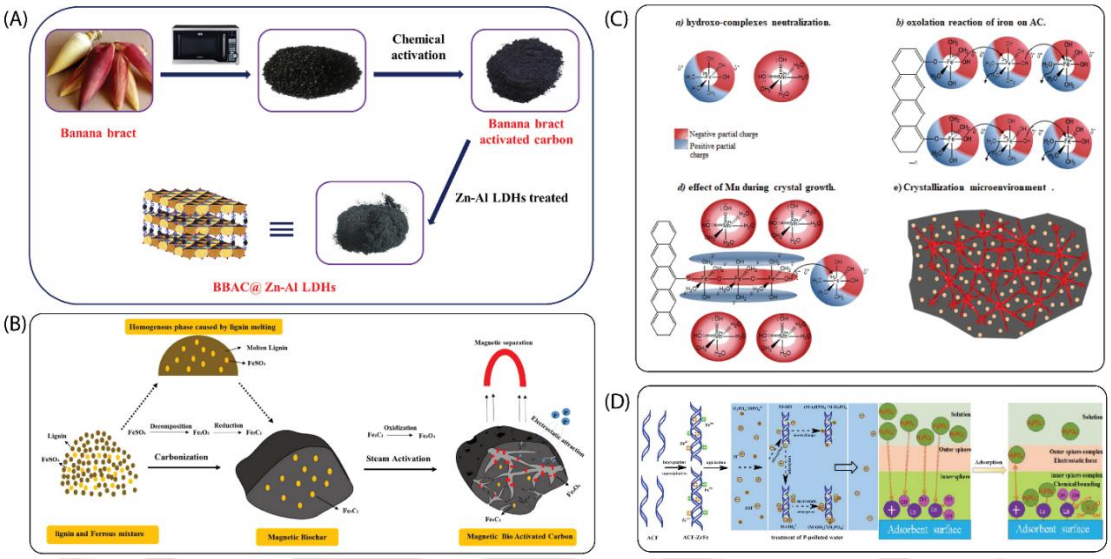

Figure 1.5. Activated carbon-based adsorbents synthesized by Karthikeyan et al. (A), Han et al. (B), Nieto-Delgado et al. (C), and Xiong et al. (D), developed for the removal of phosphate and arsenic from aqueous systems. Reproduced from ref. 18 with permission from Elsevier, Copyright 2019 (A). Reproduced from ref. 19 with permission from Elsevier, Copyright 2020 (B). Reproduced from ref. 20 with permission from Elsevier, Copyright 2019 (C). Reproduced from ref. 21 with permission from Elsevier, Copyright 2017 (D).

1.3.1.3.2. Cellulose–based bio adsorbents:

In recent years, there has been a lot of interest in using cellulose-based biomaterials (CBBs) as precursors for producing phosphate and arsenate biosorbents. These materials are abundant in reactive functional groups like –OH, allowing them to undergo several chemical transformations, such as etherification, condensation, and polymerization, which helps them become functionalized polymeric materials with improved adsorption properties. To improve the adsorption efficiency of the CBBs, surface modifications, especially cationization through metal ion loading, have been employed. Metals like Fe, Al, Mn, Zn, La, Zr, and Ce and their oxides and hydroxides introduce positively charged active sites, which

makes electrostatic attraction and complexation more likely. Fe is frequently used to remove both phosphate and arsenate, and materials modified with Zr(IV) have a particularly high affinity for phosphate, making them extremely effective and selective phosphate adsorbents.[22-27]

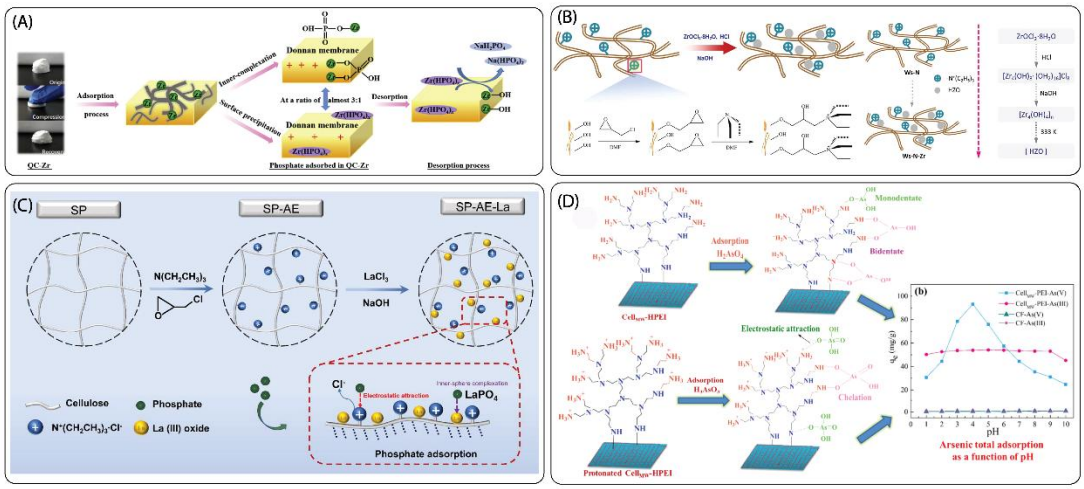

Figure 1.6. Cellulose-based adsorbents synthesized by Dong et al. (A), Qiu et al. (B), Nie et al. (C), and Chauhan et al. (D), developed for the efficient removal of phosphate and arsenic from aqueous environments. Reproduced from ref. 25 with permission from Elsevier, Copyright 2020 (A). Reproduced from ref. 26 with permission from American Chemical Society, Copyright 2015 (B). Reproduced from ref. 27 with permission from Elsevier, Copyright 2023 (C). Reproduced from ref. 24 with permission from the American Chemical Society, Copyright 2024 (D).

Despite the metal-loaded CBBs working well, their practical application is limited by metal leaching, which compromises adsorption performance and poses environmental risks. Leaching, especially lanthanum (La) and iron (Fe), reduces material stability and efficiency over repeated cycles. Cationic functionalization of CBBs using quaternary ammonium compounds has emerged as a potential approach to address metal ion leaching from metal-loaded cellulose during adsorption. Due to the low reactivity of native cellulose, cross-linking agents—particularly epichlorohydrin—are employed to enhance grafting efficiency by forming reactive cellulose ethers. Other cross-linkers have also been used, such as choline chloride derivatives, N-(3-chloro-2-hydroxypropyl) compounds, and ethylenediamine. Quaternary ammonium compounds commonly applied include poly(allylamine

hydrochloride) (PAAHCl), 3-chloro-2-hydroxypropyltrimethylammonium chloride, and triethylamine. These strategies enhance surface functionality, reduce metal leaching, and improve biosorbent performance in water treatment.[22]

1.3.1.3.3. Metal organic frameworks (MOFs):

Recently, scientists have been interested in using MOFs to remove oxoanions and other water pollutants because of their distinctive crystalline structure, large surface area, and high porosity. The adsorption of phosphate and arsenate onto the surace of the MOF-based materials is primarily governed by various mechanisms, including electrostatic interactions, ligand exchange (inner-sphere complexation), ion exchange (outer-sphere complexation), hydrogen bonding, and Lewis acid–base interactions.[28-32] Among these, especially in MOFs functionalized with amine or metal-rich sites, electrostatic attraction and ligand exchange are often the most dominant. Usually operating in synergy, these interactions help to explain the complicated and multifarious character of adsorption processes in MOFs. A thorough mechanistic understanding is necessary to guide logical material design and improve the selectivity and efficiency of MOFs to remove phosphate and arsenate in wastewater treatment. MOFs provide exceptional reusability and easy regeneration, generally accomplished by desorbing adsorbed species to regenerate active sites, thus maintaining performance across numerous operating cycles. This improves economic feasibility and minimizes waste associated with repetitive synthesis.[15, 33, 34]

Despite many advantages of MOFs over conventional adsorbents, there are still financial and environmental issues. There is a greater chance of leaching and secondary pollution because their synthesis frequently entails costly processes and hazardous materials like organic ligands and hazardous metals. Therefore, future research should prioritize the development of cost-effective, environmentally benign MOFs with enhanced selectivity and reduced affinity for non-target ions.[15, 33, 34]

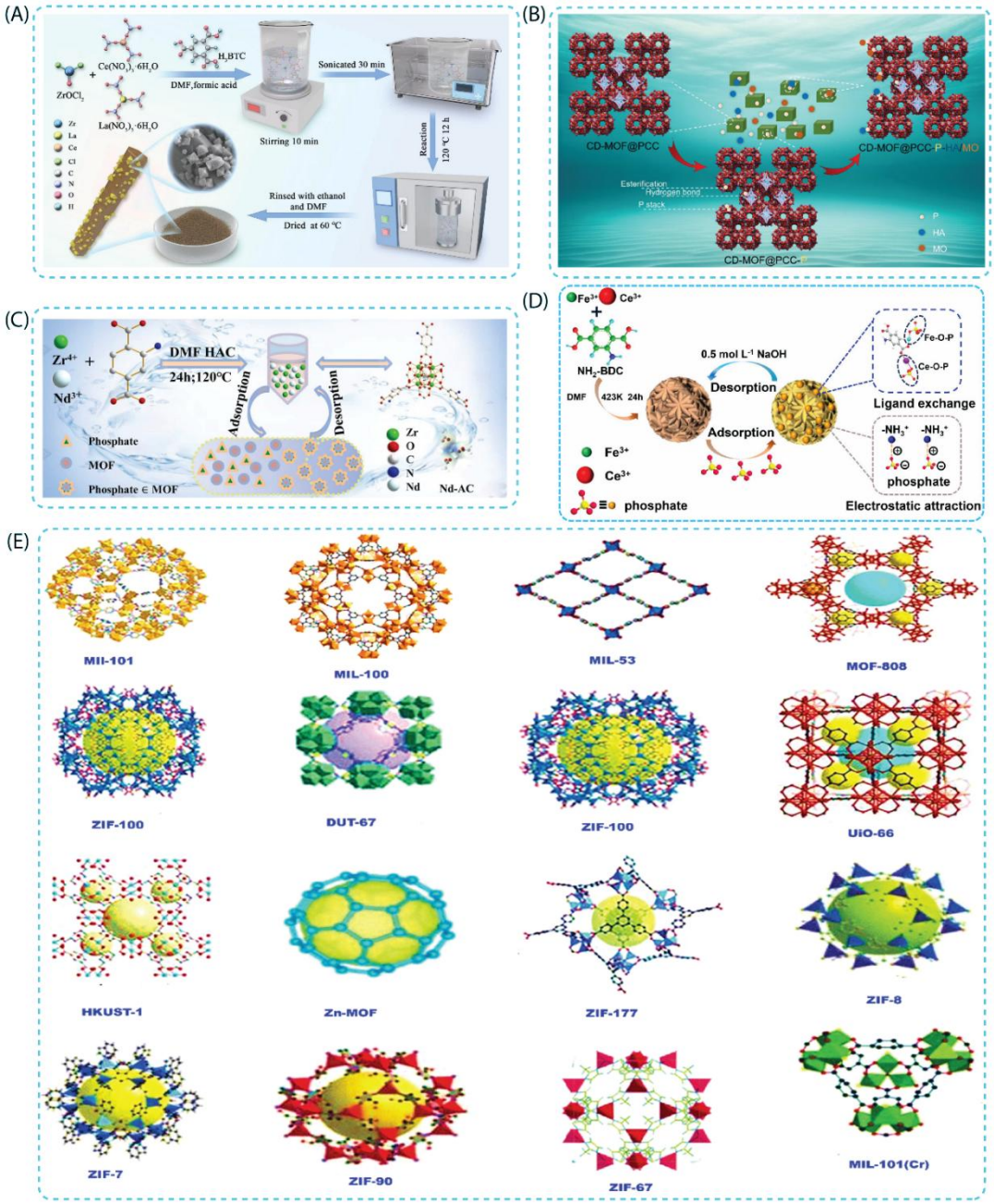

Figure 1.7. Different types of MOFs synthesized by Liu et al. (A), Quan et al. (B), Luo et al. (C), and Zhu et al. (D) for the efficient removal of phosphate and arsenic from aqueous environments. Some other reported MOFs specifically designed for arsenic removal (E). Reproduced from ref. 28 with permission from Elsevier, Copyright 2024 (A). Reproduced from ref. 29 with permission from American Chemical Society, Copyright 2024 (B). Reproduced from ref. 30 with permission from Elsevier, Copyright 2022 (C). Reproduced from ref. 31 with permission from American Chemical Society, Copyright 2024 (D). Reproduced from ref. 32 with permission from the Royal Society of Chemistry, Copyright 2025 (E).

1.3.1.3.4. Porous organic polymers (POPs):

POPs are metal-free frameworks made of light elements like C, H, O, N, and B. They have structural and physicochemical benefits over traditional porous materials. Their modular synthesis enables them to be modified before or after they undergo synthesis, which makes it possible to change their properties at the molecular level.[35-38] POPs can be either amorphous (like PAFs, HCPs, CMPs, and PIMs) or crystalline (like COFs and some CTFs), depending on their degree of long-range order.[39-46] Additionally, POPs can also be neutral or ionic (iPOPs). The latter includes cationic or anionic frameworks with a lot of ionic sites, which makes it possible to change the strength of the electrostatic interactions to improve sorption and separation.[47, 48] The following section discusses the roles of crystalline and amorphous POPs in oxoanion remediation from water.

1.3.1.3.4.1. Amorphous POPs:

As we talked about before, the unique physicochemical properties of POPs make them magnificent sorbent materials for treating wastewater, especially when it comes to removing different types of pollutants, such as oxoanions. Ion-exchange-based POPs adsorption has received a lot of attention as a good way to remove up oxoanions. In particular, iPOPs, especially those with cationic properties, have shown better performance because of the strong electrostatic interactions between the negatively charged oxoanions and the positively charged polymer frameworks.[47, 49]

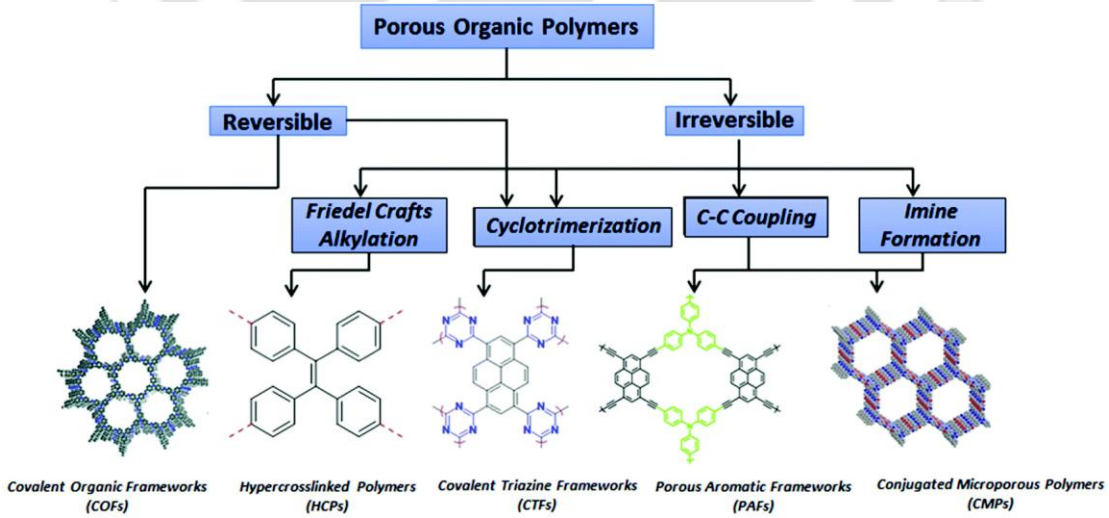

Figure 1.8. Classification of porous organic polymer (POP) frameworks and corresponding linkage-forming reactions. Reproduced from ref. 32 with permission from the Royal Society of Chemistry, Copyright 2025.

A prominent subclass of iPOPs includes imidazolium-functionalized cationic POPs, which have been extensively developed to efficiently capture oxoanions such as $Cr_2O_7^{2-}$, TcO_4^-, and ReO_4^-. Over a broad pH range, these imidazolium-based frameworks show extremely fast uptake kinetics. They maintain their adsorption efficiency under harsh chemical conditions, including prolonged exposure to 12 M HCl and 2 M NaOH.[50] These materials retain high performance over multiple adsorption–desorption cycles and show robustness in dynamic column operations, underscoring their applicability in practical wastewater treatment systems.[47, 49]

Aside from imidazolium groups, other types of cationic groups, like quaternary ammonium and viologen-based groups, have also been successfully incorporated into POP structures. These variants have shown an effective affinity, a significant ability for the removal of oxoanions with fast adsorption kinetics. These results show the versatility of cationic functionalities in tailoring POPs for oxoanion removal and suggest that quaternary ammonium- and viologen-functionalized POPs represent promising alternatives to imidazolium-based systems for efficient and sustainable oxoanion remediation.[51, 52]

1.3.1.3.4.2. Crystalline POPs:

Covalent Organic Frameworks (COFs) are a unique type of crystalline, porous polymer first introduced by Omar M. Yaghi and his research team in 2005.[40] These frameworks are interconnected by strong covalent bonds, allowing them to form large, well-organized networks in either two or three dimensions.[53, 54] The resultant structures demonstrate significant periodicity, inherent porosity, and elevated surface area. Due to these notable properties, COFs exhibit considerable potential for a range of applications, especially in the domains of wastewater treatment and environmental remediation. One of the characteristics that distinguishes COFs is their remarkable chemical and structural stability. In the context of wastewater treatment, the stability of the system is essential for providing extended operational lifetimes and consistent performance outcomes. Because of this degree of structural accuracy, COFs can identify and capture particular target molecules or ions based on their size, shape, or compatibility with functional groups. Such characteristics are especially helpful for attaining high separation efficiency and target specificity in

aqueous systems with a complex mixture of contaminants. Another important advantage of COFs is their synthetic modularity and tunability.[55]

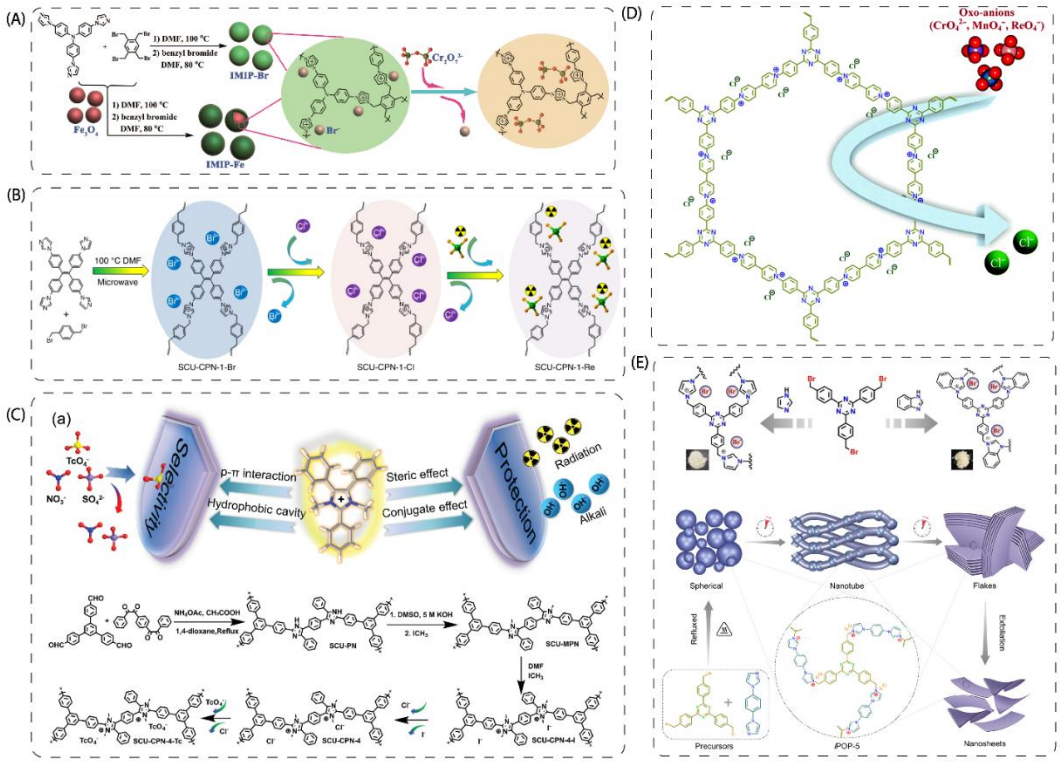

Figure 1.9. Different types of POPs reported by Sun et al. (A), Li et al. (2018) (B), Li et al. (2021) (C), Samanta et al. (D), and Mandal et al. (E), developed for the removal of various oxoanions from aqueous systems. Reproduced from ref. 35 with permission from the Royal Society of Chemistry, Copyright 2022.

The purposeful choice and alteration of organic monomeric units made possible by COF design enables customization of the framework topology, surface chemistry, and pore size.[56] Unlike MOFs, COFs are metal-free, eliminating metal ion leaching and enhancing their environmental compatibility and biocompatibility for safe water purification and reuse.[8] Moreover, the internal pore surfaces of COFs can be modified to possess hydrophobic characteristics. Using this feature allows one to improve the binding affinity for weakly hydrated anionic species. In water, metal oxoanions are usually surrounded by hydration shells that prevent them from binding easily to standard hydrophilic adsorbents. However, the hydrophobic nature of COF pores can help strip away these water shells, making it easier to capture the anions – either through hydrophobic interactions or specific anion-π binding

mechanisms.[8, 57, 58] Although COFs have great potential to remove harmful oxoanions, including phosphate, arsenate, chromate, molybdate, perrhenate, etc., their use is still understudied. These anions provide considerable challenges for selective adsorption

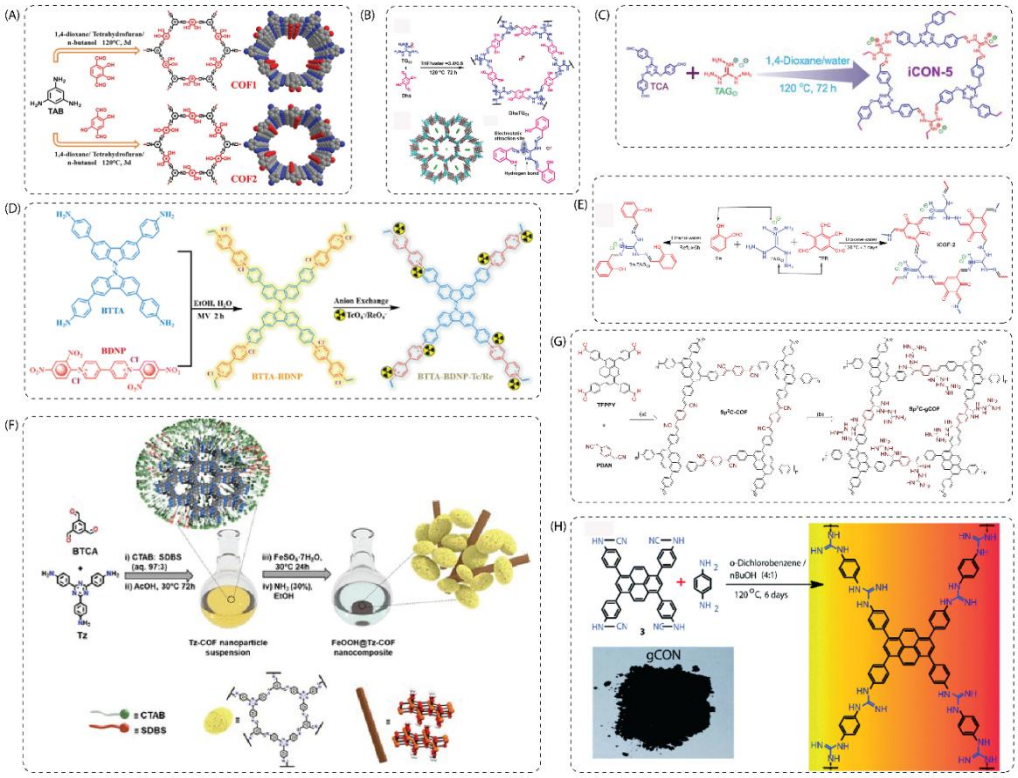

Figure 1.10. Different types of covalent organic frameworks (COFs) reported by Zhu et al. (A), Da et al. (B), Chandra et al. (C), Chen et al. (D), Hassan et al. (E), Guillem-Navajas et al. (F), Manna et al. (2023) (G), and Manna et al. (2022) (H), developed for the removal and recovery of various environmentally relevant oxoanions from aqueous systems. Reproduced from ref. 59 with permission from Elsevier, Copyright 2020 (A). Reproduced from ref. 60 with permission from Elsevier, Copyright 2019 (B). Reproduced from ref. 61 with permission from the American Chemical Society, Copyright 2022 (C). Reproduced from ref. 62 with permission from the Royal Society of Chemistry, Copyright 2023 (D). Reproduced from ref. 63 with permission from the Royal Society of Chemistry, Copyright 2023 (E). Reproduced from ref. 64 with permission from the American Chemical Society, 2022 (F). Reproduced from ref. 9 with permission from the Royal Society of Chemistry, Copyright 2023 (G). Reproduced from ref. 6 with permission from the Royal Society of Chemistry, Copyright 2022 (H).

since they usually have high hydration energies, diffuse charge densities, and complex speciation behaviour. Recent research, however, indicates that strategically functionalizing COFs – adding cationic sites, hydrogen-bonding moieties, or electron-deficient π-systems – can improve oxoanion binding efficiency. Recent research has focused on improving the ability of COFs to adsorb and recover toxic oxoanions from water more efficiently.[59-64] By modifying COFs either during synthesis or afterward, scientists can introduce ionic functional groups into the frameworks – greatly boosting their capacity to capture oxoanions. Overall, a lot of progress has been made in designing COFs that can efficiently capture Tc(VII), Re(VII), and Cr(VI) oxoanions. However, there are still relatively limited studies that focus on phosphate and arsenate sequestration, highlighting an important direction for future research.[8, 58, 65]

1.3.2. Chemical precipitation –

Chemical precipitation is a commonly implemented method in water treatment to eliminate dissolved hazardous substances, including heavy metals, metalloids, and oxoanionic contaminants. The technique functions by inducing the transformation of soluble ionic pollutants into poorly soluble or insoluble solid phases. This is accomplished by careful pH, other chemical parameter adjustments, and controlled counter-ion addition. The consequent drop in solubility helps to efficiently separate these pollutants from the liquid phase. Chemical precipitation typically follows a four-step basic process. To promote the formation of low-solubility compounds, particular precipitating agents are first added to the solution along with a pH adjustment. This is followed by a flocculation phase, during which the fine precipitate particles undergo aggregation to form larger, more easily separable flocs. After that, during the sedimentation step, these aggregates of solids settle down to the bottom of the treatment system. The last step is to separate the solid and liquid phases, which is usually done with methods like filtration, decantation, or flotation to yield a purified aqueous effluent. Common chemical precipitants in water treatment include metal salts such as $FeCl_3$, $Al_2(SO_4)_3$, $MgCl_2$, and $Ca(OH)_2$. These reagents react with dissolved pollutants – e.g., Pb^{2+}, Cd^{2+}, AsO_4^{3-}, PO_4^{3-}, and F^-, to form insoluble precipitates.[11, 14, 46]

Despite being economical and effective, chemical precipitation poses environmental and operational challenges. It generates a lot of sludges, which needs to be disposed of carefully to avoid secondary contamination. The right dosage of reagents is essential because variations could reduce efficiency and increase costs. Its performance is also quite sensitive to pH, temperature, and ionic strength; deviations cause incomplete pollutant removal. These constraints need process optimization and integration with complementary treatments to improve reliability and sustainability in water and wastewater treatment.[14, 66]

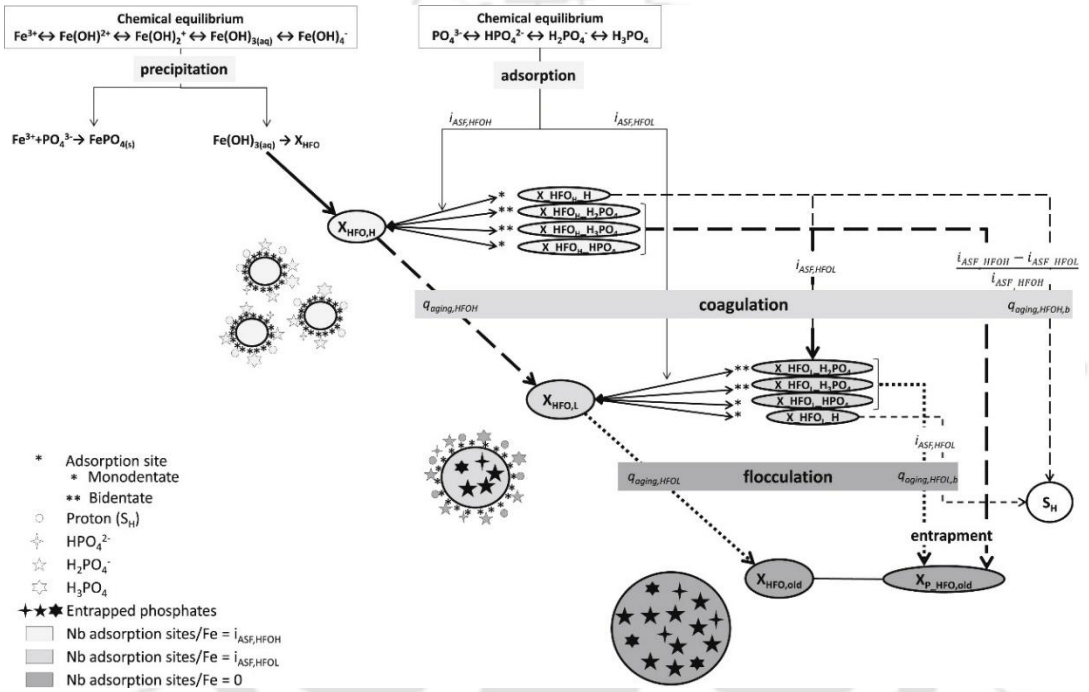

Figure 1.11. Schematic representation of phosphate removal through the chemical precipitation method. Reproduced from ref. 66 with permission from Elsevier, Copyright 2015.

1.3.3. Membrane filtration –

The tunable surface properties and high separation efficiency have also allowed membrane-based technologies to gain importance for the removal of phosphate and arsenate ions. Engineered membranes with defined pore size, selective permeability, and chemical stability enable targeted contaminant rejection based on molecular size and charge. To work well in water treatment systems, a membrane needs to have high flux, be mechanically strong, and resist chemical breakdown. One of the best things about membrane processes is that they

concentrate pollutants into small waste streams, making them easier to manage and possibly recover. Membranes also naturally reject microbes without the need for chemical additives. Microfiltration (MF), ultrafiltration (UF), nanofiltration (NF), and reverse osmosis (RO) are the main types of membrane processes. MF and UF get rid of suspended solids and pathogens, while NF and RO are suitable for the removal of dissolved ions like phosphate and arsenate. RO is better at getting rid of trace contaminants, but it needs a lot of energy and high pressure to work. Forward osmosis (FO) is a low-energy option that causes less fouling, but standard FO membranes may not meet strict regulatory standards. To get around these problems, advanced composite membranes with stronger surface charges and electrostatic properties have been made. These membranes are better at rejecting oxoanions, resisting fouling, and working reliably over time. These advancements position membrane technologies as a promising solution for complex water purification challenges.[11, 67-69]

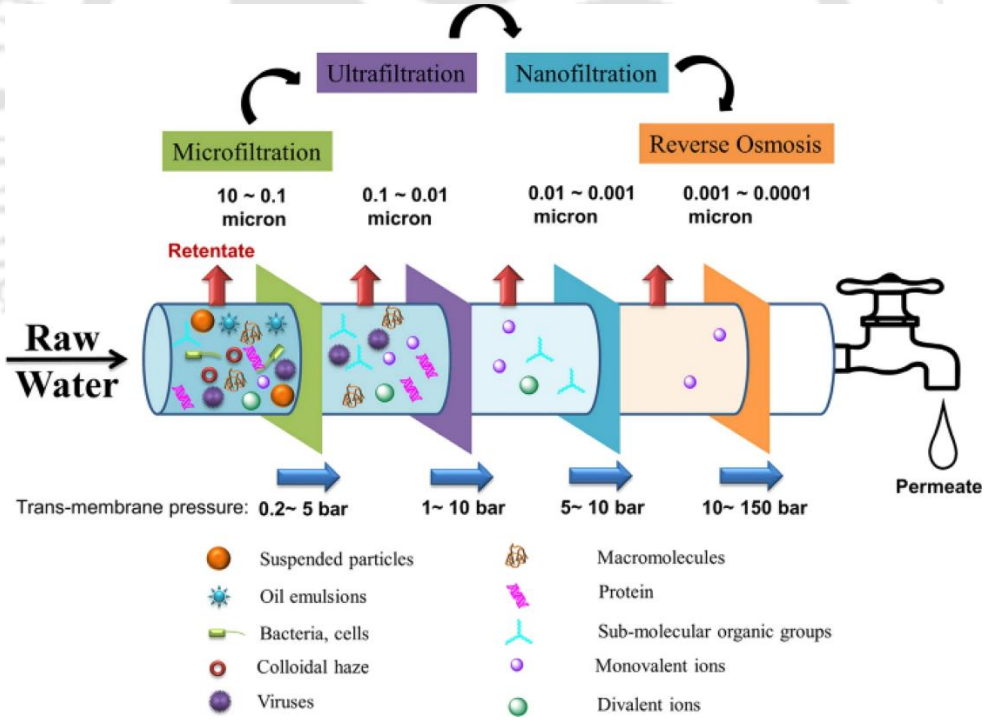

Figure 1.12. Schematic illustration of a membrane-based water treatment system. Reproduced from ref. 69 with permission from Royal Society of Chemistry, Copyright 2018.

1.3.4. Electrocoagulation method –

Electrocoagulation (EC) is an advanced water and wastewater treatment technology that removes phosphate, arsenate, and other contaminants by generating coagulant agents in situ through the electrochemical dissolution of sacrificial metal anodes, typically aluminium (Al) or iron (Fe). When electric current passes through these electrodes, metal cations (Al^{3+} or Fe^{2+}/Fe^{3+}) are released into the water. These cations hydrolyse to form metal hydroxides, which act as coagulants, destabilizing and aggregating phosphate, arsenate ions, and other contaminants into flocs that can be separated from the treated water via adsorption, precipitation, and flocculation.[11, 46, 70-72]

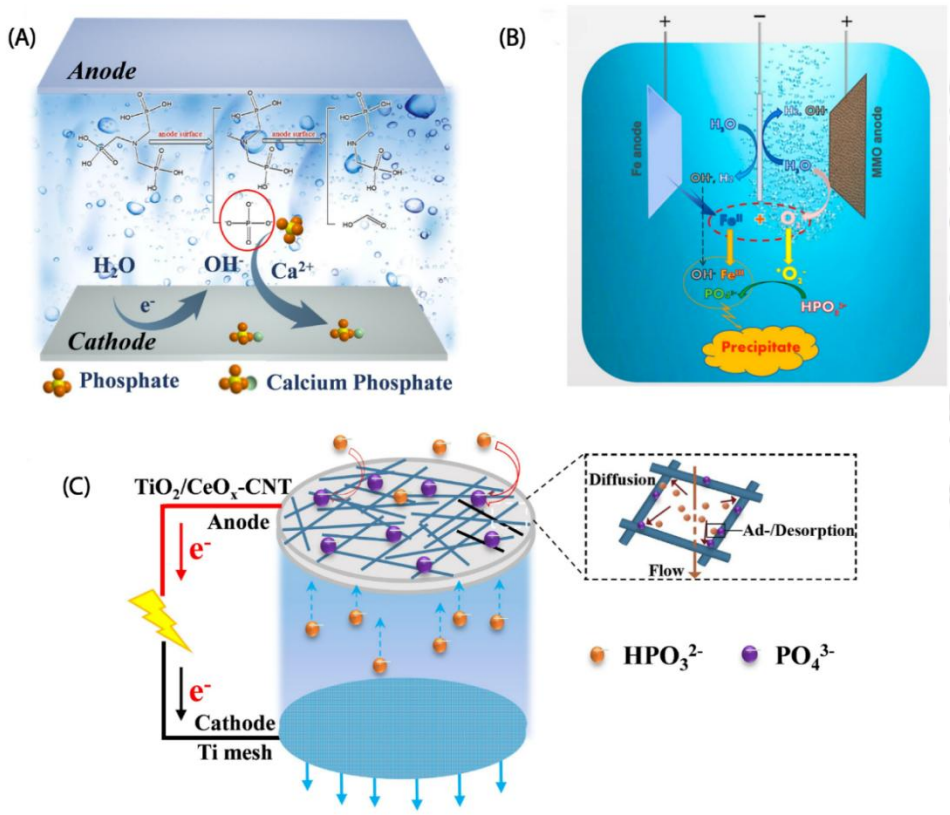

Figure 1.13. Electrochemically mediated calcium phosphate precipitation for phosphorus recovery from phosphonate-containing solutions(A), schematic representation of phosphate removal via an integrated electro-oxidation/electro-coagulation system (B), and one-step phosphite removal using an electroactive carbon nanotube (CNT) filter functionalized with TiO_2/CeO_x nanocomposites (C). Reproduced from ref. 71 with permission from Elsevier, Copyright 2009.

1.3.5. Biological method –

Phosphate removal from wastewater via microbial processes occurs through biological assimilation and indirect precipitation, primarily facilitated by enhanced biological phosphorus removal (EBPR) and microbial iron oxidation. EBPR, commonly employed in activated sludge and biological nutrient removal (BNR) systems, relies on polyphosphate-accumulating organisms (PAOs) that absorb and store phosphate as intracellular polyphosphate. In the anaerobic phase, PAOs uptake volatile fatty acids (VFAs), converting them into poly-β-hydroxyalkanoates (PHAs) using energy from polyphosphate hydrolysis and glycogen degradation. During the aerobic phase, PHAs are metabolized for phosphate uptake, polyphosphate synthesis, and cell growth. An anaerobic–anoxic variation using denitrifying PAOs (DPAOs) enables simultaneous phosphate and nitrogen removal using nitrate or nitrite as electron acceptors, reducing aeration and external carbon demands. These strategies enhance energy efficiency and cost-effectiveness, supporting integrated nutrient removal in engineered treatment systems.[73, 74]

Parallel to biological assimilation, phosphate can be removed via indirect microbial precipitation facilitated by iron oxidation. Lithotrophic iron-oxidizing bacteria, such as *Gallionella ferruginea* and *Leptothrix ochracea*, catalyze the oxidation of ferrous iron (Fe^{2+}) to ferric iron (Fe^{3+}), which subsequently reacts abiotically with phosphate to form insoluble ferric phosphate ($FePO_4$). This biogeochemical pathway provides a chemical-free approach for phosphate immobilization in iron-rich wastewater systems.[75] A similar mechanism has been proposed for arsenic removal, wherein microbial oxidation of Fe^{2+} to Fe^{3+} is followed by the precipitation and accumulation of Fe(III) oxides. These ferric oxides serve as effective adsorbents for arsenate (As(V)), thereby facilitating the removal of arsenic from solution.[74, 76]

However, while EBPR employs polyphosphate-accumulating organisms (PAOs) to remove phosphate by intracellular polyphosphate storage under alternating anaerobic and aerobic conditions, its efficiency is often compromised by competition from glycogen-accumulating organisms (GAOs), which consume VFAs without contributing to phosphorus removal. Various environmental conditions, such as low pH, high temperatures, imbalanced carbon-to-phosphorus ratios, and

low dissolved oxygen levels, promote GAO proliferation. It is vital to precisely control these parameters to maintain PAO activity. It was observed that the lack of pure PAO cultures hinders comprehensive metabolic and genomic analyses. While dependence on mixed microbial communities complicates functional understanding and targeted process optimization. Moreover, EBPR produces sludge with excess polyphosphates, posing environmental hazards and requiring expensive treatment and disposal. However, the operational complexities in small facilities and inconsistent performance due to environmental sensitivity further limit its large-scale application. Recent inclusion of innovations such as return activated sludge fermentation (S2EBPR) shows promise in enhancing the performace of EBPR by enriching adaptive PAOs and increasing VFA availability. In parallel, while environmentally friendly, biological arsenite [As(III)] oxidation is limited by slow kinetics and high sensitivity to pH, temperature, oxygen, and nutrient levels. Additional challenges include maintaining stable arsenite-oxidizing bacterial (AsOB) communities, microbial toxicity at elevated arsenic concentrations, and operational issues such as biofilm clogging. Incomplete oxidation of As(III) can hinder future adsorption of As(V), frequently requiring iron supplementation, which elevates sludge generation and further constrains the practicality of large-scale implementation.[77, 78]

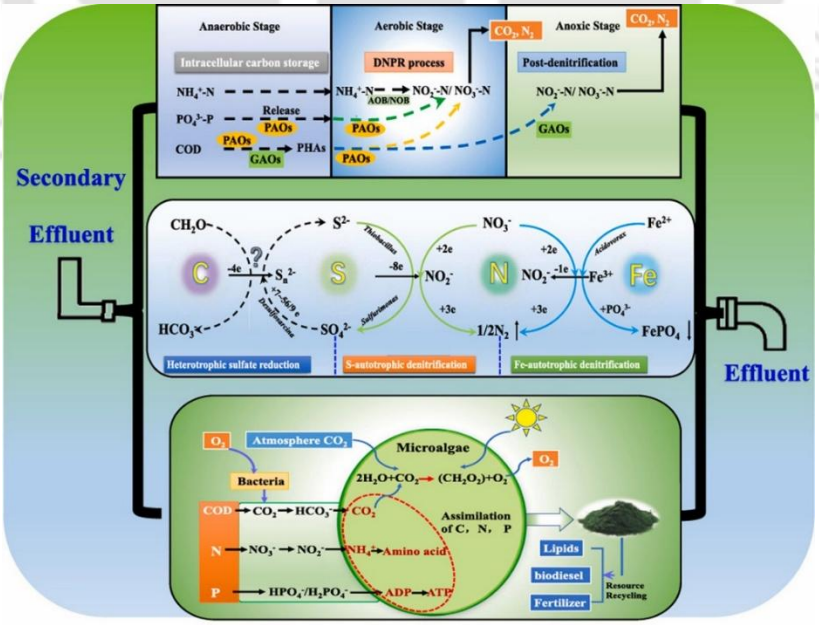

Figure 1.14. Diagrammatic illustration of phosphate removal through biological methods. Reproduced from ref. 73 with permission from Elsevier, Copyright 2007.

1.4. Comparative advantages of adsorption in oxyanion remediation

Among various physicochemical methods for wastewater treatment, adsorption is one of the most effective, selective, and long-lasting ways to remove trace-level oxyanions like phosphate (PO_4^{3-}) and arsenate (AsO_4^{3-}) from wastewater, which are usually found in natural and impacted water bodies in the microgram to milligram per litter range. Conventional techniques, including chemical precipitation, biological remediation, or membrane filtration, find them difficult to remove because of their low abundance and excellent solubility. In this regard, adsorption stands out because of its remarkable removal efficiency even at ultra-trace levels, so ensuring compliance with strict environmental and public health guidelines such as those defined by the World Health Organization (WHO) or the United States Environmental Protection Agency (USEPA).[6]

The fundamental principle behind adsorption is that phosphate and arsenate ions move from the water phase to the surface of a solid-phase adsorbent. This happens because of physicochemical interactions such as electrostatic attraction, hydrogen bonding, surface complexation, and ligand exchange mechanisms. Both batch and continuous-flow systems offer rapid kinetics, operational simplicity, and low energy and chemical requirements. Unlike membrane processes prone to fouling or precipitation methods that generate sludge, adsorption is economically and operationally advantageous, particularly for decentralized applications. A wide range of adsorbent materials – from naturally occurring minerals, biochar, and industrial by-products to synthetically engineered materials – supports its adaptability across diverse treatment contexts.[14]

The reusability of the adsorbents further improves the economic viability and environmental sustainability of the adsorption process. Many adsorbents can be reactivated by changing the pH or ionic exchange, which lowers the need for material replacement and secondary waste. One of the major advantages of adsorption is its selectivity. Advanced adsorbents can be specially functionalized with metal ions or organic ligands that allow them to selectively capture targeted oxyanions, even when other similar ions are present in the water. This targeted removal is made possible by strong chemical interactions – such as inner-sphere complexation, Lewis acid-

base reactions, and redox processes – which are especially important when dealing with contaminants like arsenic.

Adsorption is more resistant to changing water chemistries and shock conditions than other treatment methods. Biological and membrane systems are often sensitive to changes in pH, temperature, or the contaminant load in the water. However, adsorption works well in a wide range of operating conditions and water matrices. Its minimal by-product formation and compatibility with circular treatment approaches further support its environmental advantages.

Advances in material science have made it possible to develop the next generation of adsorbents, such as POPs, COFs, MOFs, and engineered nanomaterials. These materials have large surface areas, adjustable pore structures, and custom functional groups that make them better at capturing oxoanions. These new technologies make it possible for adsorption to handle more complicated treatment situations with better capacity, selectivity, and renderability. Therefore, adsorption is a perfect candidate for the remediation of phosphate and arsenate in aqueous systems since it provides a special mix of high removal efficiency, operational flexibility, cost-effectiveness, environmental sustainability, and tuned selectivity. Adsorption is likely to remain at the forefront of advanced water purification technologies as long as adsorbent design and process integration are constantly innovatively developed.

1.5. Comparative superiority of cellulose-based bio-adsorbents and COFs over conventional adsorbents

Cellulose is the most prevalent biopolymer on the earth, derived from plant biomass, agricultural waste, and industrial waste, and is therefore considered an economical and environmentally friendly precursor to prepare wastewater treatment material. Unlike less abundant and more costly biopolymers such as chitosan and alginate – limited by seasonal and regional availability – cellulose offers a continuous, large-scale supply suitable for scalable applications. Its linear polysaccharide structure with abundant reactive hydroxyl groups enables extensive chemical functionalization with multivalent metal ions (e.g., Fe^{3+}, La^{3+}, Zr^{4+}), enhancing its affinity and selectivity for phosphate via mechanisms such as electrostatic attraction, ligand exchange, and surface complexation. In contrast, other

biopolymers like lignin and starch lack comparable tunability, and chitosan suffers from reduced stability and performance under neutral to alkaline conditions. Although the surface area and porosity of raw cellulose are moderate, these characteristics can be greatly improved by processes like carbonization, hydrolysis, and nanostructuring, producing advanced materials like biochars, cellulose aerogels, and nanocellulose. These modifications improve ion diffusion and adsorption efficiency while offering superior mechanical stability and durability – particularly important in continuous-flow and multi-cycle systems. Chitosan- or alginate-based materials often have inadequate structural integrity and exhibit excessive swelling. In contrast, modified cellulose-based adsorbents keep working well even when conditions change. Functionalized cellulose materials exhibit strong phosphate binding through inner-sphere complexation with metal ions, maintaining high selectivity even in competing anions and across a broad pH range. Additionally, they exhibit outstanding mechanical and chemical stability as well as high reusability across several cycles of adsorption and desorption with mild regenerants. On the other hand, a lot of natural adsorbents, such as lignin-based materials, alginate, and chitosan, degrade or lose their effectiveness upon reuse. Economically and environmentally, cellulose-based adsorbents are compatible with green processing techniques, biodegradable, and non-toxic. Cellulose provides a more sustainable and financially feasible substitute than synthetic polymers or activated carbons, which sometimes demand energy-intensive manufacturing involving hazardous chemicals. Matching with sustainability and the circular economy, its abundance, structural adaptability, high adsorption capacity, and long-term stability position modified cellulose as a leading material for phosphate elimination in wastewater treatment.

On the other hand, within the spectrum of chemically synthesized adsorbents, COFs have recently attracted considerable interest as advanced materials for effectively eliminating environmentally significant oxyanions from water systems. Their outstanding performance exceeds that of conventional materials like MOFs, metal hydroxide nanoparticles, and amorphous POPs, mainly because of their crystalline structure, chemical tunability, and enhanced physicochemical stability. The advantages of COFs are very attractive for purifying water, particularly in harsh environmental settings where traditional adsorbents are often ineffective.[79] Their

crystalline and well-organized structure is one of the primary characteristics. Synthesis of these frameworks occurs via reversible, thermodynamically controlled polymerization reactions. The dynamic covalent bonding enables the creation of extensive frameworks and promotes self-correction throughout the synthesis process, resulting in long-range order and consistent structure. Such precision in molecular assembly enables the design of well-defined 1D channels and 2D layered structures that the selection of appropriate monomeric building blocks can tailor.

The final topological result of the COF is determined by the geometry and symmetry of these monomers, which are typically categorized as Cn units (where n is the number of symmetrical reactive groups).[56] Hexagonal, tetragonal, trigonal, rhombohedral, and dual-pore kagome structures are among the various polygonal skeletons that can be created by adjusting the geometry of these units. This level of control extends to dimensionality as well, allowing the formation of either 2D or three-dimensional (3D) COFs. In 2D frameworks, planar layers are covalently bonded and stacked through π–π interactions, forming uniform and tunable 1D channels. Conversely, 3D COFs synthesized from tetrahedral sp^3-hybridized carbon or silane-based linkers show even more specific surface areas and connected pore networks, improving their sorption capacity and enabling effective mass transport. Increased adsorption kinetics and efficiency result from the high degree of structural regularity and porosity, facilitating uniform exposure of functional adsorption sites and quick guest molecule diffusion. By contrast, amorphous POPs show heterogeneous site distribution and disordered pore structures with irregular connectivity that lower adsorption performance and slow down diffusion rates. These constraints in POPs draw attention to the significance of framework crystallinity in the structure of efficient adsorbent design.

One of the most advantageous features of COFs is their modular synthesis and functional tunability.[80] A wide range of chemically active functional groups, including triazine, bipyridine, sulfonic acid, carboxyl, guanidinium, imidazolium, quaternary ammonium moieties, etc., can be either directly incorporated into the framework during polymerization or introduced via post-synthetic modifications. These functional groups have strong and selective interactions with oxyanions through hydrogen bonding, electrostatic attraction, ion exchange, and coordination

interactions.[81] This flexibility makes it possible to customize COFs for specific oxyanions, which is not easy to accomplish with MOFs because the limitations of metal-ligand chemistry make functionalization difficult. While metal hydroxide nanoparticles also have strong chemical activity, they are often limited by their lack of functional diversity on their surfaces and their tendency to aggregate in water, which greatly reduces their effective surface area and ability for adsorption. Despite having a variety of structural types, MOFs are usually hindered by poor hydrolytic stability because of metal ion leaching or coordination network breakdown in basic or acidic environments. On the other hand, COFs exhibit remarkable resilience in a range of environmental circumstances.

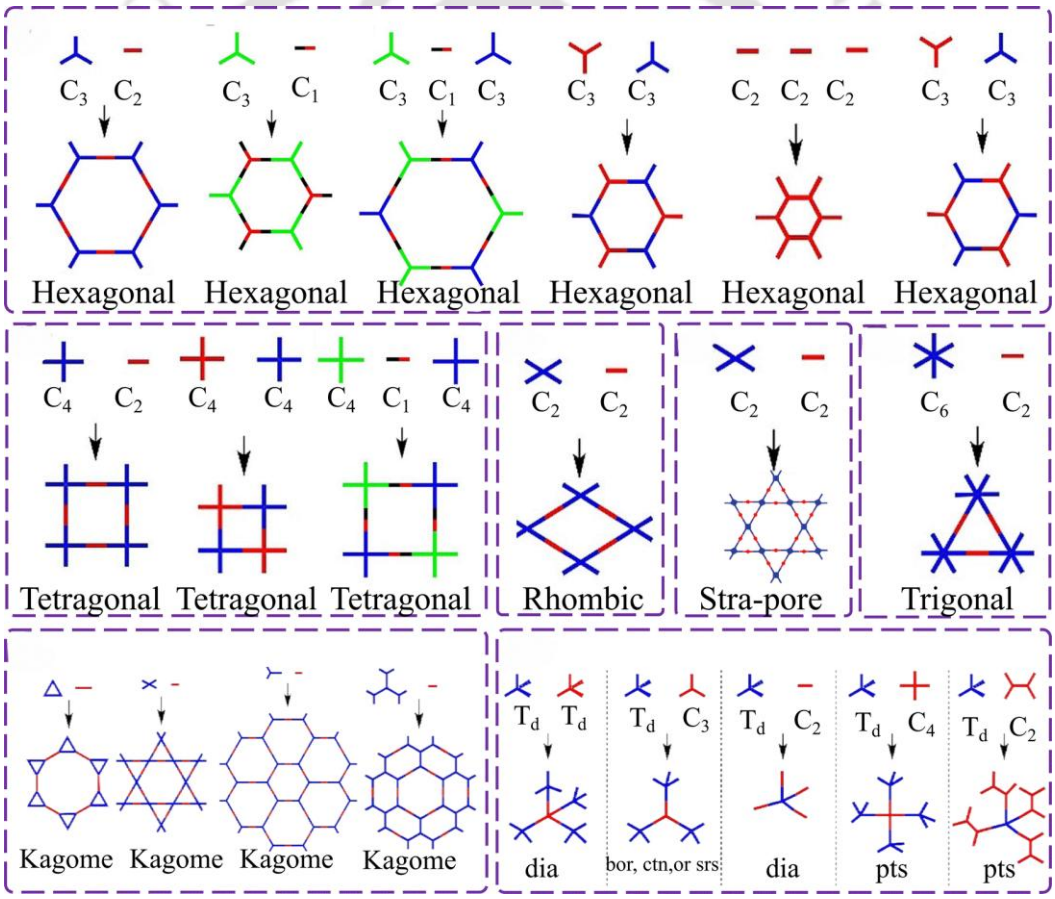

Figure 1.15. Structural representations of different COF topologies, including hexagonal, tetragonal, rhombic, star-shaped pore, trigonal, Kagome, and three-dimensional COFs, demonstrating the wide variety of pore structures and network architectures. Reproduced from ref. 56 with permission from the Royal Society of Chemistry, 2024.

The strong covalent bonds in COFs' frameworks make them very stable and resistant to chemical, thermal, and hydrolytic breakdown.[82] They remain stable across a broad pH range, in saline solutions, and in the presence of oxidants, conditions commonly encountered in real wastewater systems. This makes COFs highly suitable for practical applications in water treatment, especially when compared to MOFs and POPs, which often degrade or lose performance after multiple usage cycles.

From a performance point of view, COFs have shown that they can quickly and effectively adsorb a wide range of hazardous oxyanions, such as phosphate, nitrate, chromate, arsenate, and selenate. The primary causes for these properties are their large specific surface areas, functional groups that are easy to reach, and well-ordered channels that help intraparticle diffusion. Also, the development of COF-based hybrid materials, like COF–metal oxide composites and ionic COFs, has shown that performance metrics can be improved even more through synergistic effects, such as better redox activity and electronic conductivity. Furthermore, several hybrid systems show remarkable structural integrity over adsorption–desorption cycles and great regeneration capacity. For sustainable environmental uses, COFs' recyclability is crucial since it reduces secondary pollution from material breakdown or leaching and running costs. These systems have shown minimal capacity loss over repeated use, further solidifying their potential as practical materials for water purification.

The integrated advantages of COFs, including well-defined porosity, extensive chemical functionalization, and high thermal and chemical stability, make them a highly promising material platform for removing oxyanions from aqueous media. They successfully get around important drawbacks of other adsorbent classes, like the hydrolytic instability of MOFs, the inadequate structural definition of POPs, and issues associated with metal hydroxide surface aggregation. As a result, COFs are poised to play a central role in advancing next-generation water treatment technologies and broader environmental remediation efforts.

1.6. Research gap

Despite growing interest in sustainable materials for environmental remediation, notable research gaps remain in applying cellulose-based biomaterials

for phosphate removal and recovery from wastewater. When compared to conventional commercial or chemically engineered adsorbents, cellulose-derived adsorbents have several limitations that restrict their practical use, despite their low cost and environmental friendliness. Low adsorption capacities, slow kinetics, restricted pH operating ranges, and subpar regeneration performance are some of these disadvantages. In order to overcome these problems, researchers have investigated incorporating metal hydroxides and oxides into cellulose matrices, which increases the efficiency of phosphate adsorption. However, these modifications often lead to metal leaching during adsorption or regeneration cycles, which increases stability and environmental concerns. Also, a lot of modified cellulose materials are unstable when they are in acidic or basic conditions, which makes them less useful for treating wastewater. Recent studies demonstrate that carefully modifying cellulose with appropriate chemical groups can significantly improve its adsorption efficiency, making it competitive with synthetic substitutes.

At the same time, a group of porous crystalline materials known as COFs has shown a lot of promise in removing potentially hazardous tetrahedral oxoanions from water systems and recovering them. COFs have demonstrated superior performance in capturing high-valent transition-metal oxoanions such as Tc(VII), Re(VII), and Cr(VI) from groundwater and industrial effluents. However, the application of COFs for the selective removal of non-metal or metalloid-based oxoanions, particularly phosphate and arsenate, remains underexplored. Because of the urgent problem of eutrophication caused by excessive levels of phosphate in water, especially in regions with intensive agriculture, high population densities, and inadequate wastewater infrastructure, developing efficient COF-based adsorbents for phosphate management is timely and critical.

Only a few studies have indicated that COFs can be used to remove phosphates, even though they have a lot of potential. Manna and his coworkers have shown that a guanidine-functionalized COF (gCON) can selectively adsorb phosphate, highlighting the viability of such materials. However, broader and more systematic studies are warranted to design next-generation COFs with enhanced selectivity, capacity, and stability for phosphate remediation.

On the other hand, methods for removing arsenate that use COFs are relatively well-documented. In order to enhance arsenate capture, the post-synthesis addition of metal hydroxides or oxides, particularly those based on iron, into the COF frameworks. Despite their efficacy, these hybrid materials are vulnerable to secondary contamination due to metal ion leaching. Jansone-Popova and colleagues have developed guanidinium-functionalized COFs (iCONs) aimed at facilitating metal-free arsenate adsorption. Still, these materials often have low adsorption capacities and slow kinetics, which shows that more research is needed on metal-free COFs that have better performance metrics.

Overall, cellulose-based materials and COFs provide eco-friendly platforms for oxoanion remediation, and there are plenty of chances to improve their functionality and suitability, especially when it comes to phosphate recovery and arsenate detoxification from water systems. Advancing this field requires the development of robust, recyclable, and high-affinity adsorbents, free from the drawbacks of metal leaching and pH instability.

1.7. Thesis Overview

Based on the literature review and knowledge gap, this thesis focuses on designing, synthesising, and applying polymeric adsorbents to efficiently remove and recover environmentally hazardous oxoanions, specifically phosphate and arsenate, from water. The research primarily concentrates on developing biopolymer composites and covalent organic networks. These materials are tailored to exhibit high selectivity, recyclability, and adsorption capacity under environmentally relevant conditions.

Chapter 1 provides an in-depth analysis of the present literature on polymeric adsorbents for oxoanion remediation, especially phosphate and arsenic, emphasizing their structural properties and basic adsorption mechanisms. This chapter starts with the basis by pointing out the need for better materials and the limits of current systems.

Chapter 2 presents the development of a Zn(II)-coordinated, 1-aminoguanidine-functionalized cellulose biopolymer (Zn-gCP) with efficient phosphate removal and recovery. Guanidinium groups enabled aqueous exfoliation

and imparted broad-spectrum antibacterial activity. The study offers a sustainable route for dual-functional, reusable biopolymer adsorbents.

Chapter 3 describes the synthesis of a pH-responsive 2D covalent organic network (2D ag-CON) incorporating tris-aminoguanidine units. The material enabled rapid, selective phosphate capture and release via pH modulation. Phosphate adsorption induced a morphological shift from spherical to sheet-like structures, serving as a distinguishing feature of ag-CON.

Chapter 4 demonstrates the development of bis-imidazolium-based covalent organic network (IC-CON) for selective removal of arsenate and phosphate ions. IC-CON exhibits higher affinity for arsenate, making it suitable for arsenate extraction from phosphate-rich environments.

Chapter 5 outlines future directions for the rational design of advanced polymeric adsorbents, along with a summary of the key findings from the thesis. The chapter also highlights the importance of multifunctional polymeric materials with high efficiency, selectivity, and reusability for the sustainable management of oxoanion pollutants.

1.8. Summary

Recently, significant progress has been made in developing polymeric adsorbents and understanding their role in the efficient removal and recovery of environmentally hazardous oxoanions, specifically phosphate and arsenate, from water. Literature shows that polymeric material can still be used to tune oxoanion selectivity by adjusting the functional group and cavity size. Efficient removal and recovery of environmentally hazardous oxoanions requires a balance between a hydrophobic exterior for water insolubility and a polar oxoanion recognition motif for selective oxoanion binding. Therefore, the installation of suitable functional groups around the pores or surface of the polymers significantly influences the selective oxoanion adsorption properties. The guanidine and imidazolium are a unique class of functional groups capable of facilitating selective phosphate and arsenate adsorption in the presence of other competing anions. Suitable hydrophobic moieties allow the polymer to be easily recovered from an aqueous system. This finding has inspired the development of novel polymers with varied structures, offering potential for diverse oxoanion removal capabilities. This thesis aims to

create a collection of water-insoluble polymeric materials with high adsorption efficiencies to remove and recover oxoanions, particularly phosphate and arsenate, from contaminated water sources. The insights gained from this work contribute significantly to the advancement of next-generation adsorbents for environmental remediation and sustainable water treatment.

1.9. References

1. Pal, S. K.; Zewail, A. H., Dynamics of water in biological recognition. *Chem. Rev.* **2004,** *104* (4), 2099-2124.
2. Sponseller, R. A.; Heffernan, J. B.; Fisher, S. G., On the multiple ecological roles of water in river networks. *Ecosphere* **2013,** *4* (2), 1-14.
3. Shannon, M. A.; Bohn, P. W.; Elimelech, M.; Georgiadis, J. G.; Mariñas, B. J.; Mayes, A. M., Science and technology for water purification in the coming decades. *Nature* **2008,** *452* (7185), 301-310.
4. Falkowski, P.; Scholes, R. J.; Boyle, E.; Canadell, J.; Canfield, D.; Elser, J.; Gruber, N.; Hibbard, K.; Högberg, P.; Linder, S., The global carbon cycle: a test of our knowledge of earth as a system. *Science* **2000,** *290* (5490), 291-296.
5. Mishra, R. K., Fresh water availability and its global challenge. *bjmas* **2023,** *4* (3), 1-78.
6. Dey, S.; Das, S.; Patel, A.; Raj, K. V.; Vanka, K.; Manna, D., Antimicrobial two-dimensional covalent organic nanosheets (2D-CONs) for the fast and highly efficient capture and recovery of phosphate ions from water. *J. Mater. Chem. A* **2022,** *10* (9), 4585-4593.
7. Sun, D. T.; Peng, L.; Reeder, W. S.; Moosavi, S. M.; Tiana, D.; Britt, D. K.; Oveisi, E.; Queen, W. L., Rapid, selective heavy metal removal from water by a metal–organic framework/polydopamine composite. *ACS Cent. Sci.* **2018,** *4* (3), 349-356.
8. Zhao, L.; Liu, Q. X.; Li, C. P., Sequestration of Metal Oxoanions by Covalent Organic Frameworks. *Eur. J. Inorg. Chem.* **2025,** *28* (9), e202400639.
9. Das, S.; Hazarika, G.; Manna, D., Guanidine-functionalized fluorescent sp2 carbon-conjugated covalent organic framework for sensing and capture of Pd (II) and Cr (VI) ions. *Chem. Eur. J.* **2023,** *29* (15), e202203595.
10. Dodds, W. K.; Bouska, W. W.; Eitzmann, J. L.; Pilger, T. J.; Pitts, K. L.; Riley, A. J.; Schloesser, J. T.; Thornbrugh, D. J., Eutrophication of US freshwaters: analysis of potential economic damages. *Environ. Sci. Technol.* **2009**, 43(1) 12–19.
11. Sadee, B. A.; Zebari, S. M.; Galali, Y.; Saleem, M. F., A review on arsenic contamination in drinking water: sources, health impacts, and remediation approaches. *RSC Adv.* **2025,** *15* (4), 2684-2703.
12. Guillem-Navajas, A.; Martín-Illán, J. Á.; Salagre, E.; Michel, E. G.; Rodriguez-San-Miguel, D.; Zamora, F., Iron oxyhydroxide-covalent organic framework nanocomposite for efficient as (III) removal in water. *ACS Appl. Mater. Interfaces* **2022,** *14* (44), 50163-50170.
13. Weerasundara, L.; Ok, Y.-S.; Bundschuh, J., Selective removal of arsenic in water: A critical review. *Environ. Pollut.* **2021,** *268*, 115668.
14. Nadagouda, M. N.; Varshney, G.; Varshney, V.; Hejase, C. A., Recent Advances in Technologies for Phosphate Removal and Recovery: A Review. *ACS Environ. Au* **2024,** *4* (6), 271-291.

15. Afridi, M. N.; Adil, S.; Byambaa, B.; Sohail, M.; Bacha, A.-U.-R.; Wang, J.; Li, C., Progress, challenges, and prospects of MOF-based adsorbents for phosphate recovery from wastewater. *J. Water Process Eng.* **2024,** *63*, 105530.
16. Almanassra, I. W.; Kochkodan, V.; Mckay, G.; Atieh, M. A.; Al-Ansari, T., Review of phosphate removal from water by carbonaceous sorbents. *J. Environ. Manage.* **2021,** *287*, 112245.
17. Mohan, D.; Pittman Jr, C. U., Arsenic removal from water/wastewater using adsorbents—a critical review. *J. Hazard. Mater.* **2007,** *142* (1-2), 1-53.
18. Karthikeyan, P.; Meenakshi, S., Synthesis and characterization of Zn–Al LDHs/activated carbon composite and its adsorption properties for phosphate and nitrate ions in aqueous medium. *J. Mol. Liq.* **2019,** *296*, 111766.
19. Han, T.; Lu, X.; Sun, Y.; Jiang, J.; Yang, W.; Jönsson, P. G., Magnetic bio-activated carbon production from lignin via a streamlined process and its use in phosphate removal from aqueous solutions. *Sci. Total Environ.* **2020,** *708*, 135069.
20. Nieto-Delgado, C.; Gutiérrez-Martínez, J.; Rangel-Méndez, J. R., Modified activated carbon with interconnected fibrils of iron-oxyhydroxides using Mn2+ as morphology regulator, for a superior arsenic removal from water. *J. Environ. Sci.* **2019,** *76*, 403-414.
21. Xiong, W.; Tong, J.; Yang, Z.; Zeng, G.; Zhou, Y.; Wang, D.; Song, P.; Xu, R.; Zhang, C.; Cheng, M., Adsorption of phosphate from aqueous solution using iron-zirconium modified activated carbon nanofiber: performance and mechanism. *J. Colloid Interface Sci.* **2017,** *493*, 17-23.
22. Nguyen, T.; Ngo, H.; Guo, W.; Zhang, J.; Liang, S.; Lee, D.; Nguyen, P.; Bui, X., Modification of agricultural waste/by-products for enhanced phosphate removal and recovery: potential and obstacles. *Bioresour. Technol.* **2014,** *169*, 750-762.
23. Motloung, M. T.; Magagula, S. I.; Kaleni, A.; Sikhosana, T. S.; Lebelo, K.; Mochane, M. J., Recent advances on chemically functionalized cellulose-based materials for arsenic removal in wastewater: a review. *Water* **2023,** *15* (4), 793.
24. Chauhan, K.; Singh, P.; Sen, K.; Singhal, R. K.; Thakur, V. K., Recent Advancements in the Field of Chitosan/Cellulose-Based Nanocomposites for Maximizing Arsenic Removal from Aqueous Environment. *ACS Omega* **2024,** *9* (26), 27766-27788.
25. Dong, S.; Ji, Q.; Wang, Y.; Liu, H.; Qu, J., Enhanced phosphate removal using zirconium hydroxide encapsulated in quaternized cellulose. *J. Environ. Sci.* **2020,** *89*, 102-112.
26. Qiu, H.; Liang, C.; Zhang, X.; Chen, M.; Zhao, Y.; Tao, T.; Xu, Z.; Liu, G., Fabrication of a biomass-based hydrous zirconium oxide nanocomposite for preferable phosphate removal and recovery. *ACS Appl. Mater. Interfaces* **2015,** *7* (37), 20835-20844.
27. Nie, G.; Liu, X.; Li, X.; Meng, C.; Wang, W.; Zou, D., Efficient phosphate removal and recovery by using nanosized La (III) oxides anchored on aminated biomass waste. *Sep. Purif. Technol.* **2023,** *305*, 122513.
28. Liu, R.; Song, J.; Zhao, J.; Wang, Z.; Xu, J.; Yang, W.; Hu, J., Novel MOF (Zr)–on-MOF (Ce/La) adsorbent for efficient fluoride and phosphate removal. *Chem. Eng. J.* **2024,** *497*, 154780.
29. Quan, X.; Zhang, J., Phosphate Adsorption from Reclaimed Water via External Cage Expansion on CD-MOF Micro-Interface. *ACS EST Water* **2024,** *4* (11), 4793-4805.

30. Luo, G.; Bi, Z.; Liu, C.; Wan, Z.; Chen, Z.; Chen, M.; Huang, Z., Regenerable neodymium-doped zirconium-based MOF adsorbents for the effective removal of phosphate from water. *J. Environ. Chem. Eng.* **2022,** *10* (6), 108610.
31. Zhu, Y.; Ren, B.; Qiu, Y.; Zhou, Q.; Chang, J.; Lin, Z.; Yang, X., Nanoporous Cerium-Doped MIL-53 (Fe)-NH2 for Effective and Selective Removal of Phosphate from Wastewater. *ACS Appl. Nano Mater.* **2024,** *7* (17), 20700-20713.
32. Alam, E., Metal–organic frameworks (MOFs) for arsenic remediation: a brief overview of recent progress. *RSC Adv.* **2025,** *15* (25), 20281-20308.
33. Gao, D.; Ji, H.; Li, R.; Munir, M. T.; Wu, X.; Huang, Y.; Li, B., Advancing sustainable phosphorus removal and recovery with Metal-Organic frameworks (MOFs). *Chem. Eng. J.* **2023,** *475*, 145949.
34. Nguyen, D. A.; Nguyen, D. V.; Jeong, G.; Asghar, N.; Jang, A., Critical evaluation of hybrid metal–organic framework composites for efficient treatment of arsenic–contaminated solutions by adsorption and membrane–separation process. *Chem. Eng. J.* **2023,** *461*, 141789.
35. Kim, J. H.; Kang, D. W.; Yun, H.; Kang, M.; Singh, N.; Kim, J. S.; Hong, C. S., Post-synthetic modifications in porous organic polymers for biomedical and related applications. *Chem. Soc. Rev.* **2022,** *51* (1), 43-56.
36. Zhou, T.; Huang, X.; Ding, N.; Lin, Z.; Yao, Y.; Guo, J., Porous polyelectrolyte frameworks: synthesis, post-ionization and advanced applications. *Chem. Soc. Rev.* **2022,** *51* (1), 237-267.
37. Tan, L.; Tan, B., Hypercrosslinked porous polymer materials: design, synthesis, and applications. *Chem. Soc. Rev.* **2017,** *46* (11), 3322-3356.
38. Soliman, A. B.; Hassan, M. H.; Abugable, A. A.; Karakalos, S. G.; Alkordi, M. H., Post-Synthetic Immobilization of Ni Ions in a Porous-Organic Polymer-Graphene Composite for Non-Noble Metal Electrocatalytic Water Oxidation. *ChemCatChem* **2017,** *9* (15), 2946-2951.
39. Lee, J.-S. M.; Cooper, A. I., Advances in conjugated microporous polymers. *Chem. Rev.* **2020,** *120* (4), 2171-2214.
40. Cote, A. P.; Benin, A. I.; Ockwig, N. W.; O'Keeffe, M.; Matzger, A. J.; Yaghi, O. M., Porous, crystalline, covalent organic frameworks. *Science* **2005,** *310* (5751), 1166-1170.
41. Katekomol, P.; Roeser, J.; Bojdys, M.; Weber, J.; Thomas, A., Covalent triazine frameworks prepared from 1, 3, 5-tricyanobenzene. *Chem. Mater.* **2013,** *25* (9), 1542-1548.
42. Jiang, J.-X.; Su, F.; Trewin, A.; Wood, C. D.; Campbell, N. L.; Niu, H.; Dickinson, C.; Ganin, A. Y.; Rosseinsky, M. J.; Khimyak, Y. Z., Conjugated microporous poly (aryleneethynylene) networks. *Angew. Chem. Int. Ed.* **2007,** *119* (45), 8728-8732.
43. Xu, S.; Luo, Y.; Tan, B., Recent development of hypercrosslinked microporous organic polymers. *Macromol. Rapid Commun.* **2013,** *34* (6), 471-484.
44. Konstas, K.; Taylor, J. W.; Thornton, A. W.; Doherty, C. M.; Lim, W. X.; Bastow, T. J.; Kennedy, D. F.; Wood, C. D.; Cox, B. J.; Hill, J. M., Lithiated porous aromatic frameworks with exceptional gas storage capacity. *Angew. Chem. Int. Ed.* **2012,** *51* (27), 6639-6642.
45. Mohamed, M. G.; EL-Mahdy, A. F.; Kotp, M. G.; Kuo, S.-W., Advances in porous organic polymers: Syntheses, structures, and diverse applications. *Mater. Adv.* **2022,** *3* (2), 707-733.

46. Gomez-Suarez, M.; Chen, Y.; Zhang, J., Porous organic polymers as a promising platform for efficient capture of heavy metal pollutants in wastewater. *Polym. Chem.* **2023,** *14* (35), 4000-4032.
47. Fajal, S.; Dutta, S.; Ghosh, S. K., Porous organic polymers (POPs) for environmental remediation. *Mater. Horiz.* **2023,** *10* (10), 4083-4138.
48. Sen, A.; Dutta, S.; Dam, G. K.; Samanta, P.; Let, S.; Sharma, S.; Shirolkar, M. M.; Ghosh, S. K., Imidazolium-functionalized chemically robust ionic porous organic polymers (iPOPs) toward toxic oxo-pollutants capture from water. *Chem. Eur. J.* **2021,** *27* (53), 13442-13449.
49. Patra, K.; Pal, H., Recent advances in porous organic polymers (POPs): The emerging sorbent materials with promises towards toxic and radionuclides metal ions separations. *Mater. Today Sustain.* **2024**, *27*, 100799.
50. Sun, Q.; Zhu, L.; Aguila, B.; Thallapally, P. K.; Xu, C.; Chen, J.; Wang, S.; Rogers, D.; Ma, S., Optimizing radionuclide sequestration in anion nanotraps with record pertechnetate sorption. *Nat. Commun.* **2019,** *10* (1), 1646.
51. Banerjee, D.; Elsaidi, S. K.; Aguila, B.; Li, B.; Kim, D.; Schweiger, M. J.; Kruger, A. A.; Doonan, C. J.; Ma, S.; Thallapally, P. K., Removal of pertechnetate-related oxyanions from solution using functionalized hierarchical porous frameworks. *Chem. Eur. J.* **2016,** *22* (49), 17581-17584.
52. Samanta, P.; Chandra, P.; Dutta, S.; Desai, A. V.; Ghosh, S. K., Chemically stable ionic viologen-organic network: an efficient scavenger of toxic oxo-anions from water. *Chem. Sci.* **2018,** *9* (40), 7874-7881.
53. Zhuang, H.; Guo, C.; Huang, J.; Wang, L.; Zheng, Z.; Wang, H. N.; Chen, Y.; Lan, Y. Q., Hydrazone-Linked Covalent Organic Frameworks. *Angew. Chem. Int. Ed.* **2024,** *63* (31), e202404941.
54. Zheng, S.; Bi, S.; Fu, Y.; Wu, Y.; Liu, M.; Xu, Q.; Zeng, G., 3D crown ether covalent organic framework as interphase layer toward high-performance lithium metal batteries. *Adv. Mater.* **2024,** *36* (21), 2313076.
55. Segura, J. L.; Royuela, S.; Ramos, M. M., Post-synthetic modification of covalent organic frameworks. *Chem. Soc. Rev.* **2019,** *48* (14), 3903-3945.
56. Ge, S.; Wei, K.; Peng, W.; Huang, R.; Akinlabi, E.; Xia, H.; Shahzad, M. W.; Zhang, X.; Xu, B. B.; Jiang, J., A comprehensive review of covalent organic frameworks (COFs) and their derivatives in environmental pollution control. *Chem. Soc. Rev.* **2024,** *53,* 11259-11302.
57. Gendy, E. A.; Oyekunle, D. T.; Ifthikar, J.; Jawad, A.; Chen, Z., A review on the adsorption mechanism of different organic contaminants by covalent organic framework (COF) from the aquatic environment. *Environ. Sci. Pollut. Res.* **2022,** *29* (22), 32566-32593.
58. Mohammed, A. K.; Shetty, D., Macroscopic covalent organic framework architectures for water remediation. *Water Res. Technol.* **2021,** *7* (11), 1895-1927.
59. Zhu, D.; Zhou, S.; Zhou, Z.; Li, R.; Ye, J.; Ziyu, X.; Lan, S.; Zhang, Y.; Miao, S.; Wang, W., Highly efficient and selective removal of Cr (VI) by covalent organic frameworks: Structure, performance and mechanism. *Colloids Surf. A: Physicochem. Eng. Asp.* **2020,** *600*, 124910.
60. Da, H.-J.; Yang, C.-X.; Yan, X.-P., Cationic covalent organic nanosheets for rapid and selective capture of perrhenate: an analogue of radioactive pertechnetate from aqueous solution. *Environ. Sci. Technol.* **2019,** *53* (9), 5212-5220.

61. Chandra, S.; Hassan, A.; Prince; Alam, A.; Das, N., Rapid and efficient removal of diverse anionic water contaminants using a guanidium-based ionic covalent organic network (iCON). *ACS Appl. Polym. Mater.* **2022,** *4* (9), 6630-6641.
62. Chen, X.-R.; Zhang, C.-R.; Liu, X.; Liang, R.-P.; Qiu, J.-D., Ionic covalent organic framework for selective detection and adsorption of TcO 4−/ReO 4−. *Chem. Commun.* **2023,** *59* (62), 9521-9524.

63. Hassan, A.; Mollah, M. M. R.; Das, S.; Das, N., Rapid and selective removal of toxic and radioactive anionic pollutants using an ionic covalent organic framework (iCOF-2). *J. Mater. Chem. A* **2023,** *11* (32), 17226-17236.
64. Guillem-Navajas, A.; Martín-Illán, J. Á.; Salagre, E.; Michel, E. G.; Rodriguez-San-Miguel, D.; Zamora, F., Iron oxyhydroxide-covalent organic framework nanocomposite for efficient as (III) removal in water. *ACS Appl. Mater. Interfaces* **2022,** *14* (44), 50163-50170.
65. Xia, Z.; Zhao, Y.; Darling, S. B., Covalent organic frameworks for water treatment. *Adv. Mater. Interfaces* **2021,** *8* (1), 2001507.
66. Hauduc, H.; Takács, I.; Smith, S.; Szabó, A.; Murthy, S.; Daigger, G. T.; Sperandio, M., A dynamic physicochemical model for chemical phosphorus removal. *Water Res.* **2015,** *73*, 157-170.
67. Hube, S.; Eskafi, M.; Hrafnkelsdóttir, K. F.; Bjarnadóttir, B.; Bjarnadóttir, M. Á.; Axelsdóttir, S.; Wu, B., Direct membrane filtration for wastewater treatment and resource recovery: A review. *Sci. Total Environ.* **2020,** *710*, 136375.
68. Liao, Y.; Loh, C.-H.; Tian, M.; Wang, R.; Fane, A. G., Progress in electrospun polymeric nanofibrous membranes for water treatment: Fabrication, modification and applications. *Prog. Polym. Sci.* **2018,** *77*, 69-94.
69. Selatile, M. K.; Ray, S. S.; Ojijo, V.; Sadiku, R., Recent developments in polymeric electrospun nanofibrous membranes for seawater desalination. *RSC Adv.* **2018,** *8* (66), 37915-37938.
70. Tian, Y.; He, W.; Liang, D.; Yang, W.; Logan, B. E.; Ren, N., Effective phosphate removal for advanced water treatment using low energy, migration electric–field assisted electrocoagulation. *Water Res.* **2018,** *138*, 129-136.
71. Vasudevan, S.; Lakshmi, J.; Jayaraj, J.; Sozhan, G., Remediation of phosphate-contaminated water by electrocoagulation with aluminium, aluminium alloy and mild steel anodes. *J. Hazard. Mater.* **2009,** *164* (2-3), 1480-1486.
72. Ren, Y.; Zheng, W.; Duan, X.; Goswami, N.; Liu, Y., Recent advances in electrochemical removal and recovery of phosphorus from water: A review. *EFM* **2022,** *1* (1), 10-20.
73. Oehmen, A.; Lemos, P. C.; Carvalho, G.; Yuan, Z.; Keller, J.; Blackall, L. L.; Reis, M. A., Advances in enhanced biological phosphorus removal: from micro to macro scale. *Water Res.* **2007,** *41* (11), 2271-2300.
74. Zhou, Q.; Sun, H.; Jia, L.; Wu, W.; Wang, J., Simultaneous biological removal of nitrogen and phosphorus from secondary effluent of wastewater treatment plants by advanced treatment: A review. *Chemosphere* **2022,** *296*, 134054.
75. Wang, Y. e.; Li, J.; Zhai, S.; Wei, Z.; Feng, J., Enhanced phosphorus removal by microbial-collaborating sponge iron. *Water Sci Technol* **2015,** *72* (8), 1257-1265.
76. Katsoyiannis, I. A.; Zouboulis, A. I., Application of biological processes for the removal of arsenic from groundwaters. *Water Res.* **2004,** *38* (1), 17-26.

77. Gebremariam, S. Y.; Beutel, M. W.; Christian, D.; Hess, T. F., Research advances and challenges in the microbiology of enhanced biological phosphorus removal—a critical review. *Water Environ. Res.* **2011,** *83* (3), 195-219.
78. Straka, L. L.; Farmer, M. M.; Impastato, C. J.; Kadich, J. F.; Wells, G. F.; Kozak, J. A., Improving Enhanced Biological Phosphorus Removal with Return Activated Sludge Fermentation and Carbon Addition in a Benchtop Sequencing Batch Reactor Treating Real Wastewater. *ACS EST Water* **2024,** *4* (9), 4110-4119.
79. Akhzari, S.; Raissi, H.; Ghahari, A., Architectural design of 2D covalent organic frameworks (COFs) for pharmaceutical pollutant removal. *npj Clean Water* **2024,** *7* (1), 31.
80. Chen, F.; Guan, X.; Li, H.; Ding, J.; Zhu, L.; Tang, B.; Valtchev, V.; Yan, Y.; Qiu, S.; Fang, Q., Three-dimensional radical covalent organic frameworks as highly efficient and stable catalysts for selective oxidation of alcohols. *Angew. Chem. Int. Ed.* **2021,** *60* (41), 22230-22235.
81. Wang, W.; Gong, M.; Zhu, D.; Vakili, M.; Gholami, Z.; Jiang, H.; Zhou, S.; Qu, H., Post-synthetic thiol modification of covalent organic frameworks for mercury (II) removal from water. *Environ. Sci. Ecotech.* **2023,** *14*, 100236.
82. Liu, H.; Han, Y.; Zheng, X.; Zhao, J.; Man, Y.; Sun, L.; Zhao, Y., One-Pot Synthesis of Fully-Conjugated Chemically Stable Two-Dimensional Covalent Organic Framework. *Chin. J. Chem.* **2022,** *40* (6), 699-704.

Chapter 2

Guanidine-modified cellulose enhances capturing and recovery of phosphates from wastewater

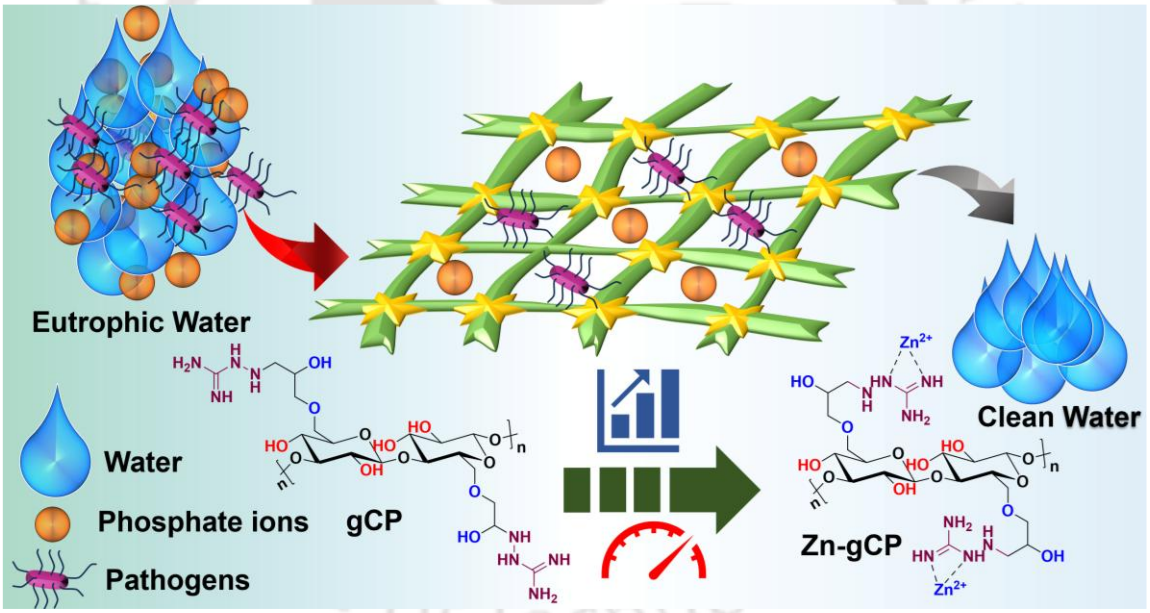

2.1. Background and objective of present work

The significance of phosphate as a nutrient in ecosystems, along with the considerable environmental issues arising from its excessive presence in water – such as eutrophication, algal blooms, and oxygen depletion – has been thoroughly discussed in chapter 1.[1, 2] These issues pose a significant risk to biodiversity and water quality, thereby underscoring the necessity for the implementation of effective phosphate management strategies.[3] It is already well documented from the detailed literature survey that among different separation techniques, adsorption-based phosphate removal and recovery is recognized as a promising strategy due to its high efficiency, operational simplicity, and recyclability.[4-9] However, conventional adsorbents, such as activated carbon, silica gel, chitosan, zeolites, biochar, etc., exhibit limited adsorption capacity and selectivity. In order to overcome these limitations, the researchers focused on the development of advanced adsorbent materials with improved efficacy, including metal oxide nanoparticles, COFs, MOFs, biomass-derived adsorbents, and porous organic polymer adsorbents. Metal nanoparticles, including zero-valent iron (nZVI) and magnetic iron oxides, enhance phosphate removal via precipitation and chemical bonding. However, their high reactivity complicates recovery due to aggregation or dispersion in water, reduces selectivity amid competing anions, and restricts their widespread applications due to environmental risks from potential metal ion leaching. Even though the porous structures and functional versatility of MOFs show excellent adsorption and recovery capabilities, because of their poor biodegradability and susceptibility to structural degradation in aqueous environments, they pose serious environmental issues. Another major problem of the MOFs for large-scale wastewater treatment is their higher production costs because of their costly metal-based precursors and intricate synthesis methods. These limitations necessitate further exploration of hybrid materials or functional modifications to enhance the sustainability and efficacy of these novel adsorbents. Recent developments in this regard have concentrated on the development of affordable and sustainable substitutes based on biomaterials. Building on these advances, this work investigates new biomaterial-based adsorbents to overcome limits of existing techniques. By integrating eco-friendly materials into wastewater treatment processes, the research aims to enhance phosphate removal efficiency while maintaining sustainability.

Recent studies demonstrated that a large number of hydroxyl groups of cellulose, hemicellulose, lignin, and other biomaterials could be easily modified with various functional moieties to remove and recover phosphates.[10, 11] Based on these reports, cellulose, which is abundant, cost-effective, and environmentally friendly, stands out as a promising precursor for the development of sorbents. Moreover, the use of chemically modified natural fibres – including cotton, coir, and several lignocellulosic materials – offers great chances to improve the application of agricultural by-products in wastewater treatment.[11-19] In spite of the economical and eco-friendly attributes of cellulose, hemicellulose, lignin, and other biomaterials, their widespread utilization in wastewater treatment is restricted by certain limitations, such as minimal adsorption capacity, a relatively slower adsorption rate, recyclability issues, and working within specific pH ranges.[19-24] In response to these challenges, we developed 1-aminoguanidine (ag)-modified cellulose, which offers a cost-effective and environmentally friendly solution, so positioning it as a potential alternative for lowering phosphate removal and recovery in wastewater treatment processes. Nonetheless, these sorbents exhibit resilience in both acidic and alkaline aqueous environments and demonstrate notably high rates of adsorption and recyclability.

Recent findings demonstrated that the guanidinium moiety efficiently and selectively binds phosphates through electrostatic and hydrogen bonding interactions.[3, 25] Inspired by these unique properties of the guanidine moiety, we developed an ag-modified cellulose-based polymer (gCP). We also identified that the gCP efficiently binds with Zn(II) ions, which allowed us to prepare Zn(II)-modified gCP (Zn-gCP). A series of physicochemical studies have confirmed the exceptional thermal and chemical stability of this biopolymer in a wide range of organic solvents, as well as in acidic or basic environments. In the presence of excessively competing counter-anions, the Zn-gCP polymer exhibits exceptional adsorption affinity for phosphate. Compared to other reported biopolymers, the Zn-gCP polymers exhibit a notably higher and faster binding affinity for phosphate anions and demonstrate enhanced recyclability. In addition, Zn-gCP polymers exhibited antimicrobial activity against gram-negative and gram-positive bacteria, which is also advantageous for effluent treatment. Overall, the outcome of this study indicates that the development of such multifunctional biopolymers has the potential to create advanced

biopolymer-based sorbents for effective effluent treatment, phosphate removal, and phosphate recovery.

2.2. Results and discussions

2.2.1. Synthesis and characterization of gCP and Zn-gCP –

The zinc-coordinated ag-functionalized polymer, Zn-gCP, was synthesized via a three-step synthetic process (Figure 2.1A). Initially, cellulose was modified with epichlorohydrin in the presence of NaOH to produce the epoxy-functionalized compound 1, with a yield of ~78% (Scheme A2.1).[26, 27] In the second step, the compound 1 reacted with 1-aminoguanidine hydrogen carbonate (reactivated by using NaOH) provided the guanidine-functionalized cellulose, gCP, exhibiting a yield of ~73% (Scheme A2.2).[26, 27] Finally, gCP reacted with Zn(II) salt (25% w/w) to produce the Zn-gCP polymer, demonstrating a yield of ~64% (Scheme A2.3). Then the reaction mixture was centrifuged, and the precipitate was repeatedly washed off with deionized water. Finally, the solid part was oven-dried overnight at 70 °C to obtain Zn(II)-loaded aminated polymer. The chemical structures and compositions of gCP and Zn-gCP polymers were characterized using several analytical techniques, including FT-IR, FESEM, FESEM-EDX, and XPS. The comparison of FT-IR spectra of compound 2.1 with cellulose shows increased peak intensities at about 901 cm^{-1} and 1223 cm^{-1}, which correspond to the asymmetric and symmetric stretching vibrations of the C-O-C bonds inside the epoxide groups, respectively (Figure A2.1).[28-30] FT-IR spectra of gCP polymer and cellulose were also compared, where the appearance of two N-H stretching peaks at 3240 cm^{-1} (free N-H) and 3123 cm^{-1} (hydrogen-bonded N-H), as well as additional intense vibrational bands at 1678 cm^{-1} (C=NH), 1493 cm^{-1} (N-H), 1346 cm^{-1} (C-N), and 1111 cm^{-1} (N-N), indicated the successful modification of cellulose with 1-aminoguanidine.[31] However, the FT-IR spectra of Zn-gCP revealed the broadening of the sharp peak at 445 cm^{-1} and the appearance of a shoulder peak around 442 cm^{-1}, signifying the coordination of Zn(II) ions with the gCP (Figure 2.1B).[32] The local bonding environments of both polymers were analysed by the XPS technique. The overlaid XPS spectra of gCP showed three characteristic peaks of carbon (C 1s) (284–289 eV), nitrogen (N 1s) (498–402 eV), and oxygen (O 1s) (530–533 eV). The core-level deconvoluted spectrum of C 1s revealed five peaks at 284.68, 285.94, 286.62, 288.41, and 288.95 eV, potentially originating from C-C/ C-H, C-N, C-O-C/ C-OH, C=NH, and $C=NH_2^+$, respectively. The deconvoluted spectrum of N 1s

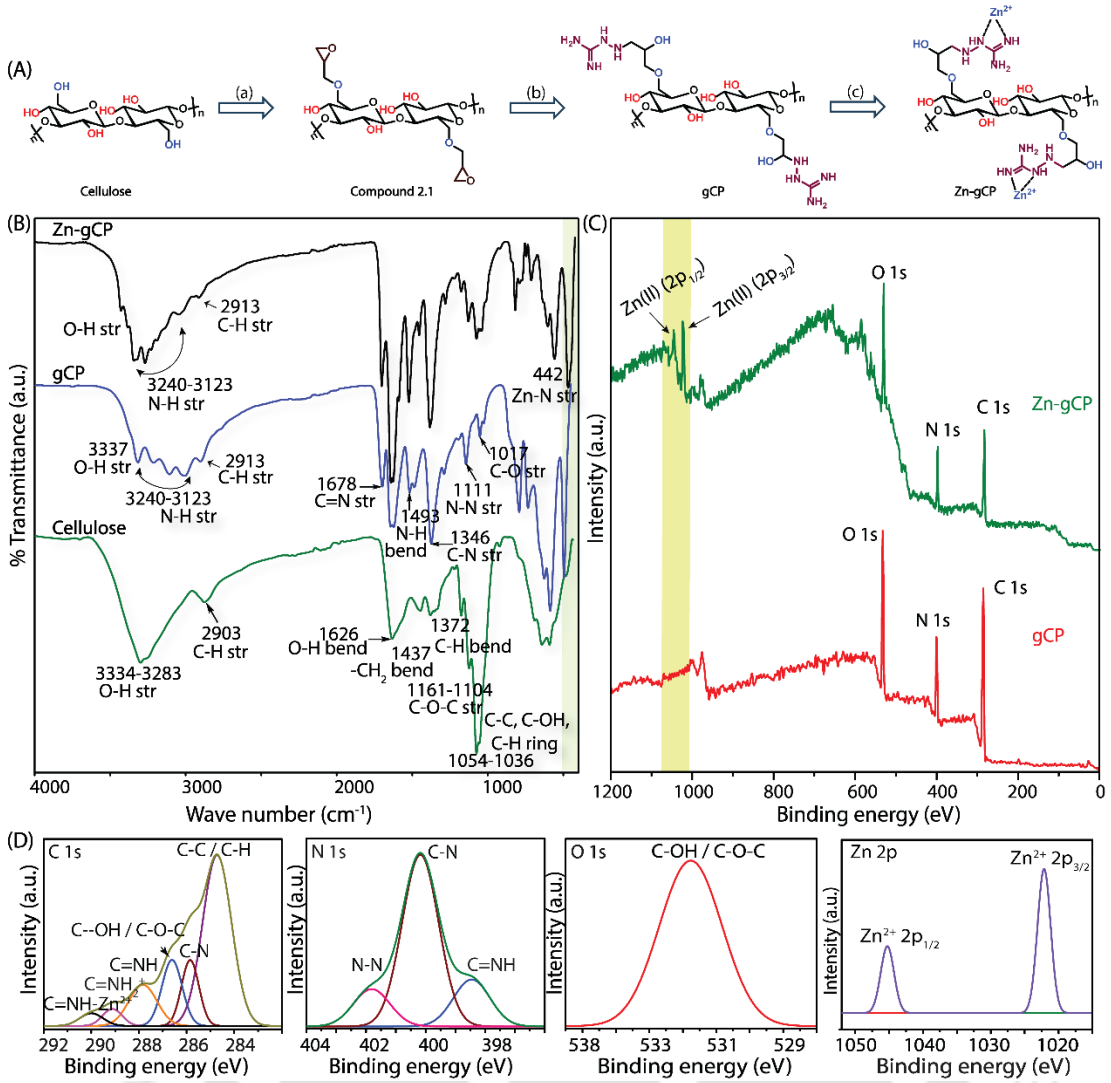

Figure 2.1. Synthetic scheme of the gCP and Zn-gCP polymers (a = epichlorohydrin, NaOH, H_2O, 0–60 °C, 3 h; b = 1-aminoguanidine hydrogen carbonate,NaOH, H_2O, rt – 0 – 60 °C, 3 h; c = $ZnCl_2.6H_2O$, H_2O, 60 °C, 12 h) (A). FT-IR of the cellulose, gCP polymer, and Zn-gCP polymer (B). XPS data profile: wide scan of the Zn-gCP polymer (C), and the deconvoluted peak of C 1s, N 1s, O 1s, and Zn 2p of the Zn-gCP polymer (D).

exhibited four peaks at 398.36, 399.48, 400.38, and 401.63 eV, corresponding to C=NH, C-N, $C=NH_2^+$, and N-N.[3] The deconvoluted spectrum of O 1s demonstrated two peaks at 530.89 and 532.70 eV, indicating C-O-C and C-OH respectively (Figure A2.2).[33] Whereas, the overlaid XPS spectra of Zn-gCP polymer showed the existence of Zn(2p) metal ions, with two new peaks appearing at 1044 eV (Zn $2p_{1/2}$) and 1021 eV (Zn $2p_{3/2}$) along with carbon (C 1s) (284–289 eV), nitrogen (N 1s) (498–402 eV), and oxygen (O 1s) (531.8 eV) (Figure 2.1C). Similarly, the C 1s core-level

deconvoluted spectrum of Zn-gCP presented six peaks at 284.72, 285.84, 286.60, 287.83, 289.12, and 290.03 eV, which could be attributed to C-C/ C-H, C-N, C-OH/ C-O-C, C=NH, C=NH_2^+, and C=NH-Zn(II). The N 1s deconvoluted spectrum showed three peaks at 398.86, 399.58, 400.39, 401.13 and 401.67 eV, potentially indicating C=NH, C-N, C=NH_2^+, N-N, and C=NH-Zn(II). The O 1s deconvoluted spectrum exhibited one peak at 531.84 eV, corresponding to C-O-C/ C-OH .[34, 35] The Zn(II) 2p deconvoluted spectrum demonstrated two peaks at 1044 eV and 1021 eV, potentially originating from Zn $2p_{1/2}$ and Zn $2p_{3/2}$, respectively (Figure 2.1D). The FESEM analysis showed that the original fibrous morphology of cellulose transformed into a more aggregate fibrous morphology in both gCP and Zn-gCP polymers (Figure 2.2A-2.2C). This transition could be due to an enhancement in crosslinking between the polymeric units, accelerated by the formation of hydrogen bonds resulting from the inclusion of ag in gCP. Additionally, the presence of Zn(II) in the Zn-gCP polymer further enhances the crosslinking efficacy through hydrogen bonding along with ag units. The FESEM-EDX analysis and elemental mapping revealed that C, N, and O are the major chemical components of gCP (Figure A2.3), whereas C, N, O, and Zn are the major chemical components of Zn-gCP polymer (Figure 2.2D and A2.4). The thermogravimetric analysis (TGA) profile revealed that the Zn-gCP polymer experience significant weight loss at around 300 °C, which is more than that of gCP polymers (200 °C) (Figure 2.2E and A2.5). This superior thermal stability of Zn-gCP polymer compared to gCP polymer could be due to the intermolecular ion-dipole interaction caused by the presence of Zn(II) ions. The Tyndall effect experiment demonstrated that both the gCP and Zn-gCP polymers exhibit dispersive properties in an aqueous medium (Figure 2.2F). The DLS measurements showed no discernible change in the hydrodynamic diameter (dH) of the polymers even after 24 h (dH~807–883 nm) (Figure A2.6). The pH-dependent zeta potential (ξ) measurements showed an alternation of the ξ values of the polymers with the pH of the aqueous medium. The ξ values of Zn-gCP reduce from +28.6 to +3.77 mV with the increase in the pH of the aqueous medium from 2 to 10. The change in ξ values of gCP also showed a similar pattern (Figure 2.2G). However, only cellulose showed negative ξ values at the above-mentioned pH range (Figure A2.7). To check the chemical stability, both polymers (5 mg) were treated with 5 mL of common organic

solvents such as acetonitrile (ACN), ethyl acetate (EtOAc), methanol (MeOH), tetrahydrofuran (THF), HCl (0.5 N), and

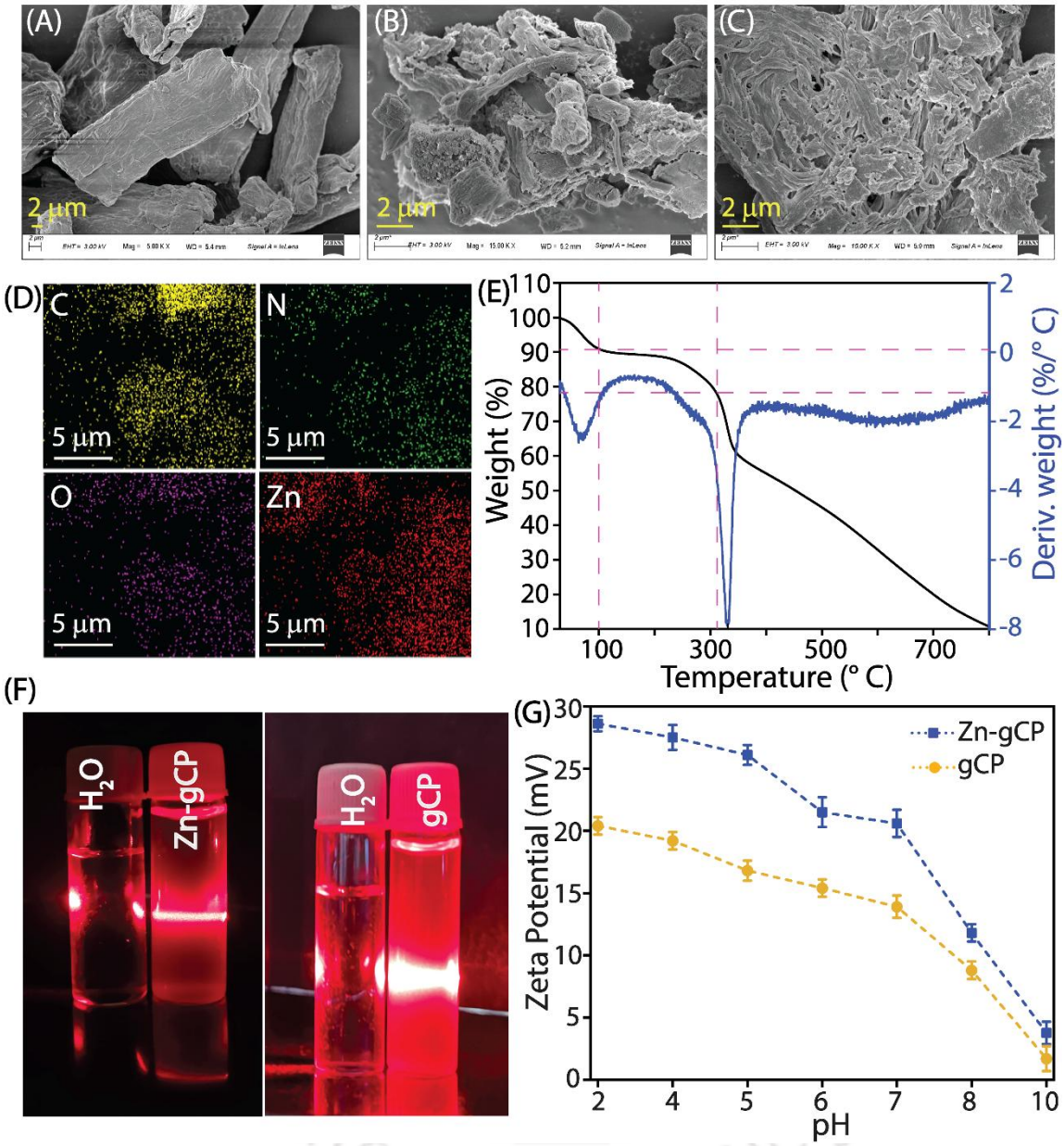

Figure 2.2. FESEM images of the cellulose (A), gCP polymer (B), and Zn-gCP polymer (C). FESEM–EDX mapping for the C, O, N, and Zn of the Zn-gCP polymer (D). TGA–DTG analysis of the Zn-gCP polymer (E). Tyndall effect demonstrated the aqueous dispersions of the gCP and Zn-gCP polymer (F). Zeta potential values of the gCP and Zn-gCP polymer at different pH values (G).

NaOH (0.5 N) for 7 days. Then, the chemical stability of the polymers was examined by FT-IR analysis. No significant alterations in the FT-IR spectra of gCP and Zn-gCP polymers before and after these treatments indicate their structural stability under

these conditions (Figure A2.8). The TGA profiles for both the polymers (gCP and Zn-gCP) before and after 7 days of treatment with HCl (0.5 N) and NaOH (0.5 N) show minor changes in the thermal integrity of both polymers (Figure A2.9). The weight loss against temperature differs in each case, but the maximum weight loss is observed around the same temperature (~ 300 °C). These changes in TGA profiles could be due to the treatment of the polymer with HCl and NaOH for 7 days. Higher concentrations of H^+ and OH^- ions could have promoted the leaching of Zn(II) from the polymer or affected the stabilization of the polymer to some extent.

2.2.2. Phosphate-binding properties of gCP and Zn-gCP polymers —

Both the guanidine moiety and Zn(II) ions are known to have a pronounced affinity for phosphate ions, primarily due to the robust hydrogen bonding and electrostatic interactions that occur between these functional groups and phosphate.[3, 25, 36] This inherent affinity inspired us to investigate the phosphate-binding capabilities of both gCP and Zn-gCP, aiming to elucidate their potential for selectively binding phosphate ions through these synergistic interactions. To perform the anion selectivity experiment, a stock solution was prepared by dissolving various sodium salts containing different anions (F^-, Cl^-, Br^-, NO_3^-, SO_4^{2-}, and HPO_4^{2-}) in Milli-Q water, each at a concentration of ~25 ppm. Subsequently, 5 mg of gCP and Zn-gCP polymers were separately added to 5 mL of the prepared stock solution, followed by agitation for 12 hours. The IC analysis revealed that both the gCP and Zn-gCP polymers showed higher phosphate binding over the other tested anions (Figure 2.3A). Conversely, the affinity of the polymer for chromate, dichromate, and arsenate anions was separately evaluated. The results indicated that the polymer exhibits relatively poorer affinity for ions as compared to the phosphate ions (Figure A2.10). Further analysis showed that the Zn-gCP and gCP polymers have >89% and >57% phosphate ion removal efficacy, respectively, from a ~25 ppm stock solution of phosphate ions. In contrast, unmodified cellulose exhibited negligible affinity for phosphate ions, implying that the incorporation of ag in gCP increased the phosphate adsorption efficacy of the polymer through hydrogen bonding and electrostatic interaction. Moreover, the introduction of Zn(II) ions into the polymer matrix (Zn-gCP) further elevated the phosphate adsorption efficiency, indicating that the presence of Zn(II) ions amplified electrostatic interactions between the polymer and phosphate ions (Figure A2.11 and A2.12). This synergistic effect, resulting from

the combined influence of ag and Zn(II) ions, substantially improved the phosphate adsorption affinity of the Zn-gCP polymer compared to the gCP polymer.[36] Due to the

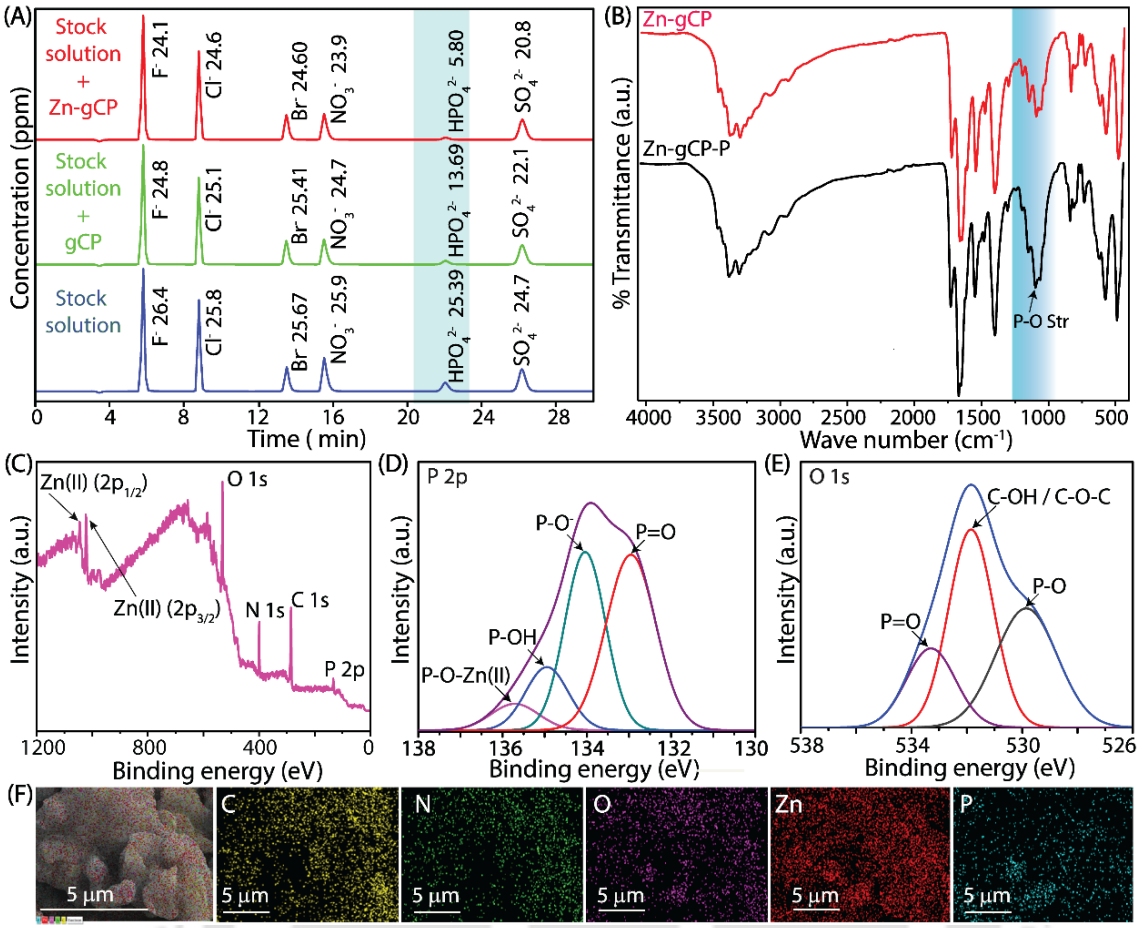

Figure 2.3. Ion chromatogram of stock solution (~25 ppm) before and after the treatment of gCP and Zn-gCP polymers (A). FT-IR of the Zn-gCP polymer before and after phosphate anion adsorption (B). XPS data profile: wide scan of the Zn-gCP polymer after phosphate anion adsorption (C), the deconvoluted peak of P 2p (D) and O 1s (E). FESEM–EDX mapping analysis for the C, O, N, Zn, and P of the Zn-gCP polymer after phosphate ion adsorption (F).

higher phosphate adsorption affinity of Zn-gCP compared to that of gCP, the subsequent studies were performed with the Zn-gCP polymer. The FT-IR, FESEM-EDX, and XPS analyses confirmed the phosphate binding ability of the polymers. The increased intensity of the FT-IR peak around 1065 cm¯1 in the phosphate-treated Zn-gCP (Zn-gCP-P) polymer indicates that the phosphate was efficiently absorbed by the Zn-gCP polymer (Figure 2.3B). The XPS analysis indicated the appearance of new peaks at 132-136 eV (P 2p) for the phosphate-treated Zn-gCP polymers compared to

that of the untreated one (Figure 2.3C). The P 2p deconvoluted spectrum showed four peaks at 132.95, 134.03, 134.94, and 135.71 eV, potentially indicating P=O, P-O, P-OH, and P-O-Zn(II), respectively. The O 1s deconvoluted spectrum exhibited three peaks at 529.85, 531.84, and 533.29 eV, corresponding to P-O^-, C-O-C/ C-OH, and P=O, respectively (Figure 2.3D-2.3E).[3] The FESEM-EDX analysis revealed that P, C, N, O, and Zn(II) are prominent elements in Zn-gCP polymers, suggesting the adsorption of phosphate (Figure 2.3F).

2.2.3. Phosphate adsorption study –

Positive surface potential values and excellent chemical and thermal stability of Zn-gCP polymers prompted us to examine their ability to adsorb phosphate from aqueous solutions. The effect of pH on the adsorption capacity of phosphate was initially studied, revealing that the acidity and basicity of the solution played a crucial role in the interaction between Zn-gCP and phosphate. The pH of the solution determines the types of phosphate present (the pKa values of the H_3PO_4 in water were 2.2, 7.2, and 12.3), which may affect their adsorption properties. Some adsorbents have pH-dependent anion adsorption properties, with maximum adsorption occurring at very acidic or basic conditions, limiting their use.[37-39] The phosphate adsorption ability of Zn-gCP was investigated at various pH values (2, 4, 5, 6, 7, 8, and 10). The Zn-gCP showed very similar phosphate adsorption capabilities across the pH range of 4 to 7, with a notable decrease in adsorption capacity as the pH of the aqueous solution dropped from 4 to 2, indicating its potential applicability for treating eutrophic waters (Figure 2.4A). Between pH 7 and 4, phosphate ions predominantly exist in the form of $H_2PO_4^-$, leading to a relatively consistent capacity for hydrogen bonding interactions with the Zn-gCP polymer. Additionally, the reduction in pH enhances the ξ of the Zn-gCP polymer, which may promote increased electrostatic interactions between the phosphate ions and the polymer. However, as the pH decreases from 4 to 2, phosphate ions shift predominantly to the H_3PO_4 form, which diminishes hydrogen bonding efficiency between the phosphate species and Zn-gCP. Despite the increase in the ξ of the Zn-gCP, the elevated concentration Cl^- ions introduced significant competition for the electrostatic binding sites on the Zn-gCP, resulting in a reduction in phosphate ion adsorption as the solution pH approached 2. However, at pH values ≥8, Zn-gCP showed significantly lower phosphate adsorption capacity. This reduction may be attributed to a weakening of

both electrostatic interactions and hydrogen bonding between ag protons and the oxygen atoms of phosphate species. At higher pH levels, the ξ of Zn-gCP (ξ = 3.77 mV at pH 10) becomes too low to sustain effective electrostatic interactions, likely leading to repulsion of phosphate ions. Furthermore, an increased abundance of OH^- ions in alkaline conditions may compete with phosphate ions for Zn(II) coordination sites, further contributing to the observed decline in adsorption efficiency. Due to almost similar adsorption capabilities of Zn-gCP across the pH range of 4 to 7, subsequent phosphate adsorption studies were conducted at pH 7. The IC studies were performed to investigate concentration-dependent phosphate adsorption. The phosphate adsorption isotherms of Zn-gCP polymers were determined by subjecting them to solutions containing varying concentrations of phosphate salt (25–1000 ppm in deionized water (Milli-Q). The solid polymer (5 mg) was added to each 5 mL of stock solution containing varying concentrations of phosphate ions (25–1000 ppm), sonicated for 10 min, and then continuously stirred for 6 h at room temperature. The concentration of phosphate ions in each stoke solution was determined using IC both before and after the treatment with the polymer. It was observed that when 5 mg of Zn-gCP polymer was introduced into a 1000 ppm concentration of phosphate, the phosphate adsorption capacity reached its maximum saturation point at 231.20 mg g^{-1} (Figure A2.13). The Langmuir and Freundlich adsorption models were used to investigate the relationship between adsorption parameters and the equilibrium concentration of phosphate. The Langmuir isotherm model indicated a maximum adsorption capacity of 310 mg g^{-1} for phosphate at pH 7 (Figure 2.4B). The phosphate adsorption isotherms of gCP polymers were also accessed under conditions similar to those of Zn-gCP polymers, revealing a maximum equilibrium adsorption capacity of 83.61 mg g^{-1} for phosphate ions from a 1000 ppm aqueous phosphate solution. The Langmuir isotherm model predicted a maximum adsorption capacity of 97 mg g^{-1} for phosphate at pH 7, which was significantly lower than that of the Zn-gCP polymer (Figure A2.14). A time-dependent IC experiment demonstrated a significant increase in phosphate adsorption. The Zn-gCP exhibited an initial adsorption capacity of 176.74 mg g^{-1} within 10 min, which reached 230.89 mg g^{-1} after 20 min at pH 7 (Figure A2.15A). The adsorption process was observed to more closely correlate with both linear and non-linear pseudo-second-order kinetics models, in

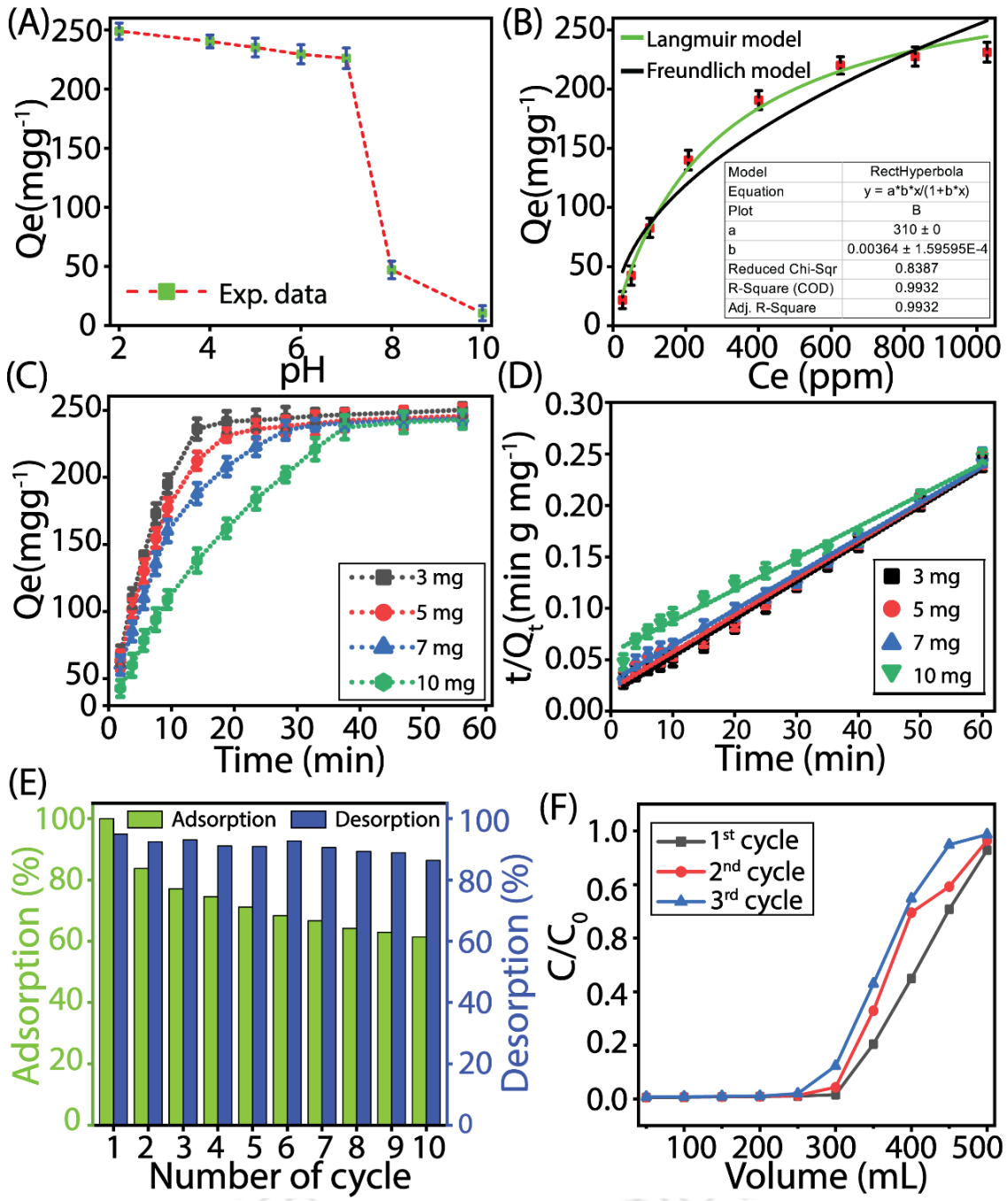

Figure 2.4. pH-dependent phosphate ion adsorption efficiency of the Zn-gCP polymer (A). Phosphate anion adsorption isotherm of Zn-gCP (B). Time-dependent adsorption isotherm of phosphate ions by the Zn-gCP polymer (3–10 mg) at pH 7.0 at room temperature (C). Pseudo-second-order kinetics curves of phosphate adsorption on Zn-gCP (3–10 mg) at pH 7.0 and room temperature (D). Phosphate ion adsorption and desorption efficiency of the Zn-gCP polymer after different cycles (E). Phosphate ion adsorption efficiency of the Zn-gCP polymer by dynamic adsorption column experiment (C_0 = initial concentration of the phosphate solution and Ce = final concentration of the phosphate solution after passing through the column) (F).

contrast to pseudo-first-order kinetics (both linear and non-linear), with correlation coefficients (R^2) > 0.99624 for the linear pseudo-second-order kinetics model and > 0.97628 for the non-linear pseudo-second-order kinetics model (Figure A2.15B – D). Similarly, kinetics studies with gCP polymer under the same conditions showed equilibrium adsorption capacity reached within 35 – 40 min, considerably slower than Zn-gCP polymer (Figure A2.16). These results indicate that the presence of Zn(II) ions enhances the electrostatic affinity of the Zn-gCP polymer for phosphate ions, that significantly contributes to a substantial enhancement in the adsorption capacity for phosphate anions as well as accelerates the adsorption rate. Time-dependent kinetic with different concentrations of Zn-gCP polymer (3 -10 mg) was studied by IC. The results were fitted to a linear pseudo-second-order model, revealing that adsorption rates decreased from 0.000809 mg g^{-1} min^{-1} to 0.000164 mg g^{-1} min^{-1} as the concentration of Zn-gCP polymer increased from 3 mg to 10 mg (Figure 4C–4D). These results demonstrate that the Zn-gCP sorbent follows a pseudo-second-order kinetic model for the removal of phosphate from aqueous solutions, exhibiting a relatively fast adsorption efficiency. To check the competing effect of coexisting anions on phosphate adsorption, stock solutions of several sodium salt anions (F^-, Cl^-, Br^-, NO_3^-, SO_4^{2-}, and phosphate) were prepared by dissolving them in Milli-Q water at a concentration ratio of 1:2 (phosphate: other anion). The IC results showed that the polymer (Zn-gCP) captured phosphate anion more preferentially (> 78%) even in the presence of the other capitating anions (Table A2.1). The phosphate removal efficiency of the Zn-gCP polymer was also assessed from a high-volume, low-concentration phosphate solution by treating 5 mg of the polymer with 50 mL of a phosphate solution at an initial concentration of 5 ppm. IC analysis revealed the reduction in the phosphate ion concentration to below 0.5 ppm after treatment with Zn-gCP, which is well below the World Health Organization (WHO) recommended threshold for phosphate in drinking water (Figure A2.17).

To evaluate the efficacy of Zn-gCP polymer in removing phosphate from real-world eutrophic water, two samples were collected from two different food manufacturing industries located in Gauripur, North Guwahati, Assam, India. The pH, ion concentrations, phosphate, and other coexisting species were all listed in Table A2.2. Zn-gCP polymer (5 mg) was treated with 5 mL of each sample, and the mixture was constantly stirred for 6 h. Subsequently, the mixture was centrifuged at 6000

rpm for 10 min, followed by filtration to separate the phosphate-adsorbed Zn-gCP and unbound phosphate in the supernatant was quantified using IC. The study demonstrated that the Zn-gCP polymers successfully reduced phosphate ion concentration to below the WHO-recommended level for phosphate discharge, even in the presence of other coexisting anions (Figure A2.18).

2.2.4. Phosphate recovery and regeneration of the Zn-gCP polymer –

To assess the viability of Zn-gCP polymer in practical applications, their ability to capture, release, and reuse phosphate was investigated. The phosphate-loaded polymers (5 mg) were kept in 5 mL of 0.5 N NaOH (pH ~13) solution for 2 h under stirring conditions. After that, the polymer was separated from the solution through centrifugation at 6000 rpm for 10 min, followed by filtration. Next, the solution was diluted 10 times to maintain the concentration of phosphate ions to 25 ppm, and the amount of released phosphate in the solution was quantified via IC. The collected polymer was then thoroughly rinsed with Milli-Q water to remove any remaining residues before being ready for the next cycle. This sequence of steps was repeated sequentially for each cycle to check the recyclability of the polymer. An analogous experiment was carried out up to ten cycles. The chromatogram result showed that Zn-gCP had > 61% adsorption efficiency of phosphate ions and > 88% desorption efficiency of phosphate ions from the Zn-gCP polymer after the 10^{th} cycle (Figure 2.4E). The decline in phosphate adsorption capacity of the Zn-gCP polymer observed from the 1^{st} to the 10^{th} adsorption cycle can be attributed to two primary factors. Firstly, during each adsorption cycle, a fraction of the active sites of the polymer become permanently blocked by non-recyclable phosphate ions, reducing the number of available adsorption sites. Secondly, the desorption process, carried out under highly basic conditions (pH ~13). Under such harsh conditions, may lead to minor leaching of Zn(II) ions from the polymer framework, potentially altering its structure and performance. The combined effect of these processes contributes to the gradual reduction in adsorption capacity over successive cycles. Nevertheless, despite this decrease, the phosphate adsorption capacity of Zn-gCP polymer in the 10^{th} cycle remains significantly higher to that of many reported biopolymers, to the best of our knowledge. The Zn(II) leaching concentrations from the Zn-gCP polymer were also analysed following the 1^{st}, 5^{th}, and 10^{th} desorption cycles of phosphate ions using ICP-MS. The results showed negligible Zn(II) leaching into the solution, with

concentrations remaining well below the limits specified by the WHO and the United States Environmental Protection Agency (US EPA) (Figure A2.19). After undergoing 10th cycles of regeneration, the polymers were subjected to various analyses, such as FTIR, FESEM, FESEM-EDX, and elemental mapping, to assess the stability of the Zn-gCP polymer after regeneration. The FTIR spectra and FESEM images of the regenerated Zn-gCP were almost identical to those of the original polymers, indicating the morphological integrity of the Zn-gCP polymers after ten cycles of regeneration (Figure A2.20A–B). FESEM-EDX and elemental mapping analysis of the regenerated Zn-gCP indicated the presence of all the elements (C, N, O, and Zn) after regeneration, suggesting their potential utility in the recovery of phosphate from aquatic systems (Figure A2.20C–D). Similarly, the time-dependent kinetics for the desorption process of phosphate-loaded Zn-gCP (5 mg) was performed, and it followed the pseudo-second-order kinetics (with rate constant = 0.000157 mg g^{-1} min^{-1}) (Figure A2.21 and A2.22). These results indicate that the synthesized Zn-gCP polymer could be an effective adsorbent for removing phosphate from wastewater. Overall, the sorption studies revealed that the adsorption of phosphate ions on this biopolymer is driven by the hydrogen bonding of ag moieties with phosphate ions (NH....O-P) and coordination of ag bound Zn(II) ions with phosphate ions.

2.2.5. Dynamic column chromatography phosphate adsorption study —

The pH-responsive sorption properties and the expeditious removal efficacy of phosphate ions by the Zn-gCP polymer, have engendered an investigative interest in assessing their capture efficiency via the column chromatographic exchange method, simulating a real-time scenario (Figure A2.23A). Based on the IC experiment, it was seen that up to 250 mL of the column eluent had phosphate concentrations lower than those recommended by the World Health Organization (WHO) in the first cycle (Figure 2.4F). The column was rejuvenated by adding 100 mL of a NaOH (0.5 N) solution before moving on to the next cycle, and over 93% of the phosphate was efficiently desorbed from the polymer through this procedure in the first cycle. The experiment was replicated up to 3 cycles, and the IC results consistently demonstrated that up to 200 – 250 mL of eluent from the column had phosphate concentrations below the WHO recommended threshold (Figure 2.4F) and efficiently removed over 85% of the phosphate from the Zn-gCP polymer after the third cycle (Figure A2.23B). These outstanding results from the use of the

column-based phosphate capture technique clearly define potential of the polymer to mimic a real-time scenario.

2.2.6. Plausible phosphate adsorption – desorption mechanisms by the Zn-gCP polymer —

In this study, phosphate adsorption experiments were conducted at pH 7. At this pH, phosphate exists in equilibrium between two forms, i.e., $H_2PO_4^-$ and HPO_4^{2-}, with $H_2PO_4^-$ being slightly more prevalent. Both phosphate forms possess hydrogen bond donor –OH groups and acceptor P=O and P–O^- groups. Through these groups, the tetrahedral phosphate ions facilitate specific hydrogen bonding interactions with the ag moieties (–NH···O=P, –NH···O–P, and C=N···HO–P). Additionally, the positive surface potential of the Zn-gCP polymer at pH 7 enhances electrostatic interactions between the phosphate ions and Zn(II) ions, as well as with the ag moieties (pKa = 11.5) of the Zn-gCP polymer. The combination of hydrogen bonding and electrostatic interactions synergistically enables the Zn-gCP polymer to effectively overcome the hydration energy barrier of phosphate ions. In contrast, due to the lack of acidic protons at pH 7, anions such as halides, nitrate, sulphate, chromate, and dichromate interact with the Zn-gCP polymer via only electrostatic interaction, resulting in a reduced affinity for these anions compared to phosphate.[25] Conversely, due to the nearly identical chemical properties of phosphate and arsenate ions, the gCP polymer demonstrates comparable removal efficacy for both, with a slight preference for phosphate ions. However, the incorporation of Zn(II) into the Zn-gCP polymer significantly enhances its selectivity and removal efficiency for phosphate over arsenate. This improved performance can be attributed to the better hydrogen bonding and electrostatic interactions between phosphate ions and the Zn-gCP framework, driven by the comparatively higher charge density of phosphate ions resulting from their smaller ionic radius, as well as the relatively higher binding affinity of Zn(ii) towards phosphate ions than arsenate ions.[40, 41] Collectively, these factors establish phosphate as the preferred ligand for both gCP and Zn-gCP polymers.

To desorb the phosphate ions from the Zn-gCP polymer for reuse, the phosphate-loaded polymer was treated with 0.5 N NaOH solution. At this basic pH (~13), phosphate ions predominantly exist as PO_4^{3-}, leading to a significant reduction in hydrogen bonding efficiency between the ag groups and phosphate ions.

Furthermore, in this elevated pH, the ag moieties are largely deprotonated (pKa of ag is 11.5), and the increased concentration of OH^- ions in the solution disrupts the electrostatic interactions between Zn-gCP polymer and phosphate ions. Consequently, under basic conditions, both hydrogen bonding and electrostatic interactions between the Zn-gCP polymer and phosphate ions are severely reduced, facilitating the desorption of phosphate ions from the surface of the Zn-gCP polymer. Thus, the polymer is effectively regenerated, allowing for subsequent phosphate adsorption cycles (Figure 2.5).

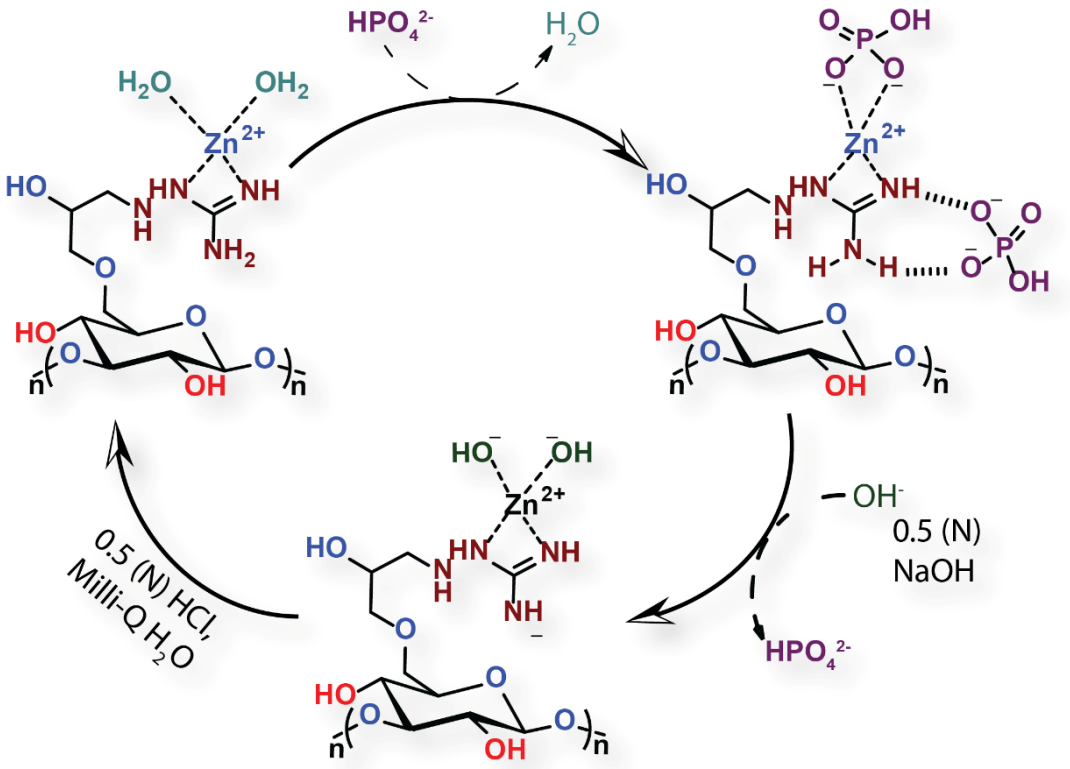

Figure 2.5. Plausible mechanistic pathways for adsorption and desorption processes.

2.3. Antibacterial activities of Zn-gCP

Purification and filtration of water include the disinfection of water or devoid of any microbial growth. A water sample devoid of bacterial growth becomes a preferred option for its further use. Hence, a polymer destined for water purification and filtration should have bactericidal efficacy. As per our earlier report, our gCON polymer studded with guanidine moiety was supposed to have antimicrobial activity. Hence, we initially analysed the antibacterial efficacy of the polymer against

Staphylococcus aureus (S. aureus), a Gram-positive bacterial strain, and Escherichia coli (E. coli), a Gram-negative bacterial strain (Figure 2.6A – B and A2.24). The polymer at different concentrations was treated with the bacterial culture after exfoliation. The bactericidal activity of the polymers was analysed after transferring

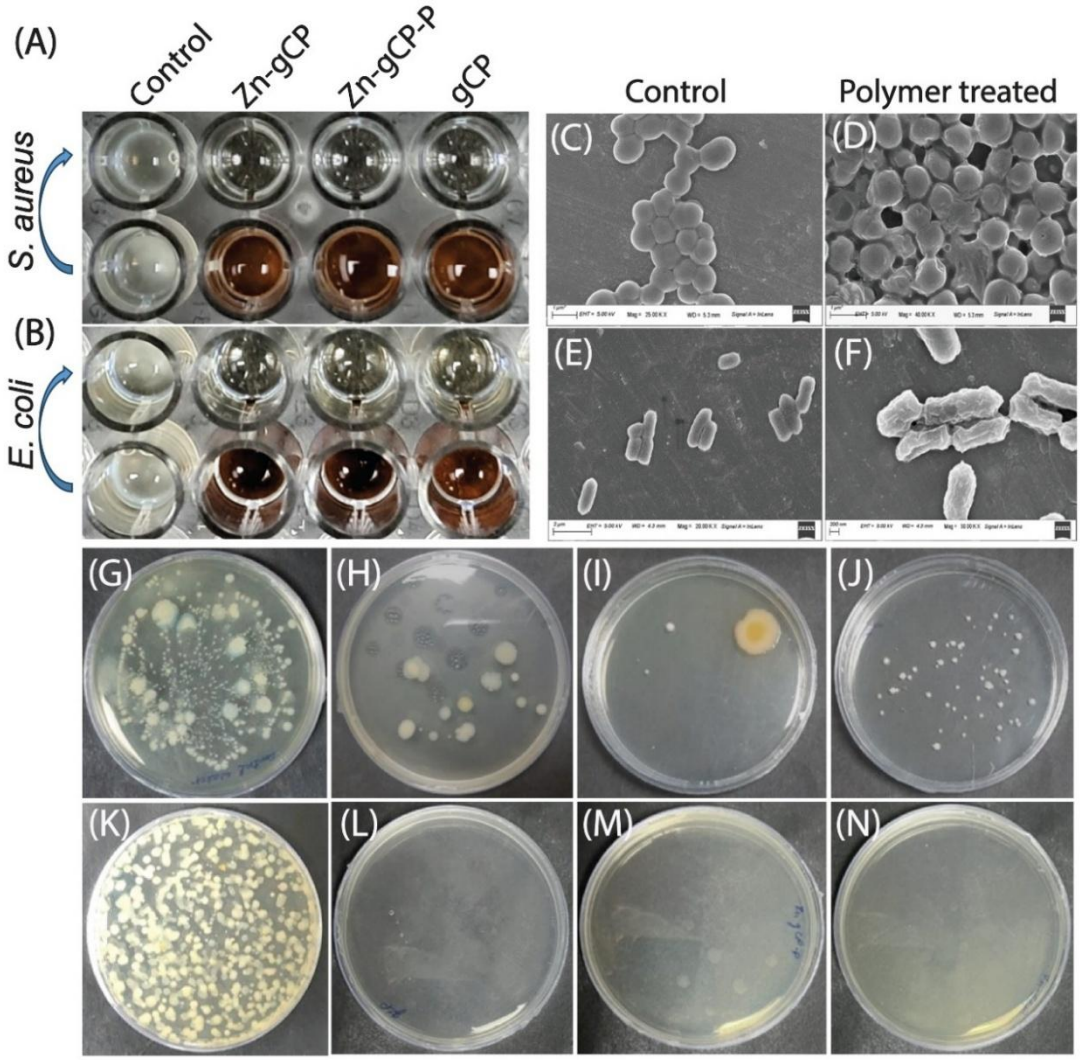

Figure 2.6. Antibacterial activity of the polymers against S. aureus (A) and E. coli (B) cells. Morphological analysis of S. aureus before (C) after (D) the treatment of polymer. Morphological analysis of E. coli before (E) after (F) the treatment of the polymer. Antibacterial activity of polymers against real water sample. Polymer untreated sample after 3 h (G). Zn-gCP–P polymer treated sample after 3 h (H). Zn-gCP polymer treated sample after 3 h (I). gCP polymer treated sample after 3 h (J). Polymer untreated sample after 6 h (K). Zn-gCP–P polymer treated sample after 6 h (L). Zn-gCP polymer treated sample after 6 h (M). gCP polymer treated sample after 6 h (N).

the treated bacterial culture into fresh media. The result indicated that the Zn-gCP polymer showed more efficient bactericidal activity than the gCP polymer. Furthermore, the antibacterial activity of the polymer (Zn-gCP-P), even after phosphate adsorption, was identical to that of the pristine polymer (Zn-gCP). The results demonstrated that at a concentration of 250 µg/mL, the gCP polymer showed bactericidal activity against S. aureus. In comparison, at 125 µg/mL concentration, both the Zn-gCP and Zn-gCP-P polymers indicated bactericidal activity. The gCP polymer displayed bactericidal activity against E. coli at 375 µg/mL, whereas the Zn-gCP and Zn- gCP-P polymers did so at a concentration of 187.5 µg/mL.

To further analyse the bactericidal activity of the polymer, morphological analysis was done against S. aureus, which represented the distorted cocci shape of the polymer-treated bacterial culture compared to the control one (Figure 2.6C – F). The antibacterial application of the Zn-gCP polymers in real water samples was also assessed by incubating the water sample with exfoliated polymers in a shaker incubator at room temperature. The growth of the microbes on the agar plate was observed, and it was surprising to note that after 6 h incubation, the agar plate showed no growth, revealing the bactericidal activity of the polymers. In our study, we also observed that the binding of Zn(II) and phosphate did not alter the bactericidal activity of the polymer (Figure 6G – N).

2.4. Summary

The widespread discharge of phosphates into aquatic environments from diverse origins not only reduces the global phosphate rock stocks but also poses a significant environmental challenge, leading to eutrophication. To address this, we developed a zinc-coordinated 1-aminoguanidine functionalized cellulose-based biopolymer (Zn-gCP) with significant thermal and chemical stability. Due to the synergistic effect caused by the ag moiety and Zn(II), the Zn-gCP polymers displayed a higher binding affinity for phosphate anions through electrostatic and hydrogen bonding interaction, even in the presence of other competing counter anions, and could be efficiently regenerated by adjusting the pH of the aqueous solution. Additionally, it exhibited antimicrobial activity, which is beneficial for effluent treatment. Overall, this study suggests that developing multifunctional biopolymers holds potential for advanced sorbents in effective effluent treatment, phosphate removal, and recovery. This polymer could also be useful in the phase-transfer of

hydrophobic nanoparticles to aqueous solutions, biomedical adhesives, fuel cells, electronic industries (including semiconducting polymers), organic catalysis and multiple biomedical applications.

2.5. Appendix section

2.5.1. General information –

All reagents used in this study were purchased from commercial sources, such as Sigma-Aldrich, and were used without further purification. The anion selectivity, adsorption, and desorption analyses by the gCP and Zn-gCP polymers were performed using a Metrohm ion chromatograph (792 Basic IC, Switzerland) equipped with a METROSEP A Supp 5-250/4.0 (6.1006.530) separation column (4 mm × 100 mm). The primary standard used in these experiments was PRIMUS multi-anion solution (10 mg/kg ± 0.2% of each ionic species) from Fluka. The UV-Vis spectroscopic measurements were performed using a Thermo SCIENTIFIC EVOLUTION 201 UV-Vis spectrophotometer equipped with 10 mm path-length quartz cuvettes, covering a wavelength range of 200 – 700 nm. The arsenate adsorption efficacy of both polymers was evaluated using a Shimadzu AA-6880F Atomic Absorption Spectrophotometer (AAS). Zn(II) leaching concentrations were determined using an Agilent 7850 Inductively Coupled Plasma Mass Spectrometer (ICP-MS). The experimental investigations utilized ultra-pure milli-Q water obtained from a PURELAB Chorus ELGA system with a resistivity of 18 MΩ. The comprehensive details of the methodologies have been provided in the supplementary information file.

2.5.2. Synthesis and characterization of the compounds –

2.5.2.1. Synthesis of compound 2.1:

First, NaOH (40 mL of 1M aq. solution) was slowly added into the suspension of cellulose (Sigma Aldrich) in water (100 g of a 1 wt %) under stirring conditions at 0 °C. Subsequently, epichlorohydrin (678 µL; excess) was gradually added to the reaction mixture and stirred for 3 h at 60 °C. After that, the reaction mixture was cooled down to room temperature, and the precipitate was collected through centrifugation at 6000 rpm for 10 min, followed by filtration. The resulting precipitate was thoroughly rinsed with deionized water multiple times to eliminate any remaining impurities from the reaction mixture and kept in the oven to dry (Scheme A2.1).[26, 27] **Characterization of the compound:** solid-state FT-IR (cm^{-1}) =

901 (s), 1054-1036 (s), 1161-1104 (s), 1223 (s), 1372 (s), 1437 (s), 1626 (s), 2903 (br), and 3334 – 3283 (br).

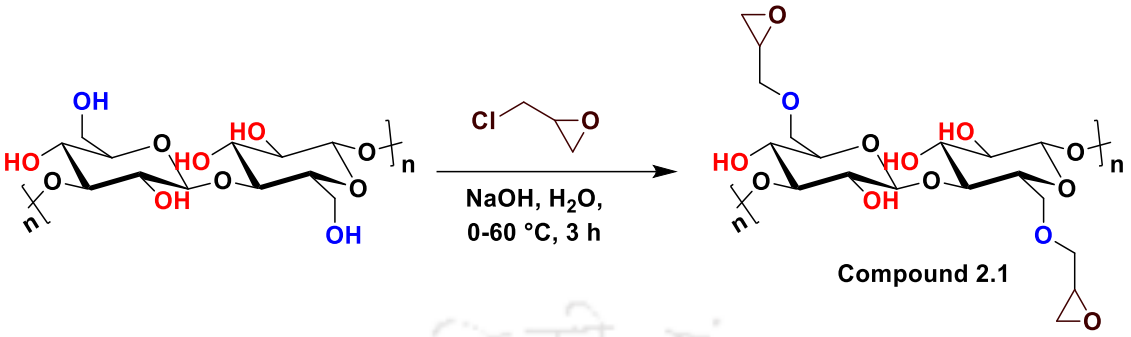

Scheme A2.1. Synthesis of epoxy-modified cellulose (compound 1).

2.5.2.2. Synthesis of gCP:

1-Aminoguanidinium hydrogen carbonate (1.6 g) was dissolved in water, and the pH of the solution was adjusted to 12 by adding NaOH. The mixture was stirred for 15 min at room temperature. Subsequently, this solution was slowly added to the suspension of compound 1 (100 g, 1 wt%) in water while being subjected to stirring at 0 °C. The temperature of the reaction mixture was then increased to 60 °C and stirred for another 3 h. Afterwards, the reaction mixture was allowed to cool down to room temperature, and the resulting solid was separated by centrifugation at 6000 rpm for 10 min, followed by filtration. The collected solid was thoroughly washed with deionized water multiple times to eliminate any remaining impurities from the reaction mixture, and it was then dried in an oven (Scheme A2.2).[26, 27] **Characterization of the compound:** solid-state FT-IR (cm^{-1}) = 1017 (s), 1111 (s), 1346 (s), 1493 (s), 1678 (s), 2913(br), 1118.2 (s), 3123 – 3240 (br) and 3337 (br).

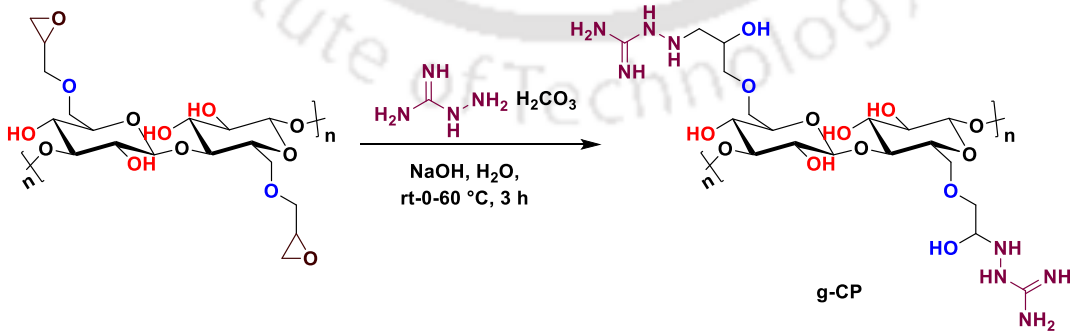

Scheme A2.2. Synthesis of guanidine functionalized cellulose polymer (g-CP).

2.5.2.3. Synthesis of Zn-gCP:

The gCP (0.2 g) was added into a stirring solution of $ZnCl_2.6H_2O$ (0.05 g) in water, and the reaction mixture was stirred at 100 °C for 12 h. Then the reaction mixture was centrifuged at 6000 rpm for 10 min, followed by filtration, and the precipitate was repeatedly washed off with deionized water. Finally, the solid part was oven-dried overnight at 70 °C to obtain Zn(II)-loaded aminated polymer (Scheme A2.3). **Characterization of the compound:** solid-state FT-IR (cm^{-1}) = 442 (br), 1017 (s), 1111 (s), 1346 (s), 1493 (s), 1678 (s), 2913 (br), 1118.2 (s), 3123 – 3240 (br) and 3337 (br).

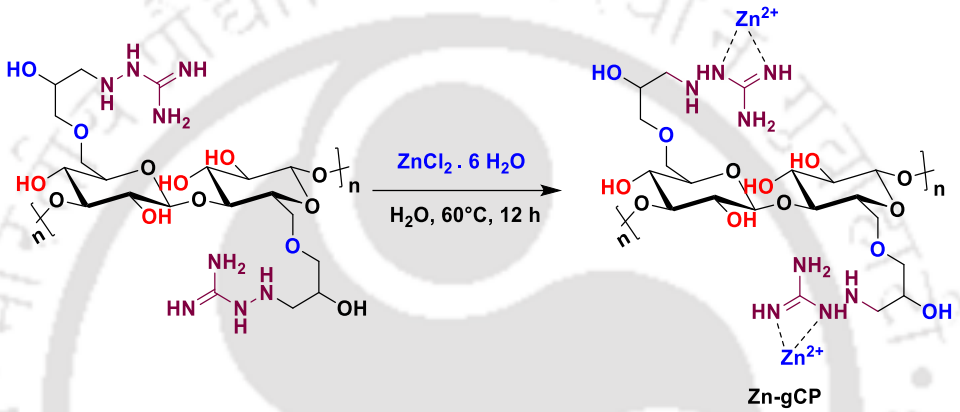

Scheme A2.3. Synthesis of Zn-complex-guanidine functionalised cellulose (Zn-gCP).

2.5.2.4. Fourier-Transform Infrared Spectroscopy (FT-IR) analysis:

The formation of the polymer was characterized by the FT-IR spectroscopic technique. The FT-IR spectra of all the samples were recorded using a Perkin Elmer instrument in attenuated total reflectance (ATR) mode over a range of 400 – 4000 cm^{-1}. In FT-IR spectra analysis, sharp peaks are denoted as "s," and broad peaks are marked as "br."

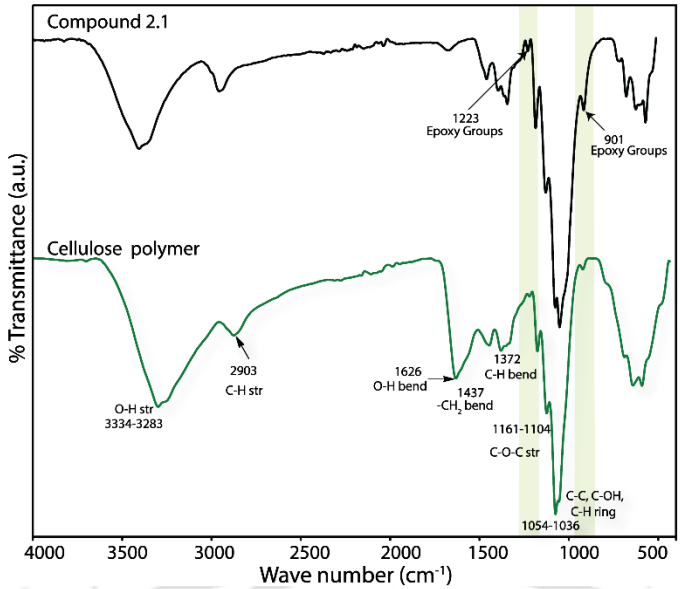

Figure A2.1. FT-IR of cellulose and compound 2.1.

2.5.2.5. X-Ray Photoelectron Spectroscopy (XPS) analysis:

XPS analyses were carried out on Thermo Fisher Scientific Instruments UK, Sr.No.- KAS2020, using an Aluminium Kα+ source to perform the elemental analysis as well as local bonding environments of all the tested samples. The samples were prepared using the drop casting dispersion method. The sample (< 0.5 mg) was dispersed in an aqueous solution (~1 mL) and deposited onto a silicon substrate, followed by incubation at room temperature to dry the sample before analysis.

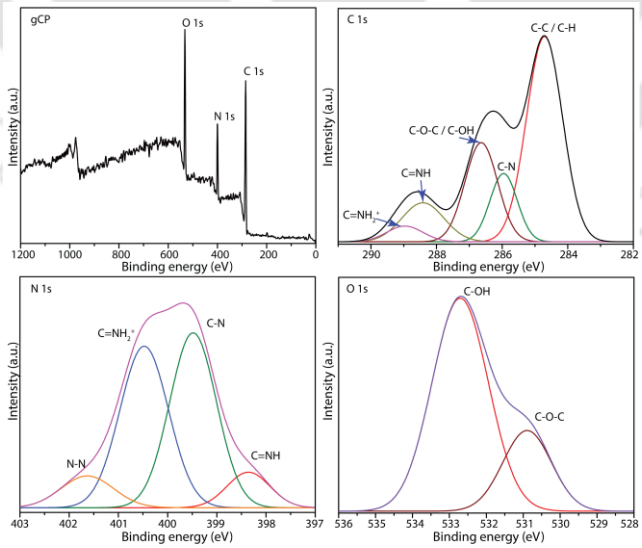

Figure A2.2. The XPS analysis of gCP polymers and XPS data profile: wide scan of gCP polymers, the deconvoluted peak of C 1s, N 1s, and O 1s.

2.5.2.6. Field Emission Scanning Electron Microscopy (FESEM) and FESEM – Energy Dispersive X-Ray Spectroscopy (FESEM-EDX) analysis:

FESEM images were taken with an OXFORD EDX FESEM instrument of the Zeiss Sigma 300 model at 3 kV to perform morphological analysis of all the tested samples. FESEM-EDX analysis was also carried out on the OXFORD EDX FESEM instrument of the Zeiss Sigma 300 model at 5 kV to determine the elemental composition of all the tested samples. For FESEM and FESEM-EDX analysis, the samples were prepared using the drop casting dispersion method as mentioned above.

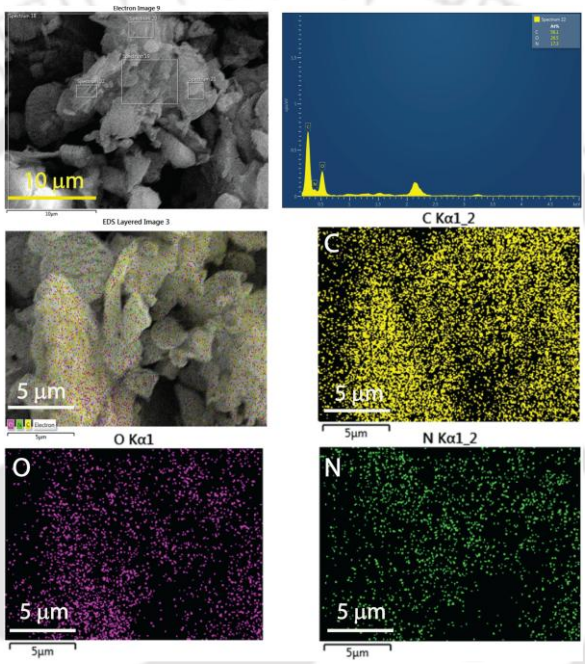

Figure A2.3. FESEM-EDX elemental mapping analysis of gCP polymer.

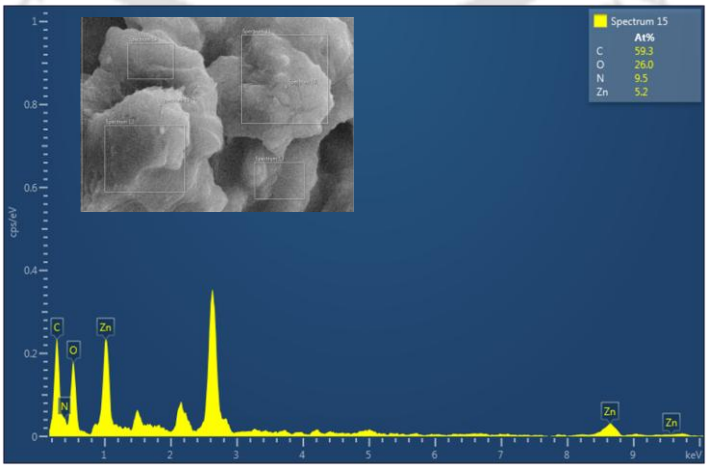

Figure A2.4. FESEM-EDX analysis of Zn-gCP polymer.

2.5.2.7. Thermogravimetric analysis (TGA):

Thermogravimetric analyses (TGA) were conducted on a Mettler-Toledo TG50 and SDT Q600 TG-DTA analyzer under an N_2 atmosphere by heating the samples (10 mg) from 20 °C to 900 °C, and the rate of heating was 10 °C min^{-1}.

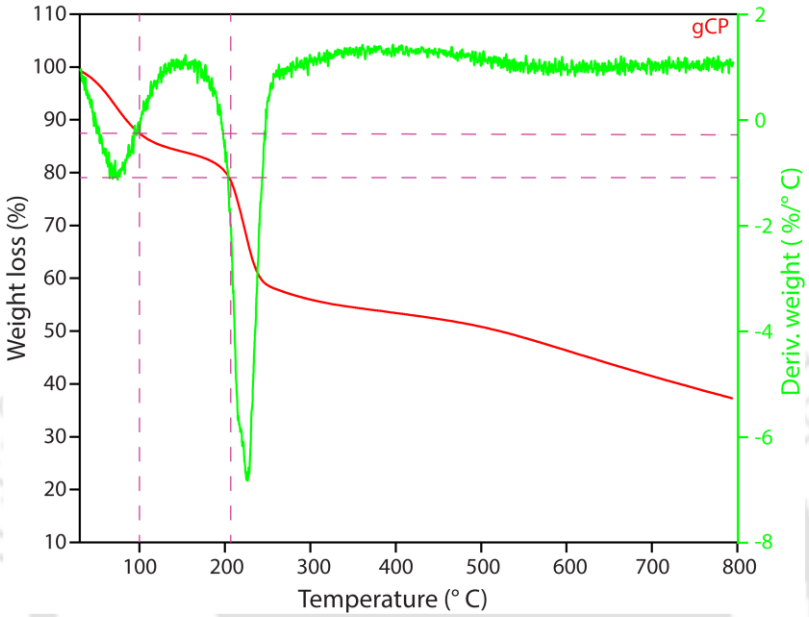

Figure A2.5. TGA-DTG plot of gCP polymer.

2.5.2.8. Dynamic light scattering (DLS) study:

The particle size of all the samples was measured through dynamic light scattering (DLS) measurement by utilizing the Zetasizer Nano ZS90 (Malvern, Westborough, MA) instrument. In order to perform DLS measurements, ≤ 0.5 mg of the polymers were mixed with 1 mL of Milli-Q water and then exposed to sonication for a period of 10 min. Subsequently, the hydrodynamic diameter was assessed at different time intervals (0 h, 12 h, 24 h, 36 h, and 72 h) at a temperature of 25 °C.

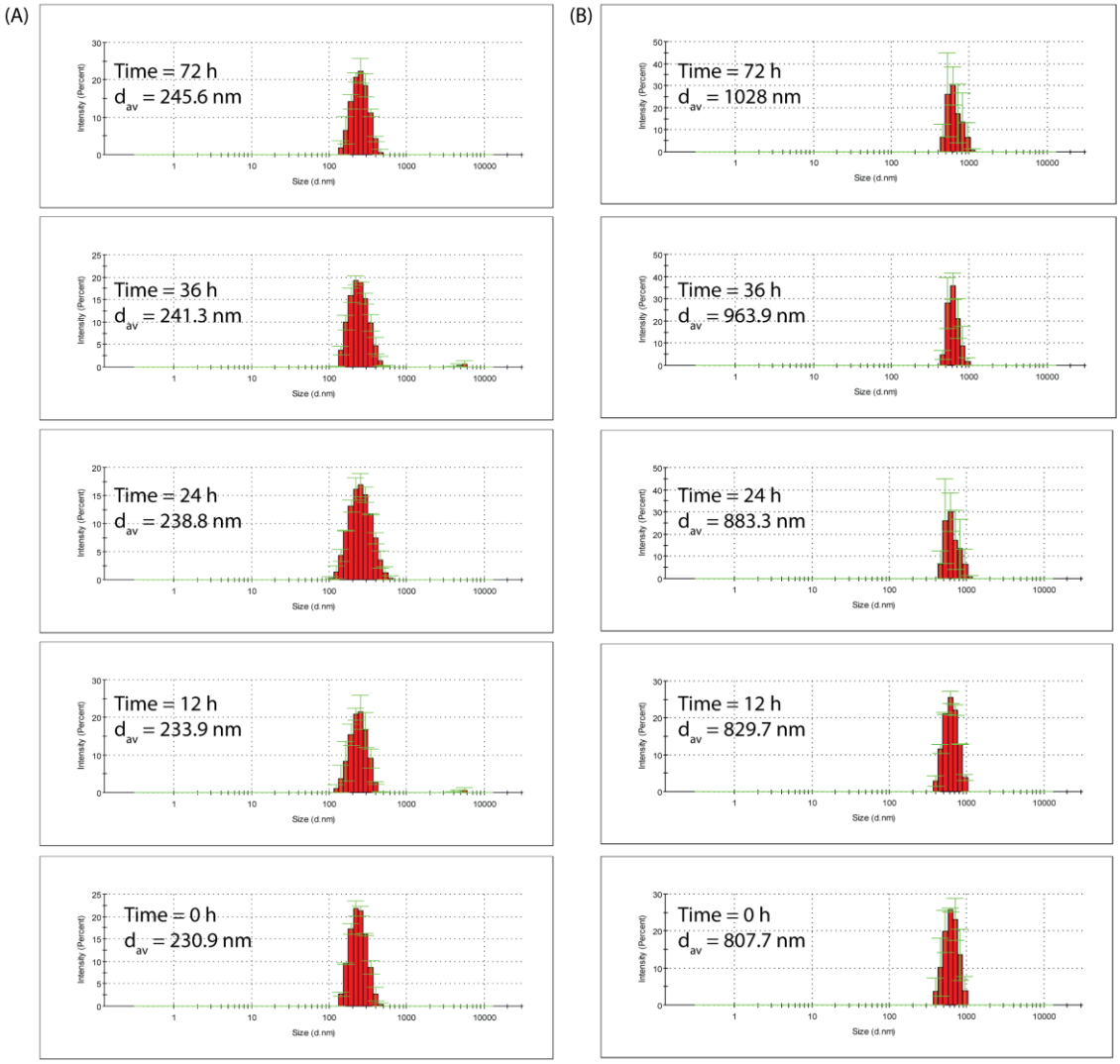

Figure A2.6. DLS measurements of unmodified cellulose (A) and Zn-gCP (B) in water at different time intervals.

2.5.2.9. Zeta potential study:

The zeta potential of all the samples was measured using the Anton Paar Litesizer DLS 500 instrument at 25 °C across a range of pH values (4, 5, 6, 7, 8, and 10). In this experiment, ≤ 0.5 mg of the polymers were mixed with 1 mL of Milli-Q water and then exposed to sonication for a period of 10 min before analysis. The pH of the solutions was adjusted by using 0.1 M HCl and 0.1 M NaOH solutions.

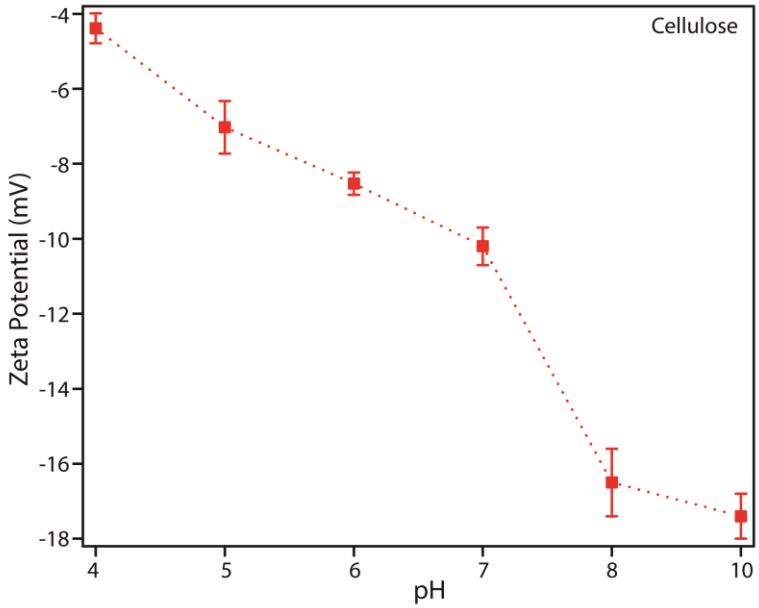

Figure A2.7. Zeta potential of the cellulose at different pH.

2.5.2.10. Chemical stability analysis of gCP and Zn-gCP polymers:

To assess the chemical stability of gCP and Zn-gCP polymers, 5 mg of each polymer was separately treated with 5 mL of common organic solvents, including acetonitrile (ACN), ethyl acetate (EtOAc), methanol (MeOH), and tetrahydrofuran (THF) for 7 days at room temperature. The polymers were then separated from the solvents by centrifugation at 6000 rpm for 10 min, followed by filtration, and dried in an oven at 70 °C for 6 h, followed by FT-IR analysis to examine their chemical stability. Additionally, to evaluate stability under acidic and basic conditions, 5 mg of each polymer was treated with 5 mL of HCl (0.5 N) and NaOH (0.5 N) for 7 days at room temperature. After this treatment, the polymers were separated by centrifugation (6000 rpm for 10 min) and dried under the same conditions, and their chemical stability was examined by FT-IR and TGA analysis.

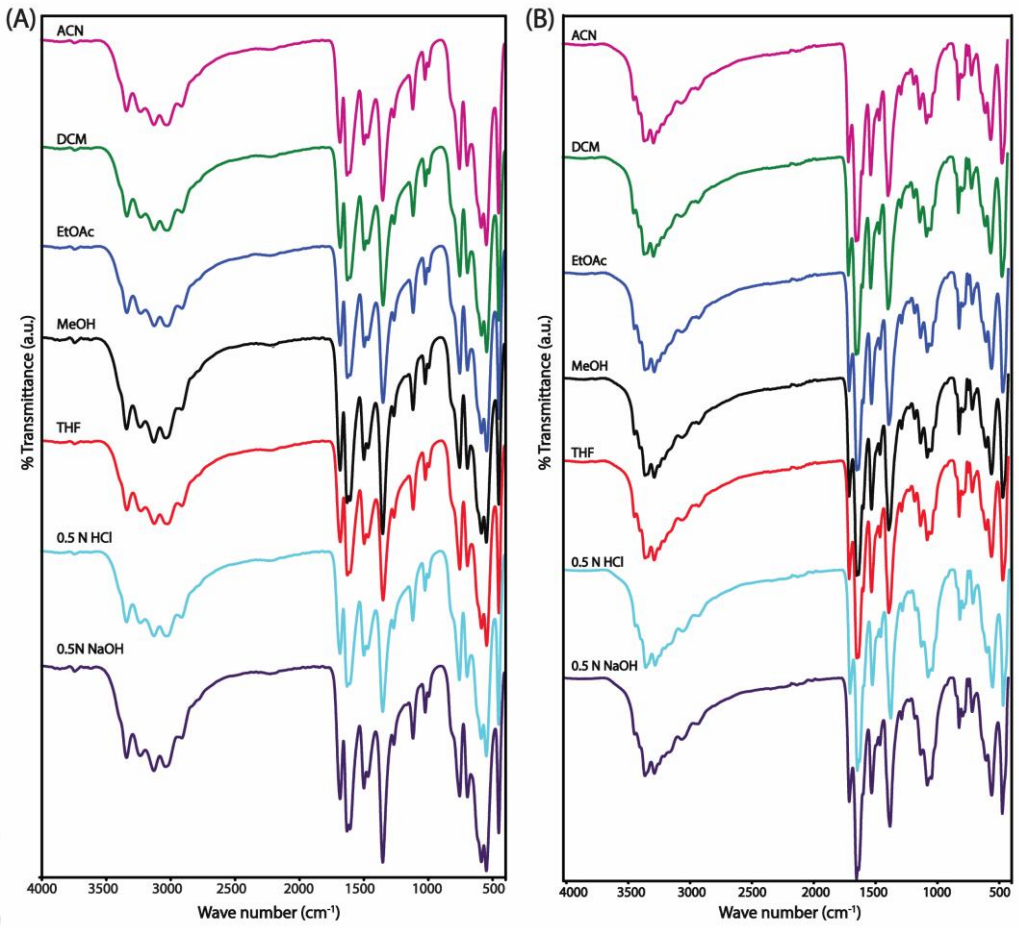

Figure A2.8. FT-IR spectra of gCP (A) and Zn-gCP (B) after the treatment (for 7 days) with ACN, DCM, EtOAc, MeOH, THF, DMF, HCl (0.5N), and NaOH (0.5N) solution.

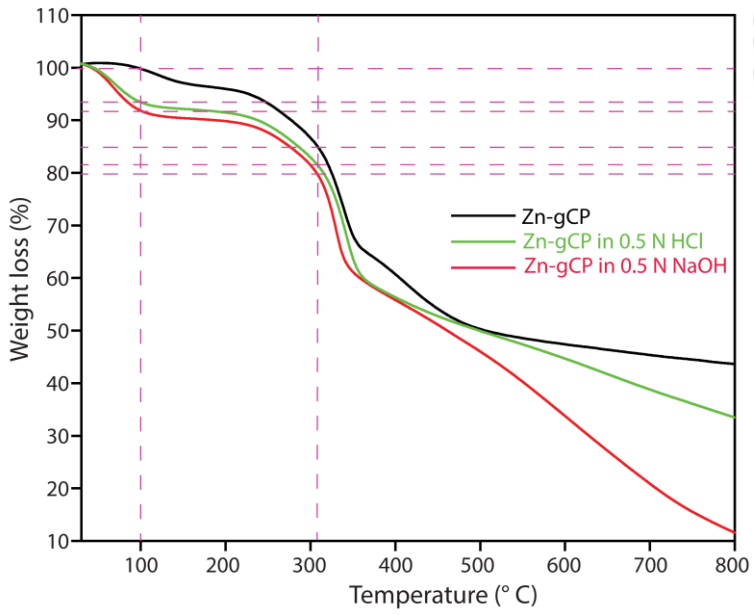

Figure A2.9. TGA plot of Zn-gCP polymer, Zn-gCP after treatment with 0.5 N HCl, and 0.5 N NaOH.

NOTE: After treatment of the Zn-gCP polymer with 0.5 N HCl for 7 days, there is a potential for the protonation of the guanidine -NH groups, which may weaken the Zn(II) coordination sites. Conversely, when the polymer is treated with 0.5 N NaOH for 7 days, the high concentration of OH^- ions could lead to the leaching of some Zn(II) ions from the polymer, forming complexes with OH^- ions. Hence, the weight loss against temperature differs in each case, but the maximum weight loss is observed at approximately the same temperature (~ 350 °C).

2.5.2.11. Tyndall effect:

In order to examine the Tyndall effect, a small quantity (<1mg) of the samples was mixed with deionized water (5 mL) and subjected to 5 min of sonication. Both the polymer solutions were then exposed to laser light source of wave length 640 – 660 nm and maximum output < 1mW, with a reference solution of normal deionized water serving as a control.

2.5.3. Equations employed for adsorption study –

2.5.3.1. Equation for the calculation of % ion adsorption:

To calculate the relative percentage of phosphate adsorption, the following equation has been used for calculation:

Percentage of adsorption,

$$Qad(\%) = \frac{(Co-Ce)}{Co} * 100\% \ldots \text{Eq. (2.1)}$$

Where *Qad(%)* is the relative percentage adsorption, C_0 and *Ce* is the concentration of anions in ppm (mg/L) before and after treatment of polymers, respectively.

2.5.3.2. Equation for the calculation of the adsorption capacity:

The adsorption capacity of Zn-gCP polymer was calculated by the following Eq. (2.2).

$$Q_e = \frac{(C_0-C_e)}{m} V\ n\ M \ldots \text{Eq. (2.2)}$$

Where, Q_e = equilibrium adsorption capacity (mg g^{-1}), Co = initial concentration (in ppm), C_e = equilibrium concentration (in ppm), V = volume of solution, m = amount of adsorbent (mg), n = dilution factor, and M = molecular weight of ion.

2.5.3.3. Equations to determine the adsorption isotherm:

To explore the adsorption patterns, Langmuir isotherm (Eq. (2.3)), and Freundlich isotherm models (Eq. (2.4)) were used to fit the adsorption data.

$$Q_e = \frac{Q_m K_l C_e}{1 + K_l C_e} \ldots \text{Eq. (2.3)}$$

$$Q_e = K_f C_e^{1/n} \ldots \text{Eq. (2.4)}$$

Where Ce is the equilibrium phosphate concentration (ppm), Q_e is the corresponding adsorption capacity (mg g^{-1}). The K_l is the Langmuir constant, and Q_m (mg g^{-1}) is the max adsorption capacity for the Langmuir model. The K_f and n are the Freundlich constant. For Freundlich adsorption isotherm, the K_f is associated with the adsorption capacity of the polymer. Whereas 1/n describes the extent of adsorption (favorable $1/n < 1$ or unfavorable $1/n > 2$).

2.5.3.4. Equations for the calculation of the adsorption kinetics:

To explore the sorption mechanism, the time-dependent adsorption data were fitted with both the linear (Eq. (2.5)) and non-linear (Eq. (2.6)) pseudo-first-order kinetics models, as well as the linear (Eq. (2.7)) and non-linear (Eq. (2.8)) pseudo-second-order kinetics models, as described below:

$$\ln(Q_e - Q_t) = lnQ_e - k_1 t \ \ldots \text{Eq. (2.5)}$$

$$Q_t = Q_e(1 - e^{-k_1 t}) \ldots \text{Eq. (2.6)}$$

$$\frac{t}{Q_t} = \frac{1}{Q_e^2 k_2} + \frac{t}{Q_e} \ldots \text{Eq. (2.7)}$$

$$Q_t = \frac{k_2 {Q_e}^2 t}{1 + k_2 Q_e t} \ldots \text{Eq. (2.8)}$$

Where Q_t and Q_e (mg g^{-1}) are the adsorption capacities of phosphate ions at time t and at equilibrium, respectively. The k_1 and k_2 (g mg min^{-1}) are the adsorption rate constants of the pseudo-first order and pseudo-second-order equations, respectively.

2.5.4. Anion selectivity study –

To determine anion selectivity by gCP and Zn-gCP polymer, a stock solution was prepared containing various anions from sodium salts (such as F^-, Cl^-, Br^-, NO_3^-, SO_4^{2-}, and phosphate) in Milli-Q water at ~25 ppm concentration for each ion. 5 mg of each polymer (gCP and Zn-gCP) were individually mixed with 5 mL of the stock solution and agitated for 12 h after that, the polymers were separated from the stoke solution by centrifugation at 6000 rpm for 10 min, followed by filtration. The IC was used to assess the concentration of anions before and after treatment of the polymer (gCP and Zn-gCP).

2.5.5. The affinity of the gCP and Zn-gCP towards chromate and dichromate ions –

5 mg of the gCP and Zn-gCP polymers was separately treated with 5 mL of ~25 ppm stock solutions of the sodium salts of chromate and dichromate. The mixtures were agitated for 6 hours at room temperature. Following that, the polymers were separated by centrifugation at 6000 rpm for 10 min, followed by filtration. The concentrations of chromate and dichromate ions before and after treatment were quantified using UV-Vis spectroscopy at 373 nm and 260 nm, respectively, using. The results revealed that the gCP and Zn-gCP polymers exhibited >20% and >30% removal efficacy of chromate, respectively, from the water. Similarly, the gCP and Zn-gCP polymers also manifest low removal efficacy, >17% and >25% of dichromate, respectively, under the same conditions.

2.5.6. The affinity of the gCP and Zn-gCP towards arsenate ions –

5 mg sample of the gCP and Zn-gCP polymers was separately treated with 5 mL of ~25 ppm stock solution of sodium arsenate and agitated for 6 hours at room temperature. The polymers were then separated from the reaction mixture by centrifugation at 6000 rpm for 10 min, followed by filtration. The concentration of arsenate in the solution before and after treatment was determined using Atomic Absorption Spectroscopy after diluting all samples 500-fold. The results indicated that the gCP and Zn-gCP polymers exhibited >43% and >59% removal efficacy of arsenate, respectively, from the stock solution.

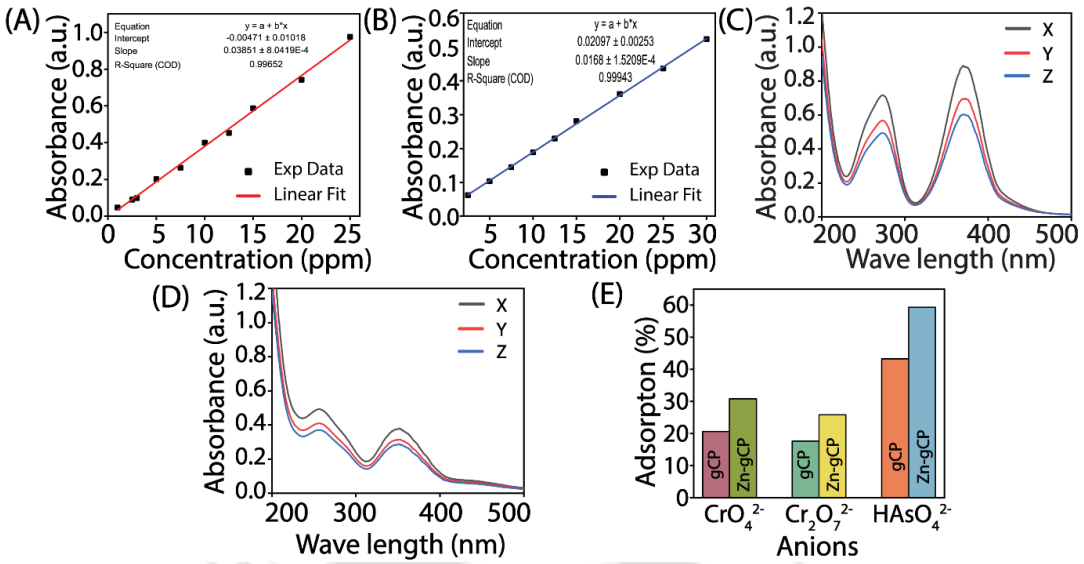

Figure A2.10. Standard calibration plot of the chromate (A), and dichromate (B) at different concentrations. UV-Vis spectra of stoke solution, after treatment with gCP and Zn-gCP polymer of chromate (C) and dichromate (D). Adsorption efficacy of gCP and Zn-gCP for chromate, dichromate and arsenate (E). (Note: X, Y, and Z are the absorbance of stoke solution, after treatment with gCP and Zn-gCP polymer respectively).

2.5.7. Phosphate adsorption experiments –

2.5.7.1. Influence of pH on phosphate capture:

To check the pH-dependency of phosphate adsorption by Zn-gCPs, seven different sets of pH values were selected for the adsorption experiments: pH 2, 4, 5, 6, 7, 8, and 10. The pH of the solutions was adjusted by HCl (0.1 M) and NaOH (0.1 M). The Zn-gCPs (5 mg) and 1000 ppm phosphate solutions (5 mL, pH = 2, 4, 5, 6, 7, 8, and 10) were mixed together and stirred at room temperature for 6 h. After that, samples were collected, and the polymers were separated by centrifugation at 6000 rpm for 10 min followed by filtration. The filtered supernatant was diluted to maintain the concentration of phosphate to 25 ppm, and an IC – based assay was performed in these solutions to measure the residual phosphate ions.

2.5.7.2. Adsorption isotherms study:

Different concentrations of phosphate ranging from 25 to 1000 ppm in 5 mL water were treated with a fixed quantity of (5 mg) gCP and Zn-gCP, and sonicated for 10 min to homogenize the polymer. Then, the samples were incubated at shaking condition for 6 h at room temperature. After that, the samples were centrifuged at

6000 rpm for 10 min and filtered to separate the phosphate-adsorbed Zn-gCP and unbound phosphate in the supernatant, which was further diluted up to 25 ppm and measured in IC.

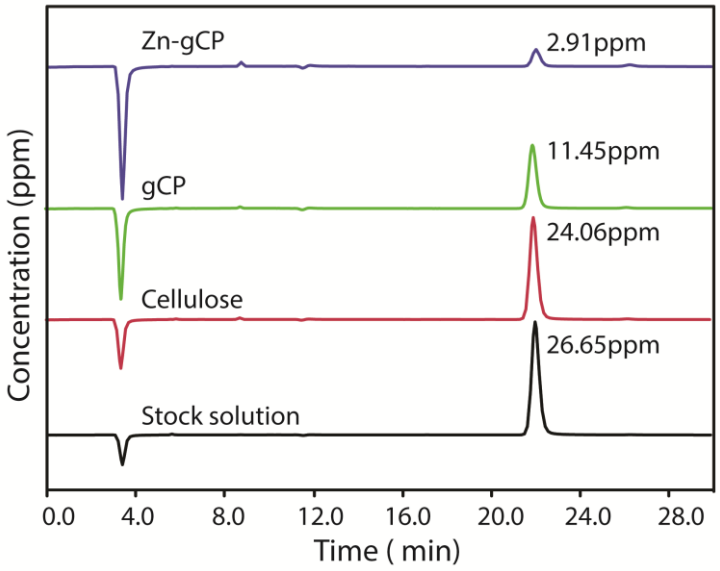

Figure A2.11. Phosphate adsorption efficacy of different polymers including cellulose, gCP and Zn-gCP polymer.

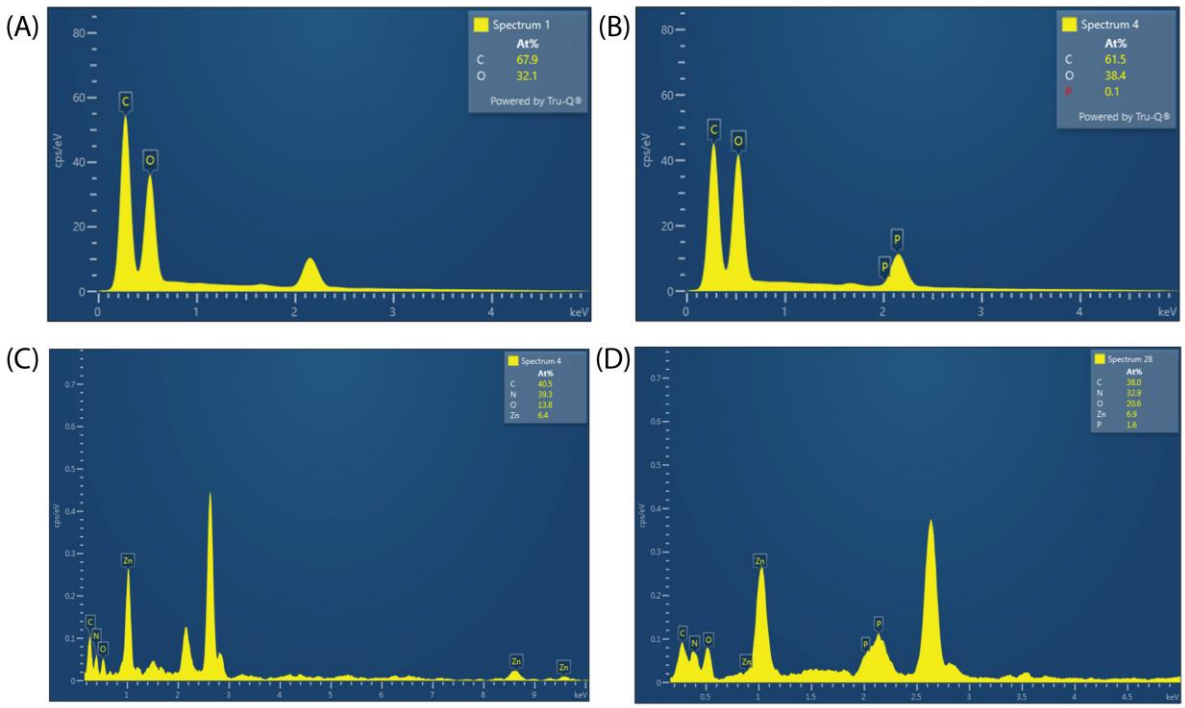

Figure A2.12. FESEM-EDX Elemental analysis of Unmodified cellulose before phosphate treatment (A), after phosphate treatment (B), Zn-gCP polymer before phosphate treatment (C), and after phosphate treatment (D).

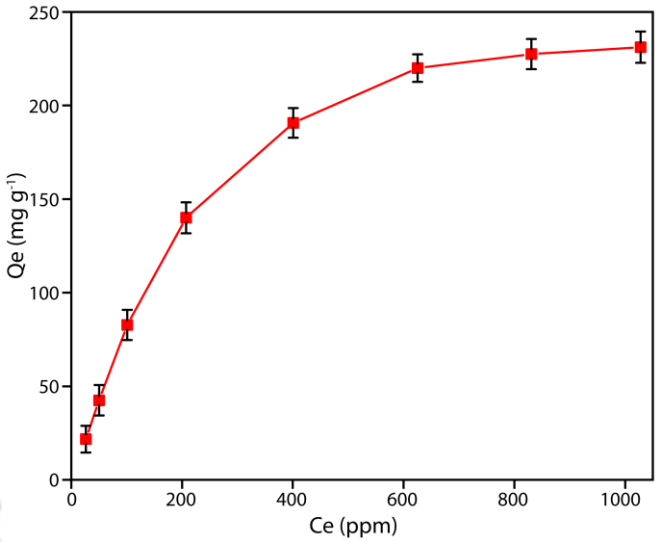

Figure A2.13. Phosphate adsorption isotherm of Zn-gCP (5 mg) at pH 7.0 under room temperature.

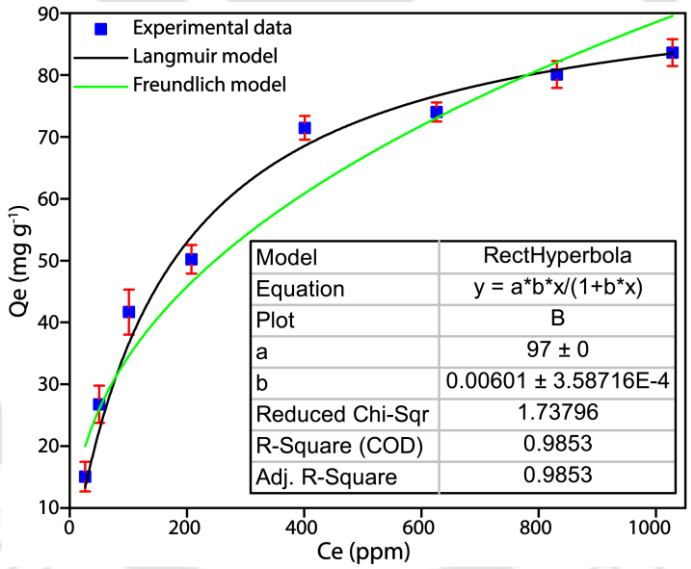

Figure A2.14. Phosphate adsorption isotherm of gCP (5 mg) at pH 7.0 under room temperature.

2.5.7.3. Adsorption kinetics study:

The phosphate adsorption kinetics onto gCP and Zn-gCP polymer over time were investigated by incubating the 5mg of the adsorbent (gCP and Zn-gCP) into 1000 ppm concentration of phosphate salt in Milli-Q water at pH ~7. At different time intervals (2, 4, 6, 8, 10, 20, 30, 40, and 60 min), samples were collected, and the polymers were separated by centrifugation at 6000 rpm for 10 min followed by

filtration. The filtered supernatant was diluted up to 40 times to achieve a phosphate concentration of 25 ppm, which was then quantified using IC.

Additionally, a kinetics study was conducted with different amounts of Zn-gCP polymer (3 mg, 5 mg, 7 mg, and 10 mg) under the same conditions. The polymer samples were subjected to incubation in a 1000 ppm phosphate salt solution in Milli-Q water at pH ~7, followed by sample collection at the aforementioned time intervals, and the polymers were separated by centrifugation at 6000 rpm for 10 min, followed by filtration. The filtered supernatant was diluted up to 40 times to achieve a phosphate concentration of 25 ppm, which was then quantified using IC.

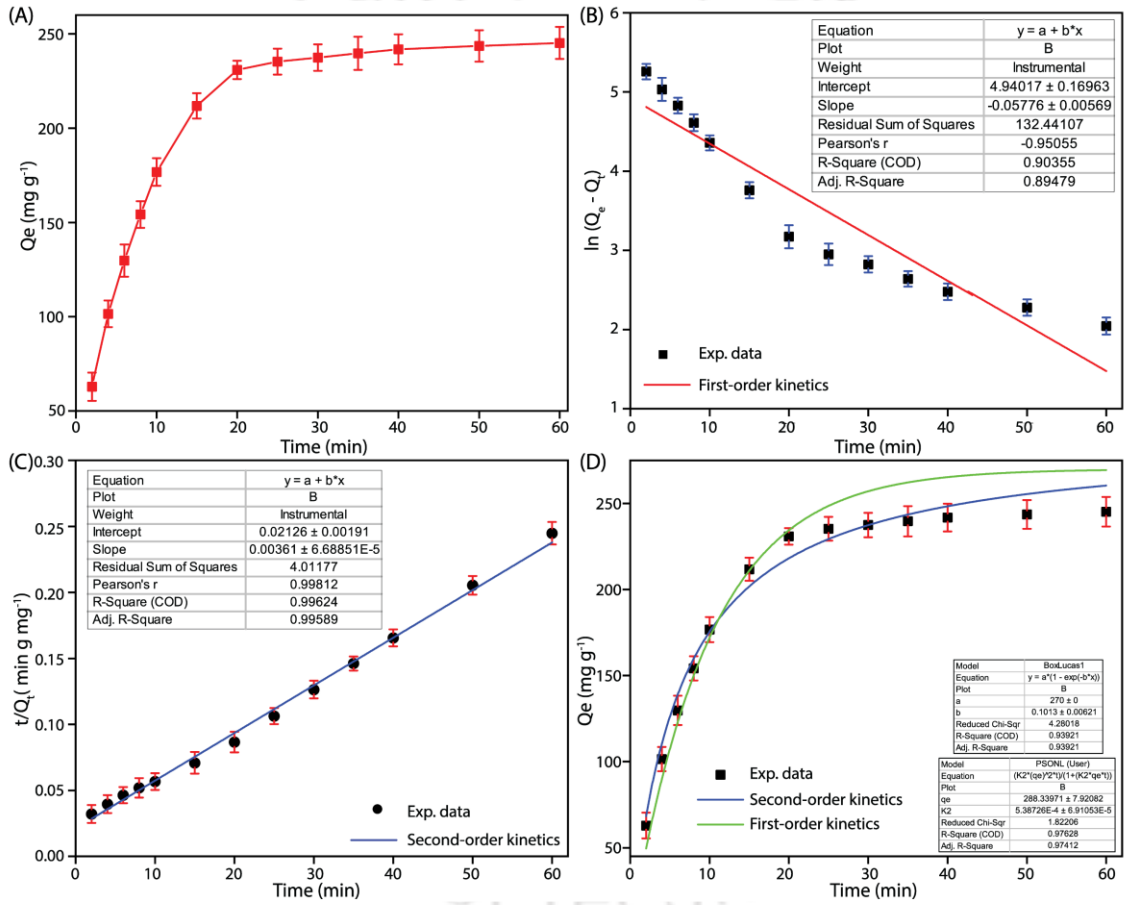

Figure A2.15. Time-dependent adsorption isotherm of phosphate by Zn-gCP (5mg) at pH 7 under room temperature(A), time-dependent adsorption efficiency of Zn-gCP (5 mg) fitted with the linear first order(B), linear second order (C), and non-linear first and second order kinetics model (D).

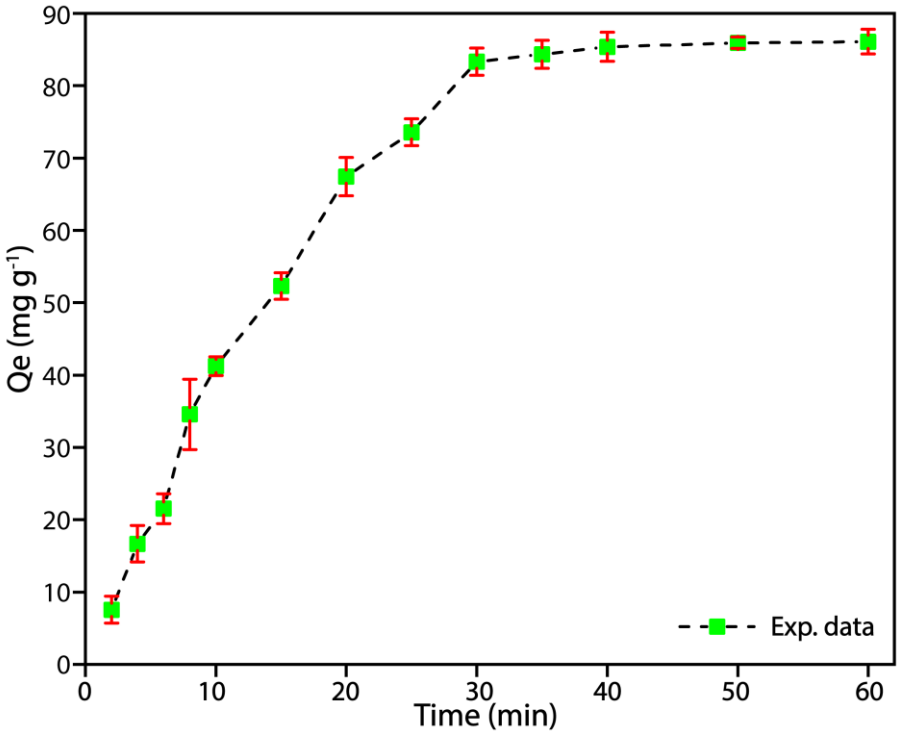

Figure A2.16. Time-dependent adsorption isotherm of phosphate by gCP (5mg) at pH 7 under room temperature.

2.5.7.4. Effect of counter anions on phosphate adsorption:

To assess the impact of competing anions on phosphate adsorption, stock solutions of several sodium salts (F^-, Cl^-, Br^-, NO_3^-, SO_4^{2-}, and phosphate) were prepared by dissolving them in Milli-Q water at a 1:2 concentration ratio (phosphate: other anions). The Zn-gCP polymer (5 mg) was mixed with 5 mL of the salt solution and agitated for 6 h after that, the polymers were separated from the stoke solution by centrifugation at 6000 rpm for 10 min, followed by filtration. The ability of the Zn-gCP polymer to adsorb phosphate ions in the presence of the other competing anions was assessed using IC.

Table A2.1: Phosphate removal efficacy of Zn-gCP in the presence of other anions.

Solutions	Initial concentration of Phosphate in presence of other anions (ppm)	Concentration of Phosphate in presence of other counter anions after treatment of with Zn-gCP (ppm)	% of removal of Phosphate in presence of other counter anions after the treatment with Zn-gCP
Only Phosphate	25.369 ± 0.045	0.490 ± 0.245	98.066 ± 0.484
Phosphate + F^-	26.480 ± 0.018	3.261 ± 0.325	87.685 ± 0.618
Phosphate + Cl^-	25.095 ± 0.033	2.121 ± 0.503	91.548 ± 1.007
Phosphate + Br^-	25.172 ± 0.051	1.488 ± 0.402	94.086 ± 0.804
Phosphate + NO_3^-	25.155 ± 0.032	3.678 ± 0.494	85.378 ± 0.992
Phosphate + SO_4^{2-}	26.005 ± 0.016	4.449 ± 0.658	82.890 ± 1.260
Phosphate + F^- + Cl^- + Br^- + NO_3^- + SO_4^{2-}	25.400 ± 0.014	5.460 ± 0.811	78.502 ± 1.602

2.5.7.5. Low-concentration of phosphate capture study:

To perform the experiment, 5 mg of the Zn-gCP polymer was treated with the phosphate solutions of volumes 50 mL at an initial concentration of 5 ppm and agitated for 6 hours. Following this, the polymer was separated from the solution via centrifugation at 6000 rpm for 10 min followed by filtration, and the concentrations of phosphate ion in the solution before and after treatment with the Zn-gCP polymer were measured using IC.

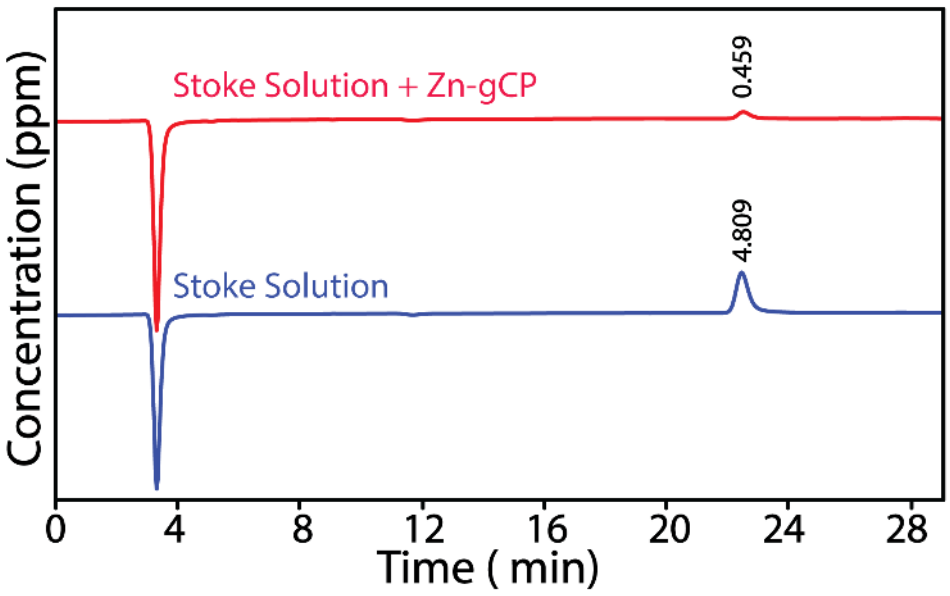

Figure A2.17. Low concentration phosphate ion adsorption study by Zn-gCP polymer.

2.5.7.6. Phosphate removal applicability with the real phosphate contaminated wastewater:

To evaluate the efficacy of Zn-gCP polymers in removing phosphate ions from real-world eutrophic water, two samples were collected from two different food manufacturing industries located in North Guwahati, Assam, India. The pH, ion concentrations, phosphate, and other coexisting species are all listed in Table A2.2. The Zn-gCP polymers (5 mg) were treated with 5 mL of each sample, and the mixture was constantly stirred for 6 h. IC was used to determine the anion concentration after centrifuging (6000 rpm for 10 min) and filtering the solution to remove the polymer. The study demonstrated that the Zn-gCP polymers successfully reduced phosphate ion concentration to below the WHO-recommended level for phosphate discharge, even in the presence of other coexisting anions. These results indicate that the synthesized Zn-gCP polymers could function as an effective adsorbent for removing phosphate from wastewater. The experiments were repeated three times, and the error bars in the figures represent the standard deviations of these three experiments.

Table A2.2. IC analysis demonstrating the concentrations of different competitive anions present before and after the treatment of Zn-gCP of samples A and B.

Sample	Existing anions (concentration in ppm)						pH
	F^-	Cl^-	Br^-	NO_3^-	Phosphate	SO_4^{2-}	
Sample A	1.161 ± 0.071	13.028 ± 0.031	0.307 ± 0.047	3.954 ± 0.05	8.012 ± 0.117	11.077 ± 0.077	5.6
After Zn-gCP treatment of sample A (A′)	1.002 ± 0.051	11.105 ± 0.022	0.247 ± 0.041	3.067 ± 0.036	0.419 ± 0.053	8.719 ± 0.057	
Sample B	1.61 ± 0.039	14.69 ± 0.061	0.271 ± 0.05	3.041 ± 0.029	6.971 ± 0.103	10.22 ± 0.063	6.1
After Zn-gCP treatment of sample B (B′)	0.297 ± .02	12.091 ± .04	0.190 ± 0.032	2.876 ± 0.022	0.398 ± 0.069	7.374 ± 0.053	

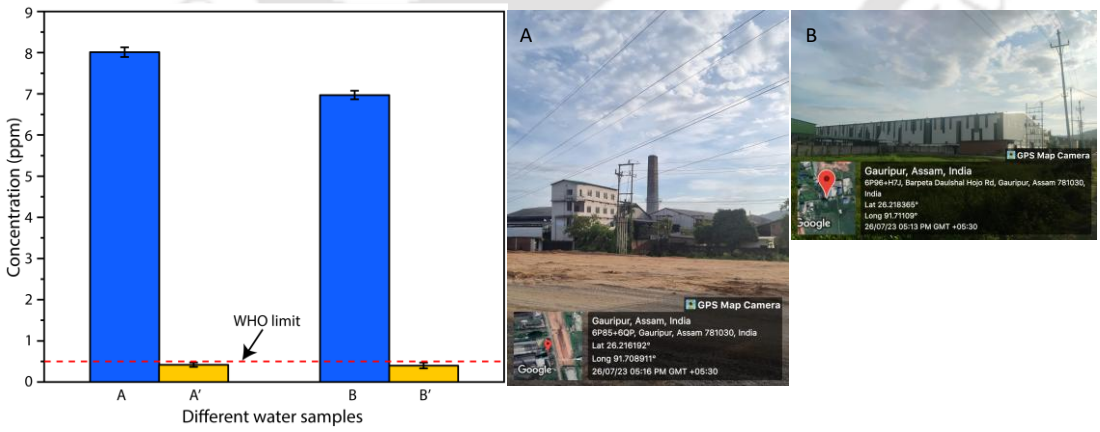

Figure A2.18. Phosphate adsorption capacity of the Zn-gCPs from the real phosphate-contaminated wastewater.

2.5.7.7. Phosphate recovery and regeneration of the Zn-gCP:

The adsorption percentage for each cycle was calculated using Equation 2.9, while the desorption efficiency for each cycle was calculated using Equation 2.10. The adsorption percentage for each cycle was calculated by taking the equilibrium adsorption capacity (Q_o) of the first cycle as 100% and the adsorption percentage of subsequent cycles expressed relative to this reference value. Conversely, the desorption percentage for each cycle was calculated considering the corresponding equilibrium adsorption capacity (Q_e) for that cycle as 100%.)

$$Qad(\%) = \frac{Qe}{Qo} * 100\% \ldots \text{Eq. (2.9)}$$

$$Qde(\%) = \frac{Qi}{Qe} * 100\% \ldots \text{Eq. (2.10)}$$

Where Q_{ad} (%) and Q_{de} (%) is the relative percentage adsorption and desorption respectively. Q_o is the equilibrium phosphate adsorption capacity in the first adsorption cycle. Q_e, is the equilibrium phosphate adsorption capacity in each adsorption cycle. Q_i is the equilibrium phosphate desorption capacity in each desorption cycle.

After undergoing the 1st, 5th, and 10th desorption cycles, the concentration of Zn(II) ions in the solution was quantified using Inductively Coupled Plasma Mass Spectrometry (ICP-MS). This analysis was conducted to evaluate the leaching of Zn(II) ions from the polymer network over multiple desorption cycles, providing insights into the stability and retention of Zn(II) within the polymer matrix.

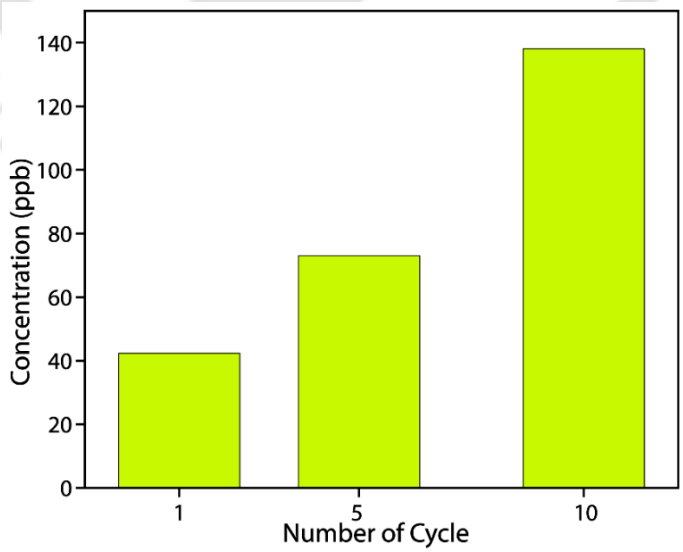

Figure A2.19. Concentration of Zn(II) in the solution after undergoing 1st , 5th and 10th cycle of desorption.

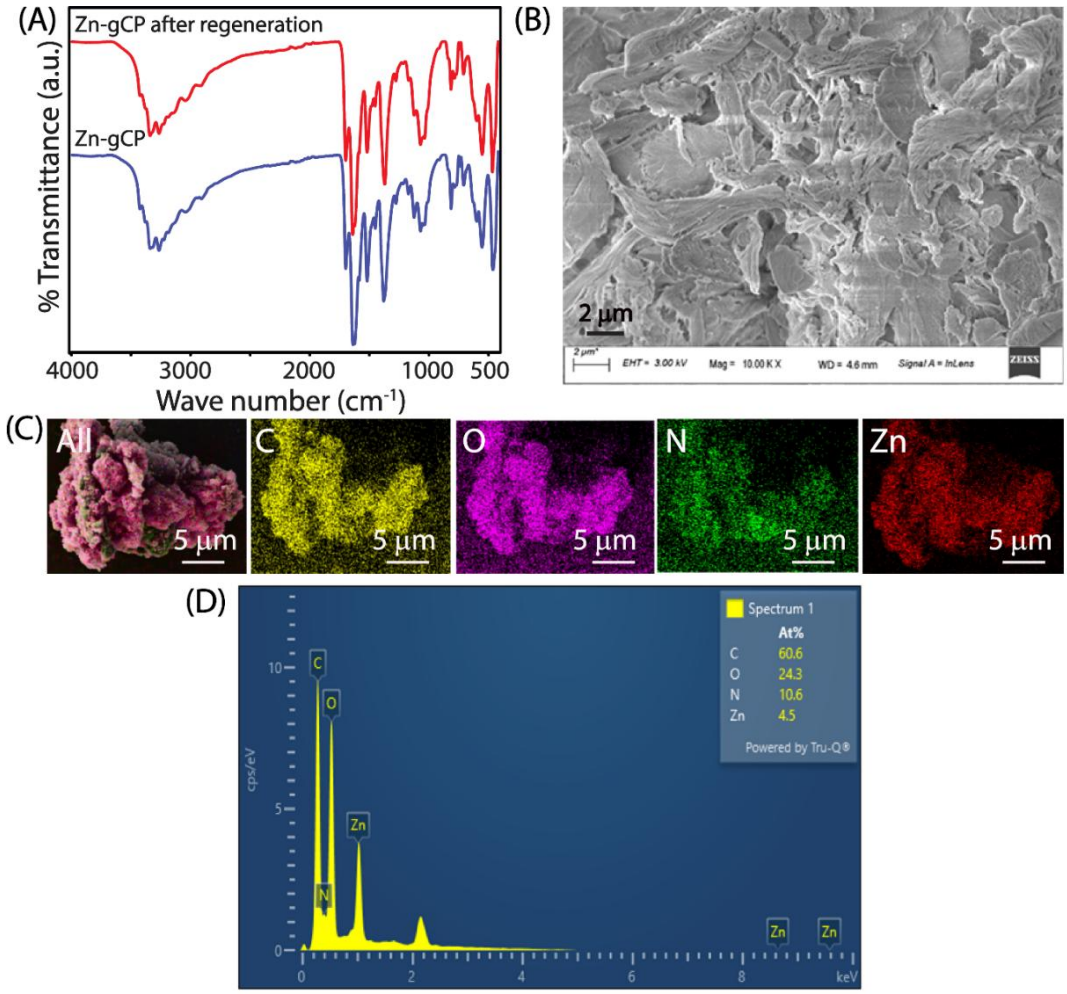

Figure A2.20. FTIR spectra (A), FESEM image (B), FESEM-Elemental mapping (C) and FESEM-EDX analysis (D) of Zn-gCP after undergoing ten cycles of regeneration.

2.5.7.8. Phosphate desorption kinetics study:

To study the desorption of phosphate from the Zn-gCP polymer, first the phosphate-loaded polymers (5 mg) were mixed with 5 mL of 0.5 N NaOH (pH ~13), and the solution was continuously stirred by an orbital shaker incubator (LabTech) at 180 rpm and 25 ^{0}C. At different time intervals (2, 4, 6, 8, 10, 20, 30, 40, and 60 min), samples were collected, and the polymers were separated by centrifugation at 6000 rpm for 10 min, followed by filtration. The filtered supernatant was diluted 10 times to maintain the concentration of phosphate to 25 ppm and quantified by IC.

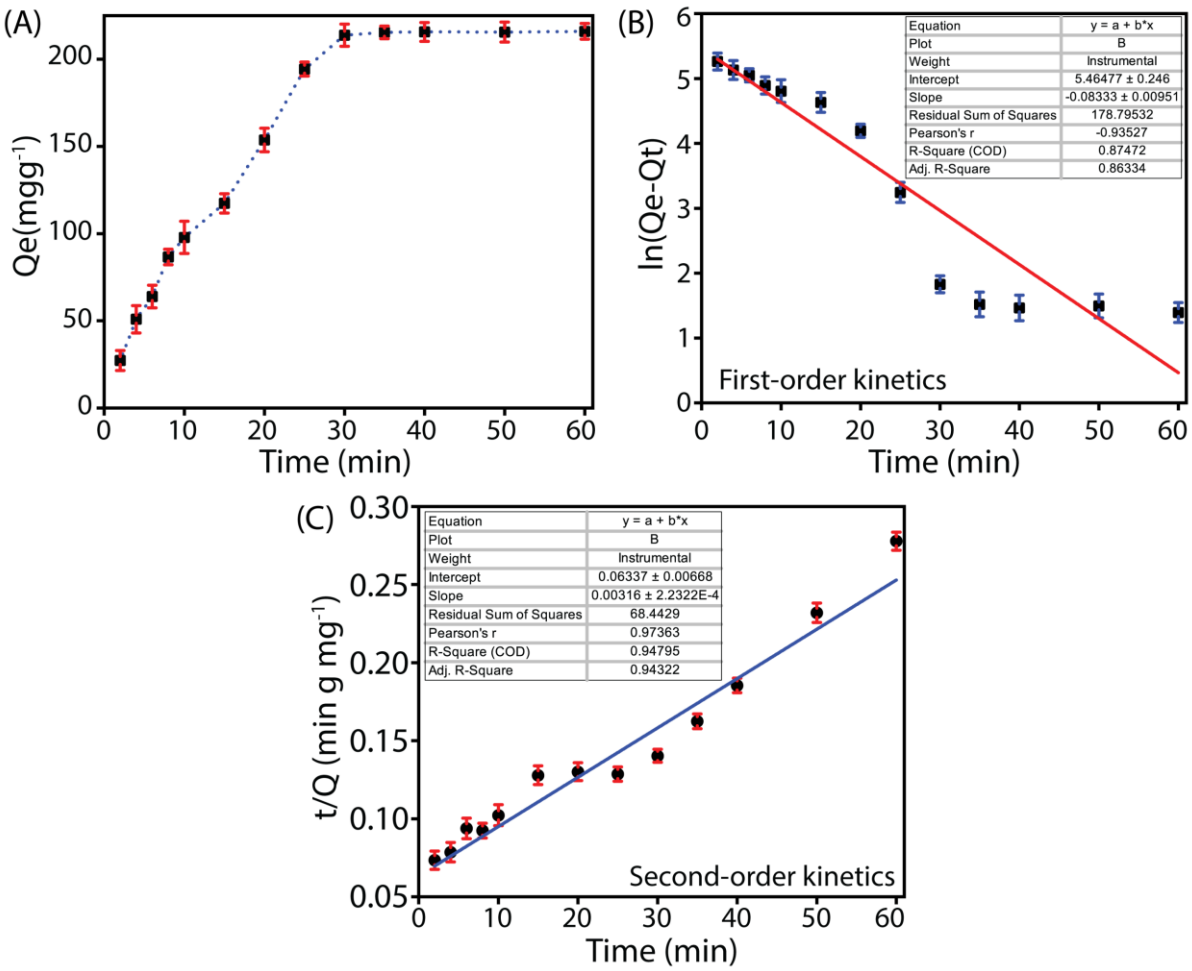

Figure A2.21. Time-dependent desorption isotherm of phosphate by Zn-gCP (5mg) at pH 7 under room temperature(A), time-dependent desorption efficiency of Zn-gCP fitted with the first order(B) and second order kinetics(C) models.

2.5.7.9. Phosphate desorption kinetics study with different amounts of phosphate loaded Zn-gCP polymer:

Phosphate desorption tendency from Zn-gCP as per time was analysed by incubating the different amounts of the phosphate loaded Zn-gCP polymer (3 mg, 5 mg, 7 mg, 10 mg) into 5 mL of 0.5 N NaOH (pH 11.5). At different time intervals (2, 4, 6, 8, 10, 20, 30, 40, and 60 min), samples were collected, and the polymers were separated by centrifugation followed by filtration. The filtered supernatant was diluted to maintain the phosphate concentration to 25 ppm and quantified by IC.

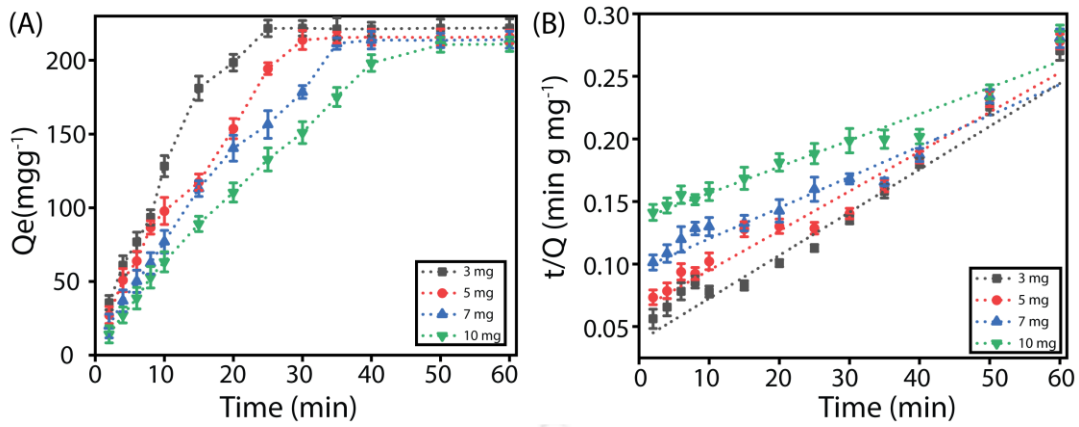

Figure A2.22. Time-dependent desorption isotherm of phosphate ions by Zn-gCP polymer (3–10 mg) at pH 7.0 at room temperature (A), pseudo-second-order kinetics curves of phosphate desorption on Zn-gCP (3,5,7, and 10mg) at pH 7.0 under room temperature (B).

2.5.7.10. Advantages of Zn-gCP compared to other reported biomaterials:

Zn-gCP, was synthesized via a three-step synthetic process. Initially, cellulose was modified with epichlorohydrin to produce the epoxy-functionalized compound 2.1. Cellulose, being a biomaterial, does not pose any significant environmental impact. Epichlorohydrin, on the other hand, is widely used in water treatment processes for the preparation of ion-exchange resins and various bio-adsorbents. The primary product of this reaction is compound 2.1, which serves as an intermediate for the synthesis of numerous water treatment adsorbents already documented in the literature. In the second step, the compound 2.1 reacted with 1-aminoguanidine, providing the guanidine-functionalized cellulose, gCP. 1-aminoguanidine is known for its various biomedical applications, including its antioxidant and antimicrobial properties, which could be advantageous for water disinfection. Finally, gCP reacted with Zn(II) salt (25% w/w) to produce the Zn-gCP polymer. Zinc is renowned for its antimicrobial properties and its strong affinity for phosphate ions. All the chemicals used for synthesizing the Zn-gCP polymer are environmentally friendly and highly cost-effective. In contrast, most reported biomaterials utilize lanthanide-based metal oxides and/ or zirconium-based metal oxides for phosphate removal from aqueous solutions, which are not only significantly more expensive but also pose severe environmental hazards as compared to zinc. Both the lanthanide and zirconium-based metal ions are notably

costlier and more toxic due to their lack of biological roles, environmental persistence, and interference with essential biological processes.

2.5.7.11. Dynamic adsorption column experiment:

A glass column of diameter ~ 0.5 cm was packed with a mixture of 50 mg of the Zn-gCP polymer and 3 g of sand with a bed length ~ 5 cm for the dynamic adsorption column experiment. Initially, 50 mL of ultrapure milli-Q water was passed through the column bed to eliminate any bubbles present. After that, 500 mL of the 50-ppm aqueous phosphate solution, along with 2 times excess the concentration of other anions (F^-, Cl^-, Br^-, NO_3^-, and SO_4^{2-}), was passed through the column bed with a flow rate of 0.5 mL/min following an equilibration time of 10 min. The eluents from the column were collected in 10 separate 50 mL batches, and the concentration of oxoanions in each batch was determined using IC. Observations revealed that up to 250 mL of the column eluent had phosphate concentrations lower than those recommended by the WHO in the first cycle. The column was rejuvenated by adding 100 mL of a NaOH (0.5 N) solution before moving on to the next cycle. Observations from the IC experiment revealed that over 93% of the phosphate was efficiently desorbed from the polymer through this procedure in the first cycle. The experiment was replicated up to 3 cycles, and the IC results consistently demonstrated that up to 200 – 250 mL of eluent from the column had phosphate concentrations below the WHO recommended threshold and efficiently removed over 85% of the phosphate from the Zn-gCP polymer after the third cycle (Figure A2.23).

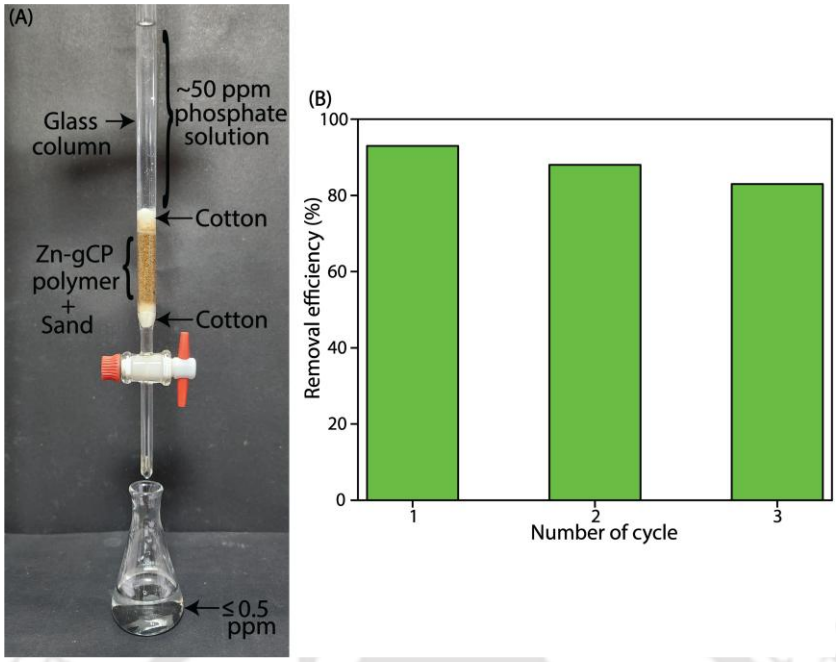

Figure A2.23. Digital image for dynamic adsorption column experiment (A). Phosphate ions desorption efficiency (%) of Zn-gCP polymer in adsorption column experiment (B).

2.5.8. Antibacterial activities of the Zn-gCP polymer –

2.5.8.1. Microbicidal efficacy of the polymers:

Antimicrobial activity of the polymers was tested against Gram-negative (*Escherichia coli*, MTCC 1687) and Gram-positive (*Staphylococcus aureus*, MTCC 96) bacteria. Glycerol stock of the bacterial strain was cultured on to agar media supplemented with Luria Bertani (LB) nutrient media at 37 °C. Single colony of the bacterial strain was cultured in broth media and grown till mid logarithmic phase in a shaker incubator at 37 °C, 180 rpm. The stock solution of the polymer was prepared in Milli-Q water with a concentration of 500 µg/mL for *Staphylococcus aureus* and 1500 µg/mL for *Escherichia coli*. The solution was then subjected to sonication and subsequently underwent serial dilution in a 96 well plate. The solution exhibits a reddish-brown colour, which can be attributed to the inherent coloration of the polymer (gCP in A, Zn-gCP in B, and Zn-gCP-P in C), which eventually diminished with dilution of the polymer solution. Bacterial culture was harvested by centrifugation and added to the 96 well plate containing the serially diluted polymers at 10^6 CFU/mL. The plate was incubated at 37 °C for 4 to 6 h. After that, 10 µL polymer treated culture was transferred to the fresh broth media (A to A′ in case of gCP

polymer, B to B′ in case of Zn-gCP polymer, C to C′ in case of Zn-gCP-P polymer, and D to D′ in case of unmodified cellulose polymer), and the plate was again incubated at 37 °C for 14 to 16 h. Due to the transfer of only 10 µL into the fresh media (190 µL), the media did not acquire the coloration of the compound as observed in the A′ (gCP), B′ (ZN-gCP), and C′ (Zn-gCP-P) samples. The bacterial growth was visually observed or measuring the optical density at 600 nm. The experimental results demonstrated that at a 250 µg/mL concentration, the gCP polymer showed bactericidal activity against *S. aureus*. In comparison, at 125 µg/mL concentration, both the Zn-gCP and Zn-gCP-P polymers indicated bactericidal activity against *S. aureus*. The gCP polymer displayed bactericidal activity against *E. coli* at 375 µg/mL, whereas the Zn-gCP and Zn-gCP-P polymers did so at a concentration of 187.5 µg/mL. However, it was evident from the experiment that unmodified cellulose did not exhibit bactericidal activity against both *S. aureus* and *E. coli*.[42, 43]

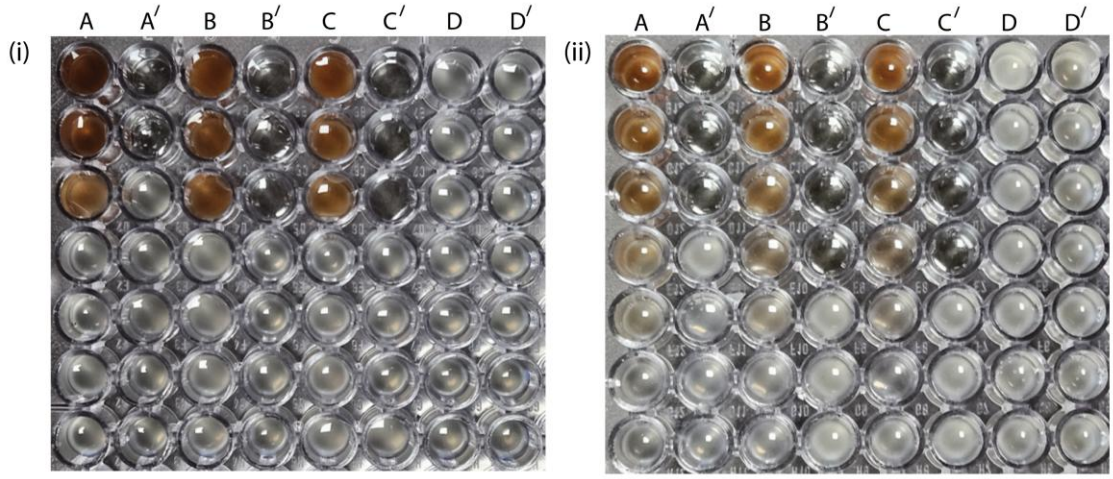

Figure A2.24. Bactericidal activity of the polymers (gCP, Zn-gCP, ZN-gCP-P, and unmodified cellulose) against *S. aureus* (i) and *E. coli* (ii). A, B, C, and D in the figure represents gCP, Zn-gCP, Zn-gCP-P, and unmodified cellulose respectively in initial antibacterial study. Whereas A′, B′, C′, and D′ represents the same after transferring the 10 µL of the compounds from A, B, C, and D respectively in fresh media for further study.

2.5.8.2. Morphological analysis of the polymer-treated bacterial cells:

The *S. aureus* bacterial cells were cultured as mentioned in the above section. Bacterial cells were treated with the polymers and incubated at 37 °C, 180 rpm. Cells were harvested by centrifugation and suspended in the buffer. Cells were fixed with

3 % glutaraldehyde and kept for 30 min and washed with Milli-Q and mounted on to glass grid. After drying the sample under laminar airflow, it was stacked onto a FESEM grid and coated with gold. Morphology was analysed at different magnifications under the microscope.

2.5.8.3. Microbicidal activity against real water sample:

To analyze the application of microbicidal polymer the water sample was collected from IITG lake and treated with the polymers at a concentration of 0.25 mg/mL. For control water sample without treatment was also taken, and all the samples were shaken for 6 h at room temperature. Water samples were plated onto agar nutrient LB media, and the plate was incubated for 16 to 20 h at 37 °C. The growth of the microbes was analyzed on the plate after the incubation.

2.6. References

1. Neal, J. F.; Zhao, W.; Grooms, A. J.; Smeltzer, M. A.; Shook, B. M.; Flood, A. H.; Allen, H. C., Interfacial supramolecular structures of amphiphilic receptors drive aqueous phosphate recognition. *J. Am. Chem. Soc.* **2019,** *141* (19), 7876-7886.
2. Xia, W.-J.; Guo, L.-X.; Yu, L.-Q.; Zhang, Q.; Xiong, J.-R.; Zhu, X.-Y.; Wang, X.-C.; Huang, B.-C.; Jin, R.-C., Phosphorus removal from diluted wastewaters using a La/C nanocomposite-doped membrane with adsorption-filtration dual functions. *Chem. Eng. J.* **2021,** *405*, 126924.
3. Dey, S.; Das, S.; Patel, A.; Raj, K. V.; Vanka, K.; Manna, D., Antimicrobial two-dimensional covalent organic nanosheets (2D-CONs) for the fast and highly efficient capture and recovery of phosphate ions from water. *J. Mater. Chem. A* **2022,** *10* (9), 4585-4593.
4. Hassan, M. H.; Stanton, R.; Secora, J.; Trivedi, D. J.; Andreescu, S.; Interfaces, Ultrafast removal of phosphate from eutrophic waters using a cerium-based metal–organic framework. *ACS Appl. Mater. Interfaces* **2020,** *12* (47), 52788-52796.
5. Desmidt, E.; Ghyselbrecht, K.; Zhang, Y.; Pinoy, L.; Van der Bruggen, B.; Verstraete, W.; Rabaey, K.; Meesschaert, B., Global phosphorus scarcity and full-scale P-recovery techniques: a review. *Crit. Rev. Environ. Sci. Technol.* **2015,** *45* (4), 336-384.
6. Oehmen, A.; Lemos, P. C.; Carvalho, G.; Yuan, Z.; Keller, J.; Blackall, L. L.; Reis, M. A., Advances in enhanced biological phosphorus removal: from micro to macro scale. *Water Res.* **2007,** *41* (11), 2271-2300.
7. Di Capua, F.; de Sario, S.; Ferraro, A.; Petrella, A.; Race, M.; Pirozzi, F.; Fratino, U.; Spasiano, D., Phosphorous removal and recovery from urban wastewater: Current practices and new directions. Sci. Total Environ. **2022,** *823*, 153750.
8. Pan, B.; Han, F.; Nie, G.; Wu, B.; He, K.; Lu, L., New strategy to enhance phosphate removal from water by hydrous manganese oxide. *Environ. Sci. Technol.* **2014,** *48* (9), 5101-5107.
9. Huang, W.; Zhu, Y.; Tang, J.; Yu, X.; Wang, X.; Li, D.; Zhang, Y., Lanthanum-doped ordered mesoporous hollow silica spheres as novel adsorbents for efficient phosphate removal. *J. Mater. Chem. A* **2014,** *2* (23), 8839-8848.

10. Nakamura, S.; Amano, M.; Saegusa, Y.; Sato, T., Preparation of aminoalkyl celluloses and their adsorption and desorption of heavy metal ions. *J. Appl. Polym. Sci.* **1992,** *45* (2), 265-271.
11. Orlando, U.; Okuda, T.; Baes, A.; Nishijima, W.; Okada, M., Chemical properties of anion-exchangers prepared from waste natural materials. *React. Funct. Polym.* **2003,** *55* (3), 311-318.
12. Gong, R.; Ding, Y.; Li, M.; Yang, C.; Liu, H.; Sun, Y., Utilization of powdered peanut hull as biosorbent for removal of anionic dyes from aqueous solution. *Dyes Pigm.* **2005,** *64* (3), 187-192.
13. Robinson, T.; Chandran, B.; Nigam, P., Removal of dyes from a synthetic textile dye effluent by biosorption on apple pomace and wheat straw. *Water Res.* **2002,** *36* (11), 2824-2830.
14. Ajmal, M.; Khan, A. H.; Ahmad, S.; Ahmad, A., Role of sawdust in the removal of copper (II) from industrial wastes. *Water Res.* **1998,** *32* (10), 3085-3091.
15. Manju, G.; Raji, C.; Anirudhan, T., Evaluation of coconut husk carbon for the removal of arsenic from water. *Water Res.* **1998,** *32* (10), 3062-3070.
16. Orlando, U.; Baes, A.; Nishijima, W.; Okada, M., Preparation of agricultural residue anion exchangers and its nitrate maximum adsorption capacity. *Chemosphere* **2002,** *48* (10), 1041-1046.
17. Anirudhan, T.; Unnithan, M. R., Arsenic (V) removal from aqueous solutions using an anion exchanger derived from coconut coir pith and its recovery. *Chemosphere* **2007,** *66* (1), 60-66.
18. Gao, B.-Y.; Xu, X.; Wang, Y.; Yue, Q.-Y.; Xu, X.-M., Preparation and characteristics of quaternary amino anion exchanger from wheat residue. *J. Hazard. Mater.* **2009,** *165* (1-3), 461-468.
19. Qiu, H.; Liang, C.; Zhang, X.; Chen, M.; Zhao, Y.; Tao, T.; Xu, Z.; Liu, G., Fabrication of a biomass-based hydrous zirconium oxide nanocomposite for preferable phosphate removal and recovery. *ACS Appl. Mater. Interfaces* **2015,** *7* (37), 20835-20844.
20. Qiu, H.; Liang, C.; Yu, J.; Zhang, Q.; Song, M.; Chen, F., Preferable phosphate sequestration by nano-La (III)(hydr) oxides modified wheat straw with excellent properties in regeneration. *Chem. Eng. J.* **2017,** *315*, 345-354.
21. Zhang, B.; Chen, N.; Feng, C.; Zhang, Z., Adsorption for phosphate by crosslinked/non-crosslinked-chitosan-Fe (III) complex sorbents: Characteristic and mechanism. *Chem. Eng. J.* **2018,** *353*, 361-372.
22. Huang, Y.; Lee, X.; Grattieri, M.; Yuan, M.; Cai, R.; Macazo, F. C.; Minteer, S. D., Modified biochar for phosphate adsorption in environmentally relevant conditions. *Chem. Eng. J.* **2020,** *380*, 122375.
23. Zong, E.; Liu, X.; Jiang, J.; Fu, S.; Chu, F., Preparation and characterization of zirconia-loaded lignocellulosic butanol residue as a biosorbent for phosphate removal from aqueous solution. *Appl. Surf. Sci.* **2016,** *387*, 419-430.
24. Zhang, M.; Lin, K.; Li, X.; Wu, L.; Yu, J.; Cao, S.; Zhang, D.; Xu, L.; Parikh, S. J.; Ok, Y. S., Removal of phosphate from water by paper mill sludge biochar. *Environ. Pollut.* **2022,** *293*, 118521.
25. Hazarika, G.; Das, S.; Das, N. M.; Manna, D., A pH-responsive covalent organic network: Morphology change leads to capture and removal of phosphate ions from water. *J. Mater. Chem. A* **2024,** *12* (30), 19559-19566.
26. Ye, X.; Wang, A.; Zhang, D.; Zhou, P.; Zhu, P., Light and pH dual-responsive spiropyran-based cellulose nanocrystals. *RSC Adv.* **2023,** *13* (17), 11495-11502.

27. Ye, X.; Wang, H.; Yu, L.; Zhou, J., Aggregation-induced emission (AIE)-labeled cellulose nanocrystals for the detection of nitrophenolic explosives in aqueous solutions. *Nanomaterials* **2019,** *9* (5), 707.
28. Van Zyl, A. J.; Graef, S. M.; Sanderson, R. D.; Klumperman, B.; Pasch, H., Monitoring the grafting of epoxidized natural rubber by size-exclusion chromatography coupled to FTIR spectroscopy. *J. Appl. Polym. Sci.,* **2003,** *88* (10), 2539-2549.
29. Somseemee, O.; Saeoui, P.; Schevenels, F. T.; Siriwong, C., Enhanced interfacial interaction between modified cellulose nanocrystals and epoxidized natural rubber via ultraviolet irradiation. *Sci. Rep.* **2022,** *12* (1), 6682.
30. Su, C.; Guo, J.; Cheng, J.; Zhang, J.; Gao, F., Heterogeneous epoxidation of microcrystalline cellulose and the toughening effect toward epoxy resin. *Ind. Eng. Chem. Res.* **2023,** *62* (6), 2671-2686.
31. Das, S.; Hazarika, G.; Manna, D., Guanidine-functionalized fluorescent sp2 carbon-conjugated covalent organic framework for sensing and capture of Pd (II) and Cr (VI) ions. *Chem. Eur. J.* **2023,** *29* (15), e202203595.
32. Anjali, K.; Nishana, L.; Christopher, J.; Sakthivel, A., Zinc-tetraphenylporphyrin grafted on functionalised mesoporous SBA-15: synthesis and utilisation for nitroaldol condensation. *J. Porous Mater.* **2020,** *27* (4), 1191-1201.
33. Wang, Q.; Xie, D.; Chen, J.; Liu, G.; Yu, M., Superhydrophobic paper fabricated via nanostructured titanium dioxide-functionalized wood cellulose fibers. *J. Mater. Sci.* **2020,** *55* (16), 7084-7094.
34. Radhakrishnan, K.; Panneerselvam, P.; Marieeswaran, M., A green synthetic route for the surface-passivation of carbon dots as an effective multifunctional fluorescent sensor for the recognition and detection of toxic metal ions from aqueous solution. *Anal. Methods* **2019,** *11* (4), 490-506.
35. Lin, L.; Song, X.; Chen, Y.; Rong, M.; Zhao, T.; Jiang, Y.; Wang, Y.; Chen, X., One-pot synthesis of highly greenish-yellow fluorescent nitrogen-doped graphene quantum dots for pyrophosphate sensing via competitive coordination with Eu 3+ ions. *Nanoscale* **2015,** *7* (37), 15427-15433.
36. Francesconi, O.; Gentili, M.; Bartoli, F.; Bencini, A.; Conti, L.; Giorgi, C.; Roelens, S., Phosphate binding by a novel Zn (II) complex featuring a trans-1, 2-diaminocyclohexane ligand. Effective anion recognition in water. *Org. Biomol. Chem.* **2015,** *13* (6), 1860-1868.
37. Ribet, S. M.; Shindel, B.; Dos Reis, R.; Nandwana, V.; Dravid, V. P., Phosphate Elimination and Recovery Lightweight (PEARL) membrane: A sustainable environmental remediation approach. *Proc. Natl. Acad. Sci. U. S. A.* **2021,** *118* (23), e2102583118.
38. Zhang, L.; Dan, H.; Bukasa, O. T.; Song, L.; Liu, Y.; Wang, L.; Li, J., Low-cost efficient magnetic adsorbent for phosphorus removal from water. *ACS Omega* **2020,** *5* (39), 25326-25333.
39. SHI, Z.-l.; LIU, F.-m.; YAO, S.-h., Adsorptive removal of phosphate from aqueous solutions using activated carbon loaded with Fe (III) oxide. *New Carbon Mater.* **2011,** *26* (4), 299-306.
40. Mekjinda, N.; Phunnarungsi, S.; Ruangpornvisuti, V.; Ritchie, R. J.; Hamachi, I.; Ojida, A.; Wongkongkatep, J., Masking phosphate with rare-earth elements enables selective detection of arsenate by dipycolylamine-ZnII chemosensor. *Sci. Rep.* **2020,** *10* (1), 2656.

41. Lee, H. N.; Swamy, K.; Kim, S. K.; Kwon, J.-Y.; Kim, Y.; Kim, S.-J.; Yoon, Y. J.; Yoon, J., Simple but effective way to sense pyrophosphate and inorganic phosphate by fluorescence changes. *Org. Lett.* **2007,** *9* (2), 243-246.
42. Zhao, S.-W.; Guo, C.-R.; Hu, Y.-Z.; Guo, Y.-R.; Pan, Q.-J., The preparation and antibacterial activity of cellulose/ZnO composite: A review. *Open Chem.* **2018,** *16* (1), 9-20.
43. Norrrahim, M. N. F.; Nurazzi, N. M.; Jenol, M. A.; Farid, M. A. A.; Janudin, N.; Ujang, F. A.; Yasim-Anuar, T. A. T.; Najmuddin, S. U. F. S.; Ilyas, R. A., Emerging development of nanocellulose as an antimicrobial material: An overview. *Mater. Adv.* **2021,** *2* (11), 3538-3551.

Chapter 3

A pH-responsive covalent organic network: Morphology change leads to capture and removal of phosphate ions from water

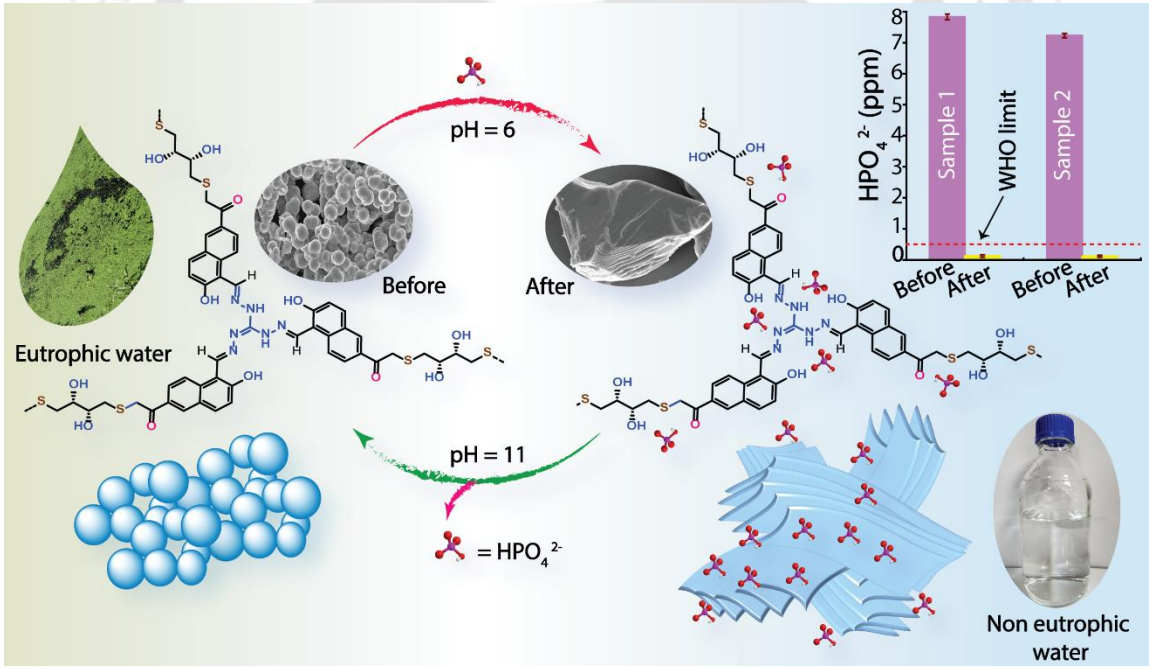

3.1. Background and objective of present work

The Zn(II)-coordinated cellulose-based biopolymer (Zn-gCP), presented in Chapter 2, has shown considerable potential for the selective removal and recovery of phosphate from aquatic systems, even in the presence of competing anions such as F^-, Cl^-, Br^-, NO_3^-, and SO_4^{2-}, achieving over 85% phosphate removal efficiency and enabling easy recovery and reuse through pH adjustment. Moreover, it exhibits antimicrobial activity against both Gram-positive and Gram-negative bacteria, making it a multifunctional and eco-friendly material for wastewater treatment. However, its comparatively lower adsorption capacity and slower kinetics with respect to advanced adsorbents such as MOFs and COFs – which generally provide higher uptake and quicker adsorption rates – could restrict its large-scale practical application.

MOFs are considered as one of the preferred materials for oxoanion adsorption among various advanced porous adsorbents, due to their large surface area and the presence of positively charged metal cations.[1-4] But their widespread use is hindered by limitations like their lack of selectivity and specificity as well as the presence of hazardous metal ions. Additionally, MOFs tend to be unstable in highly acidic or basic environments, and their high production costs limit industrial scalability. Ongoing research explores the modification of hydroxyl groups in biomaterials for phosphate removal and recovery.[5-15] Even though of this, their broad application is limited by issues like low adsorption capacity, slow adsorption rate, recyclability issues, and performance that depends on pH.[15-20] On the other hand, COFs exhibit superior chemical stability under extreme conditions, which is advantageous for applications requiring prolonged exposure to harsh environments. On the other hand, COFs are more chemically stable in extreme conditions, which is advantageous for using them in harsh environments for a long time. At the same time, their flexible design helps to control the size, shape, and function of the pores with great accuracy, making them even better for specific uses like selective adsorption and separation processes. Furthermore, the exceptional hydrolytic stability of COF enables numerous recycling opportunities through techniques like centrifugation, washing, and filtration repeatedly. In summary, COFs have great potential for the environmental remediation applications because of their naturally flexible, stable, selective, and eco-friendly nature. Our group has recently synthesized a guanidine-

based 2D COF (gCON), showing promise in wastewater treatment.[21] However, its relatively slow adsorption rate limits its broad application. To overcome this, we have further modified the guanidine moiety, resulting in the rapid synthesis of a tris-aminoguanidine-functionalized 2D COF (ag-CON), which proves to be a promising and cost-effective adsorbent for rapid phosphate removal and recovery in wastewater treatment.

The recent efforts to use guanidine-based molecules to remove phosphate from wastewater are considered to be an important advancement in the development of technology for wastewater treatment.[21, 22] These molecules are especially effective because they can form strong electrostatic interactions and hydrogen bonds with phosphate ions, making the removal process more efficient.[23, 24] One of their biggest advantages is their flexible chemical structure, which allows scientists to design adsorbents with specific properties like improved selectivity and the ability to be reused.[25, 26] Inspired by the unique properties of guanidine, we further modified it to tris-aminoguanidine to enhance phosphate binding affinity through H-bonding. Additionally, we also modified 2-hydroxynaphthaldehyde to 6,6′-(2,2′-(((2R,3R)-2,3-dihydroxybutane-1,4-diyl)bis(sulfanediyl))bis(acetyl))bis(2-hydroxy-1-naphthaldehyde) for a facile polymerization reaction with tris-aminoguanidine. This modification introduced additional hydroxy groups within the polymeric network, enhancing the H-bonding interacting sites along with the tris-aminoguanidine moiety. Furthermore, these hydroxyl groups and carbonyl groups can be attributed to promoting the interconnection between the polymeric network through hydrogen bonding, thereby enhancing the thermal and chemical stability of the polymer. Physicochemical studies show that this polymer has outstanding thermal and chemical stability across a range of conditions. It consistently displays a strong ability to absorb phosphate, even when other competing anions are present. Compared to previously reported polymers, it binds phosphate more quickly and effectively, especially under neutral to acidic conditions. It also stands out for its improved recyclability in basic environments. Interestingly, ag-CON undergoes noticeable changes in its structure depending on the presence or absence of phosphate ions. Specifically, its structure transitioned from a spherical form to a sheet-like arrangement in the presence of phosphate ions and returned to its spherical shape once the adsorbed phosphate was

removed from the polymer. These features, including pH-responsive adsorption behaviour and enhanced and selective phosphate removal affinity, make this polymer a promising material for practical water treatment processes.

3.2. Results and discussions

3.2.1. Synthesis of the ag-CON polymer –

A four-step synthetic methodology was employed in the synthesis of the ag-CON functionalized with tris-aminoguanidine. First, the acylation of 2-hydroxynaphthaldehyde with bromoacetyl bromide resulted in the formation of 6-(2-bromoacetyl)-2-hydroxy-1-naphthaldehyde (Compound 3.1) (Scheme A3.1).[27] The reaction of 6-(2-bromoacetyl)-2-hydroxy-1-naphthaldehyde was with dithiothreitol (DTT), produced the linker, 6,6'-(2,2'-(((2R,3R)-2,3-dihydroxybutane-1,4 diyl)bis(sulfanediyl))bis(acetyl))bis(2-hydroxy-1-naphthaldehyde) (Compound 3.2) (Scheme A3.2). Meanwhile, tris-aminoguanidine (Compound 3.3) was synthesized from guanidine hydrogen chloride according to the reported method (Scheme S3).[28] In the final step, a Schiff base reaction was employed, where compound 6,6'-(2,2'-(((2R,3R)-2,3-dihydroxybutane-1,4 diyl)bis(sulfanediyl))bis(acetyl))bis(2-hydroxy-1-naphthaldehyde) and compound tris-aminoguanidine were combined to yield the ag-CON in a dioxane-water solution (1:0.3) within a pyrex tube at 120 °C for 3 days (Figure 3.1A). Afterwards, the resulting yellowish precipitate was filtered and successively washed with water and different organic solvents, including methanol, ethyl acetate, dichloromethane, acetonitrile, and tetrahydrofuran. It was then dried at 70 °C for 24 h before being collected.

3.2.2. Characterization of the ag-CON polymer –

The polymer formation was initially characterized using the FT-IR technique. The FT-IR peaks at ~3317 cm^{-1} (-NH_2 stretching), ~1615 cm^{-1} (C=N stretching), and ~1291 cm^{-1} (C-N stretching) provided evidence for the existence of the tris-aminoguanidine unit within the polymer. On the other hand, the existence of the monomeric unit of 2-hydroxy-1-naphthaldehyde within the polymer was confirmed by the appearance of FT-IR peaks at ~3434 cm^{-1} (O-H stretching), ~1659 cm^{-1} (C=O stretching), and ~690 cm^{-1} (-S-) (Figure 3.1B).[29] The ^{13}C CP-MAS NMR spectrum analysis revealed distinct carbon environments within the ag-CON. Notably, the presence of the C=O unit was confirmed by a peak at δ 194.75 ppm, while signals at δ 159.30 ppm and δ 157.91 ppm corresponded to the carbon of the tris-

aminoguanidine unit and -C=N- unit, respectively, affirming the presence of tris-aminoguanidine moieties. Aryl rings, excluding the carbon atom attached to the -OH group, manifested signals in the range of δ 135-108 ppm. Furthermore, aromatic and aliphatic carbons attached to the -OH group were identified at δ 166.89 ppm and δ 78.68 ppm, respectively. Aliphatic carbon atoms dispersed within the polymer were evidenced by broad peaks spanning δ 40 - 30 ppm (Figure 3.1C). The overlaid XPS spectra of ag-CON revealed characteristic peaks for oxygen (O 1s) at 534-531 eV, nitrogen (N 1s) at 401–399 eV, carbon (C 1s) at 289–284 eV, and two peaks for

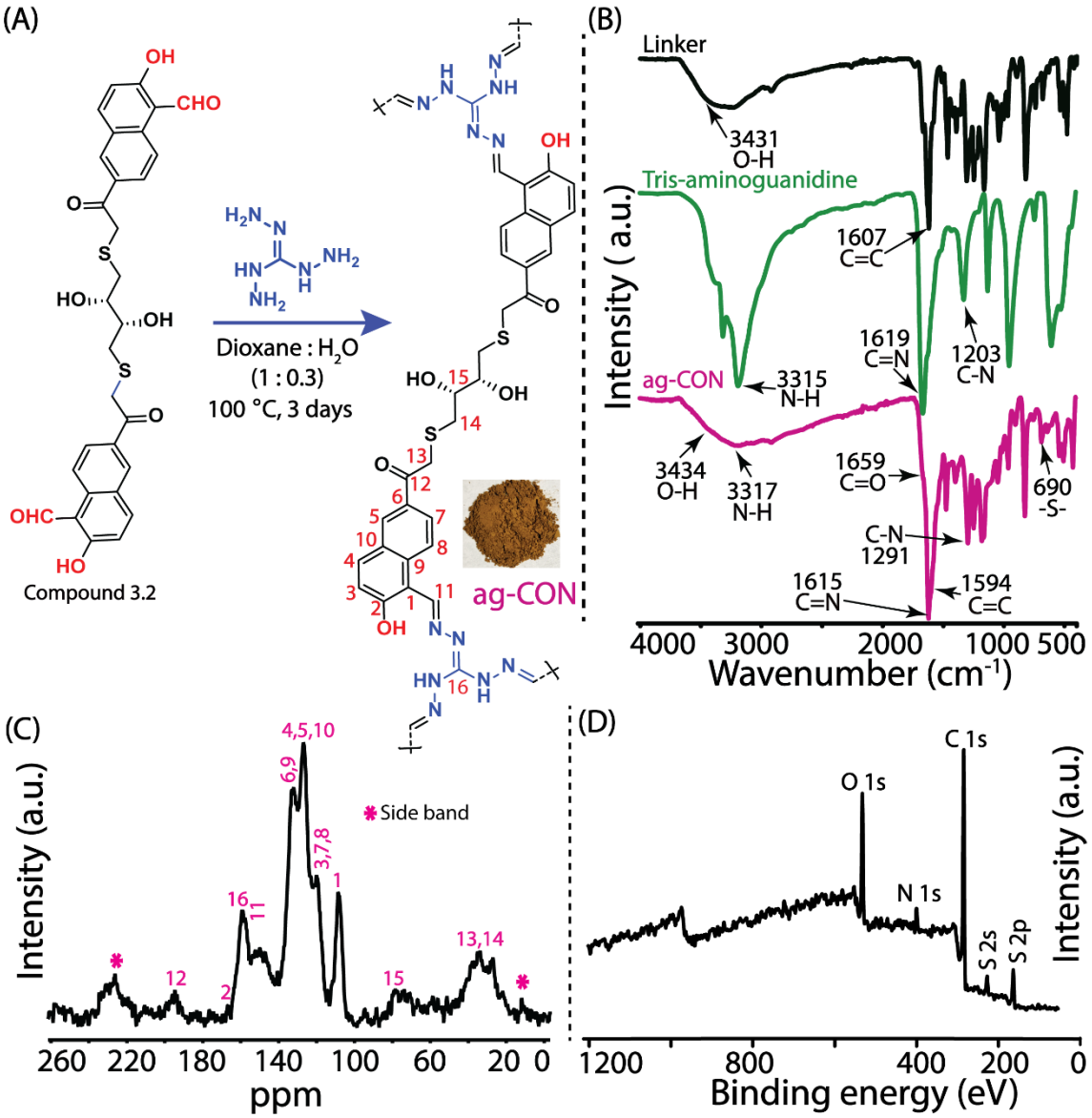

Figure 3.1. Synthetic route to ag-CON (A). FT-IR spectra of linker, tris-aminoguanidine, and ag-CON (B). The solid-state ^{13}C NMR spectra of ag-CON (C). XPS data profile (wide scan) of ag-CON (D).

sulphur (S 2s and S 2p) at 165-163 eV (Figure 3.1D). Deconvolution of the C 1s spectrum exhibited six peaks at 288.01, 287.13, 286.38, 285.66, 285.01, and 284.37 eV, attributed to C-OH, C=O, C-S-C, C=N, C-C, and C=C, respectively (Figure A3.1A). Analysis of the N 1s spectrum unveiled peaks at 400.66 and 399.78 eV, corresponding to C=N and -NH- functionalities (Figure A3.1B). The O 1s spectrum showed peaks at 533.42, 532.53, and 531.60 eV, representing C=C-OH, C-C-OH, and C=O, respectively (Figure A3.1C). Additionally, sulfur exhibited peaks at 164.40 and 163.32 eV for S $2p_{1/2}$ and S $2p_{3/2}$, providing insights into its chemical environment (Figure A3.1D). The Powder X-ray Diffraction (PXRD) analysis indicated that the synthesized polymer exhibited significantly low crystallinity, as evidenced by the initial broad peak observed at $2\theta = 3.32°$ (Figure 3.2A). Also, the fact that there was a board peak at $2\theta = 24.17°$ showed that the aromatic ring layers did not interact well with each other when stacking.[21] This lack of stacking could potentially be attributed to the interference caused by tris-aminoguanidine moieties, disrupting the π-π stacking interactions among the aromatic moieties within the ag-CON. In addition, the TEM-selected area electron diffraction (TEM-SAED) pattern further confirmed the low crystalline nature of the ag-CON, with a few intense spots (Figure A3.2).[30] The FESEM and TEM analyses revealed the spherical shape morphology of the polymer (Figure 3.2B – C). The morphological analysis performed using AFM also revealed a similar pattern (Figure A3.5). FESEM-EDX and elemental mapping analyses reveal the uniform presence of C, O, N, and S as the main chemical constituents in the polymer (Figure 3.2D and A3.6). The TGA result revealed a minor decrease in weight observed within the temperature range of 90 °C – 100 °C, which could be due to the removal of water molecules that were adsorbed onto the sample. Subsequently, a notable reduction in weight was observed at around >300 °C, indicating the deterioration of the molecular framework of the polymer (Figure 3.2E). Therefore, TGA analysis demonstrated that the ag-CON polymer exhibited a very low char residue. This enhanced thermal stability observed in the ag-CON may stem from hydrogen bonding and ion-dipole interactions facilitated by the -NH, -OH, and C=O functional groups embedded within the polymeric network.

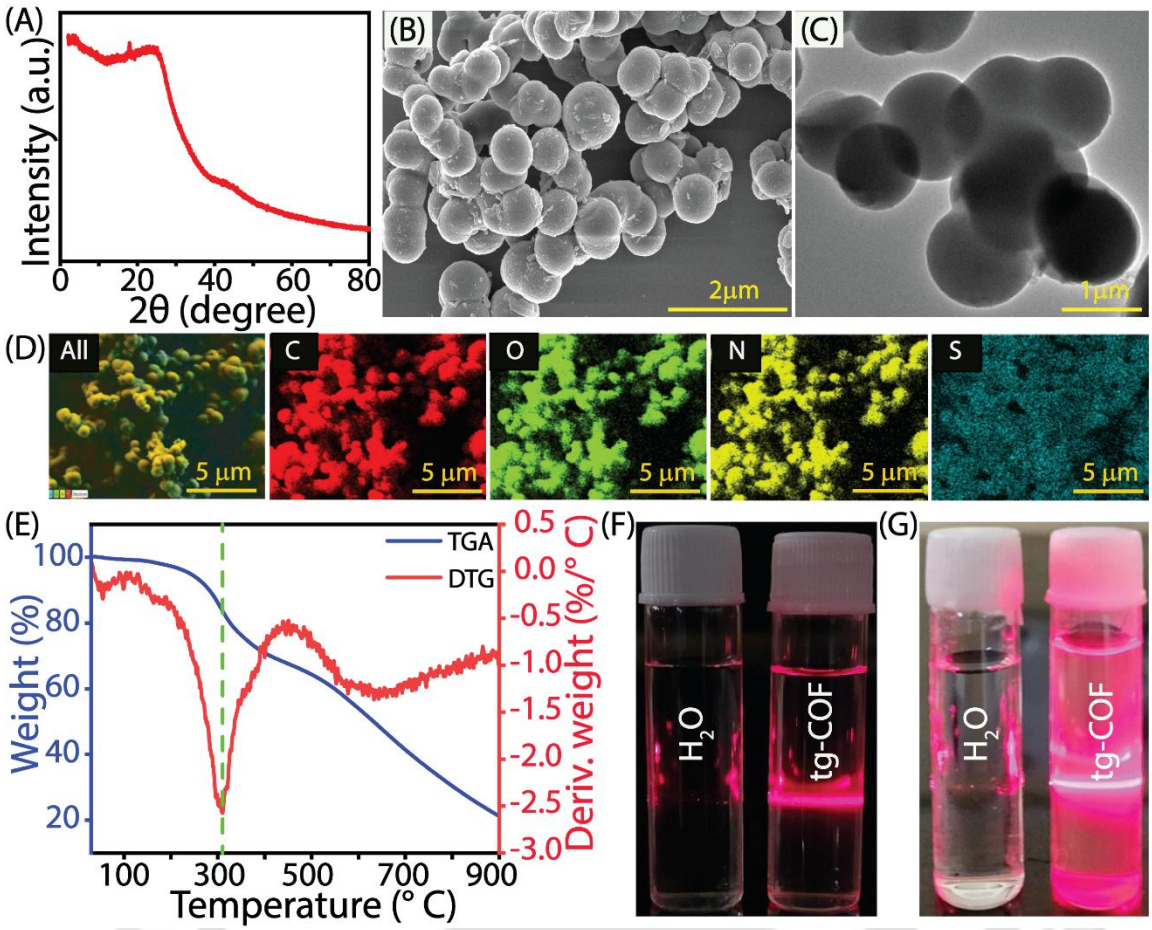

Figure 3.2. Characterization of ag-CON by PXRD (A), FESEM (B), and TEM (C) analyses. The FESEM mapping analysis for the C, O, N, and S of ag-CON (D). The TGA-DTG analysis of ag-CON (E). Tyndall effect of light in the aqueous dispersions of ag-CON at 0 h (F) and after 48 h (G).

To evaluate the porosity and surface area of the polymer, Brunauer-Emmett-Teller (BET) analysis was performed. At cryogenic temperatures (77.3 K), the polymer exhibited a surface area of 169.633 m^2g^{-1}, determined from the nitrogen adsorption-desorption isotherm (Figure A3.7A). The total pore volume, measured at a relative pressure of 0.9 (P/P_0), was found to be 3.120 cm^3g^{-1}. The average pore size distribution obtained via the Barrett–Joyner–Halenda (BJH) method was found to be 3.35 nm, displaying close agreement with the proposed structure (Figure A3.7B and A3.8). The observed porosity in ag-CON could be attributed to the absence of counter anions and the hydrogen bonding interactions between the OH and C=O groups in the two layers of the ag-CON polymer, which restrict free rotation.[29] The zeta-potential analysis revealed a significant change in the surface potential of the

polymer across various pH levels (Figure A3.9). When the pH of the aqueous solution decreased from 7 to 2, there was a noticeable increase in the surface potential from ξ = 16 mV to ξ = 44 mV. In a similar manner, when the pH increased from 8 to 12, there was a corresponding decrease from ξ = 3.6 mV to ξ = -51 mV. This pH-dependent change in surface potential is probably caused by the protonation and deprotonation of the -NH group of the tris-aminoguanidine moiety as well as the -OH groups within the polymer network at various pH levels. The dispersive property of the polymer in an aqueous medium was characterized by the Tyndall effect, signifying the stable colloidal suspension of the polymer over 48 h (Figure 3.2F – G). The DLS experiment further demonstrated that the particle size of the polymer remained within the range of ~1000 nm in an aqueous environment even after the 24 h duration (Figure A3.10). In order to assess the chemical stability, the polymer was treated with commonly used organic solvents, including acetonitrile (ACN), dichloromethane (DCM), ethyl acetate (EtOAc), methanol (MeOH), tetrahydrofuran (THF), and acetone, as well as HCl (3 N) and NaOH (3 N), over a period of 14 days. The unchanged FT-IR spectra of the polymer before and after the treatments indicate their structural integrity under these circumstances (Figure A3.11A). Additionally, morphological (FESEM) and thermal (TGA) analysis under acidic and basic conditions over a 14-day period validate the morphological and thermal stability of the polymer (Figure A11B – E).

3.2.3. Phosphate ion selectivity study –

The guanidium moiety is widely recognized for its selective and robust affinity of the phosphate ions due to its strong hydrogen bonding and salt bridge interaction properties. Inspired by the pH-responsive surface charge alternation and impressive chemical and thermal stability of ag-CON, we were prompted to explore the adsorption affinity of the polymer towards phosphate and other anions in aqueous conditions. The affinity of the ag-CON towards different anions in the aqueous medium was initially assessed using ion IC techniques in the presence of sodium salts of various anions, including F^-, Cl^-, Br^-, NO_3^-, SO_4^{2-} and HPO_4^{2-}. The results demonstrated that the polymer exhibited significantly higher specificity towards phosphate anions compared to the other tested anions (Figure 3.3A). The tetrahedral geometry and the presence of both hydrogen bond donor and acceptor groups within the phosphate anions enable effective spatial alignment with the tris-

aminoguanidine moieties of the ag-CON polymer, making it a better candidate for adsorption compared to other tested anions. Additionally, due to the larger difference in electronegativity, the guanidine preferentially interacts with phosphate over sulphate ions. The strong binding efficiency of the ag-CON polymer also enhances its ability to overcome the hydration energy barrier of phosphate ions.[21-24, 31, 32] The initial phosphate binding ability of the ag-CON was assessed through FT-IR, XPS, and FESEM-EDX analysis. Upon analysing the FT-IR spectra of the polymer before and after phosphate treatment, a noticeable increase in the intensity of the peak at 1070 cm¯1 was observed in the phosphate-treated polymer, indicating the successful phosphate adsorption by the polymer (Figure 3.3B). XPS analysis revealed distinct peaks within the range of 132-136 eV, which especially correspond to the P 2p in the phosphate-treated polymer, in contrast to the untreated polymer (Figure 3.3C). The P 2p deconvoluted spectrum exhibited three distinct peaks at 132.33, 133.12, and 134.16 eV, potentially indicative of P=O, P-O, and P-OH, respectively (Figure A3.12A). Similarly, the O 1s deconvoluted spectrum displayed two new peaks at 530.91 and 533.11 eV, corresponding to $P\text{-}O^-$ and P=O moieties, respectively (Figure A3.12B). Interestingly, the FESEM and TEM images revealed that the original spherical shape morphology of the ag-CON was converted to a sheet-like arrangement after the phosphate adsorption (Figure 3.3D – E). This alternation in the morphology of ag-CON in the presence of phosphate ions could be attributed to various factors. Firstly, phosphate ions may engage in specific intermolecular interactions with functional groups or sites on the polymer surface, such as hydrogen bonding or electrostatic interactions, prompting rearrangements of polymer chains favouring sheet-like arrangements. Additionally, the altered surface energy induced by phosphate ions might promote the adoption of a lower energy configuration, potentially leading to the stabilization of the sheet-like morphology. Conformational changes in the polymer chains, driven by molecular recognition or binding interactions with phosphate ions, could further facilitate the transition to a sheet-like structure. Furthermore, the influence of the ionic environment on the distribution of charges or ions at the interface may contribute to the observed morphological transformation. Moreover, it was observed that the extent of conversion from the spherical to a sheet-like arrangement of the ag-CON increased proportionally with the concentration of aqueous phosphate ion solution (Figure A3.13). This

observation supports the conclusion that the presence of phosphate ions directly correlates with the morphological transformation from spherical to sheet-like arrangement in the ag-CON. Additionally, the FESEM-EDX analysis disclosed the prominent presence of P along with C, O, N, and S within the polymer (Figure 3.3F). These studies provide strong evidence of phosphate adsorption by the ag-CON.

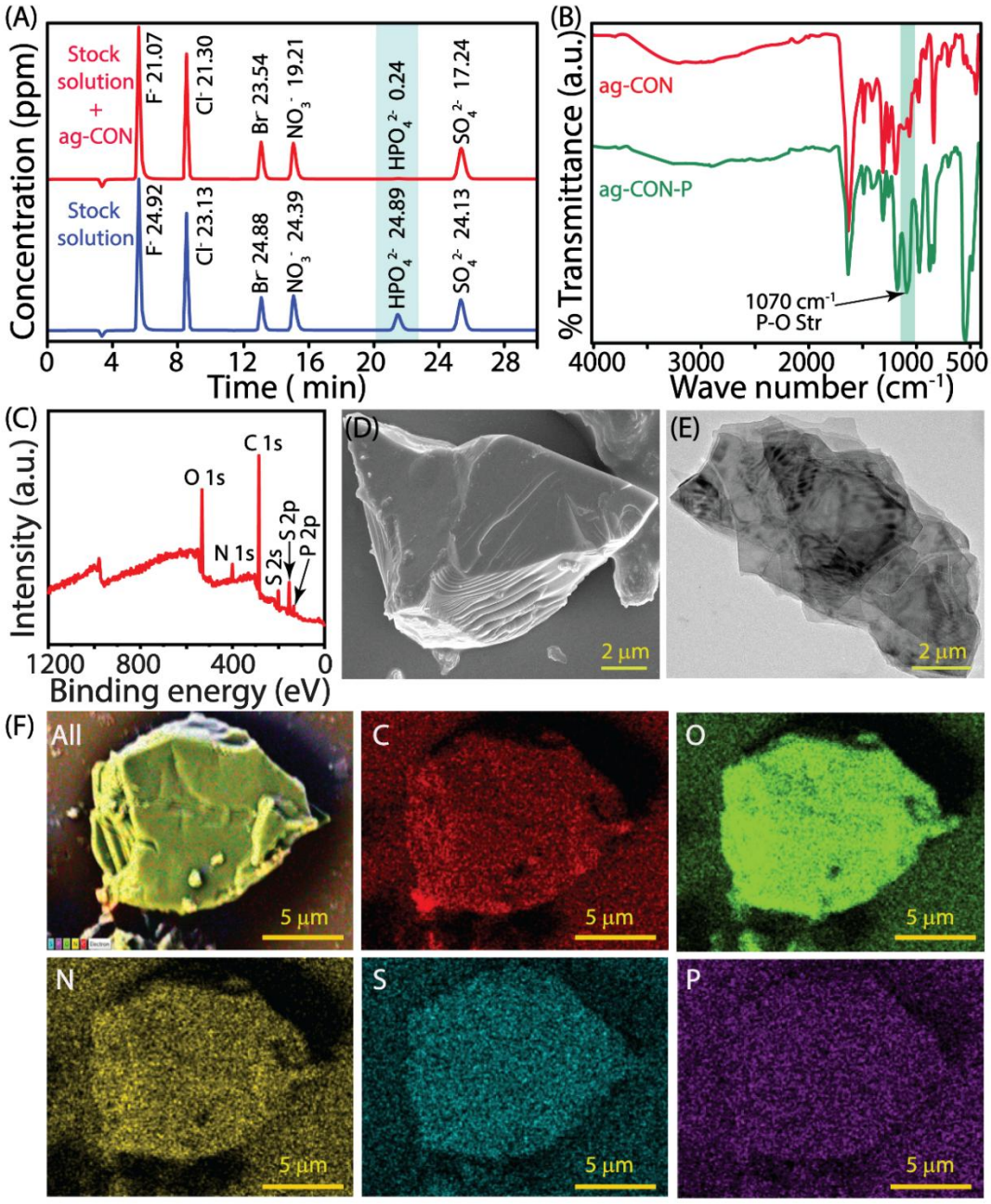

Figure 3.3. Ion chromatograms in the absence and presence of ag-CON (A). FT-IR spectra of ag-CON before and after phosphate anions adsorption (B). XPS data profile (wide scan) of ag-CON after phosphate anions adsorption (C). The FESEM(D) and TEM (E) images of ag-CON after phosphate adsorption. The FESEM mapping analysis for the C, O, N, S, and P of ag-CON after phosphate anions adsorption (F).

3.2.4. Removal and recovery of phosphate –

Motivated by the excellent selectivity for phosphate ions, an extensive investigation was conducted into the adsorption behaviour of phosphate ions by a polymer in an aqueous medium using ion chromatographic methods. The initial investigation explored the influence of pH on phosphate adsorption capacity, revealing the crucial role of the acidity and basicity of the solution in influencing the interaction between the polymer and phosphate. Notably, the polymer exhibited significant phosphate adsorption capabilities between pH 4-7, indicating its potential for treating eutrophic water. Furthermore, the highest adsorption capacity of the ag-CON was observed at pH 6, with a subsequent decline as the pH of the aqueous medium increased from 8 to 12 (Figure 3.4A). The observed variations in capture performance are attributable to the differing forms of phosphate present in solution across varying pH conditions (notably, the pKa values of H_3PO_4 in water were 2.2, 7.2, and 12.3), potentially influencing their adsorption capabilities.[21] In acidic conditions, although the surface potential of the ag-CON increases, the reduced negative charge on phosphate could diminish the electrostatic interaction between the polymer and phosphate. Furthermore, the high concentration of Cl^- ions increases the competition for binding sites on the polymer, which ultimately reduces the phosphate adsorption efficiency as pH decreases. On increasing the pH, the negative charge on the phosphate increases, but the negative surface potential of the polymer, as well as the excess OH^- ions in the solution, also decrease the adsorption affinity of the polymer at the basic pH. Since the polymer has the maximum adsorption affinity at pH 6, all subsequent adsorption-based studies were conducted at pH 6.

In the concentration-dependent phosphate ion adsorption study, phosphate solutions ranging from 20 ppm to 1000 ppm were prepared using sodium phosphate salt in Milli-Q water. Each solution was treated with 5 mg of ag-CON, undergoing sonication for 10 minutes, followed by continuous stirring for 6 h at room temperature. The IC measurements were employed to quantify phosphate ion concentrations before and after adsorption. Notably, the polymer exhibited the highest affinity for phosphate ions at 1000 ppm concentration, with an equilibrium adsorption capacity of 389.473 mg g^{-1}. Langmuir and Freundlich adsorption models were applied to explore the correlation between adsorption parameters and

phosphate equilibrium concentration, revealing a maximum adsorption capacity of 719 mg g^{-1} at pH 6 using the Langmuir model (Figure 3.4B). Time-dependent kinetics aligned with the pseudo-second-order model, and the equilibrium adsorption reached within 60 sec with the rate constant 0.0000663 mg $g^{-1}sec^{-1}$ (R^2 = 0.99178) for 5 mg ag-CON (Figure A3.15). Moreover, increasing polymer quantity from 3 to 10 mg decreased adsorption rates from 0.0007526 mg g^{-1} sec^{-1} to 0.0000703 mg g^{-1} sec^{-1}, indicative of second-order kinetics (Figure 3.4C and A3.16). Overall, the polymer demonstrates efficient phosphate removal with rapid adsorption kinetics, suggesting practical utility in phosphate removal processes. Further, the temperature-dependent phosphate ion adsorption study demonstrated that the equilibrium phosphate ion adsorption capacity (Qe) of the ag-CON decreased from 389.473 to 307.074 mg g^{-1} as the temperature increased from 298 K to 343 K (Figure A3.17).

For practical implications of ag-CON in extracting phosphate ions, it is crucial to evaluate the ability of the polymer to effectively bind with phosphate ions in the presence of other competing ions such as Cl^-, F^-, NO_3^-, Br^-, SO_4^{2-}, Na^+, K^+, Rb^+, Cs^+, Mg^{2+}, and Al^{3+}, which are prevalent in eutrophic water or industrial wastewater. These ions could potentially interfere with the process of phosphate ions adsorption by competing for identical adsorption sites on the polymer. Selectivity, therefore, becomes pivotal for successful phosphate ions extraction and recovery. The IC analyses were conducted to assess the capacity of the ag-CON to adsorb phosphates in the presence of a 100-fold excess of interfering ions. Results revealed that the polymer could preferentially adsorb phosphate ions with a selectivity of 90% over other coexisting anions, nearly consistent with its adsorption capacity in the absence of these coexisting anions and also displayed a pronounced preference for capturing the phosphate ions, even in the presence of different coexisting metal ions (Figure A3.18, and A3.19). This study emphasizes the resilient performance of the polymer and suggests minimal interference from coexisting ions. This rapid and selective phosphate ion removal efficacy from the wastewater makes the polymer a promising material for practical applications. To evaluate the phosphate removal efficacy of the ag-CON from a very low-concentration phosphate solution, a solution containing ~500 ppb phosphate was utilized. The IC analysis confirmed a reduction in phosphate ion concentration to below 15 ppb following treatment with the ag-CON.

Additionally, in the presence of 100 ppm interfering ions, as mentioned above, the polymer effectively lowered the phosphate concentration to below 25 ppb from ~500 ppb, indicating its ability to selectively adsorb phosphate ions even in the presence of an excess amount of other competing ions (Figure A3.20). These results suggest that the ag-CON exhibits selective removal of trace phosphate ions even under elevated interfering anion concentrations. Thus, the ag-CON exhibits promising potential for targeted removal of trace phosphate ions in complex aqueous environments. In order to assess the effectiveness of the polymer in the removal of phosphate from eutrophic water in real-world conditions, two samples were obtained from two distinct food manufacturing facilities situated in Gauripur, North Guwahati, Assam, India. The pH, ion concentrations of phosphate, and other coexisting ions were all presented in Table S1. The IC-based study provides evidence that the polymer effectively decreased the concentration of phosphate anions to a level below the recommended threshold for phosphate discharge by the World Health Organization (WHO), even in the presence of other coexisting anions (Figure 3.4D). These results suggest that the polymer exhibits promising potential as a proficient adsorbent for the removal of phosphate from wastewater.

To explore the capability of the polymer to release and recycle the adsorbed phosphate, the phosphate-loaded polymers (5 mg) were submerged in a 5 mL solution of NaOH (0.5 N) with a pH of ~13 and agitated for a duration of 2 h. After that, the solution was collected and analysed to quantify the recovered phosphate ions using the IC technique. Subsequently, the pH of the polymer solution was neutralized to 7 by adding HCl (0.1 M). Then, the polymer was collected via centrifugation and filtration, followed by a meticulous washing with Milli-Q water to eliminate any lingering residues before being ready for the next cycle. A similar experiment was performed for a total of ten cycles. The IC data indicates that the ag-CON exhibits a potential to adsorb >78% phosphate and desorb >90% of the adsorbed phosphate even after ten consecutive cycles (Figure 3.4E). The chemical and thermal stability of the regenerated polymer was evaluated through comprehensive analysis methods, including FTIR, PXRD, FESEM, TEM, FESEM-EDX, elemental mapping, and TGA. The preservation of the chemical stability of the regenerated polymer was confirmed through the analysis of FTIR and PXRD spectra, which closely resembled the pristine polymer (Figure A3.21A – B). Analysis of FESEM

and TEM images revealed that upon removal of adsorbed phosphate, the surface morphology of the ag-CON shifted to a spherical shape (Figure A21C – D). This observation implies that in the absence of phosphate ions, the ag-CON reverted back to its original pristine spherical morphology. The striking similarity between the TGA graph of the regenerated polymer and the pristine one indicates the thermal stability of the polymer after undergoing 10 cycles of regeneration. (Figure A3.21E). Additionally, FESEM-EDX analysis and elemental mapping verified the presence of all constituent elements (C, O, N, and S) in the regenerated polymer (Figure A21F – H). These observations collectively indicate that the polymers retain their capability to extract phosphate from aquatic environments efficiently. Furthermore, we also analysed the kinetics of phosphate desorption from the phosphate-loaded ag-CON. The results revealed that the polymer efficiently released the highest quantity of adsorbed phosphate within 25 min (Figure A3.23).

The pH-based sorption properties of phosphate ions by the ag-CON inspired us to investigate their capture efficacy using the chromatographic column exchange method, which mimicked the real-time scenario (Figure A3.25A). The solution of phosphate ions (50 ppm) was passed through the column. The visual observation (no change in the colour in a mixture of ammonium molybdate and concentrated nitric acid solutions) and ion chromatographic studies revealed that the concentrations of phosphate ions were found to be below the level recommended by the WHO (Figure A3.25B). Before proceeding to the next cycle, the column was revitalized with 100 mL NaOH (0.5 N) solution. Experimental data revealed efficient desorption of over 90% of phosphate from the polymer (Figure A3.25C). The experiment was repeated for 3 cycles, consistently yielding phosphate concentrations below the WHO-recommended threshold in 250–300 mL of eluent, demonstrating the ability of the polymer to accurately mimic real-time scenarios (Figure 3.4F).

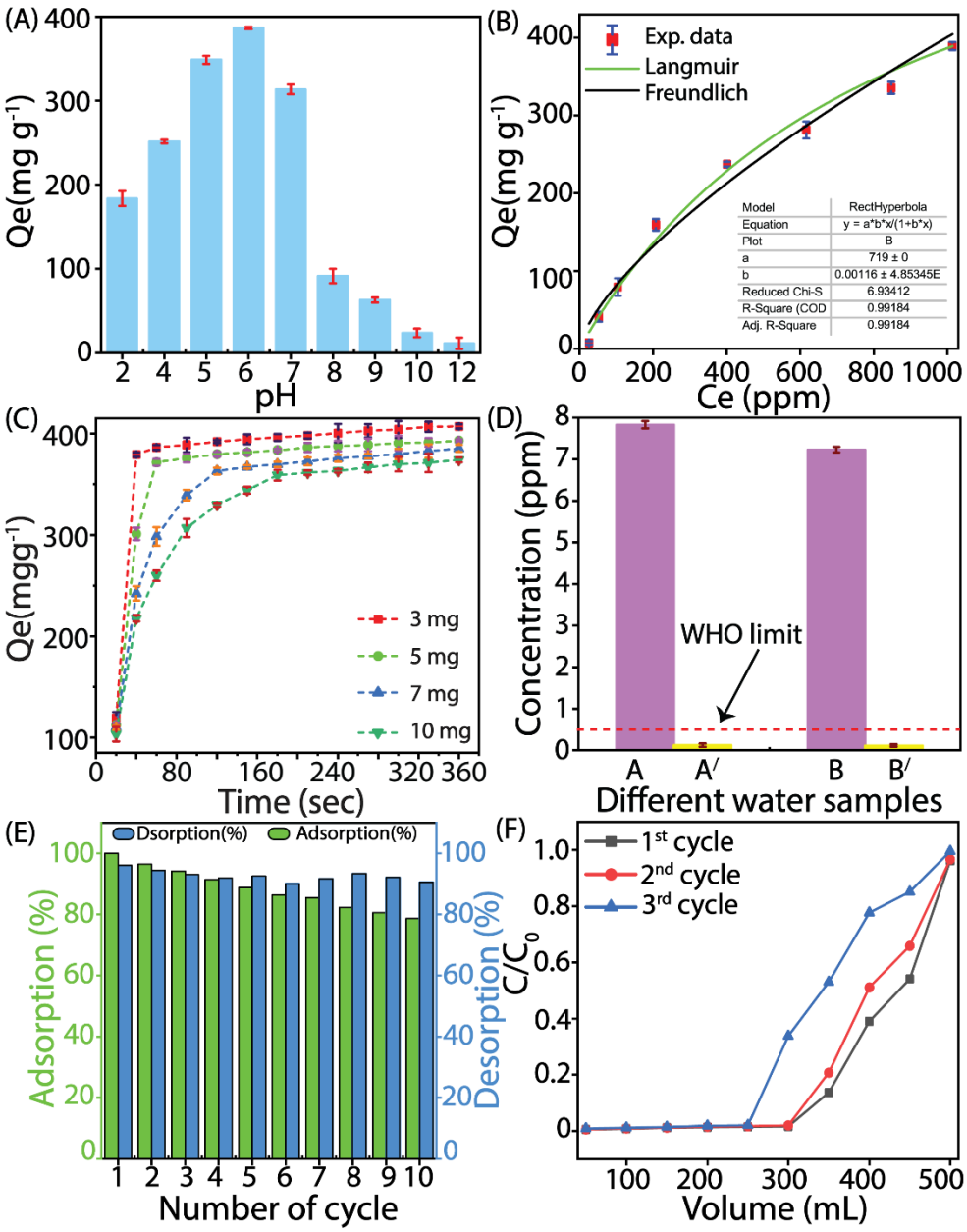

Figure 3.4. The pH-dependent phosphate ion adsorption efficiency of ag-CON (A). Phosphate ion adsorption isotherm of ag-CON (B). Time-dependent adsorption isotherm of phosphate ions by ag-CON (3-10 mg) at pH 6.0 under room temperature (C). Phosphate adsorption capacity of the ag-CON from the real phosphate-contaminated wastewater (D). Phosphate ions adsorption and desorption efficiency of ag-CON after different cycles (E). Phosphate ions adsorption efficiency of the ag-CON by dynamic adsorption column experiment (C_0 = Initial concentration of the phosphate solution and C = Final concentration of the phosphate solution after passing through the column) (F).

3.2.5. Mechanism for phosphate adsorption –

To elucidate the interaction between the polymer backbone and phosphate anions, XPS analysis was conducted. Comparison of the deconvoluted XPS spectrum of the N 1s peak before and after phosphate adsorption revealed the shift in both binding energy peaks of C=N and -NH- from 400.660 eV and 399.785 eV to 400.339 eV and 399.453 eV repetitively (Figure 3.5A). This shift towards lower binding energies strongly suggests an interaction between the tris-aminoguanidine units of the polymer and phosphate anions. Moreover, the observed shift in binding energy peaks of the C 1s of the aromatic moiety and O 1s towards lower binding energy regions in the deconvoluted XPS spectrum after phosphate adsorption indicates interaction between phosphate and carbon of the aromatic moiety, -OH, and C=O units (Figure 5B – 5C). The results of the XPS analysis revealed that all the mentioned functionalities synergistically contribute to the process of phosphate ion removal from aqueous media through hydrogen bonding and electrostatic interactions. The existence of numerous adsorption sites within the polymeric network may also collectively enhance its adsorption capacity for phosphate ions. As these interactions are predominantly noncovalent, they have minimal impact on the changes in the binding energy of the elements.[33-35]

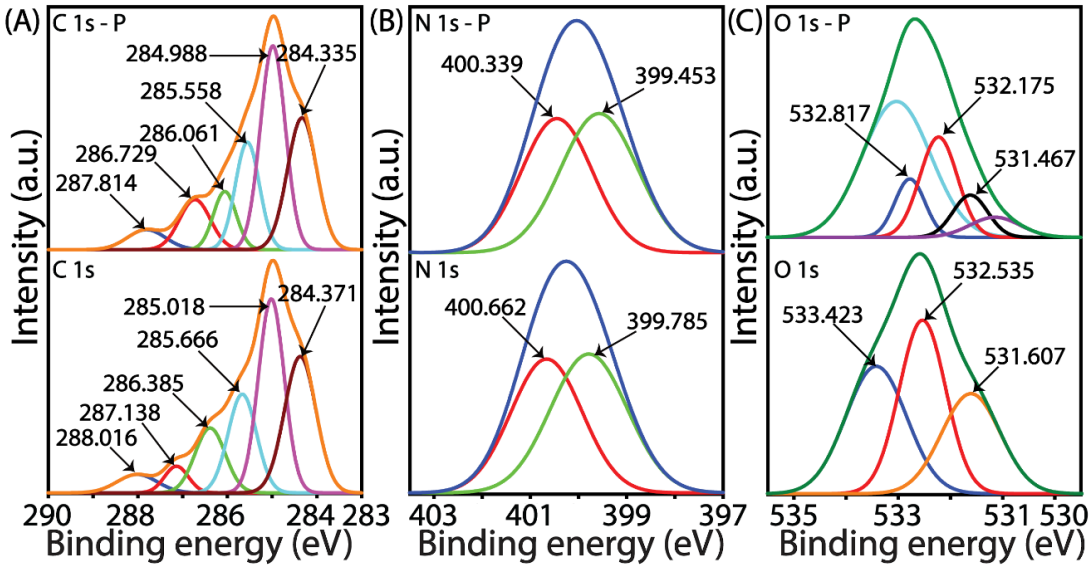

Figure 3.5. Deconvoluted XPS spectra before phosphate adsorption (C 1s, N 1s, and O 1s) and after phosphate adsorption (C 1s-P, N 1s-P, and O 1s-P) for the C 1s (A), N 1s (B), and O 1s (C) of the ag-CON.

3.2.6. Probable mechanism for the morphological changes of polymer with phosphate anions –

The morphological analyses of only ag-CON polymer showed nano-spherical structural arrangements; however, in the presence of phosphate ions, the ag-CON showed multilayer sheet-like structural arrangements. The ag-CON polymer contains tris-aminoguanidine moieties, which have both hydrogen donating (–NH) and hydrogen bond accepting (C=N) capabilities. Upon contact with tetrahedral phosphate ions, which possess both hydrogen bond donor units (–OH) and acceptor units (P=O and P–O^-), strong non-covalent interactions occur primarily through hydrogen bonding and electrostatic interactions. These robust interactions facilitate the interlayer self-assembly phenomenon between the phosphate anions and the ag-CON polymer, transforming the spherical ag-CON polymer into a multilayer sheet-like structural arrangement.[36] Additionally, the hydrogen bonding among the side chain hydroxyl and carbonyl groups (from DTT moiety) of the ag-CON polymer could contribute to this multilayer self-assembly process, resulting in the formation of nanosheet-like structures. The transformation from the nano-spherical to a multilayer sheet-like structural arrangement progressively increased with the concentration of phosphate anions in the aqueous solution. When NaOH (0.5 N) is added, this multilayer sheet-like structure reverts to its original nano-spherical form, which could be due to the disruption of the hydrogen bonding and electrostatic interactions at this pH (~13) (Figure 36).

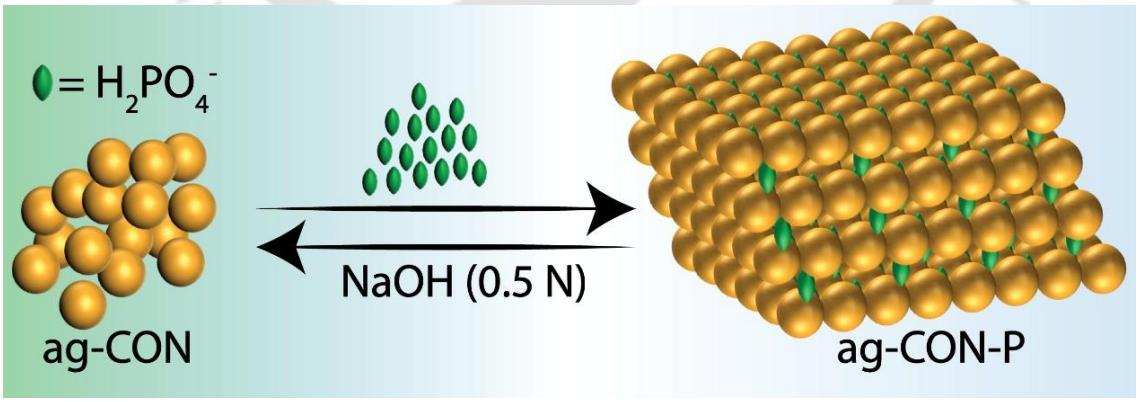

Figure 3.6. The pictorial representation of the transformation from spherical to sheetlike structure of ag-CON polymer after phosphate ions adsorption.

3.3. Summary

In summary, we developed tris-aminoguanidine functionalized CON with DTT linkers to address the environmental challenge posed by excessive phosphate levels in aquatic ecosystems. The excellent thermal and chemical stability in various organic solvents and under significant acidic and basic pH conditions render this tris-aminoguanidine -based polymer highly suitable for applications in harsh environments. Due to the presence of the tris-aminoguanidine moiety, the polymer exhibited high selectivity for phosphate ions even in the presence of excess competing anions, demonstrating a maximum adsorption capacity of 719 mg g^{-1} at pH 6. The presence of the tris-aminoguanidine moiety facilitates the capture of phosphate anions through the mediation of hydrogen bonding and salt bridge interactions. The pH-responsive surface potential variation nature of the polymer allowed for efficient regeneration simply by adjusting the pH of the aqueous solution using a NaOH (0.5 N) solution. The polymer exhibited a negligible phosphate anion removal efficacy reduction from the aqueous phase throughout 10 cycles. On the other hand, the transition in surface morphology of the ag-CON from a spherical to a sheet-like configuration and subsequently reverting to a spherical form, influenced by the presence or absence of phosphate ions, confers a unique characteristic to the ag-CON. Considering these observations, the synthesized polymer holds significant promise as an effective material for the selective capture, recovery, and removal of valuable and hazardous anions such as phosphate from wastewater, even in harsh conditions. For practical industrial applications, ag-CON can be fabricated into composite membranes, and these membranes can be integrated into filtration systems, offering an efficient solution for removing excess phosphate from industrial effluents and environmental remediation purposes.[37] The presence of the tris-aminoguanidine moiety could be advantageous for developing antibacterial materials. Furthermore, this polymer holds potential applications in the phase transfer of hydrophobic nanoparticles to aqueous solutions, biomedical adhesives, fuel cells, electronic industries (including semiconducting polymers), organic catalysis, and various biomedical applications.

3.4. Appendix Section

3.4.1. General information–

All reagents were purchased from Sigma-Aldrich, Merck, Himedia and other commercial sources and used directly without further purification. The column chromatography was performed using 60–120 mesh silica gels. Reactions were monitored by thin-layer chromatography (TLC) on silica gel 60 F254 (0.25 mm). The ^{1}H NMR and ^{13}C NMR were recorded at 400 or 600 and 100 or 151 MHz with Varian AS400 spectrometer and Brucker spectrometer, respectively. The chemical shifts were reported in parts per million (δ) using DMSO-d_6, $CDCl_3$ as internal solvent. The coupling constant (J values) and chemical shifts (δ_{ppm}) were reported in Hertz (Hz) and parts per million (ppm), respectively, downfield from tetramethylsilane using residual chloroform (d = 7.24 for ^{1}H NMR, d = 77.23 for ^{13}C NMR) as an internal standard. Multiplicities are reported as follows: s (singlet), d (doublet), t (triplet), m (multiplet), and br (broadened). High-resolution mass spectra (HRMS) were recorded at Agilent Q-TOF mass spectrometer with Z-spray source using built-in software for analysis of the recorded data.

3.4.2. Synthesis and characterization of the polymers–

3.4.2.1. Synthesis of 6-(2-bromoacetyl)-2-hydroxy-1-naphthaldehyde (Compound 3.1):

In a stirring solution of aluminium chloride ($AlCl_3$) (930 mg, 7 mmol, 6 equiv.) in 40 mL of dichloromethane (DCM), bromoacetyl bromide (586.2 mg, 3 mmol, 2.5 equiv.) was gradually added at 0 °C. Then the temperature of the mixture was brought to 10 °C, and the mixture was stirred for 2 hours. After 2 h in that mixture, a solution of 2-hydroxynapthaldhyde (200 mg, 1.16 mmol) in DCM was added slowly, followed by raising the temperature to 45 °C, and the mixture was stirred for 24 h. Then, the reaction mixture was quenched with ice water. Next, the product was extracted with DCM. The product was purified through column chromatography using an EtOAc/Hexane 20% mixture. A yellow-coloured solid was obtained with a 78% yield.[27] **Characterization of the compound:** ^{1}H NMR (600 MHz, $CDCl_3$) δ_{ppm}: 13.36 (s, 1H), 10.85 (s, 1H), 8.48-8.48 (d, 1H), 8.47-8.45 (s, 1H), 8.22-8.20 (m, 1H), 8.14-8.12 (d, 1H), 7.28-7.28 (d, 1H), 4.56 (s, 2H).^{13}C NMR (151 MHz, $CDCl_3$) δ_{ppm}: 193.11, 190.52, 166.93, 140.17, 136.21, 131.84, 129.99, 127.93, 127.59, 126.90, 120.75, 119.42, 111.37, 77.24, 77.02, 76.81, 30.39. **HRMS (ESI) m/z:** calculated for $C_{13}H_9BrO_3$ $(M–H)^-$: 290.9662, found: 290.9962.

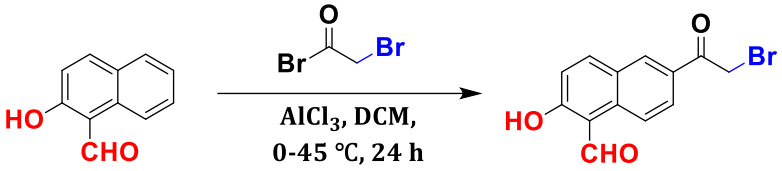

Compound 3.1

Scheme A3.1. Synthesis of 6-(2-bromoacetyl)-2-hydroxy-1-naphthaldehyde from 2-hydroxy-1-naphthaldehyde.

3.4.2.2. Synthesis of 6,6'-(2,2'-(((2R,3R)-2,3-dihydroxybutane-1,4 diyl) bis(sulfanediyl)) bis(acetyl)) bis(2-hydroxy-1-naphthaldehyde) (Compound 3.2):

To the stirring solution of 6-(2-bromoacetyl)-2-hydroxy-1-naphthaldehyde from 2-hydroxy-1-naphthaldehyde (500 mg, 1.7 mmol, 1.00 equiv.) in 1,4-dioxane (20 mL), 1,4-dithiothreitol (131.55 mg, 0.853 mmol, 0.5 equiv.) and trimethylamine (0.240 mL) in 1,4-dioxane was added at 0 ℃. After that, the reaction mixture was stirred for 2 h at room temperature monitored by TLC. Next, the solvent was evaporated under reduced pressure, and the product was purified through column chromatography using 30 % EtOAc / hexane, and a dark orange-coloured crystalline solid **(B)** was obtained, exhibiting a yield of 62%. **Characterization of the compound:** ^{1}H NMR (600 MHz, DMSO-d_6) δ_{ppm}: 12.21 (s, 2H), 10.78 (s, 2H), 9.02-9.01 (d, 2H), 8.61-8.60(d, 2H), 8.27-8.26 (d, 2H), 8.10-8.08 (m, 2H), 7.33-7.32 (d, 2H), 5.76 (s, 1H), 4.13-4.07 (m, 2H), 3.17 (s, 4H), 2.69-2.66 (m, 2H), 2.62-2.59 (m, 2H).^{13}C NMR (151 MHz, DMSO-d_6) δ_{ppm}: 140.01, 134.81, 131.51, 131.18, 128.15, 127.16, 123.33, 120.24, 113.13, 71.56, 55.40, 49.08, 37.86, 35.33. **HRMS (ESI) m/z:** calculated for $C_{30}H_{26}O_8S_2$ $(M + Na)^+$: 601.0961, found: 601.0968 and $(M + K)^+$: 617.0701 found 617.0701.

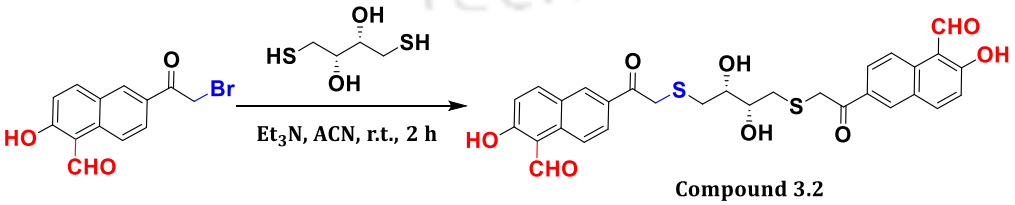

Compound 3.2

Scheme A3.2. Synthesis of compound 6,6'-(2,2'-(((2R,3R)-2,3-dihydroxybutane-1,4 diyl) bis(sulfanediyl)) bis(acetyl)) bis(2-hydroxy-1-naphthaldehyde).

3.4.2.3. Synthesis of tris-aminoguanidine (Compound 3.3):

To the stirring solution of guanidine hydrochloride (500 mg, 5.23 mmol, 1.00 equiv.) in 1,4-dioxane (30 mL), hydrazine monohydrate (0.9 mL, 17.79 mmol, 3.40 equiv.) was added and, after that, a clear solution formed. The reaction mixture was refluxed for 3 h, and a white solid precipitate was formed. Then, the solid precipitate was filtered and washed with 1,4-dioxane (30 mL). The solid was dried under a high vacuum, affording the tris-aminoguanidine as a colourless solid with a 96% yield.[28]

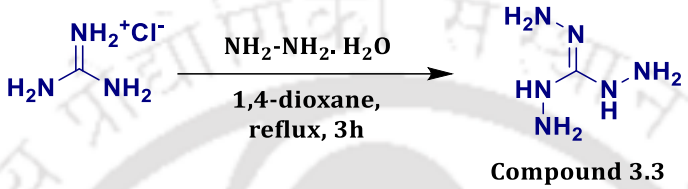

Scheme A3.3. Synthesis of tris-aminoguanidine.

3.4.2.4. Synthesis of ag-CON Polymer:

Initially, 20 mg (0.0345 mmol) of compound 6,6'-(2,2'-(((2R,3R)-2,3-dihydroxybutane-1,4 diyl) bis(sulfanediyl)) bis(acetyl)) bis(2-hydroxy-1-naphthaldehyde) (B) and 3.29 mg (0.0228 mmol) of compound tris-aminoguanidine (C) were taken in a Pyrex tube and dissolved in a dioxane and water solution at a ratio of 1:0.3. Following this, the mixture was vacuum sealed in the Pyrex tube and subjected to sonication for 15 minutes. Subsequently, the sealed tube was heated to 110 ˚C and left to react for a period of 3 days. A solid yellow product formed within the flask, adhering to its walls during this time. The compound was then isolated through filtration and underwent multiple washes with deionized water and various organic solvents, including ethanol, acetonitrile and tetrahydrofuran. After thorough drying in an oven at 70 ˚C for 24 hours, the resulting compound was collected for further use, exhibiting a yield of 92%. Characterization of the compound: solid-state FT-IR (cm^{-1}) = ~3434 cm^{-1} (s), 3317 cm^{-1} (s), **1659 cm^{-1} (s), 1615 cm^{-1} (s), 1594 cm^{-1} (s) 1291 cm^{-1} (s), and 690 cm^{-1} (s) (Figure 1A).**

3.4.2.5. FT-IR spectroscopy analysis:

FT-IR analysis was carried out following the procedure outlined in section 2.5.2.4

3.4.2.6. XPS analysis:

XPS analysis was carried out following the procedure outlined in section 2.5.2.5

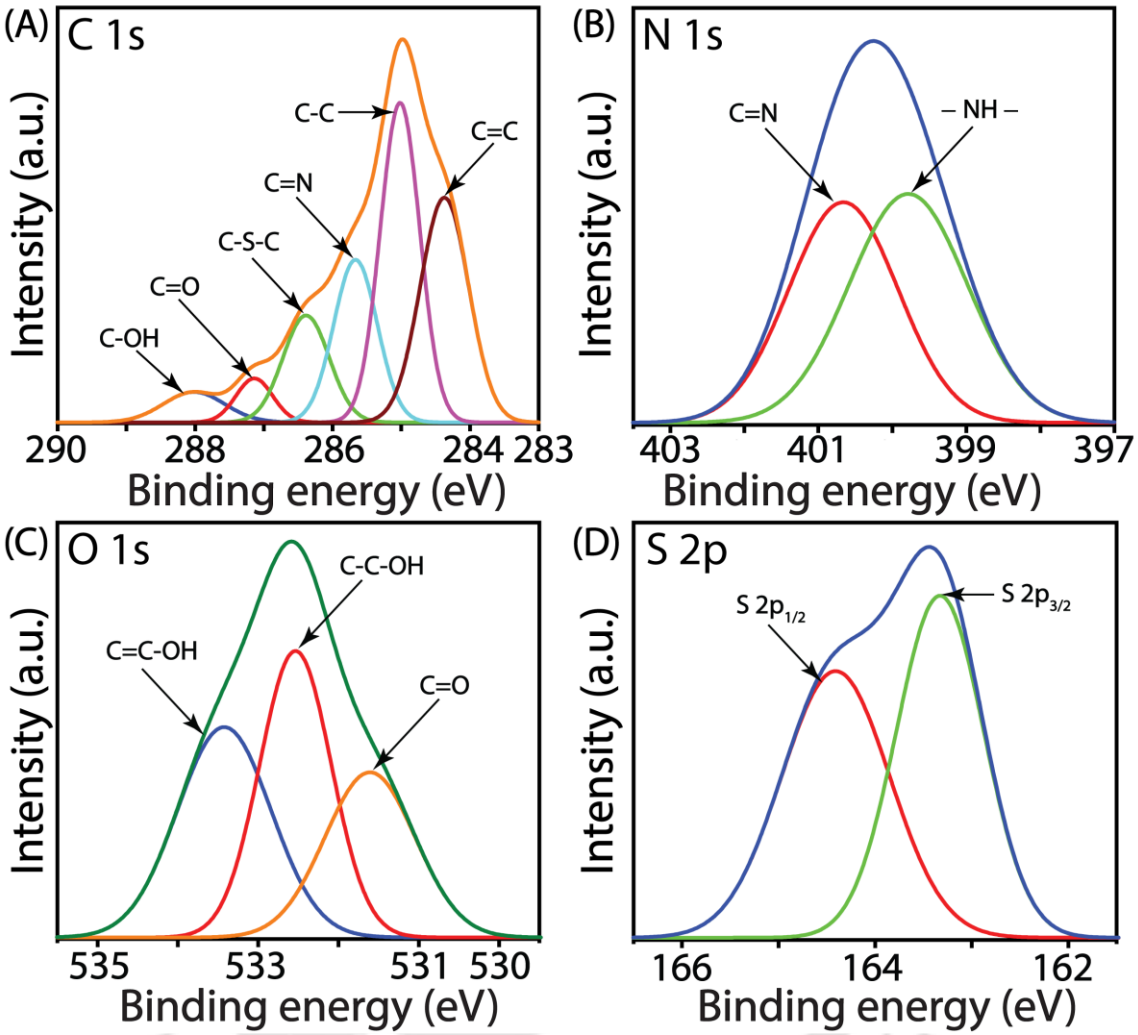

Figure A3.1. XPS data profile: the deconvoluted peak of C 1s (A), N 1s (B), O 1s (C), and S 2p (D) of **ag-CON** polymer.

3.4.2.7. Powder X-ray Diffraction (PXRD) analysis:

The polymer was analysed using PXRD at room temperature. The analysis was conducted using the Phillips PAN analytical diffractometer with Cu Kα radiation (α = 1.5406 Å, 40 kV, 40 mA) and the Rigaku MicroMax 007HF diffractometer.

3.4.2.8. FESEM analysis:

FESEM analysis was carried out following the procedure outlined in section 2.5.2.6

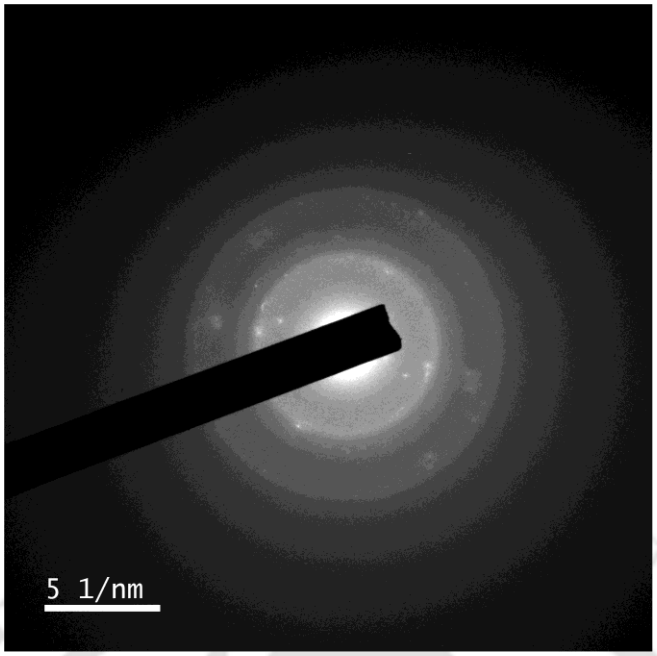

Figure A3.2. Transmission electron microscopy -selected area electron diffraction (TEM-SAED) image of **ag-CON** polymer.

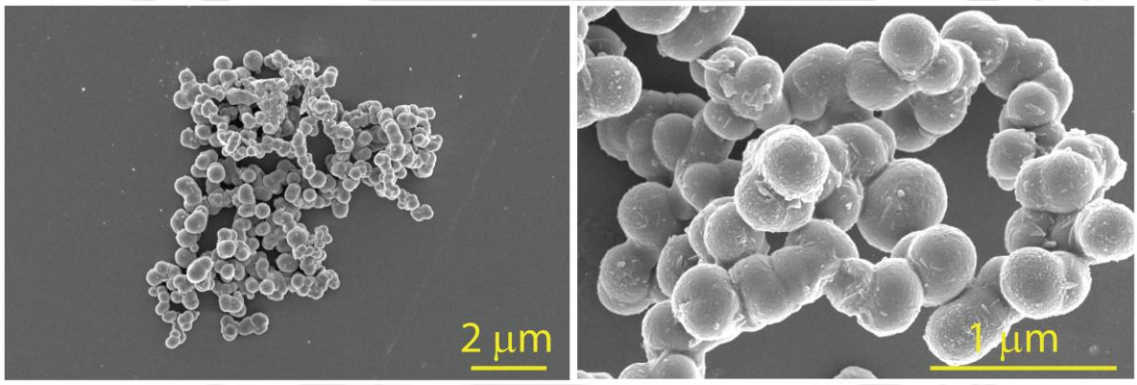

Figure A3.3. Additional FESEM images of **ag-CON** polymer at different magnifications.

3.4.2.9. Transmission Electron Microscopy (TEM) analysis:

Samples were prepared for TEM analysis using the drop-cast method. At first, a small quantity of the polymer was dispersed in milli-Q water, and 10 µL of the suspension solution was deposited onto a carbon-coated copper grid and left to settle for 5 min. Following the gentle blotting of the grid with filter paper, it was allowed to dry overnight at room temperature. The transmission electron microscope utilized for TEM imaging was the JEOL JEM 2100, operating at a maximum accelerating voltage of 200 kV.

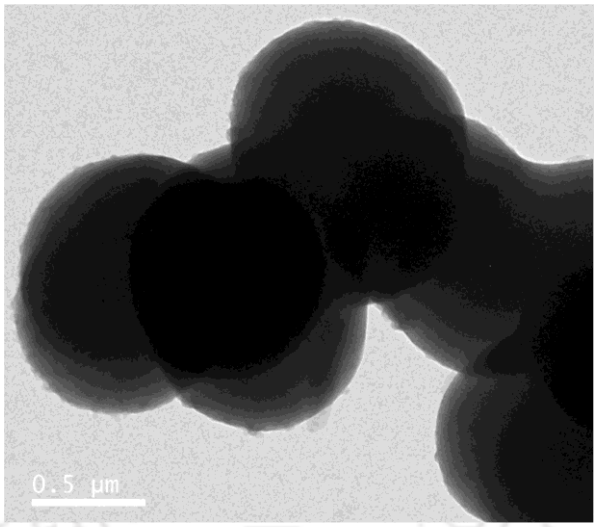

Figure A3.4. Additional TEM image of **ag-CON** polymer.

3.4.2.10. Atomic Force Microscopy (AFM) analysis:

For analysis using Atomic Force Microscopy (AFM), the samples were prepared using the drop-casting technique. 5 µL of polymer suspension in milli-Q water solutions is placed on a silicon wafer and allowed to dry overnight at room temperature. AFM images were captured to analyse the morphology and height profile of the polymer. Asylum AFM AC 240 TS-R3 silicon cantilever probes were used to image the samples. Images of the samples were acquired and analysed through standard AC mode imaging, including topographic, amplitude, and phase images.

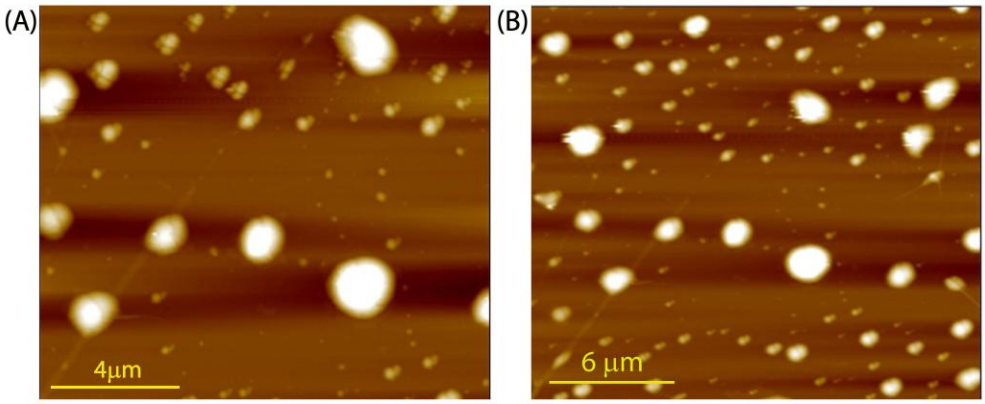

Figure A3.5. Additional AFM image of **ag-CON** polymer.

3.4.2.11. FESEM-EDX and elemental mapping analysis:

FESEM-EDX analysis was carried out following the procedure outlined in Section 2.5.2.6.

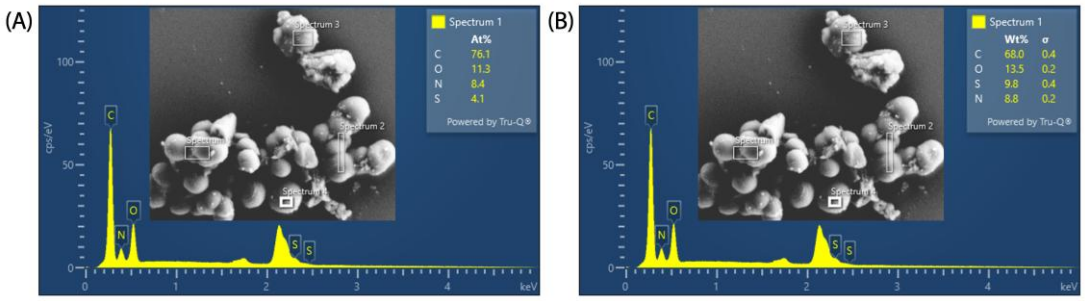

Figure A3.6. FESEM-EDX analysis of **ag-CON** polymer in atomic % (A) and weight % (B).

3.4.2.12. TGA:

TGA was carried out following the procedure outlined in section 2.5.2.7

3.4.2.13. Nitrogen adsorption BET experiments:

The BET adsorption experiment was conducted using Quantachrome Quadrasorb automatic and Autosorb IQ instruments. Nitrogen adsorption isotherms were measured at 77.3 K, facilitated by a liquid nitrogen bath. Prior to surface area analysis, **ag-CON** samples underwent activation at 150 °C for 24 hours under vacuum. The porosity assessment of BIP involved N_2 adsorption on activated samples at 77.3 K, while the average pore diameter was determined using Barrett–Joyner–Halenda (BJH) method. The Brunauer-Emmet-Teller (BET) surface area of BIP was calculated via multipoint BET analysis, with 'P' and 'P_0' representing the equilibrium and saturation pressure of nitrogen within the experimental setup, respectively.

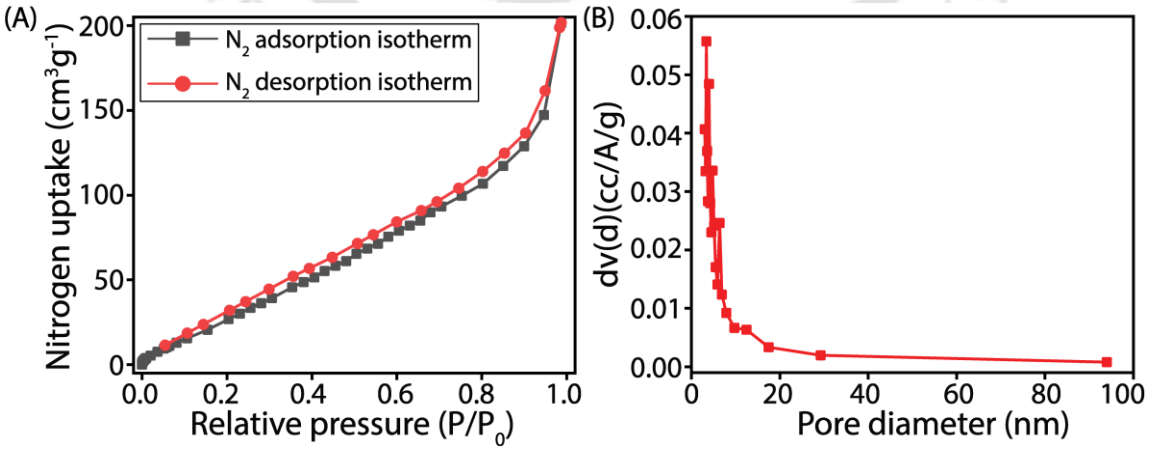

Figure A3.7. Nitrogen adsorption isotherm (A) and the pore-size distribution (B) of **ag-CON** polymer.

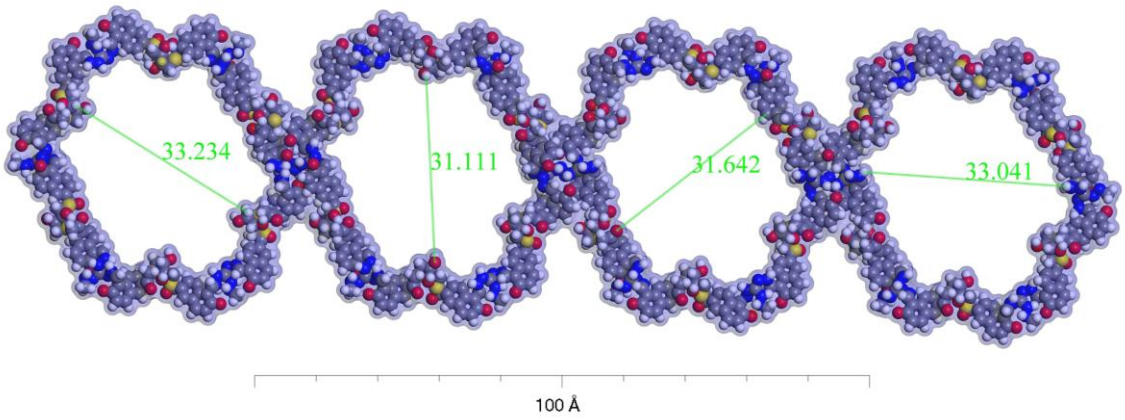

Figure A3.8. Space-filling model of **ag-CON** polymer illustrating the individual pore structure, grey = carbon, red = oxygen, blue = nitrogen, yellow = sulphur, and white = hydrogen (this model was drawn in Materials Studio).

3.4.2.14. Zeta potential study:

Zeta potential study was carried out following the procedure outlined in Section 2.5.2.9.

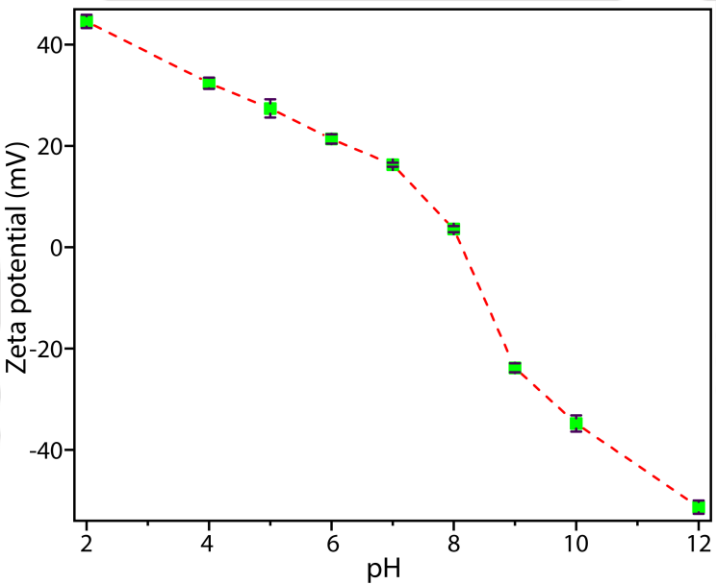

Figure A3.9. Zeta potential of **ag-CON** polymer at different pH.

3.4.2.15. Tyndall effect:

Tyndall effect analysis was carried out following the procedure outlined in section 2.5.2.11

3.4.2.16. DLS study of the ag-CON polymer:

DLS study was carried out following the procedure outlined in section 2.5.2.8

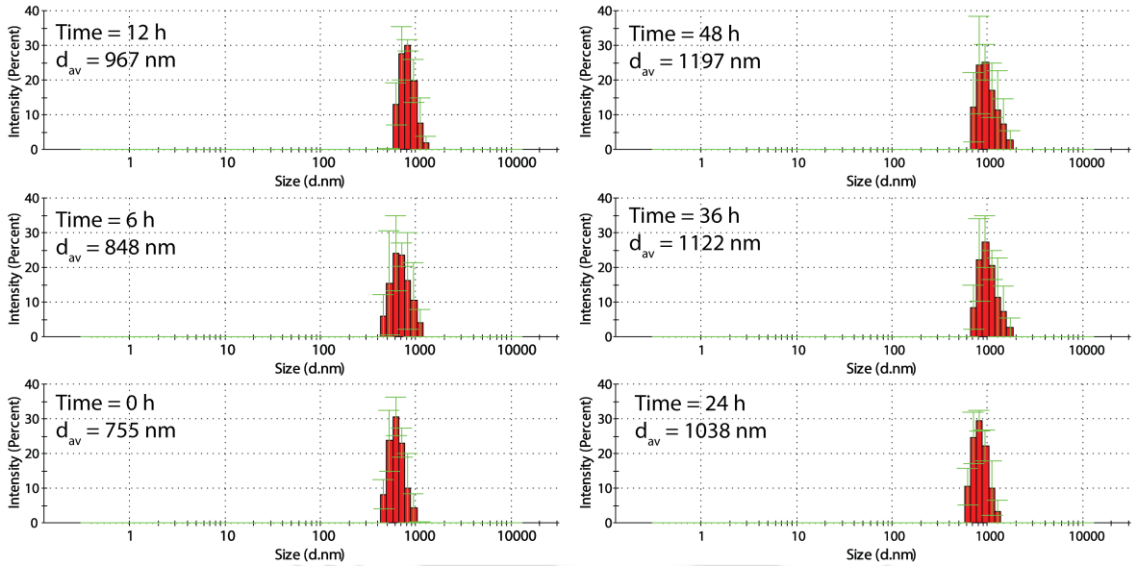

Figure A3.10. DLS measurements of **ag-CON** polymer in water at different time intervals.

3.4.2.17. Chemical stability analysis of the ag-CON polymer:

The polymer was subjected to treatment with various organic solvents such as acetonitrile (ACN), dichloromethane (DCM), ethyl acetate (EtOAc), methanol (MeOH), tetrahydrofuran (THF), acetone, along with 3 N hydrochloric acid (HCl) and 3 N sodium hydroxide (NaOH) solutions for a period of 14 days to evaluate its chemical stability. Following this, their chemical stability was evaluated through Fourier Transform Infrared (FT-IR) analysis.

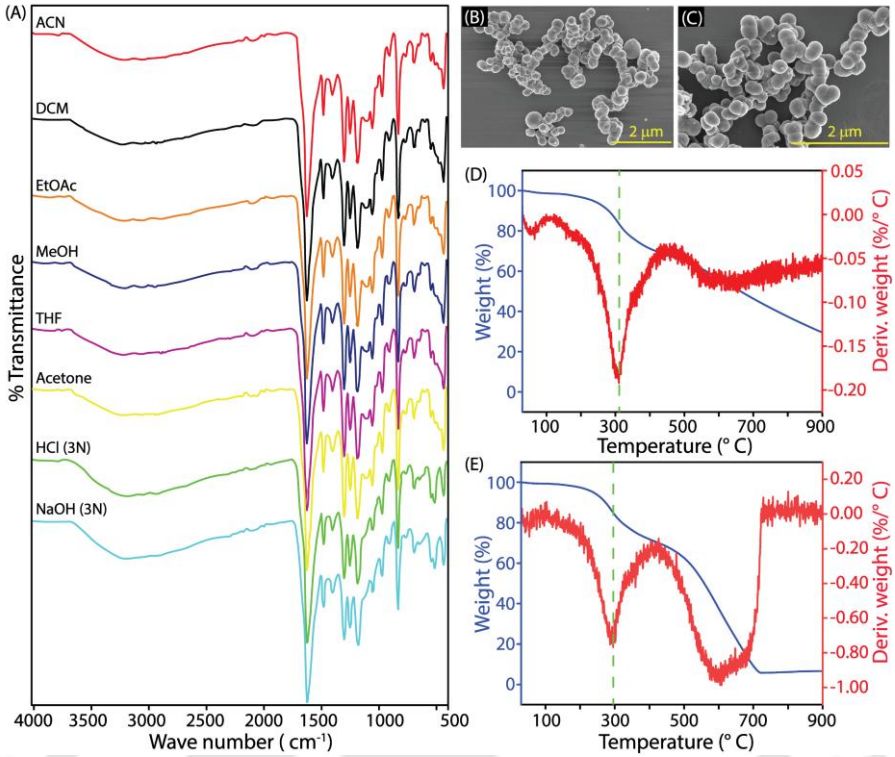

Figure A3.11. FT-IR spectra of **ag-CON** polymer after the treatment (for 14 days) with ACN, DCM, EtOAc, MeOH, THF, DMF, Acetone, HCl (3 N), and NaOH (3 N) solution (A). FESEM images of **ag-CON** polymer after treatment with 3 N NaOH (A) and 3 N HCl (B) for 14 days. TGA graph of **ag-CON** polymer after treatment with 3 N NaOH (A) and 3 N HCl (B) for 14 days.

3.4.3. Selectivity experiments –

3.4.3.1. Anion Selectivity Study:

Anion Selectivity Study was carried out following the procedure outlined in Section 2.5.3.5.

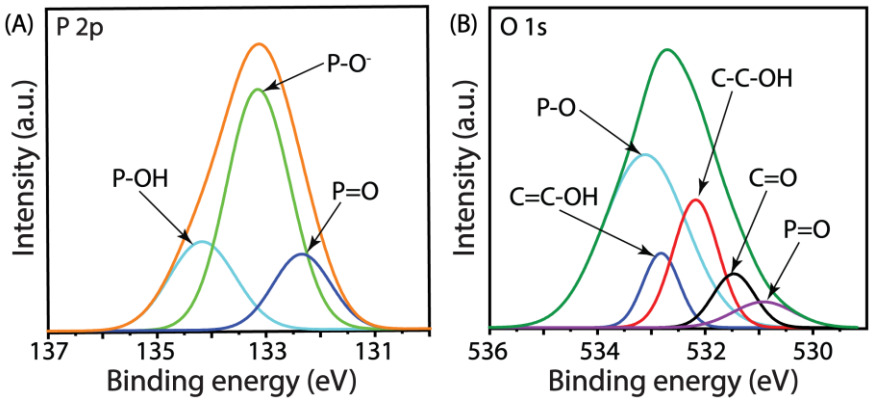

Figure A3.12. XPS data profile: the deconvoluted peak of P2p (A), and O1s (B) of **ag-CON** polymer after phosphate adsorption.

3.4.3.2. Physical characterization for phosphate adsorption by ag-CON polymer:

The phosphate binding ability of the **ag-CON** polymer was assessed through a series of analytical techniques, such as FTIR, XPS, FESEM-EDX, and mapping analysis. In this experiment, a 5 mg sample of the **ag-CON** polymer was subjected to treatment with a 5 mL solution containing 25 ppm of phosphate. The mixture was then sonicated for a duration of 10 minutes to ensure uniformity of the polymer. Next, the samples underwent incubation under shaking conditions for a duration of 6 hours. Following this, the samples underwent centrifugation and filtration to isolate the phosphate-adsorbed **ag-CON** polymer. Prior to the analysis, the **ag-CON** polymer with adsorbed phosphate was rinsed with milli-Q water and subjected to overnight drying using hot air.

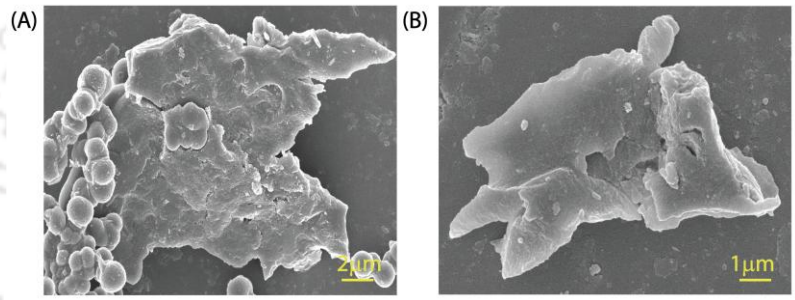

Figure A3.13. FESEM images of **ag-CON** polymer after treatment with 50 ppm phosphate solution (A) and 500 ppm phosphate solution.

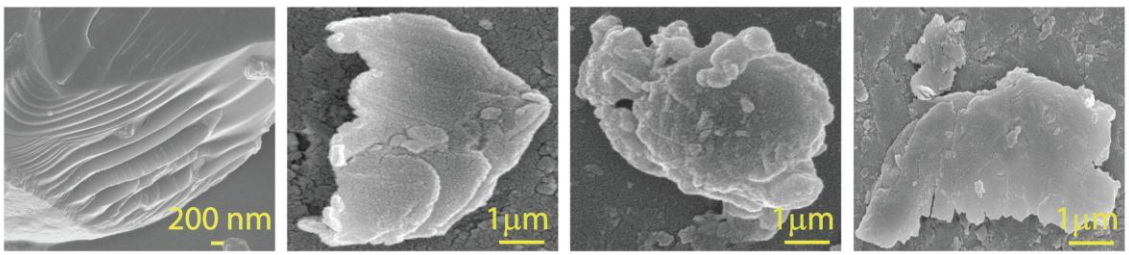

Figure A3.14. Additional FESEM images of **ag-CON** polymer after the treatment with 1000 ppm phosphate solution.

3.4.4. Equation employed for adsorption study –

3.4.4.1. Equation for the calculation of % ion adsorption:

The relative percentage of phosphate ions absorbed from water was carried out following the equation 2.1, outlined in Section 2.5.3.1.

3.4.4.2. Equation for the calculation of the adsorption capacity:

The adsorption capacity of the **ag-CON** polymer was quantified using the equation 2.2, outlined in section 2.5.3.2.

3.4.4.3. Equation for the adsorption isotherm experiment:

The adsorption isotherm patterns were explored using equations 2.3 and 2.4, as outlined in section 2.5.3.3.

3.4.4.4. Adsorption kinetics equations:

The adsorption kinetics patterns were explored using equations 2.5 and 2.7, as outlined in section 2.5.3.4.

3.4.5. Phosphate adsorption experiments –

3.4.5.1. Influence of pH on phosphate ion capture:

The impact of pH on the adsorption of phosphate ions by the ag-CON polymer was investigated using the procedure outlined in Section 2.5.4.1., across different pH levels (4, 5, 6, 7, 8, and 10).

3.4.5.2. Adsorption isotherms experiment:

The efficiency of phosphate ion adsorption by the polymer was assessed using the procedure outlined in Section 2.5.4.2.

3.4.5.3. Adsorption kinetics experiment:

The affinity of phosphate for the polymer over time was assessed using the procedure outlined in Section 2.5.4.3 at various time intervals (20, 40, 60, 90, 120, 150, 180, 210, 240, 270, 300, 330, and 360 seconds).

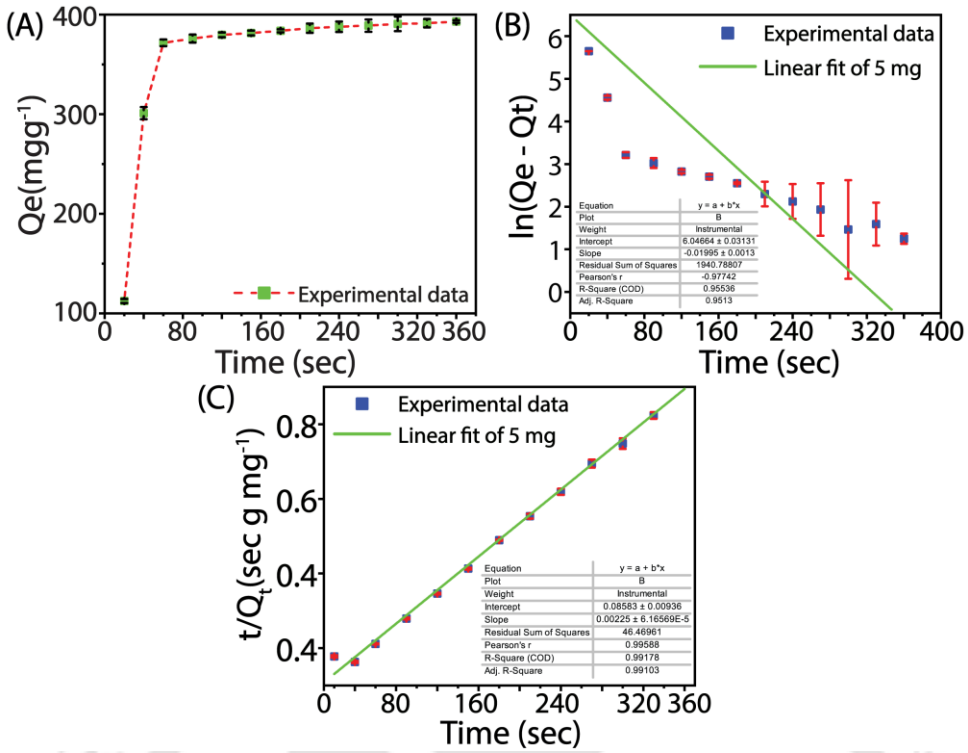

Figure A3.15. Time-dependent desorption isotherm of phosphate by **ag-CON** (5 mg) at pH 6 under room temperature(A), time-dependent desorption efficiency of **ag-CON** fitted with the first order (B) and second order kinetics (C) models.

3.4.5.4. Adsorption kinetics study with different amounts of ag-CON polymer:

The phosphate adsorption behaviour over time, various concentrations of polymer (3 mg, 5 mg, 7 mg, and 10 mg) were assessed using the procedure outlined in Section 2.5.4.3. at various time intervals (20, 40, 60, 90, 120, 150, 180, 210, 240, 270, 300, 330, and 360 seconds).

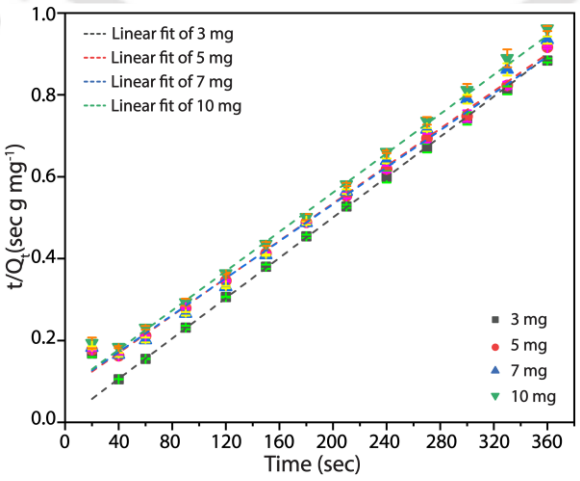

Figure A3.16. Pseudo-second-order kinetics curves of phosphate adsorption on **ag-CON** (3-10 mg) at pH 6.0 under room temperature.

3.4.5.5. Effect of temperature on phosphate adsorption:

To investigate the influence of temperature on phosphate adsorption, four batches of 5 mL 1000 ppm phosphate solution were mixed with 5 mg of the **ag-CON** polymer and agitated individually for 6 hours at varying temperatures (298 K, 313 K, 328 K, and 343 K) at pH 6. Subsequently, the **ag-CON** polymers were separated from the phosphate solution through centrifugation, and the concentration of the phosphate solution before and after the addition of the **ag-CON** polymer was measured using IC.

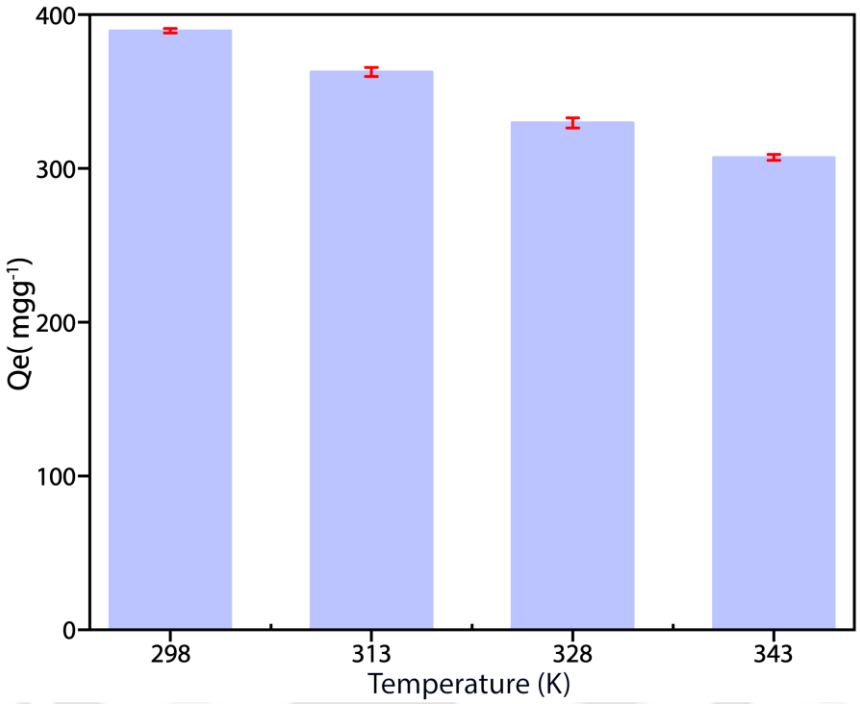

Figure A3.17. The equilibrium adsorption capacity by **ag-CON** polymer at different temperatures.

3.4.5.6. Effect of counter anions on phosphate adsorption:

To explore the impact of competing anions on phosphate adsorption, stock solutions of various sodium salts (F^-, Cl^-, Br^-, NO_3^-, SO_4^{2-}, and HPO_4^{2-}) in Milli-Q water at a 1:100 concentration ratio (phosphate: other anion) were prepared. Subsequently, 5 mg of the **ag-CON** polymer was mixed with 5 mL of each salt solution and agitated for 6 hours. The efficacy of anion adsorption by the **ag-CON** polymer was assessed using IC. Remarkably, the results demonstrated that the **ag-CON** polymer displayed a pronounced preference for capturing the HPO_4^{2-} anion, even in the presence of other competing anions.

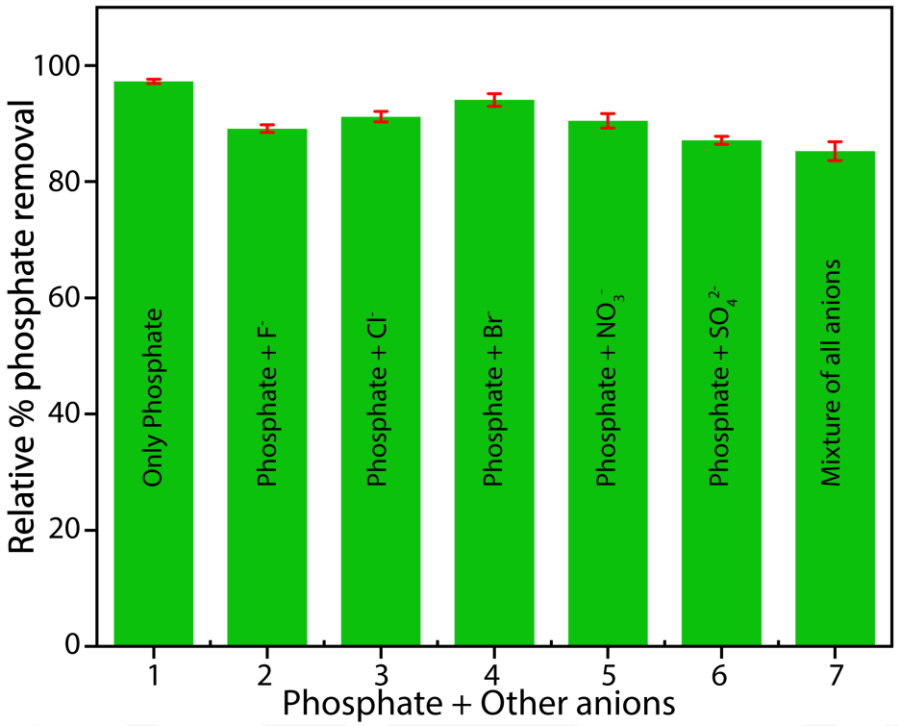

Figure A3.18. Bar diagram for phosphate removal efficiency of **ag-CON** polymer in the presence of F^-, Cl^-, Br^-, NO_3^- and SO_4^{2-} anions.

3.4.5.7. Effect of different metal ions on phosphate adsorption:

From the effect of counter anions on phosphate ion adsorption experiments, it is clear that Cl^- ions have a negligible impact on phosphate ion adsorption by the **ag-CON** polymer. Due to the limiting solubility issue of different metal phosphates, we have selectively chosen the metal chloride salts of Na^+, K^+, Rb^+, Cs^+, Mg^{2+}, and Al^{3+} to analyse the impact of different metal ions on phosphate adsorption. To perform the experiment, stock solutions of the aforementioned metal ions along with phosphate in Milli-Q water at a 1:100 concentration ratio (phosphate: other metal ion) were prepared. Subsequently, 5 mg of the **ag-CON** polymer was mixed with 5 mL of each salt solution and agitated for 6 hours. The efficacy of the phosphate adsorption in the presence of these cations by the **ag-CON** polymer was assessed using IC. Remarkably, the results demonstrated that the **ag-CON** polymer displayed a pronounced preference for capturing the phosphate anion, even in the presence of different metal ions. Furthermore, the results reveal that with an increased positive charge density on the metal ions, the phosphate binding affinity of the **ag-CON** polymer slightly reduces because of the affinity of metal ions binding (from monovalent to trivalent) into the coordination sites (-OH, and -NH) of the polymer.

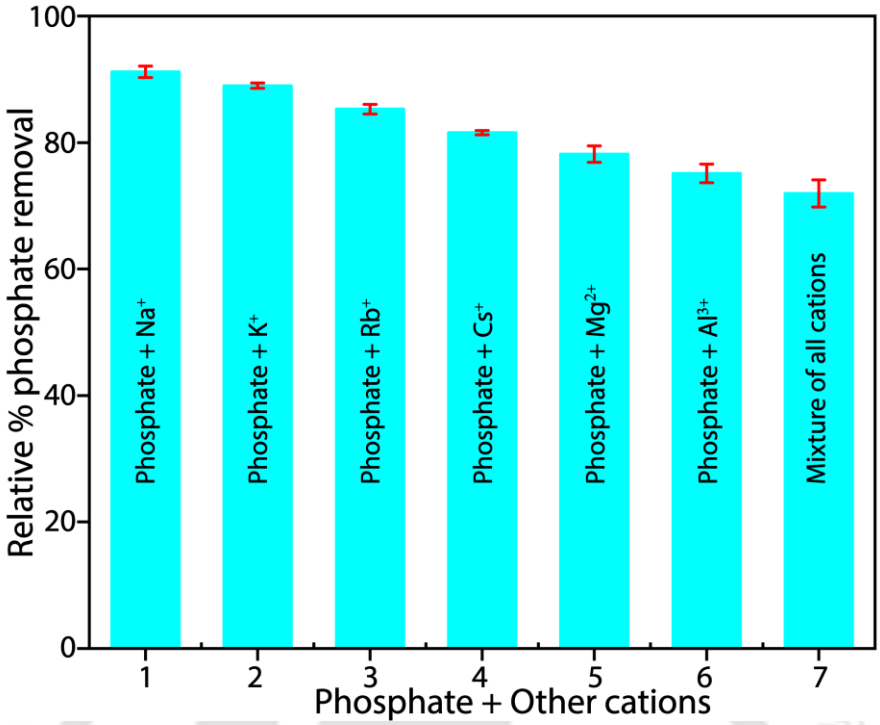

Figure A3.19. Bar diagram for phosphate removal efficiency of **ag-CON** polymer in the presence of Na^+, K^+, Rb^+, Cs^+, Mg^{2+}, and Al^{3+} cations.

3.4.5.8. Low-concentration of phosphate capture study:

To assess the **ag-CON** polymer's effectiveness in adsorbing low-concentration phosphate, a ~ 0.5 ppm phosphate stock solution was initially prepared. Subsequently, 5 mg of the **ag-CON** polymer was combined with 5 mL of the stock solution and agitated for 6 hours. Following this, the polymer was separated from the solution via centrifugation, and the phosphate solution's concentrations before and after treatment with the **ag-CON** polymer were measured using IC.

To evaluate the influence of interfering anions on the low-concentration phosphate adsorption process by the **ag-CON** polymer, a stock solution was prepared containing ~ 0.5 ppm phosphate ions and 100 ppm of other competing anions as mentioned above. Next, 5 mg of the **ag-CON** polymer was mixed with 5 mL of the stock solution and agitated for 6 hours. Subsequently, the **ag-CON** polymer was separated from the phosphate solution using centrifugation, and the phosphate ion concentrations before and after treatment with the **ag-CON** polymer were quantified via IC.

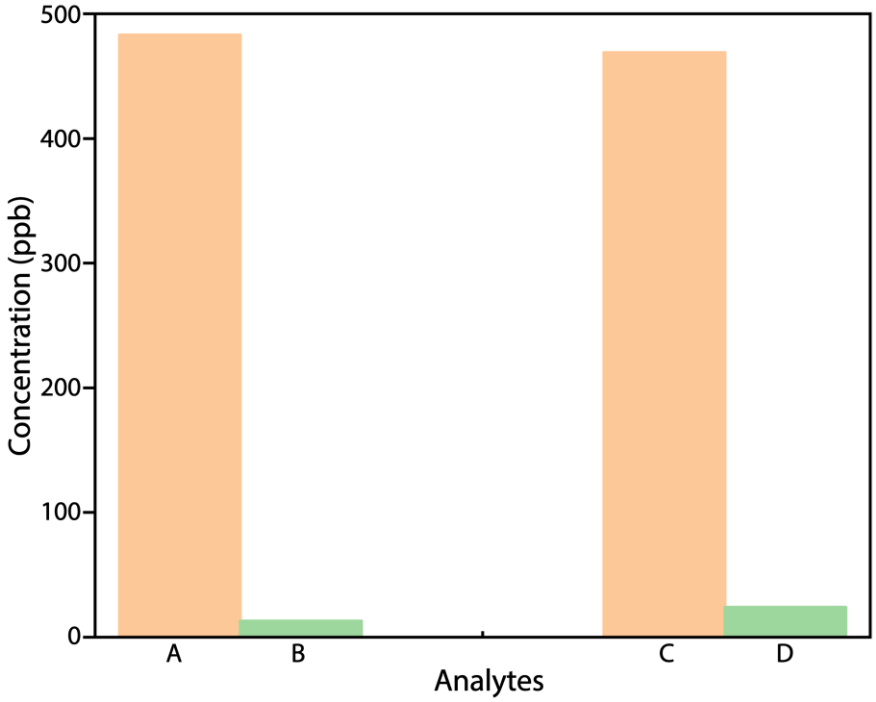

Figure A3.20. Low concentration phosphate ion capture study by **ag-CON** polymer: Concentration of only phosphate ion stock solution before (A) and after (B) the treatment with **ag-CON** polymer. The concentration of phosphate ion in the phosphate and interfering anions mixture before (C) and after (D) the treatment with **ag-CON** polymer.

3.4.5.9. Phosphate removal applicability with the real phosphate contaminated wastewater:

The efficacy of the polymer in removing phosphate from eutrophic water under real-world conditions was assessed using the procedure outlined in Section 2.5.4.6.

Table A3.1. Ion chromatographic analysis demonstrating the concentrations of different competitive anions present before and after the treatment of **ag-CON** of samples A and B.

Sample	Existing anions (concentration in ppm)						pH
	F^-	Cl^-	Br^-	NO_3^-	HPO_4^{2-}	SO_4^{2-}	
Sample A	1.17 ± 0.065	12.87 ± 0.053	0.32 ± 0.037	4.10 ± 0.031	7.82 ± 0.089	11.17 ± 0.042	5.8
After **ag-CON** treatment of sample A (A′)	0.92 ± 0.027	10.55 ± 0.043	0.26 ± 0.033	3.13 ± 0.018	0.12± 0.042	7.18 ± 0.089	
Sample B	1.43 ± 0.027	12.05 ± 0.061	0.24 ± 0.032	3.61 ± 0.046	7.23± 0.068	10.35 ± 0.061	6.2
After **ag-CON** treatment of sample B (B′)	01.04 ± .041	10.12 ± .054	0.23 ± 0.026	2.56 ± 0.039	0.11 ± 0.029	6.52 ± 0.007	

3.4.5.10. Regeneration study of the ag-CON polymer:

The reusability of the polymer was assessed through a series of batch studies involving the repetitive cycles of phosphate adsorption and desorption. During each adsorption cycle, a 5 mg sample of the polymer underwent treatment with a 1000 ppm phosphate solution (5 mL) for a duration of 6 hours. Following the mixing process, the samples were subjected to incubation under shaking conditions for a period of 6 hours. Subsequently, centrifugation and filtration procedures were employed to isolate the polymer, which had adsorbed phosphate, from the unbound phosphate ions present in the supernatant. The supernatant was then diluted to a concentration of 25 ppm, and the concentration of unbound phosphate ions was quantified using IC. The removal of adsorbed phosphate from the polymer was achieved by submerging it in a 5 mL, NaOH (0.5 N) solution with a pH of ~13 at room temperature for a duration of 2 hours. After that, the solution was collected and analysed to quantify the recovered phosphate ions using the ion chromatography technique. Before the subsequent adsorption cycle, the pH of the polymer solution was neutralized to 7 by adding 0.1M HCl. Then, the polymer was collected via centrifugation and filtration, followed by meticulous washing with Milli-Q water to

eliminate any lingering residues. The IC data reveals that the polymer has a high adsorption rate of over 78% for phosphate, and it also shows that the polymer is capable of desorbing more than 90% of the phosphate even after undergoing ten consecutive cycles.

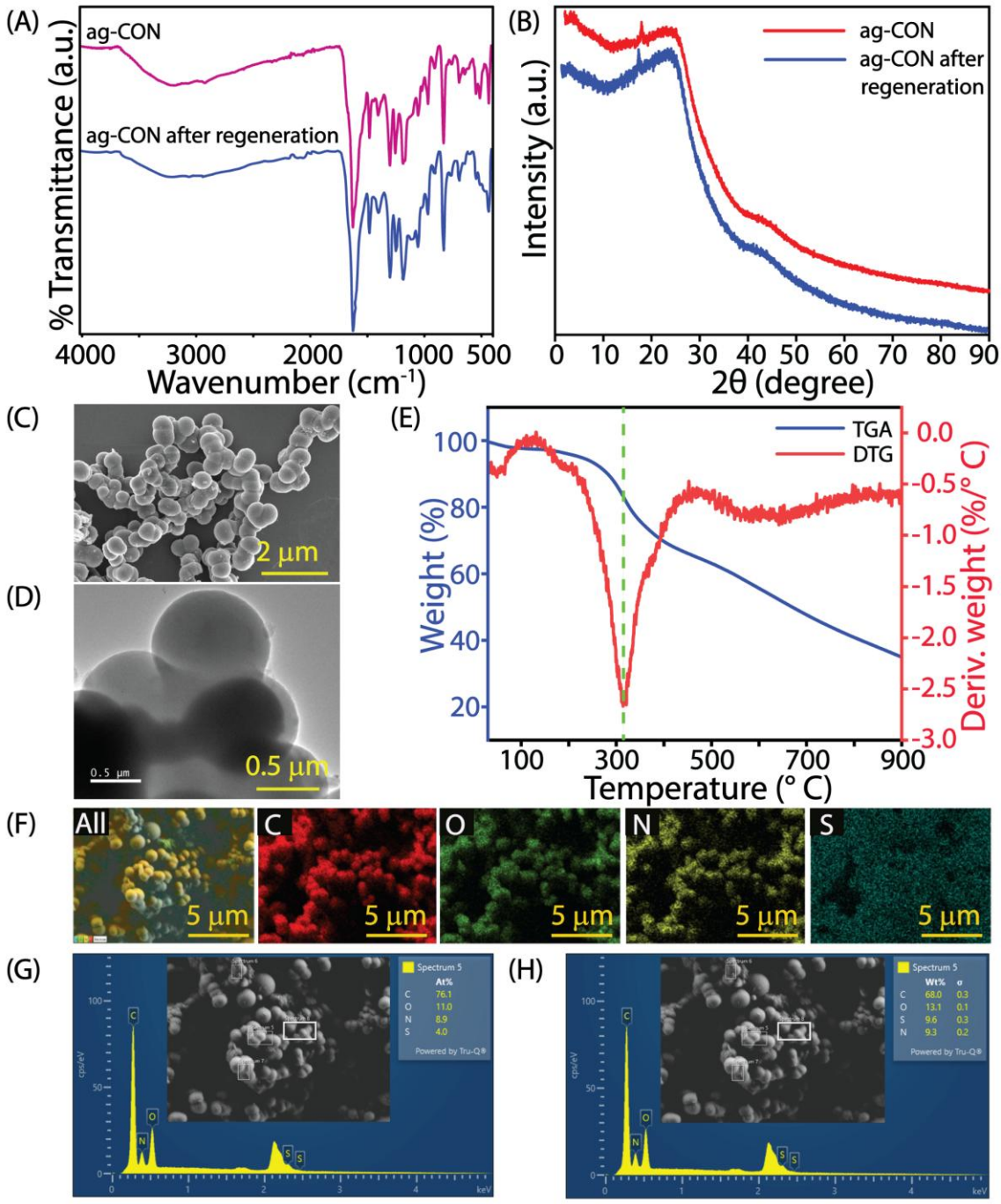

Figure A3.21. FT-IR (A), PXRD (B), FESEM image (C), TEM image (D), FESEM mapping (F) and elemental analysis in atomic % (G) and weight % (H) of **ag-CON** polymer after undergoing ten cycles of regeneration.

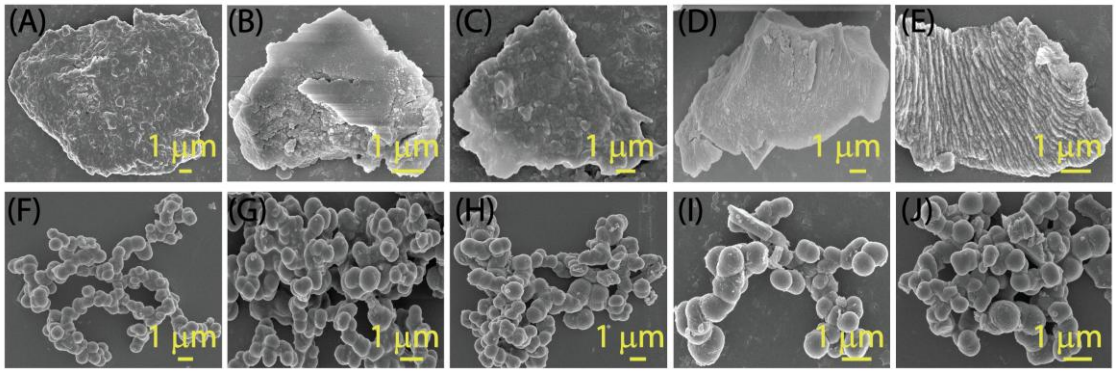

Figure A3.22. FESEM images of **ag-CON** polymer after 2nd (A), 4th (B), 6th (C), 8th (D) and 10th (E) cycle of phosphate adsorption. FESEM images of **ag-CON** polymer after 2nd (F), 4th (G), 6th (H), 8th (I) and 10th (J) cycle of phosphate desorption.

3.4.5.11. Phosphate desorption kinetics study:

The phosphate desorption kinetics from the ag-CON polymer were assessed using the procedure outlined in Section 2.5.4.8 at varying time intervals (ranging from 50 to 1200 seconds).

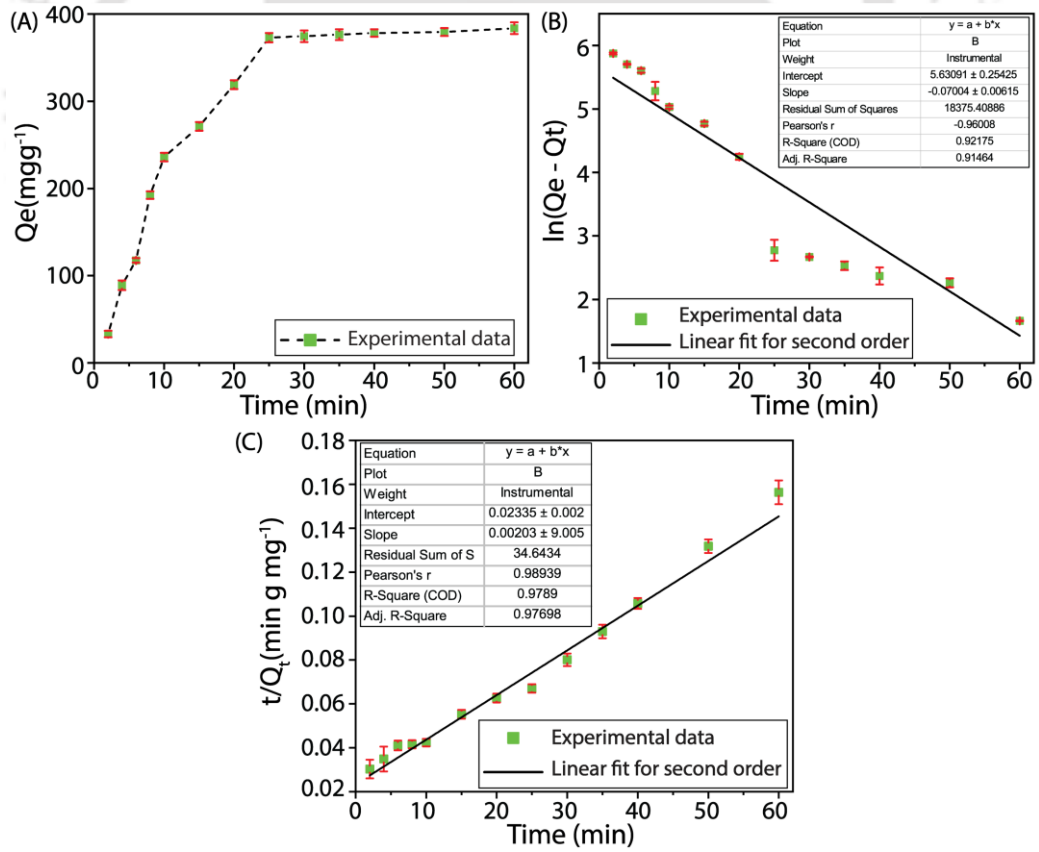

Figure A3.23. Time-dependent desorption isotherm of phosphate by **ag-CON** (5mg) under room temperature(A), time-dependent desorption efficiency of **ag-CON** fitted with the first order(B) and second order kinetics(C) models.

3.4.5.12. Proposed phosphate adsorption-desorption mechanisms by the ag-CON polymer:

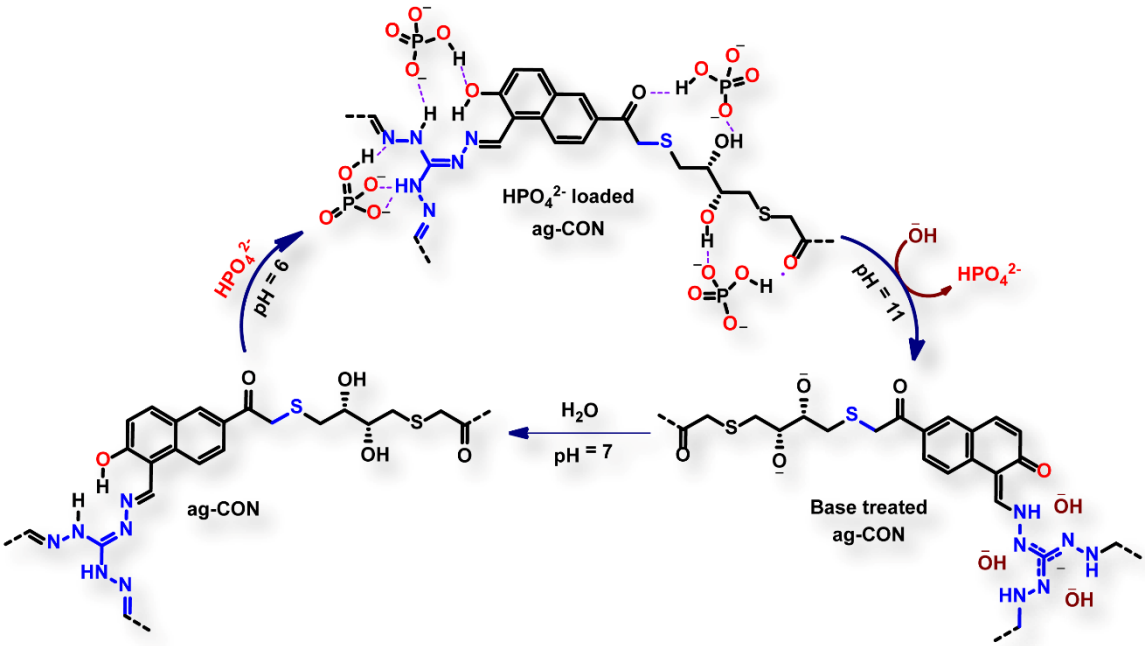

Figure A3.24. Possible mechanistic pathways for adsorption and desorption process by **ag-CON** polymer.

3.4.5.13. Dynamic adsorption column experiment:

An experimental setup was prepared using a glass column with a diameter of approximately 0.5 cm. The column was filled with 50 mg of the **ag-CON** polymer and 3 g of sand, creating a bed length of approximately 5 cm. Initially, 50 mL of ultrapure milli-Q water was carefully passed through the column bed to remove bubbles. After that, 500 mL of a 50 ppm aqueous phosphate solution, along with ten-fold excess other anions (F^-, Cl^-, Br^-, NO_3^-, and SO_4^{2-}), was passed through the column with a flow rate of 0.5 mL/min. The eluents from the column were collected in 10 separate 50 mL batches, and the concentration of each batch was determined using IC. Observations revealed phosphate concentrations of up to 300 mL in column eluents were lower than the level recommended by the World Health Organization (WHO). Before proceeding to the next cycle, the column was revitalized with 100 mL of a 1M NaOH solution. Experimental data revealed efficient desorption of over 93% phosphate from the polymer. The experiment was repeated for 3 cycles, consistently yielding phosphate concentrations below the WHO-recommended threshold in 250 – 300 mL

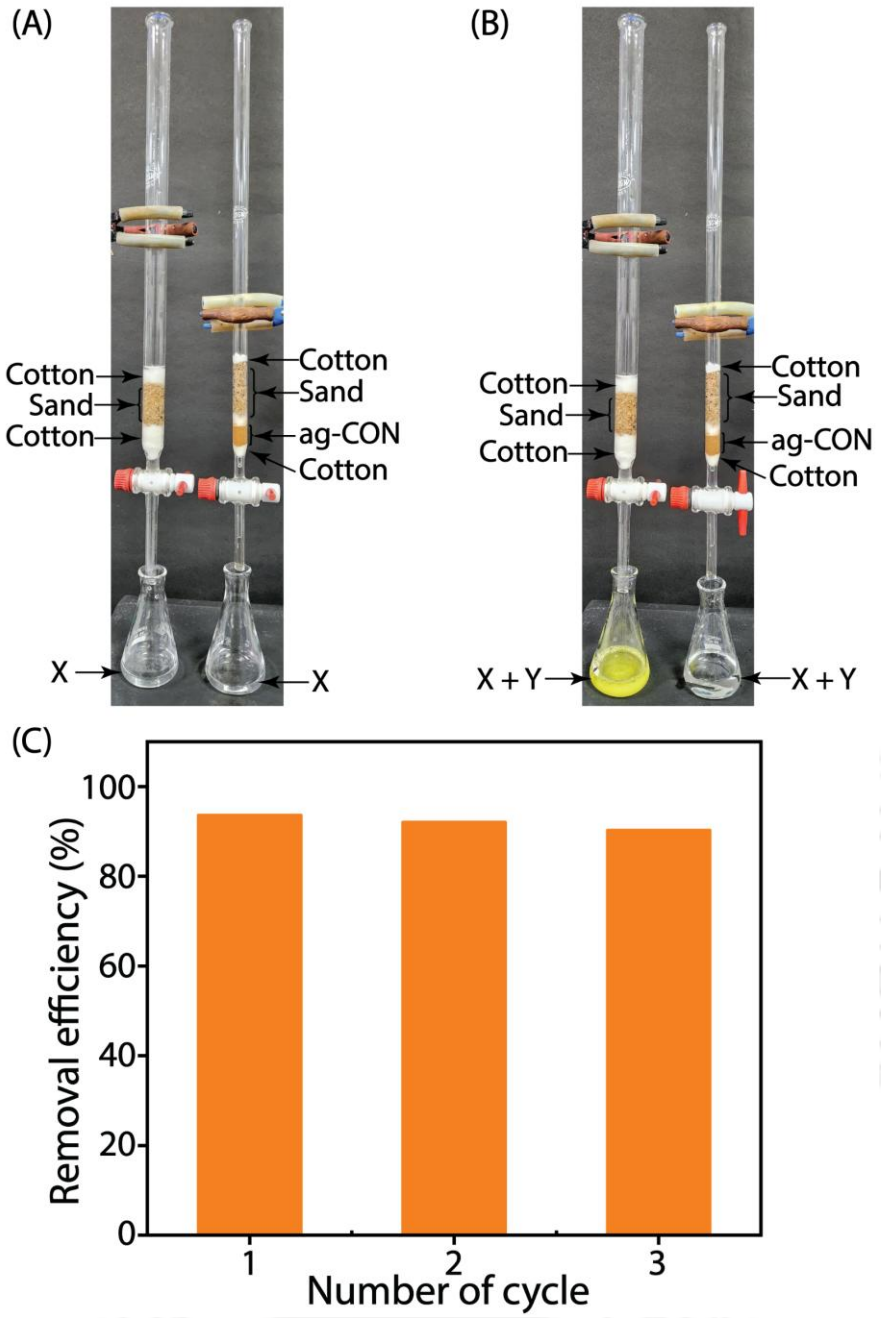

Figure A3.25. Digital image for dynamic adsorption column experiment before (A) and after (B) phosphate adsorption, here X = mixture ammonium molybdate hexahydrate and concentrated HNO_3 solution, and Y = eluents that passed through the column. Phosphate ions desorption efficiency (%) of **ag-CON** polymer in adsorption column experiment (C).

of column eluent and efficiently removing over 90% of the phosphate from the **ag-CON** polymer after the third cycle, showcasing the ability of the polymer to effectively replicate real-time scenarios. For visual observation, two conical flasks were each

filled with 10 mL of an aqueous solution comprising ammonium molybdate tetrahydrate and concentrated nitric acid. Two columns were prepared, one containing a mixture of **ag-CON** polymer and sand in a specified ratio, while the other contained only sand. Subsequently, approximately equal volumes of 50 ppm phosphate solutions were passed through each column. A notable colour change, from colourless to yellow, was discerned in the solution of molybdate tetrahydrate and concentrated nitric acid upon elution through the sand-packed column. Conversely, no colour change was observed in the solution eluted through the column packed with **ag-CON** polymer. These visual distinctions indicate that the presence of phosphate ions in the eluent passing through the column packed with **ag-CON** polymer was significantly lower than in the sand-packed column. This leads to the conclusion that the **ag-CON** polymer efficiently adsorbed phosphate ions, resulting in minimal colour change in the solution. Conversely, in the absence of **ag-CON** polymer, the sand-packed column allowed phosphate ions to pass through, inducing the observed colour change in the solution.

3.4.6. ^{1}H NMR and ^{13}C NMR spectra of synthesized compounds –

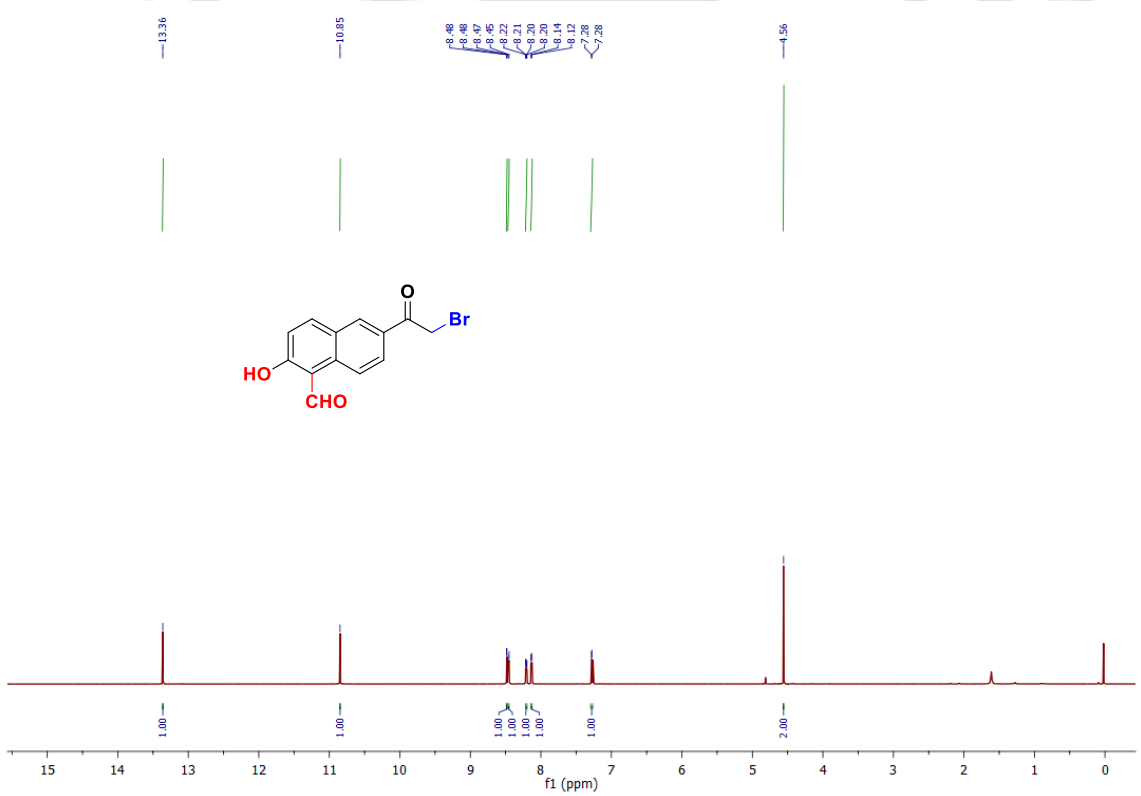

Figure A3.26. ^{1}H NMR spectra of 6-(2-bromoacetyl)-2-hydroxy-1-naphthaldehyde.

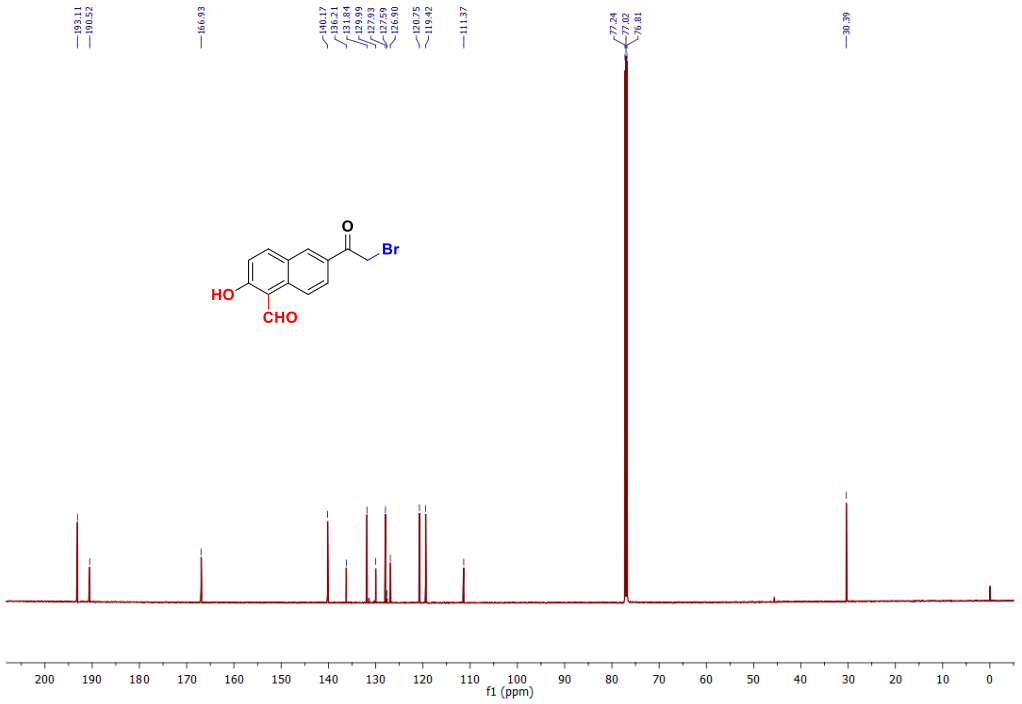

Figure A3.27. ^{13}C NMR spectra of 6-(2-bromoacetyl)-2-hydroxy-1-naphthaldehyde.

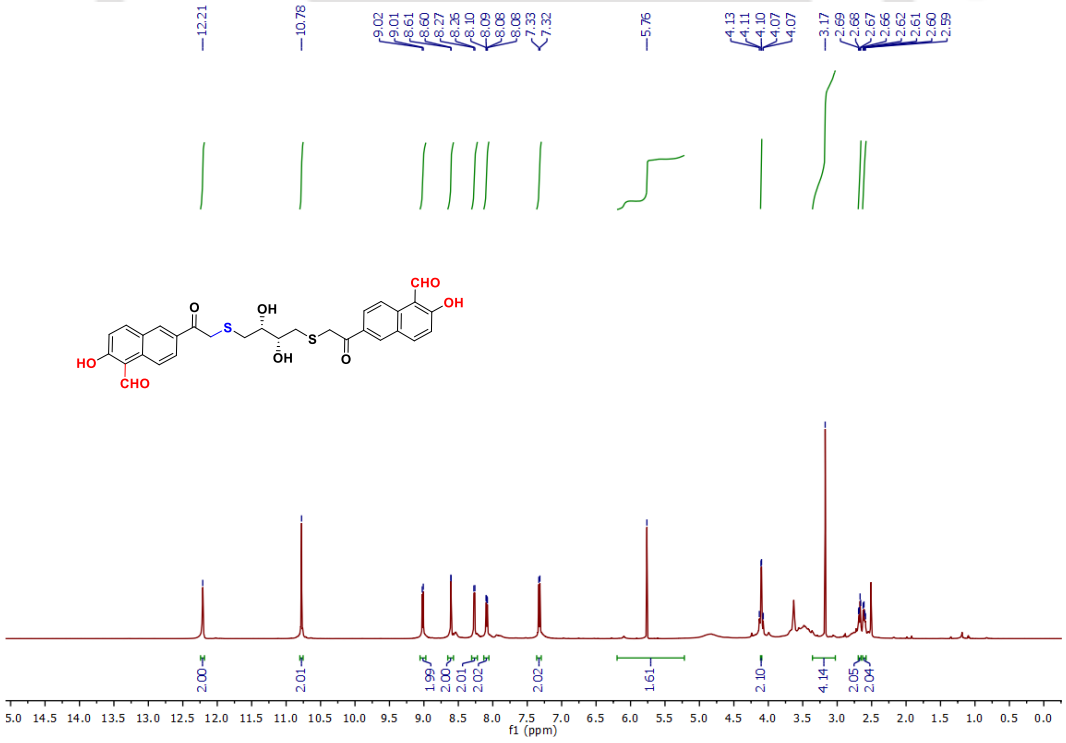

Figure A3.28. ^{1}H NMR spectra of 6,6'-(2,2'-(((2R,3R)-2,3-dihydroxybutane-1,4 diyl) bis(sulfanediyl)) bis(acetyl)) bis(2-hydroxy-1-naphthaldehyde).

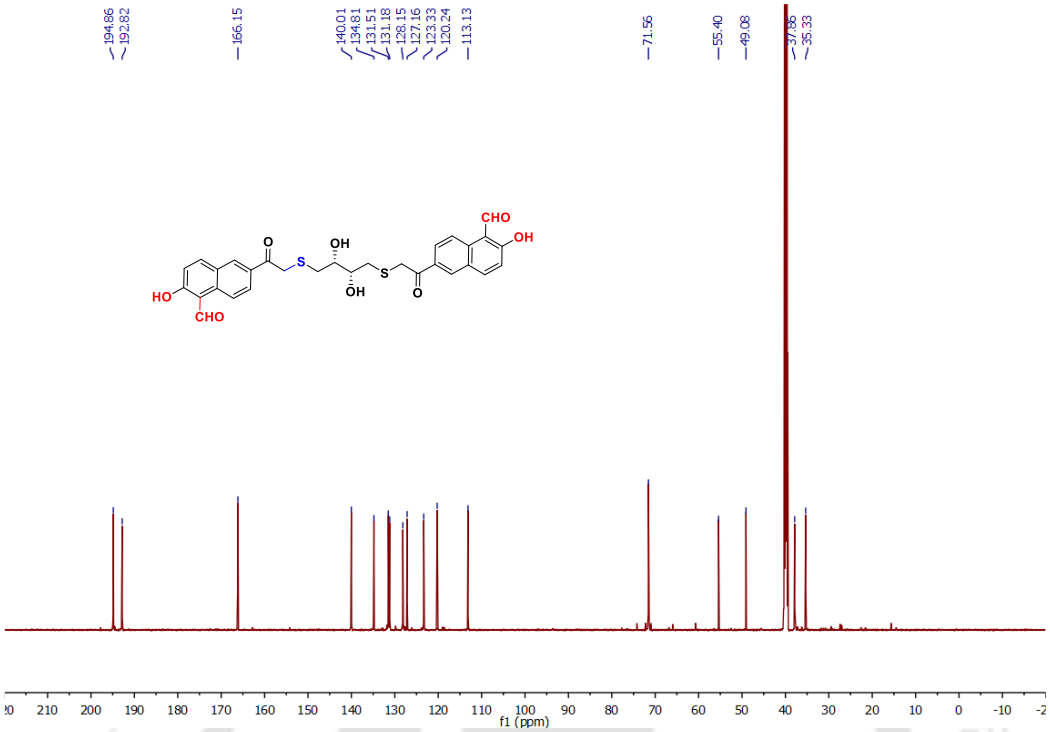

Figure A3.29. ^{13}C NMR (B) spectra of 6,6'-(2,2'-(((2R,3R)-2,3-dihydroxybutane-1,4 diyl) bis(sulfanediyl)) bis(acetyl)) bis(2-hydroxy-1-naphthaldehyde).

3.5. References

1. Hassan, M. H.; Stanton, R.; Secora, J.; Trivedi, D. J.; Andreescu, S., Ultrafast removal of phosphate from eutrophic waters using a cerium-based metal–organic framework. *ACS Appl. Mater. Interfaces* **2020,** *12* (47), 52788-52796.
2. Fang, L.; Liu, R.; Li, J.; Xu, C.; Huang, L.-Z.; Wang, D., Magnetite/Lanthanum hydroxide for phosphate sequestration and recovery from lake and the attenuation effects of sediment particles. *Water Res.* **2018,** *130*, 243-254.
3. Shang, D.; Li, D.; Chen, B.; Luo, B.; Huang, Y.; Shi, W., 2D–2D SnS2/covalent organic framework heterojunction photocatalysts for highly enhanced solar-driven hydrogen evolution without cocatalysts. *ACS Sustainable Chem. Eng.* **2021,** *9* (42), 14238-14248.
4. Hou, J.; Wang, H.; Zhang, H., Zirconium metal–organic framework materials for efficient ion adsorption and sieving. *Ind. Eng. Chem. Res.* **2020,** *59* (29), 12907-12923.
5. Ribet, S. M.; Shindel, B.; Dos Reis, R.; Nandwana, V.; Dravid, V. P., Phosphate Elimination and Recovery Lightweight (PEARL) membrane: A sustainable environmental remediation approach. *Proc. Natl. Acad. Sci. U. S. A.* **2021,** *118* (23), e2102583118.
6. Nakamura, S.; Amano, M.; Saegusa, Y.; Sato, T., Preparation of aminoalkyl celluloses and their adsorption and desorption of heavy metal ions. *J. Appl. Polym. Sci.* **1992,** *45* (2), 265-271.
7. Orlando, U.; Okuda, T.; Baes, A.; Nishijima, W.; Okada, M., Chemical properties of anion-exchangers prepared from waste natural materials. *React. Funct. Polym.* **2003,** *55* (3), 311-318.

8. Orlando, U.; Okuda, T.; Baes, A.; Nishijima, W.; Okada, M., Chemical properties of anion-exchangers prepared from waste natural materials. *Dyes Pigm.* **2003,** *55* (3), 311-318.
9. Robinson, T.; Chandran, B.; Nigam, P., Removal of dyes from a synthetic textile dye effluent by biosorption on apple pomace and wheat straw. *Water Res.* **2002,** *36* (11), 2824-2830.
10. Ajmal, M.; Khan, A. H.; Ahmad, S.; Ahmad, A., Role of sawdust in the removal of copper (II) from industrial wastes. *Water Res.* **1998,** *32* (10), 3085-3091.
11. Manju, G.; Raji, C.; Anirudhan, T., Evaluation of coconut husk carbon for the removal of arsenic from water. *Water Res.* **1998,** *32* (10), 3062-3070.
12. Orlando, U.; Baes, A.; Nishijima, W.; Okada, M., Preparation of agricultural residue anion exchangers and its nitrate maximum adsorption capacity. *Chemosphere* **2002,** *48* (10), 1041-1046.
13. Anirudhan, T.; Unnithan, M. R., Arsenic (V) removal from aqueous solutions using an anion exchanger derived from coconut coir pith and its recovery. *Chemosphere* **2007,** *66* (1), 60-66.
14. Gao, B.-Y.; Xu, X.; Wang, Y.; Yue, Q.-Y.; Xu, X.-M., Preparation and characteristics of quaternary amino anion exchanger from wheat residue. *J. Hazard. Mater.* **2009,** *165* (1-3), 461-468.
15. Qiu, H.; Liang, C.; Zhang, X.; Chen, M.; Zhao, Y.; Tao, T.; Xu, Z.; Liu, G., Fabrication of a biomass-based hydrous zirconium oxide nanocomposite for preferable phosphate removal and recovery. *ACS Appl. Mater. Interfaces* **2015,** *7* (37), 20835-20844.
16. Qiu, H.; Liang, C.; Yu, J.; Zhang, Q.; Song, M.; Chen, F., Preferable phosphate sequestration by nano-La (III)(hydr) oxides modified wheat straw with excellent properties in regeneration. *J. Chem. Eng.* **2017,** *315*, 345-354.
17. Zhang, B.; Chen, N.; Feng, C.; Zhang, Z., Adsorption for phosphate by crosslinked/non-crosslinked-chitosan-Fe (III) complex sorbents: Characteristic and mechanism. *Chem. Eng. J.* **2018,** *353*, 361-372.
18. Huang, Y.; Lee, X.; Grattieri, M.; Yuan, M.; Cai, R.; Macazo, F. C.; Minteer, S. D., Modified biochar for phosphate adsorption in environmentally relevant conditions. *Chem. Eng. J.* **2020,** *380*, 122375.
19. Zong, E.; Liu, X.; Jiang, J.; Fu, S.; Chu, F., Preparation and characterization of zirconia-loaded lignocellulosic butanol residue as a biosorbent for phosphate removal from aqueous solution. *Appl. Surf. Sci.* **2016,** *387*, 419-430.
20. Zhang, M.; Lin, K.; Li, X.; Wu, L.; Yu, J.; Cao, S.; Zhang, D.; Xu, L.; Parikh, S. J.; Ok, Y. S., Removal of phosphate from water by paper mill sludge biochar. *Environ. Pollut.* **2022,** *293*, 118521.
21. Dey, S.; Das, S.; Patel, A.; Raj, K. V.; Vanka, K.; Manna, D., Antimicrobial two-dimensional covalent organic nanosheets (2D-CONs) for the fast and highly efficient capture and recovery of phosphate ions from water. *J. Mater. Chem. A* **2022,** *10* (9), 4585-4593.
22. Neal, J. F.; Zhao, W.; Grooms, A. J.; Smeltzer, M. A.; Shook, B. M.; Flood, A. H.; Allen, H. C., Interfacial supramolecular structures of amphiphilic receptors drive aqueous phosphate recognition. *J. Am. Chem. Soc.* **2019,** *141* (19), 7876-7886.
23. Kato, Y.; Conn, M. M.; Rebek, J. J., Water-soluble receptors for cyclic-AMP and their use for evaluating phosphate-guanidinium interactions. *J. Am. Chem. Soc.* **1994,** *116* (8), 3279-3284.

24. Paltrinieri, L.; Wang, M.; Sachdeva, S.; Besseling, N. A.; Sudhölter, E. J.; De Smet, L. C., Fe 3 O 4 nanoparticles coated with a guanidinium-functionalized polyelectrolyte extend the pH range for phosphate binding. *J. Mater. Chem. A* **2017,** *5* (35), 18476-18485.
25. Zhang, Z.; Dong, X.; Yin, J.; Li, Z.-G.; Li, X.; Zhang, D.; Pan, T.; Lei, Q.; Liu, X.; Xie, Y., Chemically stable guanidinium covalent organic framework for the efficient capture of low-concentration iodine at high temperatures. *J. Am. Chem. Soc.* **2022,** *144* (15), 6821-6829.
26. Das, S.; Hazarika, G.; Manna, D., Guanidine-functionalized fluorescent sp2 carbon-conjugated covalent organic framework for sensing and capture of Pd (II) and Cr (VI) ions. *Chem. Eur. J.* **2023,** *29* (15), e202203595.
27. Roy, B.; Mengji, R.; Roy, S.; Pal, B.; Jana, A.; Singh, N. P., NIR-responsive lysosomotropic phototrigger: an "AIE+ ESIPT" active naphthalene-based single-component photoresponsive nanocarrier with two-photon uncaging and real-time monitoring ability. *ACS Appl. Mater. Interfaces* **2022,** *14* (4), 4862-4870.
28. Schnell, S. D.; Hoff, L. V.; Panchagnula, A.; Wurzenberger, M. H.; Klapötke, T. M.; Sieber, S.; Linden, A.; Gademann, K., 3-Bromotetrazine: labelling of macromolecules via monosubstituted bifunctional s-tetrazines. *Chem. Sci.* **2020,** *11* (11), 3042-3047.
29. Mitra, S.; Kandambeth, S.; Biswal, B. P.; Khayum M, A.; Choudhury, C. K.; Mehta, M.; Kaur, G.; Banerjee, S.; Prabhune, A.; Verma, S., Self-exfoliated guanidinium-based ionic covalent organic nanosheets (iCONs). *J. Am. Chem. Soc.* **2016,** *138* (8), 2823-2828.
30. Vidyasagar, D.; Ghugal, S. G.; Umare, S. S.; Banavoth, M., Extended π-conjugative np type homostructural graphitic carbon nitride for photodegradation and charge-storage applications. *Sci. Rep.* **2019,** *9* (1), 7186.
31. Gao, F.; Shi, W.; Dai, R.; Wang, Z., Effective and selective removal of phosphate from wastewater using guanidinium-functionalized polyelectrolyte-modified electrodes in capacitive deionization. *ACS EST Water* **2021,** *2* (1), 237-246.
32. Rosa, N. M.; Ferreira, F. H. d. C.; Farrell, N. P.; Costa, L. A. S., TriplatinNC and biomolecules: building models based on non-covalent interactions. *Front. Chem.* **2019,** *7*, 307.
33. Zhu, X.; Li, B.; Yang, J.; Li, Y.; Zhao, W.; Shi, J.; Gu, J., Effective adsorption and enhanced removal of organophosphorus pesticides from aqueous solution by Zr-based MOFs of UiO-67. *ACS Appl. Mater. Interfaces* **2015,** *7* (1), 223-231.
34. Min, X.; Wu, X.; Shao, P.; Ren, Z.; Ding, L.; Luo, X., Ultra-high capacity of lanthanum-doped UiO-66 for phosphate capture: unusual doping of lanthanum by the reduction of coordination number. *Chem. Eng. J.* **2019,** *358*, 321-330.
35. Yang, J.; Dai, Y.; Zhu, X.; Wang, Z.; Li, Y.; Zhuang, Q.; Shi, J.; Gu, J., Metal–organic frameworks with inherent recognition sites for selective phosphate sensing through their coordination-induced fluorescence enhancement effect. *J. Mater. Chem. A* **2015,** *3* (14), 7445-7452.
36. Xing, P.; Li, Y.; Xue, S.; Fiona Phua, S. Z.; Ding, C.; Chen, H.; Zhao, Y., Occurrence of chiral nanostructures induced by multiple hydrogen bonds. *J. Am. Chem. Soc.* **2019,** *141* (25), 9946-9954.
37. McNair, R.; Kumar, S.; Wonanke, A. D.; Addicoat, M. A.; Dryfe, R. A.; Szekely, G., Ionic covalent organic nanosheet (iCON)–quaternized polybenzimidazole nanocomposite anion-exchange membranes to enhance the performance of membrane capacitive deionization. *Desalination* **2022,** *533*, 115777.

Chapter 4

Bis-imidazolium linked covalent organic network effectively removes arsenate from water and wastewater containing phosphates

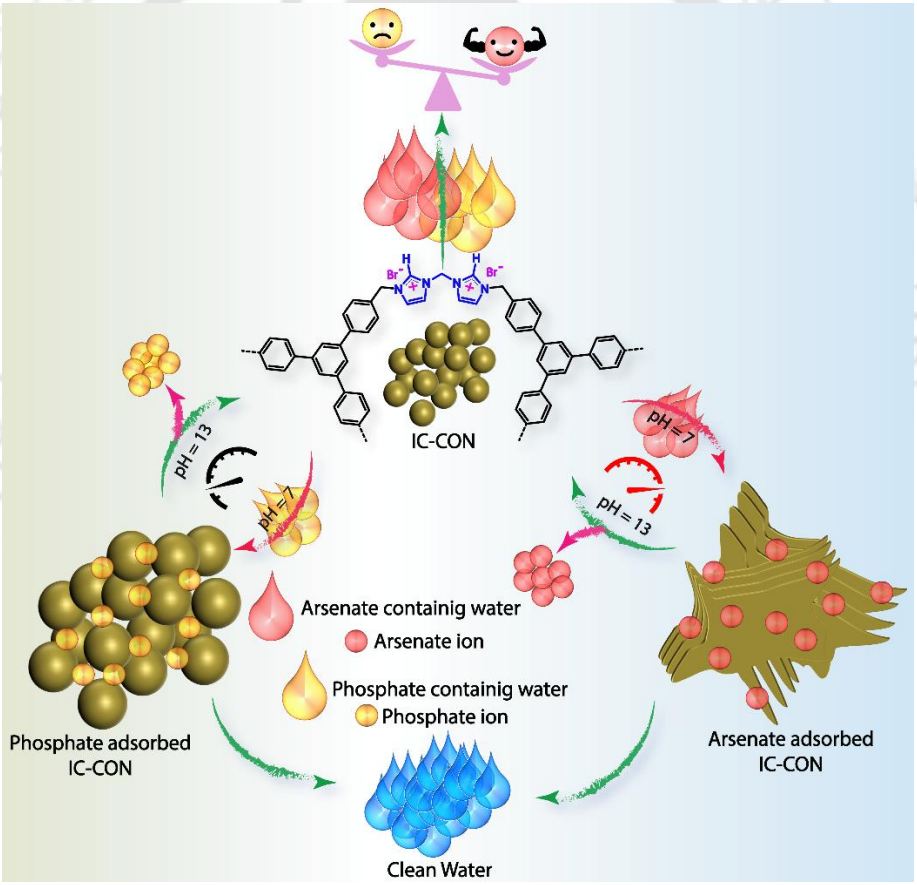

4.1. Background and objective of present work

Similar to phosphate, arsenic has been identified as a major worldwide environmental problem, particularly in aquatic environments, because of its strong toxicity and persistent character.[1-4] Whether acute or chronic, exposure to arsenic-contaminated water has major negative effects on health, including organ malfunction, developmental abnormalities, and possible carcinogenesis. The majority of arsenic pollution originates from geogenic sources, but human activity has greatly increased its release into natural water systems, especially in industrial sectors like mining, metallurgy, and the production of glass, pesticides, and semiconductors.[5-9] This problem has been exacerbated by the growing industrialization and population growth, leading to elevated levels of arsenic in surface and groundwater in different regions of the world.

Although numerous strategies have been proposed for arsenic removal, many of the existing materials suffer from limited adsorption capacities and poor selectivity.[10-21] A key challenge in the development of efficient arsenic adsorbents lies in the chemical similarity between arsenate and phosphate, both existing as tetrahedral oxoanions in aqueous media. Due to this resemblance, many materials exhibit a preferential or non-selective affinity toward phosphate over arsenate, making it difficult to achieve selective arsenic removal in phosphate-rich environments such as agricultural runoff or natural water sources.

To address this issue, the present work aims to develop a selective adsorbent capable of differentiating arsenate from phosphate ions in aqueous systems. Literature evidence indicates that imidazole and its derivatives, particularly imidazolium moieties, display significant affinity towards arsenate due to their ability to engage in electrostatic and hydrogen-bonding interactions.[22-26] Various imidazolium-based platforms – including ionic liquids, organic polymers, COFs, MOFs, and POPs – have been reported for arsenate recognition and adsorption. However, these systems often either favor phosphate over arsenate or demonstrate suboptimal adsorption performance. Motivated by the documented interactions of imidazolium compounds with oxoanions, we have successfully designed and synthesized an ionic bis-imidazolium-based dicationic covalent organic network (IC-CON), aiming to serve as a promising platform for efficient and selective water purification applications. The integration of 5'-phenyl-1,1':3',1''-terphenyl moieties

into the IC-CON framework significantly enhances intermolecular stacking through π–π interactions. These interactions are a crucial factor contributing to the high thermal and chemical stability of IC-CON, even after it is exposed to various organic solvents and under acidic or basic conditions. Furthermore, the incorporation of bis-imidazolium moieties into the polymer backbone may substantially influence the morphology of the resulting network. The positively charged bis-imidazolium units generate strong electrostatic repulsion between the growing polymer chains during synthesis of IC-CON, which may promote thermodynamically favorable spherical morphologies. Beyond morphological control, the bis-imidazolium units may also impact the internal pore environment. Bromide ions, serving as counterions to the cationic imidazolium sites, are electrostatically associated with the framework and may occupy the internal pores of the polymer network. Temporally blocking the pore channels might lead to a decrease in accessible pore size. Simultaneously, the presence of these counterions may improve the adsorption capacity of the polymer through an ion exchange mechanism, affecting its general functional performance. A comprehensive series of adsorption studies has shown that IC-CON is highly effective in removing and recovering arsenate and phosphate ions from aqueous solutions. Multiple noncovalent interaction sites, including hydrogen bonding, electrostatic interactions, and exchangeable bromide ions within the polymeric framework, account for IC-CON's enhanced adsorption performance. These interactions synergistically improve its adsorption capacity and kinetics. Notably, IC-CON exhibits higher adsorption efficiency and faster adsorption kinetics for arsenate compared to phosphate despite its ability to selectively adsorb both ions in the presence of competing anions. Furthermore, when exposed to equimolar concentrations of arsenate and phosphate, IC-CON demonstrates a stronger affinity for arsenate. This underscores its potential for the targeted removal of arsenate from phosphate-rich water systems. The anion-responsive morphological changes of IC-CON result in unique chemical properties. IC-CON demonstrates selectivity for both arsenate and phosphate; however, a shift in its structure from a spherical form to a sheet-like structure, followed by a return to the spherical shape, was only observed during the adsorption and desorption of arsenate. No such transformation occurred with phosphate. For this reason, IC-CON expresses great potential as a sustainable water treatment technique since it offers fast and efficient adsorption, improved selectivity,

and recyclability to eliminate phosphorous and arsenic. This positions it as an optimal choice for advanced water treatment and environmental remediation applications.

4.2. Results and discussions

4.2.1. Design and synthesis of the IC-CON polymer –

The imidazolium-based organic moieties have been previously recognized for their selective and strong affinity for arsenic and biological phosphate.[27, 28] The successful application of imidazolium- based moieties in detecting arsenic and phosphate ions prompted us to develop a bis-imidazolium linker to synthesize a cationic covalent organic network (IC-CON). Since arsenic and phosphate exist as oxoanions in water, we hypothesize that the dicationic linker of IC-CON will facilitate strong electrostatic interactions, while the acidic protons present in the imidazolium moieties (+N=C-H) will enable strong hydrogen-bonding interactions with these oxoanions in the aqueous medium. The combination of these two noncovalent interactions is expected to enhance the removal and recovery of arsenic and phosphate at specific pH levels.

In this context, the IC-CON was synthesized via a solvothermal method by refluxing di(1H-imidazol-1-yl) methane with 1,3,5-Tris[4-(bromomethyl) phenyl] benzene in a 1:1 ratio of dry acetonitrile and tetrahydrofuran at 100 °C for 48 hours under an inert atmosphere (Figure 4.1A and Scheme A4.1 – 4.4). The resulting white solid precipitate was collected through filtration, followed by thorough washing with a series of organic solvents, including acetonitrile and tetrahydrofuran. Subsequently, the final product was dried at 70 °C for 24 hours before being collected for further analysis.

4.2.2. Structural characterization of the IC-CON polymer –

The FT-IR analysis of the IC-CON exhibits characteristic peaks at ~ 3029 cm^{-1} (aromatic =C-H stretching), ~1600–1500 cm^{-1} (C=C and C-C ring stretching), ~1020 cm^{-1} (in-plane C-H bending), and ~829 cm^{-1} (out-of-plane C-H bending), confirming the presence of the 5'-phenyl-1,1':3',1''-terphenyl unit. Additionally, the presence of a di(1H-imidazol-1-yl) methane unit is evidenced by peaks at ~1350 cm^{-1} (C-N stretching), ~1153 cm^{-1}, and ~757 cm^{-1} (C=N-C stretching). Furthermore, the peaks observed at ~3000 – 2900 cm^{-1} (CH_2 asymmetric and symmetric vibrations), ~1443 cm^{-1} (scissoring), ~1288–1208 cm^{-1} (wagging and twisting), and ~690 cm^{-1}

(rocking) verify the existence of a methylene group bridging compound 4.2 and compound 4.3 in the polymer (Figure 4.1B).[29] The presence of aromatic carbon atoms within the polymeric network was verified by the appearance of peaks in the range of δ 120–140 ppm in the ^{13}C cross-polarization magic angle spinning nuclear magnetic resonance (^{13}C CP-MAS NMR) spectroscopy analysis of IC-CON. Furthermore, the NMR peak at δ 140 ppm indicates the presence of the carbon

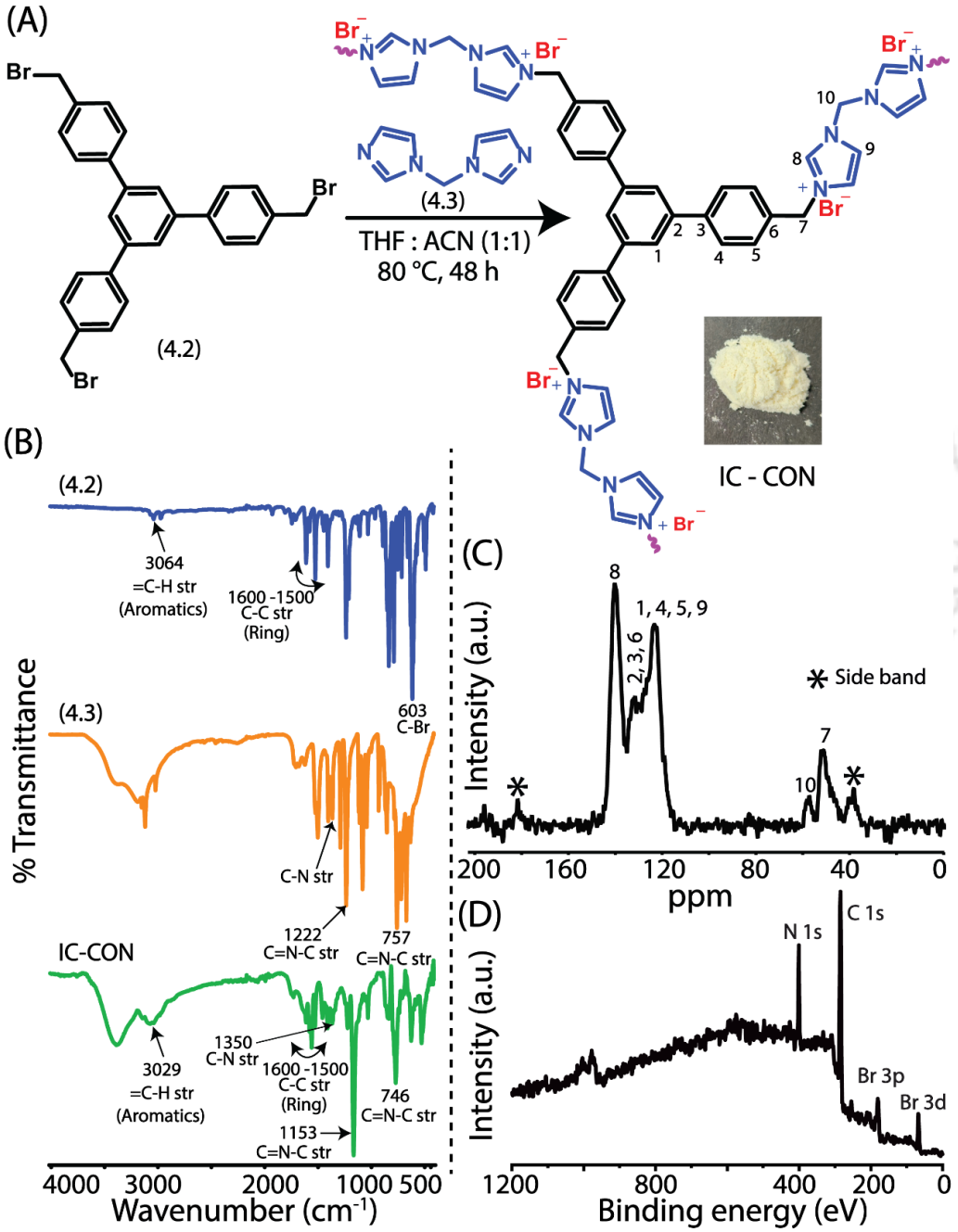

Figure 4.1. Synthetic route to IC-CON (A). FT-IR spectra of the compound 4.2, compound 4.3, and IC-CON (B). The solid-state ^{13}C NMR spectra of IC-CON (C). XPS data profile (wide scan) of IC-CON (D).

atom between the two nitrogen atoms (-N-C=N^+-) in the bis-imidazolium moieties in the IC-CON network. Additionally, the peaks at δ 53 ppm and δ 58 ppm confirmed the existence of the methylene groups that connected the two imidazolium units and linked compounds 2 and 3 in the IC-CON, respectively (Figure 4.1C).[29] The X-ray photoelectron spectroscopy (XPS) survey profile exhibited distinctive peaks that corresponded to nitrogen (N 1s) at 398 – 402 eV, carbon (C 1s) at 284 – 289 eV, and bromine (Br 3p) at 64 – 70 eV and (Br 3d) at 175 – 183 eV (Figure 4.1D).[29] These peaks in the XPS spectra indicate the existence of bromine as counter anions as well as the incorporation of carbon and nitrogen inside the IC-CON framework. Two deconvoluted peaks in the high-resolution C 1s XPS spectra at 284.69 eV and 286.3 eV, respectively, corresponded to phenyl carbon and imidazolium carbon. Characteristic peaks at 401.66 eV on the N 1s spectra were ascribed to quaternary nitrogen in the imidazolium moiety. Additionally, Br $3d_{5/2}$ and Br $3d_{3/2}$ peaks were assigned at 66.46 eV and 67.78 eV from the analysis of the high-resolution XPS spectrum of Br (Figure A4.1). The overall XPS analyses confirmed the presence of all the chemically different environments of C, N, and Br inside the IC-CON framework. The relatively low crystalline structure of IC-CON is evidenced by the weak peak at 2θ = 3.50° and the sharp peak at 2θ = 18.14° observed in the Powder X-ray Diffraction (PXRD) analysis. A broad peak at 2θ = 24.90° indicates π–π stacking interactions among the aromatic moieties within the polymeric network (Figure 4.2A and S2).[15, 30] Furthermore, the intense spots in the selected area electron diffraction (SAED) pattern obtained from transmission electron microscopy (TEM) further confirm the crystalline structure of the IC-CON (Figure A4.3).[15]

The surface morphology of IC-CON was examined using field-emission scanning electron microscopy (FESEM), field-emission transmission electron microscopy (FETEM), and atomic force microscopy (AFM). FESEM and FETEM studies confirmed the distorted or partially agglomerated spherical surface morphology of IC-CON, while high-resolution transmission electron microscopy (HRTEM) pictures showed a consistently corrugated nanosheet structure (Figure 4.2B – D). Moreover, the AFM study verified a comparable morphological pattern (Figure 4.2E). The deviation from an ideal spherical morphology observed in IC-CON can be attributed to the interplay between electrostatic repulsion and π–π stacking interactions. The presence of positively charged bis-imidazolium moieties induces

significant electrostatic repulsion among the growing polymer chains, which Favors the formation of discrete spherical particles during the polymerization process. Additionally, the reaction conditions and solvent environment further assist in stabilizing these spherical structures. However, the incorporation of 4,4''-dimethyl-5'-(p-tolyl)-1,1':3',1''-terphenyl units introduces extended π–π stacking interactions that facilitate intermolecular aggregation, thereby perturbing the uniformity of the spherical morphology. As a result, IC-CON exhibits deviation from an ideal spherical form, often presenting as distorted or partially agglomerated spherical particles. The FESEM-EDX and elemental mapping showed that carbon (C) and nitrogen (N), along with bromide (Br^-), were evenly distributed as the main chemical components in the IC-CON network (Figure 4.2F and Figure A4.4 – 4.5). Thermogravimetric analysis (TGA), conducted under a nitrogen atmosphere, showed minor weight loss up to 350 °C, followed by significant weight loss, indicating the degradation of the IC-CON framework (Figure 4.2G). The observed thermal stability is most certainly contributed by the strong π–π stacking interactions among the aromatic groups in the IC-CON. The Brunauer-Emmett-Teller (BET) method was employed to evaluate the surface area and porosity of the polymer. Based on the nitrogen adsorption-desorption isotherm analysis conducted at cryogenic temperatures (77.3 K), the polymer exhibited a surface area of 49.697 $m^2\ g^{-1}$ (Figure A4.6A). At a relative pressure (P/P_0) of 0.199858, the total pore volume was determined to be 0.051 $cm^3\ g^{-1}$. Furthermore, pore size distribution analysis using the Barrett–Joyner–Halenda (BJH) method indicated an average pore diameter of 4.03 nm (Figure A4.6B). Zeta potential analysis showed that the surface potential of the polymer rose from +7 mV to +45 mV as the pH dropped from 7 to 2, then dropped to -54 mV as the pH raised to 12, most likely due to the protonation and deprotonation of the imidazole moiety within the IC-CON framework at different pH levels (Figure A4.7). The Tyndall effect experiment revealed that the polymer showed a stable colloidal suspension throughout 48 hours, demonstrating its highly dispersive nature in aqueous solution (Figure A4.8). Furthermore, as witnessed by the dynamic light scattering (DLS) study, the polymer maintained its particle size close to 1000 nm in an aqueous media even 48 hours after sonication (Figure A4.9). The retention of identical FT-IR spectra of the polymer before and after being exposed to frequently used organic solvents, including acetonitrile (ACN), dichloromethane (DCM), ethyl acetate (EtOAc),

methanol (MeOH), tetrahydrofuran (THF), and acetone, along with 5 N HCl and 5 N NaOH, over 21 days, indicates its remarkable chemical resistance under such harsh conditions (Figure A4.10A). Additionally, the consistent FESEM images and TGA profile of the IC-CON following exposure to HCl (5 N) and NaOH (5 N) confirm its significant morphological and thermal stability in both acidic and basic aqueous environments respectively (Figure A4.10B – E).

4.2.3. Binding efficacy of IC-CON for arsenate and phosphate ions –

The binding efficacy of IC-CON toward arsenic is initially to be evaluated by treating 5 mg of IC-CON with 5 mL of 20 ppm aqueous arsenic solution for 5 minutes. We assessed the arsenate content in the solution both before and after the treatment of IC-

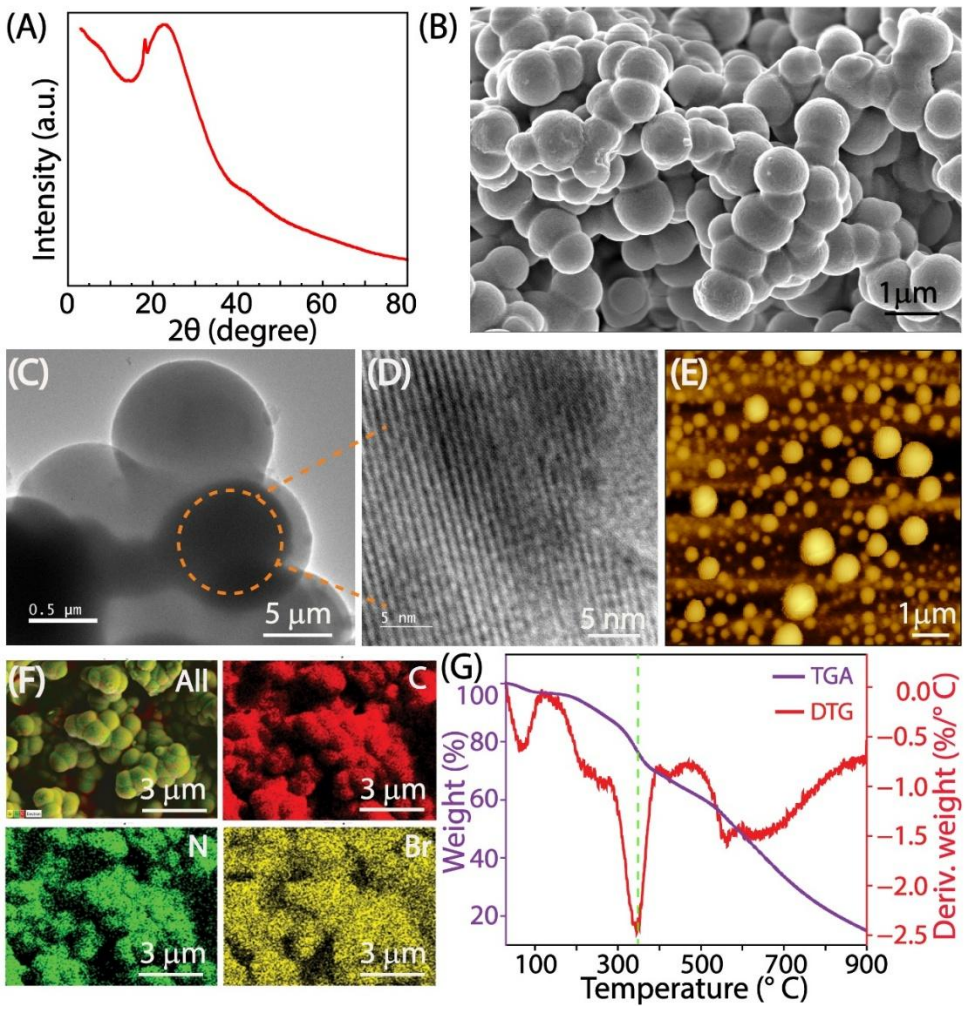

Figure 4.2. Characterization of IC-CON by PXRD (A), FESEM (B), TEM (C), HRTEM(D) and AFM (E) analyses. The FESEM mapping analysis for the C, N, and Br of IC-CON (F). The TGA-DTG analysis of IC-CON (G).

CON using inductively coupled plasma mass spectrometry (ICP-MS). ICP-MS results demonstrated a clear drop in arsenic level to less than 3 ppb following treatment, which revealed a strong binding affinity of IC-CON for arsenic. Complementing analytical methods, including FT-IR, XPS, FESEM-EDX, and FESEM elemental mapping, confirmed this affinity of IC-CON towards arsenic. In FT-IR analysis, post-arsenate adsorption, a prominent peak emerges at 895 cm^{-1}, indicative of the combined symmetric and asymmetric stretching vibrations of the As–O band. A shoulder peak appears at 740 cm^{-1}, ascribed to the asymmetric stretching vibrations of the As–OH band (Figure 4.3A).[31] The XPS survey spectra of arsenate-treated IC-CON showed a new peak in the 44–46 eV range, indicative of As 3d, therefore providing further evidence of arsenate adsorption (Figure 4.3B). The high-resolution deconvolution of the As 3d area revealed peaks at 44 eV and 45 eV aligned with the As 3d5/2 and As 3d3/2 states, respectively (Figure 4.3C). In the O 1s area, the deconvolution shows peaks at 529.85 eV and 533.29 eV, which are the As–O^-/As–OH and As=O species, respectively (Figure 4.3D). Moreover, elemental mapping and FESEM-EDX confirmed, coupled with carbon and nitrogen, the notable concentration of arsenic in the polymer matrix (Figure 4.3E and A4.11– A4.12).

Encouraged by the high efficacy of IC-CON in arsenate adsorption, its capacity for phosphate removal was subsequently examined due to the chemical similarity between arsenate and phosphate. For this purpose, 5 mg of IC-CON was treated with 5 mL of a 20-ppm phosphate solution for 5 minutes. Ion chromatography (IC) was used to determine the phosphate concentrations in the solution before and after the IC-CON treatment. The IC study revealed a significant phosphate-binding capacity for IC-CON, reducing phosphate concentration to less than 700 ppb. Further confirmation came from applying the same analytical techniques applied for arsenic. The FT-IR spectra of IC-CON displayed a new peak at 1067 cm^{-1} following phosphate treatment that would be ascribed to P–O stretching vibrations (Figure A4.13A). XPS analyses validated these results; the survey spectrum shows a peak matching P 2p orbitals in the treated sample (Figure A4.13B). High-resolution deconvolution of the P 2p region revealed corresponding P=O, P-O, and P-OH states at 132.05, 133.44, and 134.89 eV, respectively (Figure A4.13C). Deconvolution of the O 1s area revealed peaks corresponding to P=O species at 529.85 eV and P–O^-/P–OH at 533.29 eV

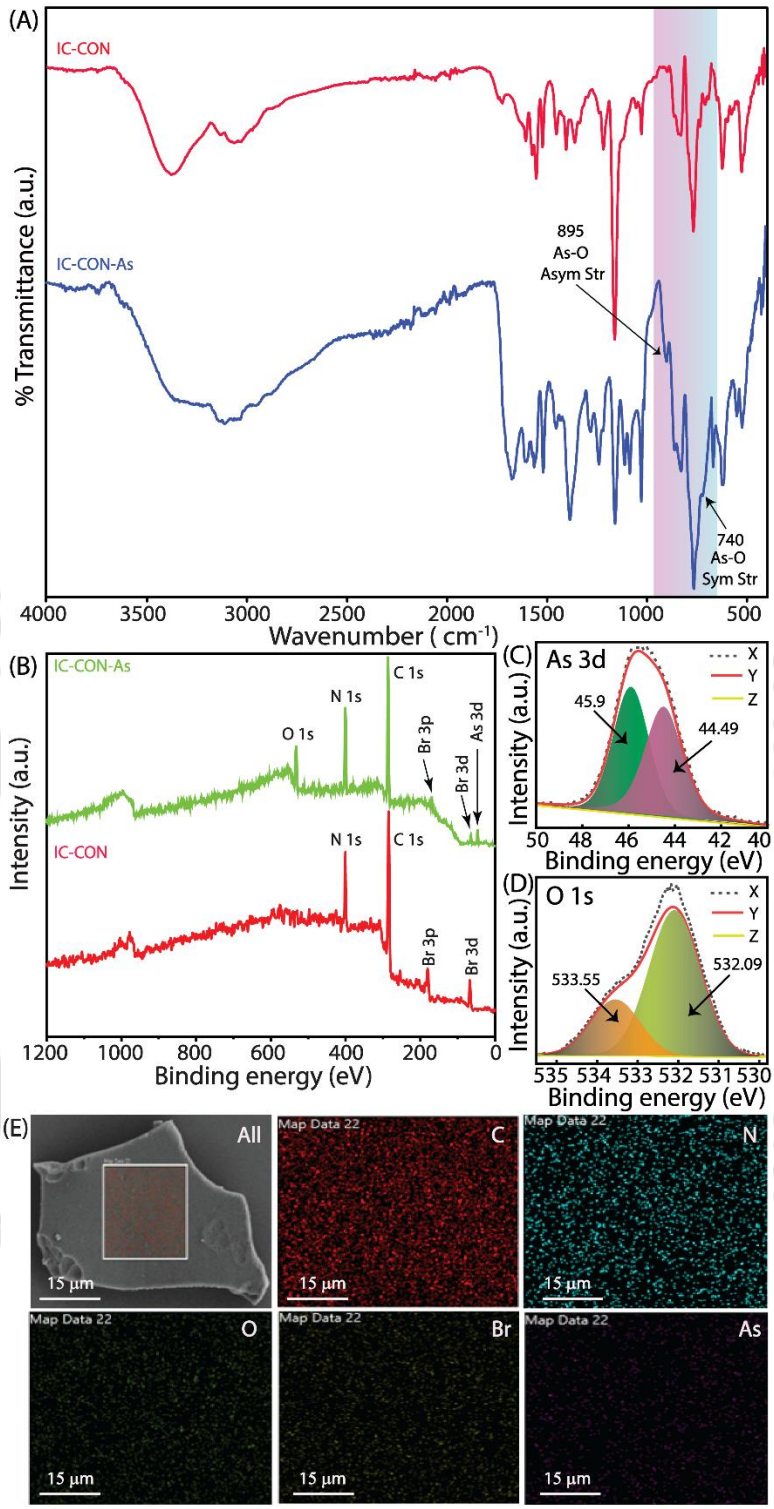

Figure 4.3. FT-IR spectra of IC-CON before and after arsenate anion adsorption (A). XPS data profile (wide scan) of IC-CON before and after the arsenate anion adsorption (B). The XPS deconvoluted peaks of As 3d (C) and O 1s (D). The FESEM mapping analysis for the C, N, O, Br and As of IC-CON after arsenate anion adsorption (E). (Note: In **Figure** 4.**3C** and **Figure 4.3D**, X, Y, and Z correspond to the experimental data, fitted curve, and background signal, respectively).

(Figure A4.13D).[32] Elemental mapping and FESEM-EDX validated the presence of N, C, O, and P in the polymer matrix (Figure A4.13E and A4.13F). The comprehensive analytical results provided the flexibility and effectiveness of IC-CON in binding both arsenate and phosphate, therefore verifying its possible use as a suitable material for the remediation of the environment.

4.2.4. Removal and recovery of arsenate and phosphate ions –

Inspired by the above-described experimental results, an extensive investigation was conducted on the adsorption of arsenate ions by the IC-CON polymer in aqueous media. Since the distribution of arsenic species in solution is pH-dependent (pKa values of H_3AsO_4: 2.2, 6.9, and 11.5), the initial study focused on the effect of pH on the adsorption capacity of arsenic ions since it might greatly alter their adsorption behavior. Arsenate ions showed the best adsorption effectiveness at pH 7; thus, all the adsorption-based studies were carried out at this pH (Figure 4.4A). A correlation between the adsorption isotherm data and the equilibrium concentration of arsenate ions was determined by applying the single-site Langmuir and Freundlich models. The plot of equilibrium concentration (C_e) against equilibrium adsorption capacity (Q_e) demonstrated a strong correlation with the Langmuir adsorption model, exhibiting a correlation coefficient (R^2 > 0.996). The Langmuir model indicated a maximum capacity for arsenate adsorption of 698 mg g^{-1} (Figure 4.4B). Time-dependent adsorption experiments showed that IC-CON was able to remove over 87% of the arsenate ions from the stock solution in just 15 seconds, and it reached equilibrium adsorption in less than 30 seconds (Figure 4.4C). The t/Q_t versus t graph, representing the adsorption capacity at time t, adhered to the pseudo-second-order kinetic model, resulting in a rate constant of 0.000944643 mg g^{-1} sec^{-1} and a correlation coefficient (R^2 > 0.999) (Figure A4.14). Furthermore, kinetic investigations conducted at different polymer concentrations revealed a decline in adsorption rates from 0.001375803 mg g^{-1} sec^{-1} to 0.0002452 mg g^{-1} sec^{-1} as the polymer dosage was elevated from 3 mg to 10 mg, thereby reinforcing the pseudo-second-order adsorption kinetics of arsenate ions by IC-CON (Figure A4.15).

Encouraged by the remarkable performance of the IC-CON polymer in the adsorption of arsenate, similar investigations were carried out to evaluate its affinity for phosphate ions, as IC-CON also shows substantial binding affinity for this ion.

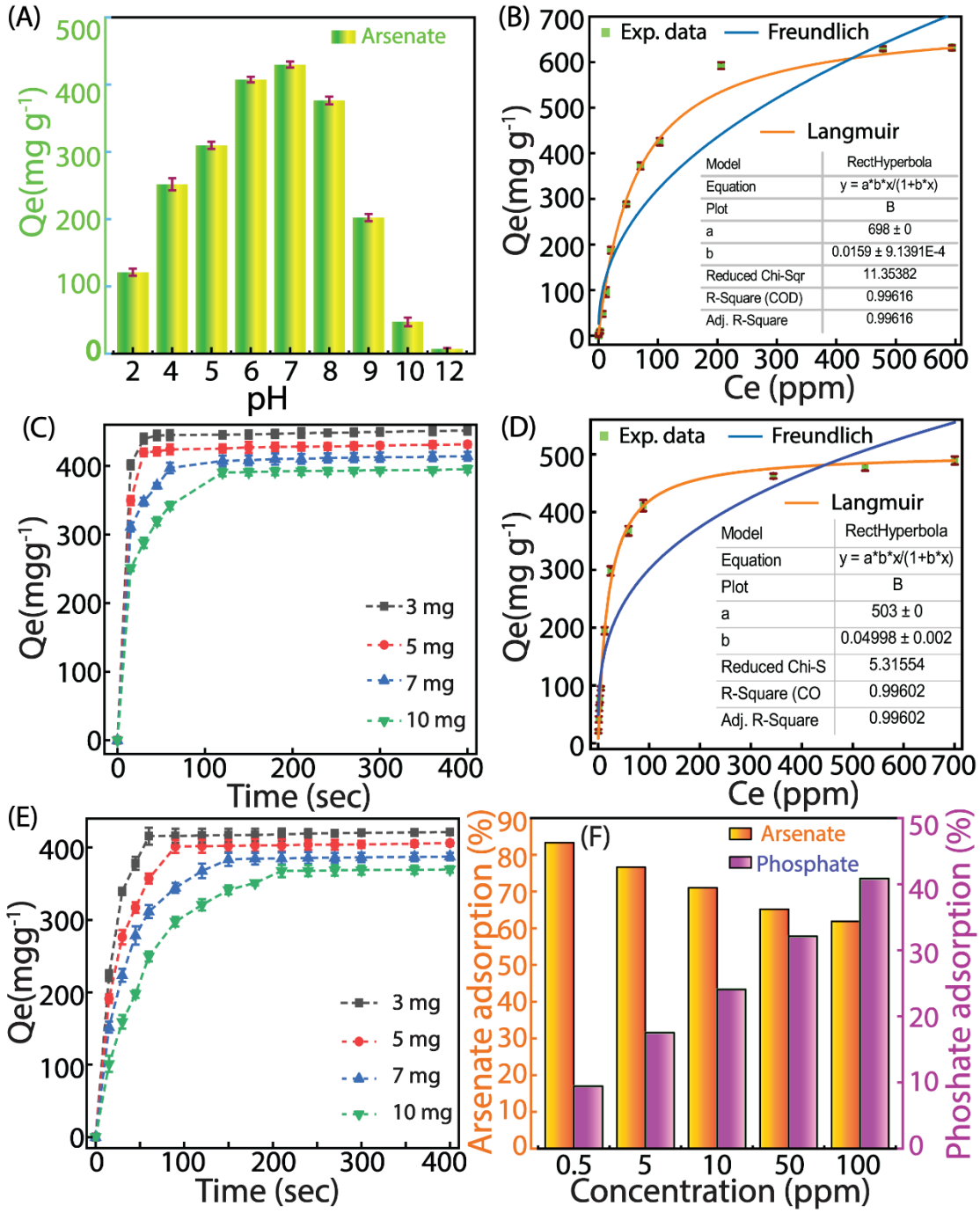

Figure 4.4. The pH-dependent arsenate ion adsorption efficiency of IC-CON (A). Arsenate ion adsorption isotherm of IC-CON (B). Time-dependent adsorption isotherm of arsenate ions by IC-CON (3–10 mg) at pH 7.0 under room temperature (C). Phosphate ion adsorption isotherm of IC-CON (D). Time-dependent adsorption isotherm of phosphate ions by IC-CON (3–10 mg) at pH 7.0 under room temperature (E). Adsorption efficiency of IC-CON from varying concentrations of 1:1 stock solution of arsenate and phosphate ions (F).

Depending on the pH, phosphate ions exist in several oxoanion forms; the pKa values of H_3PO_4 in water are 2.1, 7.2, and 12.3. Therefore, the first tests of phosphate adsorption capability were carried out throughout different pH ranges from 2 to 12. The data showed that pH 6 to 7 had the best adsorption effectiveness; hence, all later experiments were conducted at pH 7 (Figure A4.16). The Langmuir model effectively described the phosphate adsorption data with a maximum adsorption capacity of 503 mg g^{-1} (Figure 4.4D). Following the pseudo-second-order kinetic model, kinetic studies demonstrated a fast adsorption rate and equilibrium reached in 90 seconds (Figure 4.4E and A4.17– 4.18). The notable adsorption capacities and fast kinetic rates found show that the IC-CON polymer efficiently adsorbs both arsenate and phosphate ions, therefore suggesting its possible use in wastewater treatment systems. Moreover, the temperature-dependent arsenate and phosphate ion adsorption experiment revealed a reduced equilibrium ion adsorption capacity (Qe) of IC-CON as the temperature increased from 298 K to 343 K (Figure A4.19).

4.2.5. Effect of counter ions on arsenate and phosphate adsorption –

Analyzing the effectiveness of IC-CON in adsorbing arsenate and phosphate ions, especially in the presence of competing anions, is crucial. These competing anions can interfere with the adsorption process by competing for the same binding sites. Therefore, selectivity is essential for the efficient extraction and recovery of phosphorus and arsenic ions. First, the adsorption performance of IC-CON for arsenate and phosphate was evaluated under several competing anion conditions, including Cl^-, F^-, NO_3^-, SO_4^{2-}, and CO_3^{2-}. Two-component stock solutions with varying ratios of arsenate or phosphate to competing ions (1:1, 1:10, 1:50, and 1:100) have been formulated to assess the influence of these competing anions on adsorption efficacy. The results show that the adsorption process of arsenate and phosphate ions is not much influenced by these oxoanions. Particularly, IC-CON exhibits a preference for arsenate with a 93% selectivity while phosphate is adsorbed with a selectivity of 87% in the presence of competing anions (Figure A4.20). The resulting selectivity values were almost identical to those obtained in the absence of competing ions. Furthermore, the results suggest that arsenic had a steeper adsorption isotherm than phosphate. The observed ordered pattern for the adsorption is Arsenate > phosphate > CO_3^{2-} > SO_4^{2-} > NO_3^- > F^-. The reduced adsorption efficacy of arsenate and phosphate in the presence of CO_3^{2-}, SO_4^{2-}, and NO_3^- is ascribed to the interaction

between the oxygen-containing groups of these anions and the acidic imidazolium protons of the IC-CON framework via hydrogen bonds, which partially hampers the chelation, ion exchange, and hydrogen bonding of arsenate and phosphate with the IC-CON. Furthermore, the selectivity of IC-CON for arsenate and phosphate was assessed in the presence of prevalent competing metal ions (Na^+, K^+, Rb^+, Cs^+, Mg^{2+}, and Al^{3+}). These investigations show that IC-CON has low interaction with metal ions and very specific behavior for arsenate and phosphate (Figure A4.21).

The adsorption effectiveness of IC-CON toward arsenate ions in the presence of rhenate and chromate ions was also assessed. Two separate stock solutions with a 1:1 molar ratio of arsenate to chromate or rhenate were used for this investigation, and the adsorption capacity of IC-CON for arsenate ions from these mixed-ion solutions was evaluated. More than 68% of the arsenate ions from the 1:1 stock solution of arsenate and chromate and above 64% of the arsenate ions from the 1:1 stock solution of arsenate and rhenate were shown to be efficiently adsorbed by IC-CON. The experimental results indicated that IC-CON could adsorb over 62% of phosphate ions from the 1:1 stock solution of phosphate and chromate and more than 57% of phosphate ions from the 1:1 stock solution of phosphate and rhenate (Figure A4.22).

4.2.6. Adsorption efficiency of IC-CON in equimolar binary solutions of arsenate and phosphate ions —

The adsorption efficacy of IC-CON was evaluated using binary stock solutions that contained equal amounts of arsenate and phosphate, with concentrations ranging from 0.5 ppm to 100 ppm (Figure 4.4F). IC-CON showed a significantly higher adsorption rate and improved adsorption efficiency for arsenic in all tested solutions. Additionally, it demonstrated a greater affinity for arsenate compared to phosphate across all analyzed stock solutions. The experimental data provided additional confirmation that IC-CON effectively adsorbed both ions from aqueous solutions, demonstrating a notably higher adsorption efficacy and a more rapid removal rate for arsenate. The improved efficiency underscores the capability of IC-CON as a remarkable material for the selective extraction of arsenate from phosphate-rich contaminated water sources.

4.2.7. Recyclability tests for arsenate and phosphate removal –

For practical applications, it is essential for an adsorbent to maintain its adsorption efficiency over multiple regeneration cycles without significant performance loss or structural degradation. This ensures cost-effective manufacturing and facilitates the recovery of the adsorbed species. In this study, we investigated the adsorption and desorption performance of IC-CON for arsenate and phosphate ions across 15 consecutive cycles. The low adsorption efficiency of IC-CON at high pH (>10) motivates us to choose NaOH (0.5 N) followed by NaBr (0.1 N) as the desorbing agent for regeneration. Up to the 12th cycle, IC-CON maintained more than 90% of its initial arsenate adsorption capacity; thereafter, the capacity progressively dropped to 85% (Figure A4.23A). In a comparable manner, phosphate adsorption was sustained at levels exceeding 86% through the 10th cycle, subsequently declining to 79% following 15th cycles (Figure A4.23B). The IC-CON exhibited a notable release of over 93% of the adsorbed arsenate and phosphate in each cycle. Upon the completion of 15 regeneration cycles, the polymer was subjected to FTIR, FESEM, FESEM-EDX, elemental mapping, and thermogravimetric analysis (TGA) to assess its chemical and thermal stability. The FTIR spectra, FESEM-EDX, and elemental mapping analyses of the regenerated IC-CON exhibited a strong similarity to the pristine IC-CON, thereby affirming the maintenance of its chemical integrity. The FESEM and TEM imaging following arsenate and phosphate desorption, exhibited a nearly identical morphological pattern to the untreated IC-CON, hence confirming the morphological stability of IC-CON even after 15 regeneration cycles. The TGA profile of IC-CON following 15 cycles of arsenate adsorption and desorption indicated that the polymer remains stable at temperatures exceeding 300 °C, reflecting its thermal stability even after repeated regeneration cycles (Figure A4.24 – 4.25). We also investigated the kinetics of arsenate and phosphate ion desorption from the IC-CON. The results showed that after 20 min and 30 min, respectively, the IC-CON effectively released the maximum quantity of adsorbed arsenate and phosphate ions (Figure A4.26 – 4.27). The combined results show the great potential of IC-CON as a robust and effective adsorbent for phosphate and arsenic extraction from aquatic environments.

4.2.8. Morphological analysis after arsenate and phosphate ions adsorption–

We investigated the morphology of IC-CON upon the adsorption of arsenate and phosphate ions using FESEM, TEM, and AFM techniques. The FESEM analysis revealed a significant transformation in the morphology of IC-CON from a spherical form to a sheet-like structure following arsenate adsorption (Figure 4.5A – 4.5B). Both TEM and AFM further confirmed this structural rearrangement after arsenate adsorption, providing additional evidence of this morphological shift (Figure A4.28 – 4.29). In contrast, the morphological analysis of IC-CON upon phosphate ion adsorption, as observed through FESEM, showed a morphology similar to that of the pristine IC-CON. However, there was an increase in the size of the spherical particles, expanding from approximately 800 – 900 nm to 1900 – 2000 nm. These observations suggest that IC-CON undergoes anion-responsive morphological transformations, with significant changes occurring only in the presence of arsenate ions, even though it can adsorb both arsenate and phosphate ions effectively. After the desorption of both arsenate and phosphate ions, the morphology of IC-CON returned to its original spherical shape, with the particle size reverting to its initial size range (Figure 4.5C – 4.5F). Additionally, the different adsorption behaviors of IC-CON for phosphate and arsenate ions were visually evident. When IC-CON was placed in an arsenate stock

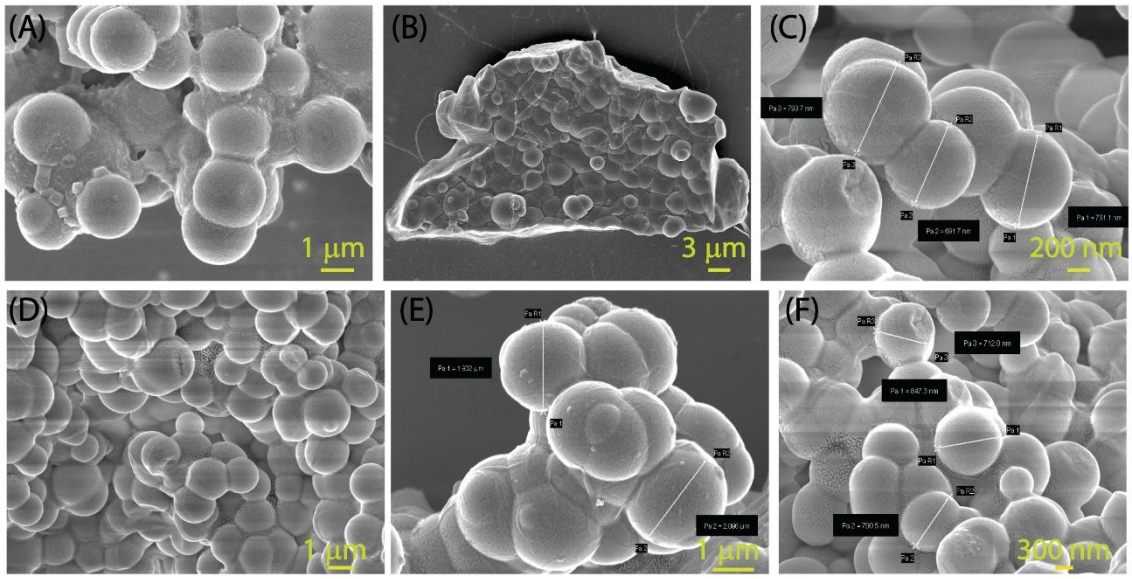

Figure 4.5. FESEM image of IC-CON(A), after arsenate adsorption (B), and after arsenate desorption (C). FESEM images of IC-CON (D), after phosphate adsorption (E), and after phosphate desorption (F).

solution, rapid precipitation occurred at the bottom of the vial within 10 minutes. In contrast, the phosphate-treated IC-CON remained stably dispersed as a colloidal suspension (Figure A4.30). The DLS measurements revealed a significant increase in the hydrodynamic diameter of arsenate-adsorbed IC-CON, exceeding 5300 nm. In comparison, the size of phosphate-adsorbed IC-CON remained around 1800 nm (Figure A4.31). This notable increase in particle size with arsenate adsorption indicates greater agglomeration, likely aiding the transformation from a sheet-like shape to rapid precipitation. Conversely, the smaller particle size and stable colloidal nature of phosphate-adsorbed IC-CON suggest that reduced agglomeration in the presence of phosphate ions prevents any morphological alteration. The morphological transformation of IC-CON in the presence of arsenate, as opposed to phosphate, can be explained by differences in ionic size, charge distribution, and hydration energy between the two ions. Arsenate has a larger ionic radius compared to phosphate, allowing it to integrate more effectively into the mesoporous cavities of IC-CON. In contrast, the higher hydration energy of phosphate creates a barrier that limits its interaction with IC-CON, thus preventing significant structural changes. The notable increase in hydrodynamic size (approximately 5300 nm) indicates a transition from a spherical to a sheet-like shape. This transformation is likely due to enhanced interactions between arsenate and IC-CON, which promote substantial agglomeration. The selective change in surface morphology may be a result of arsenic's ability to integrate more firmly within the IC-CON framework. This integration could lead to localized structural stress and rearrangement, whereas phosphate does not induce similar effects.

4.2.9. Mechanism for arsenate and phosphate adsorption –

The polymeric framework of IC-CON contains multiple interaction sites that allow for the adsorption of arsenate and phosphate ions through various noncovalent interactions. The acidic proton (N-CH-N^+=) promotes hydrogen bonding, while the positively charged quaternary nitrogen enables electrostatic interactions with both anions. To investigate the adsorption mechanism, ion chromatography (IC) analysis was conducted on two distinct stock solutions: arsenate and phosphate ions, both before and after treatment with IC-CON. The results showed a bromide peak emerging after the treatment of IC-CON, which was absent in the initial stock solutions (Figure A4.32 – 4.33). This suggests an anion-

exchange mechanism, in which Br^- ions were replaced by arsenate and phosphate ions. X-ray photoelectron spectroscopy (XPS) analysis further supported these interactions. A detailed comparative analysis of the high-resolution N 1s and C 1s core-level spectra for pristine IC-CON, arsenate-loaded IC-CON (IC-CON-As), phosphate-loaded IC-CON (IC-CON-P), and the corresponding desorbed samples (IC-CON-As-D and IC-CON-P-D) provides valuable insights into the adsorption mechanism. A noticeable shift in binding energy was observed in the N 1s spectra from 401.64 eV (IC-CON) to 401.37 eV (IC-CON-P) and 401.21 eV (IC-CON-As), indicating strong interactions between the bis-imidazolium nitrogen centres and the respective anionic species (Figure 4.6A). Upon desorption, the binding energy reverted to 401.52 eV (IC-CON-P-D) and 401.55 eV (IC-CON-As-D), suggesting the reversibility of the interaction with the imidazolium moieties (Figure A4.34A). Similarly, in the C 1s spectra, the binding energy associated with the bis-imidazolium carbon atoms decreased from 286.30 eV (IC-CON) to 285.92 eV (IC-CON-P) and 285.78 eV (IC-CON-As) (Figure 4.6B). After desorption, the binding energy shifted back to 286.23 eV (IC-CON-As-D) and 284.19 eV (IC-CON-P-D), further confirming the active involvement of bis-imidazolium units in the adsorption and desorption processes of arsenate and phosphate ions (Figure A4.34B).

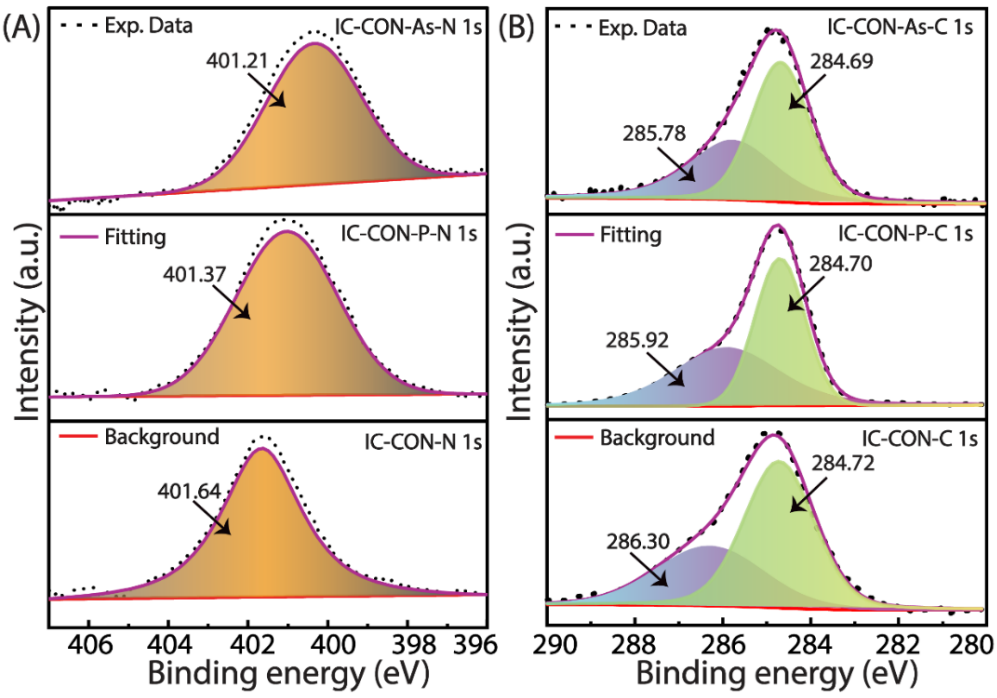

Figure 4.6. Deconvoluted XPS spectra for the N 1s (A) and the C 1s (B) of IC-CON before and after the adsorption of arsenate and phosphate ions.

4.2.10. Dynamic column chromatography-based adsorption –

The rapid adsorption kinetics and pH-responsive regeneration properties of IC-CON led to an investigation into its effectiveness in removing arsenate and phosphate ions using dynamic column chromatography to mimic real-time conditions. Two columns were filled with IC-CON, and then 500 mL of a 0.5 ppm arsenate aqueous solution and 500 mL of a 50-ppm phosphate aqueous solution, each with a tenfold excess of competing anions, were passed through the respective columns (Figure A4.36A). The results showed that up to 350 mL of effluent from the column contained arsenate and phosphate levels below the WHO-recommended limits during the first adsorption cycle. To facilitate the desorption of the adsorbed ions and regenerate the column, 100 mL of a 0.5 N NaOH solution, followed by 50 mL of a 0.1 N NaBr solution, was introduced into the column under controlled flow conditions. This process was repeated for five consecutive cycles, during which arsenate concentrations in the 300–350 mL of effluent and phosphate concentrations in the 250–350 mL of effluent remained within WHO safety limits (Figure A4.36B – 4.36E). The adsorption of phosphate by IC-CON was visually confirmed by the absence of any colour change in the mixture of ammonium molybdate and concentrated nitric acid solutions (Figure A4.36F). These findings demonstrate the high efficiency, reusability, and potential of IC-CON for practical wastewater treatment applications.

4.3. Summary

Arsenic and phosphate-based oxyanions are significant contaminants in water that pose serious risks to public health and environmental integrity. This research focuses on the synthesis of bis-imidazolium-based polymeric cationic frameworks (IC-CON) designed for the selective adsorption of arsenate and phosphate ions from water. Comprehensive studies on adsorption revealed that the bis-imidazolium-based dicationic linker-functionalized IC-CON demonstrates notable capacities for adsorption, rapid kinetics, and pronounced selectivity for binding arsenate and phosphate ions, even in the presence of common competing anions and metal ions. The mechanisms behind adsorption—identified as anion exchange, hydrogen bonding, and electrostatic interactions—were clarified through the application of IC and XPS analyses. Additionally, IC-CON showed remarkable recyclability, maintaining adsorption efficiency across 15 cycles. Effortless

regeneration was achieved using 0.5N NaOH followed by NaBr (0.1 N). The fast adsorption kinetics prompted the exploration of continuous flow applications using column chromatography, which yielded promising results. During the arsenate adsorption-desorption process, IC-CON exhibited notable ion-responsive morphological transformations, shifting from a spherical to a sheet-like configuration during adsorption and reverting to the original spherical form after desorption. In contrast, similar changes were not observed during phosphate binding. Although IC-CON demonstrates a high affinity for both arsenate and phosphate, it exhibited a greater adsorption affinity for arsenate when both ions were present in equimolar concentrations. This research highlights that IC-CON is an exceptionally effective material for the extraction and recovery of harmful anions from wastewater, underscoring its potential for environmental remediation. The presence of bis-imidazolium moieties suggests additional functionalities, including antibacterial properties, applications in fuel cells, organic catalysis, and semiconducting polymer technologies.

4.4. Appendix section

4.4.1. General information—

All reagents were purchased from Sigma-Aldrich, Merck, Himedia and other commercial sources and used directly without further purification. The column chromatography was performed using 60 –120 mesh silica gels. Reactions were monitored by thin-layer chromatography (TLC) on silica gel 60 F254 (0.25 mm). The ^{1}H NMR and ^{13}C NMR were recorded at 400 or 600 and 100 or 151 MHz with Varian AS400 spectrometer and Brucker spectrometer, respectively. The chemical shifts were reported in parts per million (δ) using DMSO-d_6, $CDCl_3$ as internal solvent. The coupling constant (J values) and chemical shifts (δ_{ppm}) were reported in Hertz (Hz) and parts per million (ppm), respectively, downfield from tetramethylsilane using residual chloroform (d = 7.24 for ^{1}H NMR, d = 77.23 for ^{13}C NMR) as an internal standard. Multiplicities are reported as follows: s (singlet), d (doublet), t (triplet), m (multiplet), and br (broadened). High-resolution mass spectra (HRMS) were recorded at Agilent Q-TOF mass spectrometer with Z-spray source using built-in software for analysis of the recorded data. The maximum number of experiments was repeated three times, and the mean value obtained for each case was reported. The error bars in the figures represent the standard deviations of these repetitions.

In the Fourier Transform Infrared Spectroscopy (FT-IR) analysis, sharp peaks are labelled as "S," and broad peaks are marked as "br."The arsenate and phosphate adsorption experimental procedures involve conducting batch experiments in 10 mL glass vials.

4.4.2. Synthesis and characterization –

4.4.2.1. Synthesis of 4,4′′-dimethyl-5′-(p-tolyl)-1,1′:3′,1′′-terphenyl (Compound 4.1):

1-(p-tolyl)ethan-1-one (500 mg, 3.72 mmol, 1.0 eq.) and p-Toluenesulfonic acid (64.05 mg, 0.37 mmol, 0.1 eq.) were taken in a round bottom flask followed by addition of dry acetonitrile. Then the mixture was refluxed at 146 °C for 16 – 20 h, and the progress of the reaction was monitored by TLC. After maximum consumption of 1-(p-tolyl)ethan-1-one, the solvent was evaporated under reduced pressure, and excess p-Toluenesulfonic acid was neutralised by $NaHCO_3$. The organic layer was extracted in DCM, and the crude product was purified through silica gel column chromatography with a solvent gradient system using ethyl acetate and hexane (0–3% EtOAc in hexanes) to obtain the pure product as a white solid (976.42 mg; 75.19% yield). **Characterization of the compound:** ^{1}H NMR (600 MHz, $CDCl_3$): δ_{ppm} 7.78 (s, 2H), 7.63–7.65 (d, 4H), 7.32–7.34 (d, 4H), 2.46 (s, 6H), ^{13}C NMR (151 MHz, $CDCl_3$): δ_{ppm} 142.21, 138.44, 137.30, 129.57, 127.22, 124.61, 21.17; **HRMS (ESI) calcd. for $C_{27}H_{24}$ [M+H]$^+$**: 349.1951, found: 349.1829.

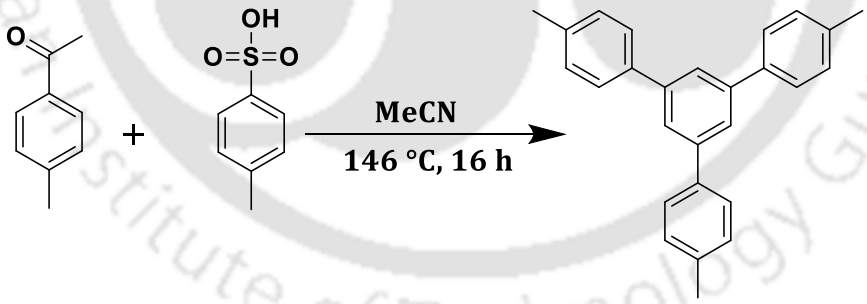

Compound 4.1

Scheme A4.1. Synthesis of 4,4′′-dimethyl-5′-(p-tolyl)-1,1′:3′,1′′-terphenyl (compound 1).

4.4.2.2. Synthesis of 4,4′′-bis(bromomethyl)-5′-(4-(bromomethyl) phenyl)-1,1′ (Compound 4.2):

Compound 1(50 mg, 0.143 m mol, 1 eq.), *N*-Bromosuccinimide (89.38 mg, 0.430 mmol, 3 eq.) and benzoyl peroxide (0.84 mg) were taken in a round bottom flask followed by addition of chloroform. Then the mixture was refluxed at 60 °C for

24 h, and the progress of the reaction was monitored by TLC. After maximum consumption of compound 1, the solvent was evaporated under reduced pressure. The organic layer was extracted in EtOAc, and the crude product was purified through silica gel column chromatography with a solvent gradient system using ethyl acetate and hexane (0 – 5% EtOAc in hexanes) to obtain the pure product as a white solid (976.42 mg; 75.19% yield**). Characterization of the compound:** ^{1}H NMR (600 MHz, $CDCl_3$): δ_{ppm} 7.78 (s, 3H), 7.68–7.69 (d, 6H), 7.53–7.54 (d, 6H), 4.60 (s, 6H), ^{13}C NMR (151 MHz, $CDCl_3$): δ_{ppm} 141.79, 141.06, 137.28, 129.66, 127.76, 125.33, 33.25; **HRMS (ESI) calcd. for $C_{27}H_{21}Br_3$ [M+H]$^+$:** 582.9266, found: 582.9065.

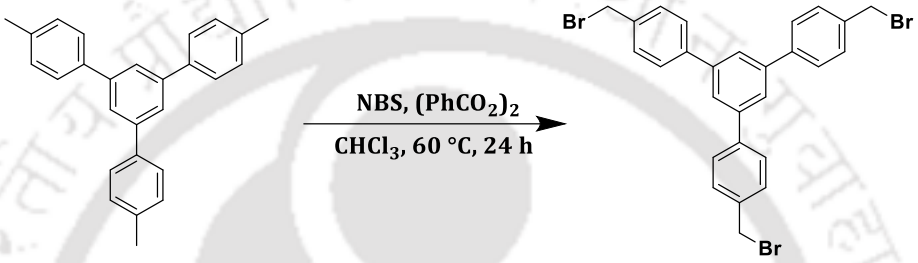

Compound 4.2

Scheme A4.2. Synthesis of 4,4′′-bis(bromomethyl)-5′-(4-(bromomethyl) phenyl)-1,1′ (compound 4.2).

4.4.2.3. Synthesis of di(1*H*-imidazol-1-yl) methane (Compound 4.3):

A mixture of imidazole (500 mg, 7.34 mmol, 1 eq.) and tetrabutylammonium bromide (47.35 mg,0.146 mmol, 0.02 eq.) in DCM and 45% NaOH (11 mL) solution was reflux at 45 °C for 16 h, and the progress of the reaction was monitored by TLC. After completion of the reaction, the volatile was removed from the reaction mixture and the crude product was purified through silica gel column chromatography with a solvent gradient system using MeOH and DCM (0 – 10% MeOH in DCM) to obtain the pure product as a white solid (976.42 mg; 75.19% yield). **Characterization of the compound:** ^{1}H NMR (600 MHz, $CDCl_3$): δ_{ppm} 7.93 (s, 2H), 7.39 (s, 2H), 6.91 (d, 2H), 6.22 (s, 2H), ^{13}C NMR (151 MHz, CDCl3): δ_{ppm} 137.77, 129.58, 119.59, 55.31; **HRMS (ESI) calcd. for $C_7H_8N_4$ [M+H]$^+$:** 149.0822, found: 149.0824.

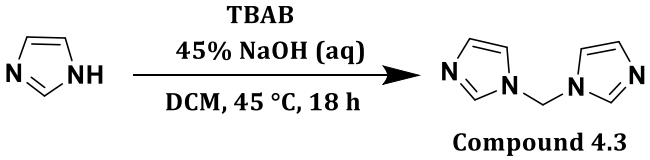

Compound 4.3

Scheme A4.3. Synthesis of di(1*H*-imidazol-1-yl) methane (compound 4.3).

4.4.2.4. Synthesis of IC-CON polymer:

Compound **4.**2 and compound 4.3 were taken in a sealed tube, followed by the addition of 1:1 dry acetonitrile and tetrahydrofuran solvent. Then, the mixture was refluxed at 80 °C for 48 h under inert conditions. After that, the white solid precepted was filtered and washed with various organic solvents, followed by acetonitrile and tetrahydrofuran several times. The compound was dried at 70 °C 24 h and collected. **Characterization of the compound: solid-state FT-IR (cm^{-1}):** 3064 (br), 1600-1500, 1443 (S), 1396 (S), 1350 (S), 1153(S), 1020 (S), 829 (S), 757 (S).

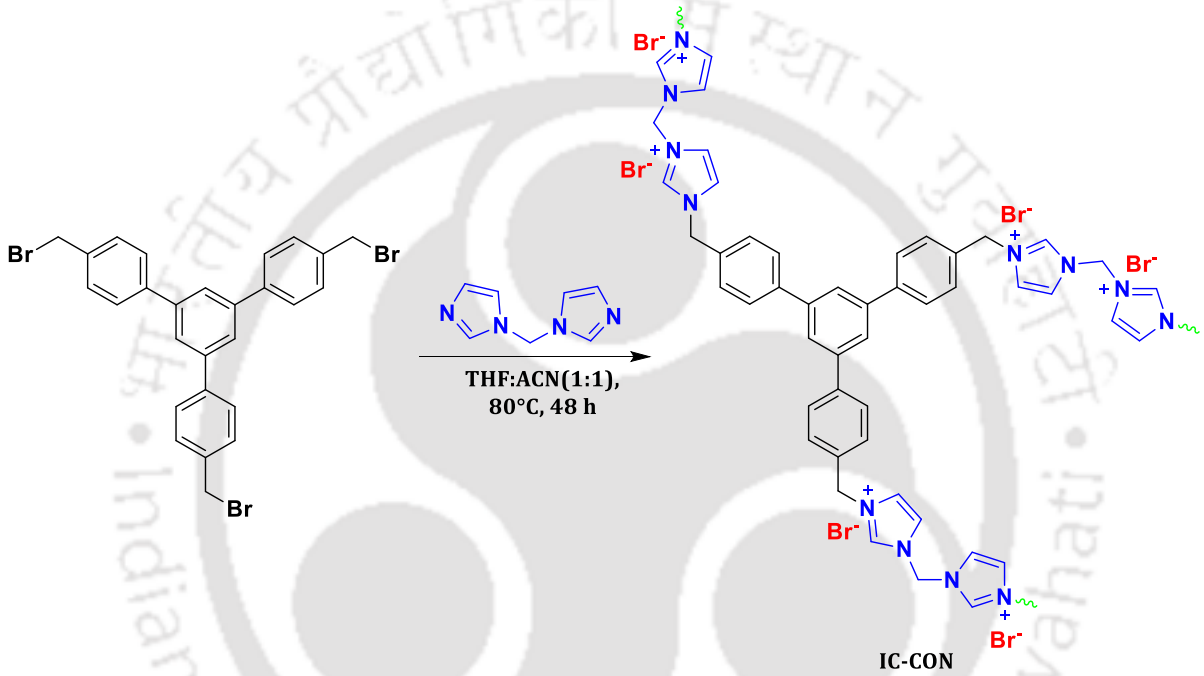

Scheme A4.4. Synthesis of bis-imidazolium-based cationic covalent organic network (IC-CON).

4.4.2.5. FT-IR spectroscopy analysis:

FT-IR analysis was carried out following the procedure outlined in section 2.5.2.4

4.4.2.6. XPS analysis:

XPS analysis was carried out following the procedure outlined in section 2.5.2.5

4.4.2.7. PXRD analysis:

PXRD analysis was carried out following the procedure outlined in section 3.4.2.6

4.4.2.8. FESEM and FESEM-EDX analysis:

FESEM and FESEM-EDX analysis was carried out following the procedure outlined in Section 2.5.2.6

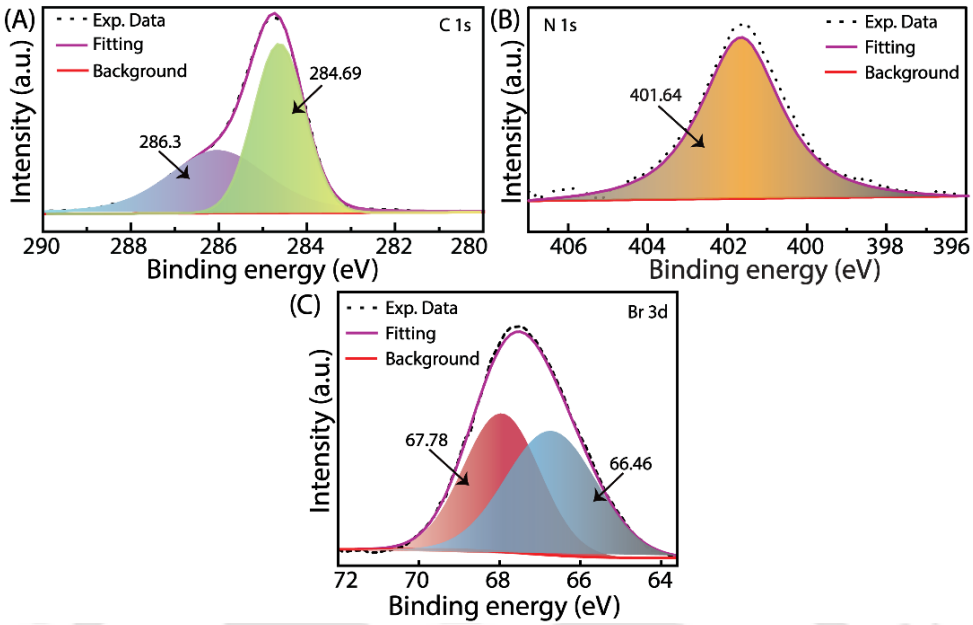

Figure A4.1. XPS data profile: the deconvoluted peak of C 1s (A), N 1s (B), and Br 3d of IC-CON.

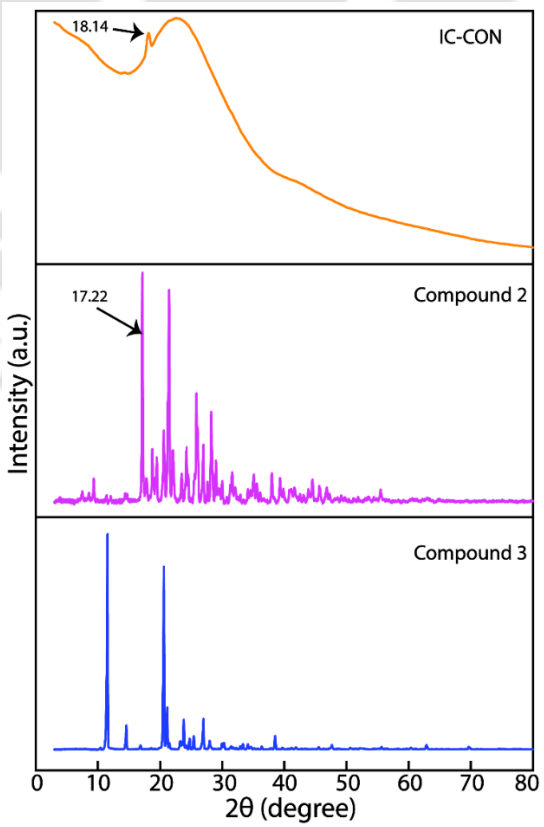

Figure 4.2. Comparative PXRD analyses of compounds 2 and 3 with IC-CON.

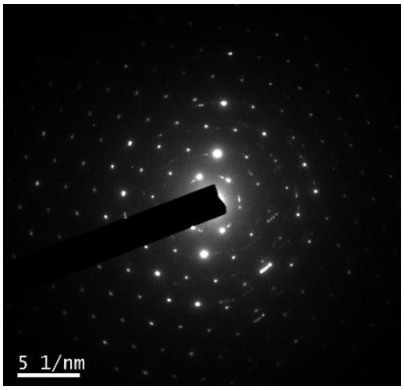

Figure A4.3. Transmission electron microscopy -selected area electron diffraction (TEM-SAED) image of **IC-CON** polymer.

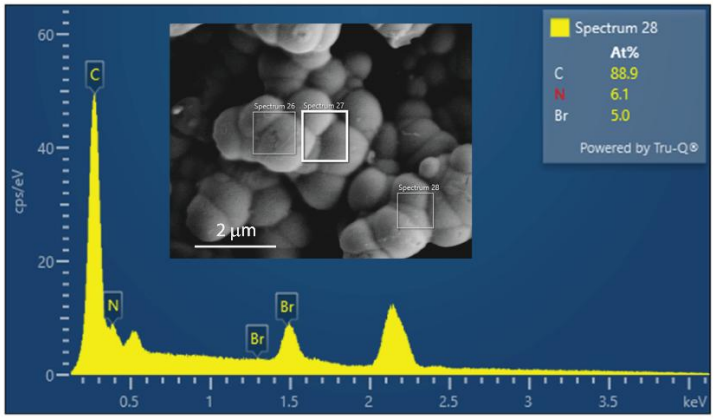

Figure A4.4. FESEM-EDX analysis of **IC-CON** polymer in atomic %.

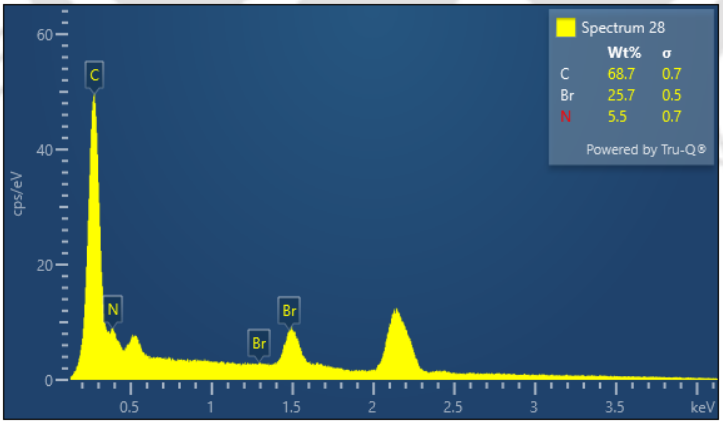

Figure A4.5. FESEM-EDX analysis of **IC-CON** polymer in weight %.

4.4.2.9. TEM analysis:

TEM analysis was carried out following the procedure outlined in section 3.4.2.8

4.4.2.10. AFM analysis:

AFM analysis was carried out following the procedure outlined in section 3.4.2.9

4.4.2.11. TGA:

TGA was carried out following the procedure outlined in section 2.5.2.7

4.4.2.12. Nitrogen adsorption Brunauer-Emmett-Teller (BET) experiments:

BET analysis was carried out following the procedure outlined in section 3.4.2.12

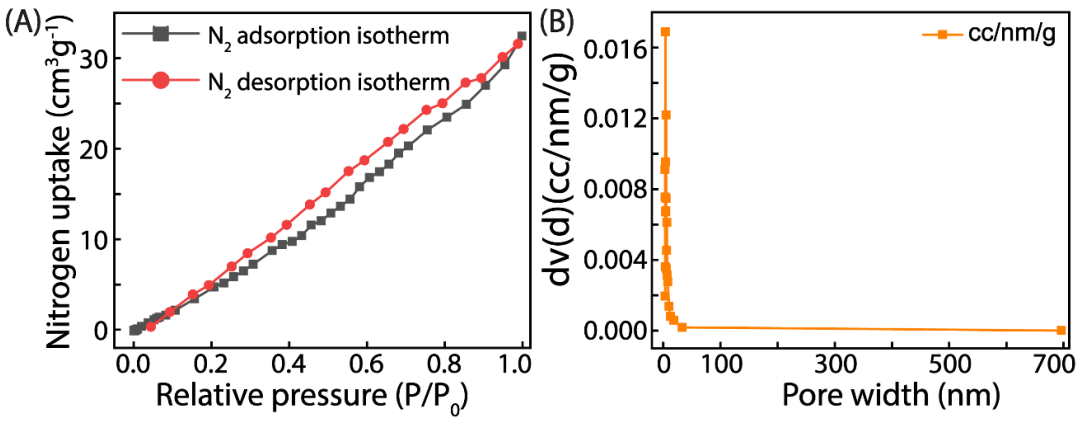

Figure A4.6. Nitrogen adsorption isotherm (A) and the pore-size distribution (B) of **IC-CON** polymer.

4.4.2.13. Zeta potential study:

Zeta potential analysis was carried out following the procedure outlined in section 3.4.2.13

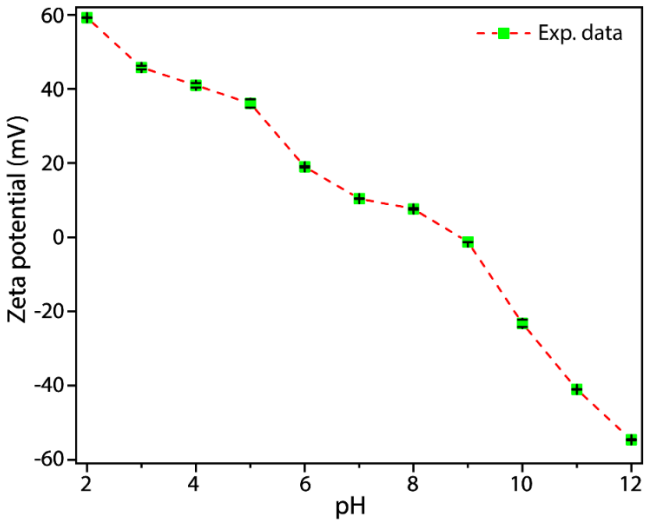

Figure A4.7. Zeta potential of **IC-CON** polymer at different pH.

4.4.2.14. Tyndall effect:

Tyndall effect analysis was carried out following the procedure outlined in section 2.5.2.11

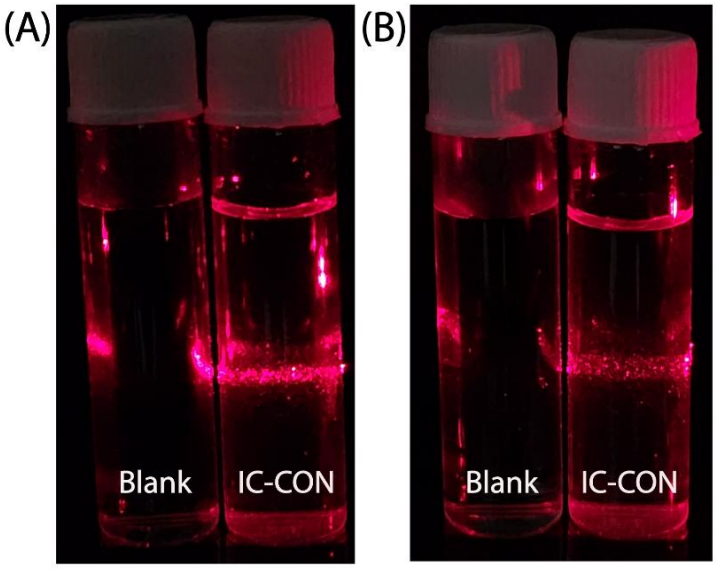

Figure A4.8. Tyndall effect of light in the aqueous dispersions of **IC-CON** after 2 min (A) and 48 h (B) of sonication.

4.4.2.15. DLS study of the IC-CON:

DLS analysis was carried out following the procedure outlined in section 2.5.2.8

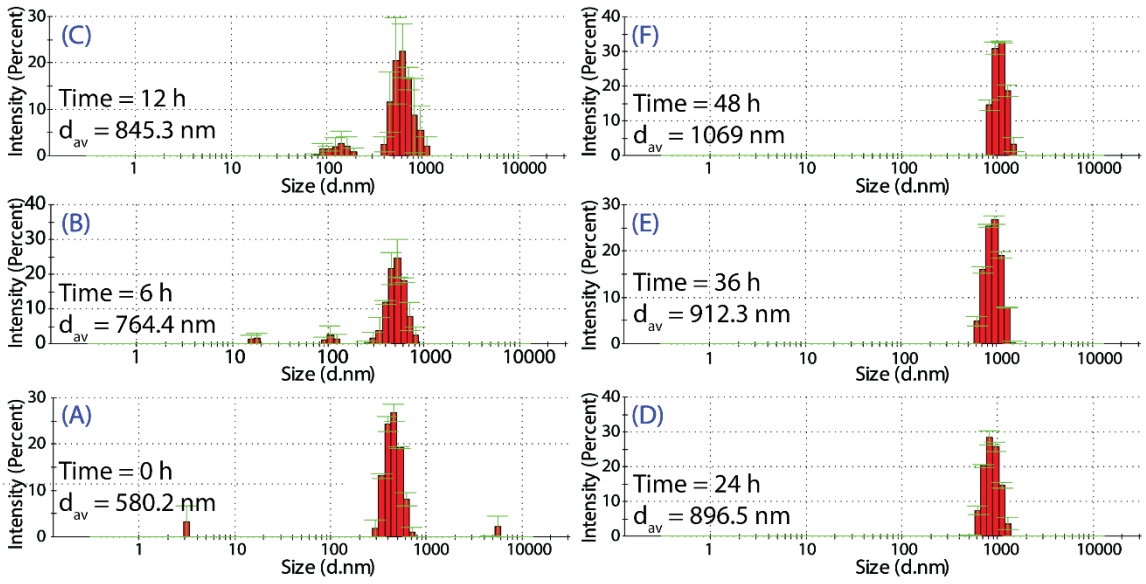

Figure A4.9. DLS measurements of IC-CON polymer in water at different time intervals.

4.4.2.16. Chemical stability analysis of the IC-CON:

To access the chemical stability of the IC-CON in different organic solvents, 5 mg of the polymer was separately treated with 5 mL of acetonitrile (ACN), dichloromethane (DCM), ethyl acetate (EtOAc), methanol (MeOH), tetrahydrofuran (THF), and acetone for 21 days. Subsequently, the polymers were isolated from the solvents using centrifugation at 8000 rpm for 5 min, followed by filtration by using a 0.45 μm syringe filter (Axiva). FT-IR analysis was then performed to assess the chemical stability of the polymer after oven drying at 75 °C for 8 h. Additionally, the stability of the IC-CON in basic and acidic solutions was accessed by treating 5 mg of the polymer in 5 mL of HCl (3 N) and NaOH (3 N) for 21 days at room temperature. Following this, the polymers were separated and dried in the same manner as mentioned above, and FT-IR analysis was performed to assess their chemical stability. Furthermore, morphological and thermal stability were assessed using FESEM and TGA on the same IC-CON samples after exposure to the acidic and basic conditions.

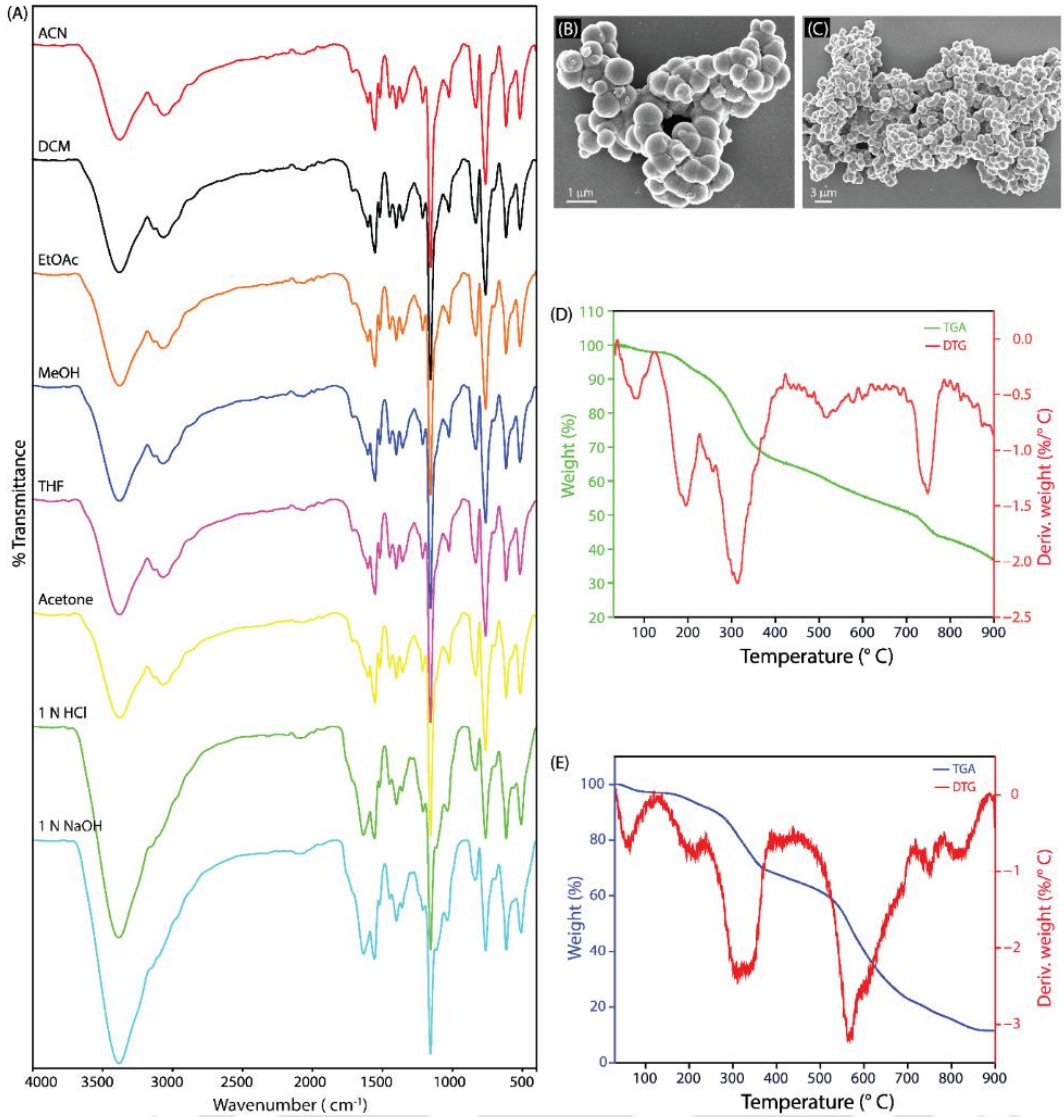

Figure A4.10. FT-IR spectra of **IC-CON** polymer after the treatment (for 21 days) with ACN, DCM, EtOAc, MeOH, THF, DMF, Acetone, HCl (3 N), and NaOH (3 N) solution (A). FESEM images of **IC-CON** polymer after treatment with 3 N NaOH (A) and 3 N HCl (B) for 21 days. TGA graph of **IC-CON** polymer after treatment with 3 N NaOH (A) and 3 N HCl (B) for 21 days.

4.4.3. Equations employed for adsorption study –

4.4.3.1. Equation for the calculation of % ion adsorption:

The relative percentage of phosphate ions absorbed from water was carried out following the equation 2.1, outlined in section 2.5.3.1

4.4.3.2. Equation for the calculation of the adsorption capacity:

The adsorption capacity of the IC-CON polymer was quantified using the equation 2.2, outlined in section 2.5.3.2

4.4.3.3. Equations to determine the adsorption isotherm:

The adsorption isotherm patterns were explored using equations 2.3 and 2.4, as outlined in section 2.5.3.3

4.4.3.4. Equations for the calculation of the adsorption kinetics:

The adsorption kinetics patterns were explored using equations 2.5 and 2.7, as outlined in section 2.5.3.4

4.4.4. Arsenate and phosphate adsorption study:

All arsenate ion adsorption studies, including selectivity, adsorption isotherm, kinetics, recyclability, and desorption isotherm experiments, were conducted using an Agilent 7850 Inductively Coupled Plasma Mass Spectrometer (ICP-MS). The residual solute concentration in the solution was quantified by comparison with a calibration curve constructed from certified standard solutions of known concentrations. In contrast, all phosphate ion adsorption experiments were performed using a Metrohm ion chromatograph (792 Basic IC, Switzerland) equipped with a METROSEP A Supp 5-250/4.0 (6.1006.530) separation column (4 mm × 100 mm). The primary standard employed for these measurements was the PRIMUS multi-anion solution (10 mg/kg ± 0.2% for each ionic species) from Fluka. Prior to analysis, arsenate ion solutions were diluted with 2% HNO_3, whereas phosphate ion solutions were diluted using Milli-Q water.

4.4.4.1. Initial binding efficacy study of IC-CON for arsenate and phosphate ions:

This study aimed to evaluate the initial binding efficacy of IC-CON toward arsenate and phosphate ions. The adsorption performance of IC-CON was first assessed for arsenate, followed by an evaluation of its phosphate adsorption capacity upon demonstrating significant arsenate binding efficacy.

For the adsorption experiments, 5 mg of IC-CON was dispersed in 5 mL of a 20-ppm arsenate solution and subjected to sonication for 1 min. The mixture was then agitated at 180 rpm for 5 min using an orbital shaker. Subsequently, the IC-CON was separated from the solution via centrifugation at 8000 rpm for 5 min, followed by filtration through 0.45 µm syringe filters (Axiva). The filtrates containing arsenate were diluted 20-fold to ensure arsenate ion concentrations remained below 1 ppm. The arsenate concentration in the solution before and after IC-CON treatment was quantified.

Encouraged by the high arsenate adsorption efficacy, the phosphate removal capacity of IC-CON was investigated following the same experimental protocol.

Furthermore, the binding efficacy of IC-CON toward arsenate and phosphate was validated using complementary analytical techniques, including Fourier transform infrared spectroscopy (FT-IR), X-ray photoelectron spectroscopy (XPS), field emission scanning electron microscopy coupled with energy dispersive X-ray spectroscopy (FESEM-EDX), and elemental mapping analysis.

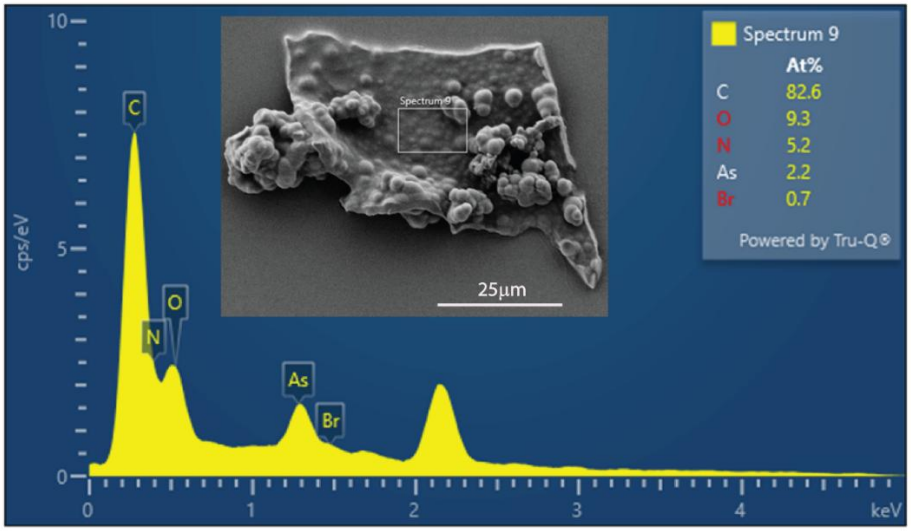

Figure A4.11. FESEM-EDX analysis of **IC-CON** polymer after arsenate adsorption in atomic %.

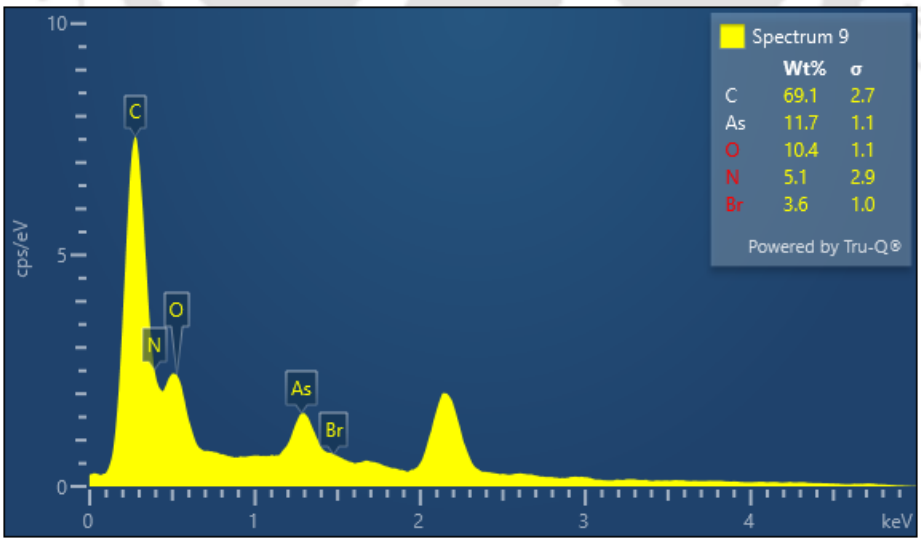

Figure A4.12. FESEM-EDX analysis of **IC-CON** polymer after arsenate adsorption in weight %.

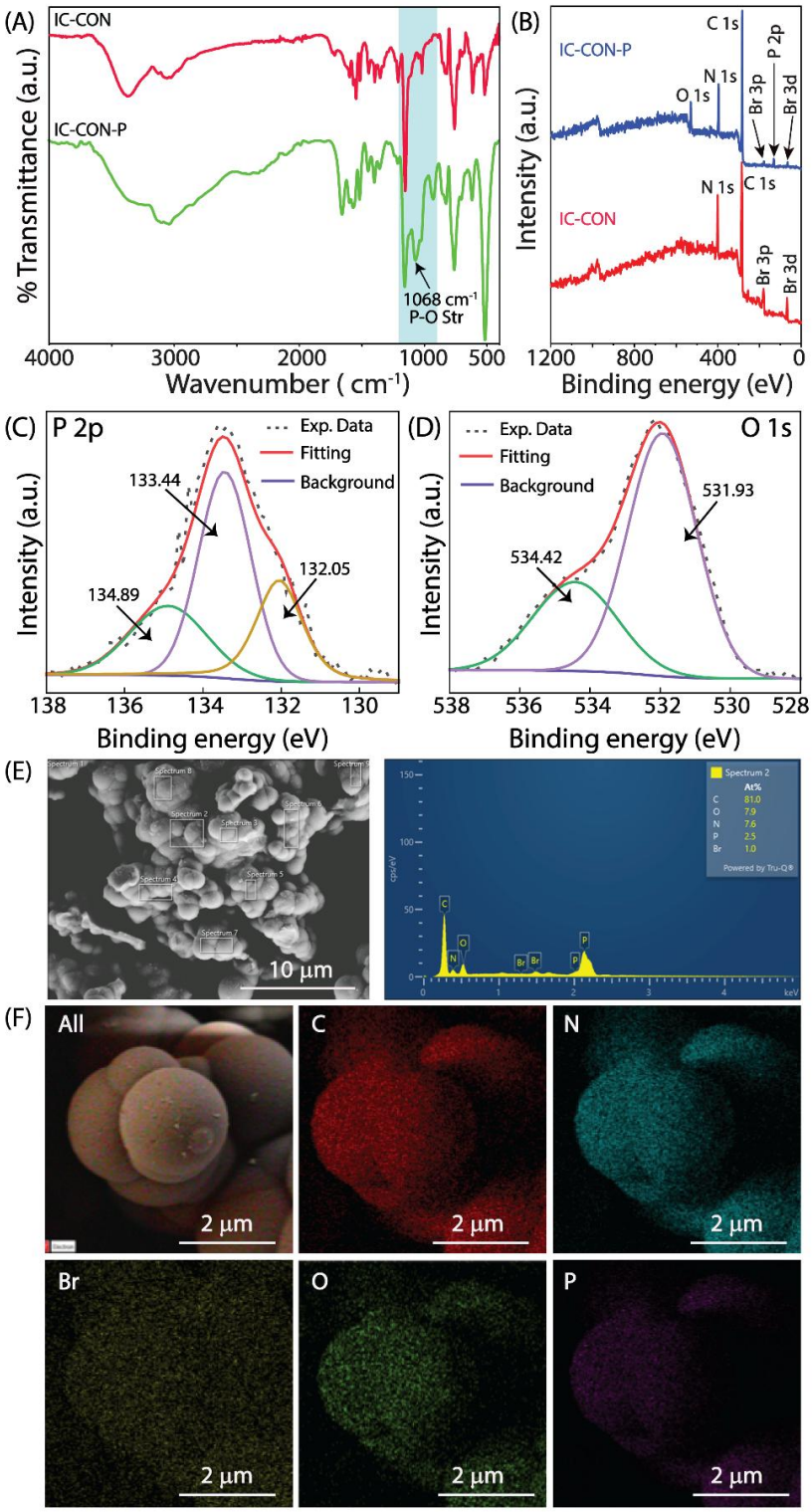

Figure A4.13. FT-IR spectra of **IC-CON** before and after phosphate anion adsorption (A). XPS data profile (wide scan) of **IC-CON** after phosphate anion adsorption (B). XPS data profile: the deconvoluted peak of P 2p (C), and O1s (D) of **IC-CON** polymer after phosphate adsorption. FESEM-EDX analysis of **IC-CON** polymer after phosphate adsorption in atomic % (E). The FESEM mapping analysis for the C, O, N, Br and P of **IC-CON** after phosphate anion adsorption (F).

4.4.4.2. Influence of pH on adsorption experiments:

To evaluate the effect of pH on the adsorption of arsenate and phosphate ions by IC-CON, adsorption experiments were conducted over a pH range of 2 to 12. The pH of the solutions was adjusted using 0.1 M HCl and 0.1 M NaOH. In each experiment, 5 mg of the polymer was added to 5 mL of a 500-ppm arsenate ion solution prepared at different pH values (2, 4, 5, 6, 7, 8, 10, and 12) and agitated in an orbital shaker at 180 rpm for 6 hours at 25 °C. Following adsorption, the polymer was separated from the solution via centrifugation at 8000 rpm for 5 minutes, followed by filtration using a 0.45 µm syringe filter (Axiva). The residual arsenate ion concentration in the supernatant was determined using ICP-MS. Prior to analysis, the supernatants were diluted 500 times to maintain arsenate ion concentrations below 1 ppm. The equilibrium adsorption capacity of the polymer for arsenate ions was subsequently calculated using equation 2.2.

Similarly, the effect of pH on phosphate ion adsorption was investigated following the same procedure. In this case, IC was employed to quantify the phosphate ion concentration in the supernatants before and after treatment with IC-CON. To ensure phosphate ion concentrations remained below 20 ppm, each solution was diluted 25 times before IC analysis.

The results of the above analyses reveal that both the arsenate and phosphate ion adsorption capacities reach their maximum values under near-neutral conditions (pH 6–8). The adsorption of arsenate and phosphate ions by IC-CON is predominantly influenced by two non-covalent interactions: hydrogen bonding with the acidic C–H protons near the quaternary nitrogen centers and electrostatic attraction between the quaternary nitrogen and the anionic species. The zeta potential study revealed that the surface potential of IC-CON increases from +7 mV at pH 7 to +45 mV at pH 2, signifying a higher positively charged surface in acidic environments. Despite the increased positive surface charge at lower pH, the adsorption efficacy of both arsenate and phosphate ions decreases. This decrease can be ascribed to two key factors. Initially, the elevated concentration of chloride ions (Cl^-) in acidic conditions competes with arsenate and phosphate for electrostatic binding sites on IC-CON, diminishing their absorption; additionally, the increased protonation of arsenate and phosphate ions at low pH reduces their net negative charge, thereby weakening electrostatic interactions with the cationic IC-CON

surface. As pH rises from 7 to 12, arsenate and phosphate ions undergo gradual deprotonation, resulting in an increase in their negative charge. At alkaline pH, IC-CON exhibits a negative zeta potential, resulting in electrostatic repulsion between the polymer and the anions and hence reducing adsorption. Moreover, the higher concentration of hydroxide ions (OH^-) at high pH competes with arsenate and phosphate for binding sites. Furthermore, the deprotonation of the oxyanions at elevated pH diminishes their hydrogen-bonding ability, hence further reducing interaction with the IC-CON framework. At pH 7, IC-CON exhibits a moderately positive zeta potential (~+7 mV), signifying the presence of quaternary ammonium groups that can participate in electrostatic interactions with arsenate and phosphate ions. At this pH, arsenate predominantly exists as $H_2AsO_4^-$ and $HAsO_4^{2-}$, while phosphate also exists as $H_2PO_4^-$ and HPO_4^{2-} species, which possess hydroxyl functionalities that can engage in directional hydrogen bonding with the electron-deficient –C–H protons adjacent to the quaternary nitrogen atoms on the imidazolium rings, thus improving overall adsorption efficacy. Furthermore, the negligible concentration of competing anions such as Cl^- or OH^- at neutral pH helps IC-CON to selectively interact with target arsenate and phosphate ions. This diminished ionic competition, along with synergistic hydrogen bonding and electrostatic attraction, enhances both enthalpic and entropic factors in the adsorption process. Most natural groundwater sources have a pH between 5 and 8, and IC-CON demonstrated enhanced adsorption capacity under near-neutral conditions (pH 6–8), indicating its potential for practical application in diverse water treatment processes.[33]

4.4.4.3. Adsorption isotherms study:

To evaluate the adsorption isotherms of arsenate and phosphate ions by the polymer, aqueous solutions of arsenate and phosphate ions were prepared at varying concentrations ranging from 1 to 1200 ppm in Milli-Q water. 5 mL of each solution was individually treated with 5 mg of the IC-CON, followed by sonication for 1 minute to ensure homogeneous dispersion. The samples were then incubated under continuous shaking at 180 rpm in an orbital shaker at room temperature for 6 hours. After incubation, the polymer was separated from the solution via centrifugation at 8000 rpm for 5 minutes, followed by filtration using 0.45 µm syringe filters (Axiva). The filtered supernatants containing arsenate were diluted to maintain arsenate ion

concentrations below 1 ppm, while the phosphate-containing supernatants were diluted to maintain phosphate ion concentrations below 20 ppm prior to analysis. The equilibrium concentrations of arsenate and phosphate ions were then determined using equation 2.2. To further analyse the adsorption behaviour, both the Langmuir and Freundlich isotherm models, as described in equations 2.3 and 2.4, respectively, were employed to assess the relationship between adsorption parameters and equilibrium concentrations. These models were also used to determine the maximum adsorption capacity of the polymer for arsenate and phosphate ions.

4.4.4.4. Adsorption kinetics study:

The adsorption kinetics of arsenate and phosphate ions onto the polymer were evaluated by monitoring their uptake from aqueous solutions over various time intervals: 15, 30, 45, 60, 90, 120, 150, 180, 210, 240, 270, 300, 360 and 400 seconds. In each experiment, 5 mg of IC-CON was incubated with 5 mL of a 500-ppm aqueous solution of arsenate or phosphate at pH 7. At each designated time point, approximately 100 µL of the solution was collected, and the polymer was separated via centrifugation at 8000 rpm for 5 minutes, followed by filtration through 0.45 µm syringe filters (Axiva). The filtered supernatants containing arsenate ions were diluted 500 times to maintain concentrations below 1 ppm before analysis via ICP-MS. Similarly, the filtered phosphate-containing supernatants were diluted 25 times to maintain phosphate ion concentrations below 20 ppm before analysis using IC. The equilibrium concentrations of arsenate and phosphate ions were then calculated using Equation 2. The adsorption kinetics of arsenate and phosphate ions onto the polymer were further characterized by fitting the experimental data to both pseudo-first-order and pseudo-second-order kinetic models, as described by equations 2.5 and 2.7, respectively.

Additionally, to investigate the effect of polymer concentration on adsorption kinetics, experiments were conducted using varying amounts of IC-CON (3 mg, 5 mg, 7 mg, and 10 mg), each incubated with 5 mL of a 500-ppm aqueous solution of arsenate or phosphate at pH 7. The kinetics study for each polymer concentration was performed following the same protocol as described above.

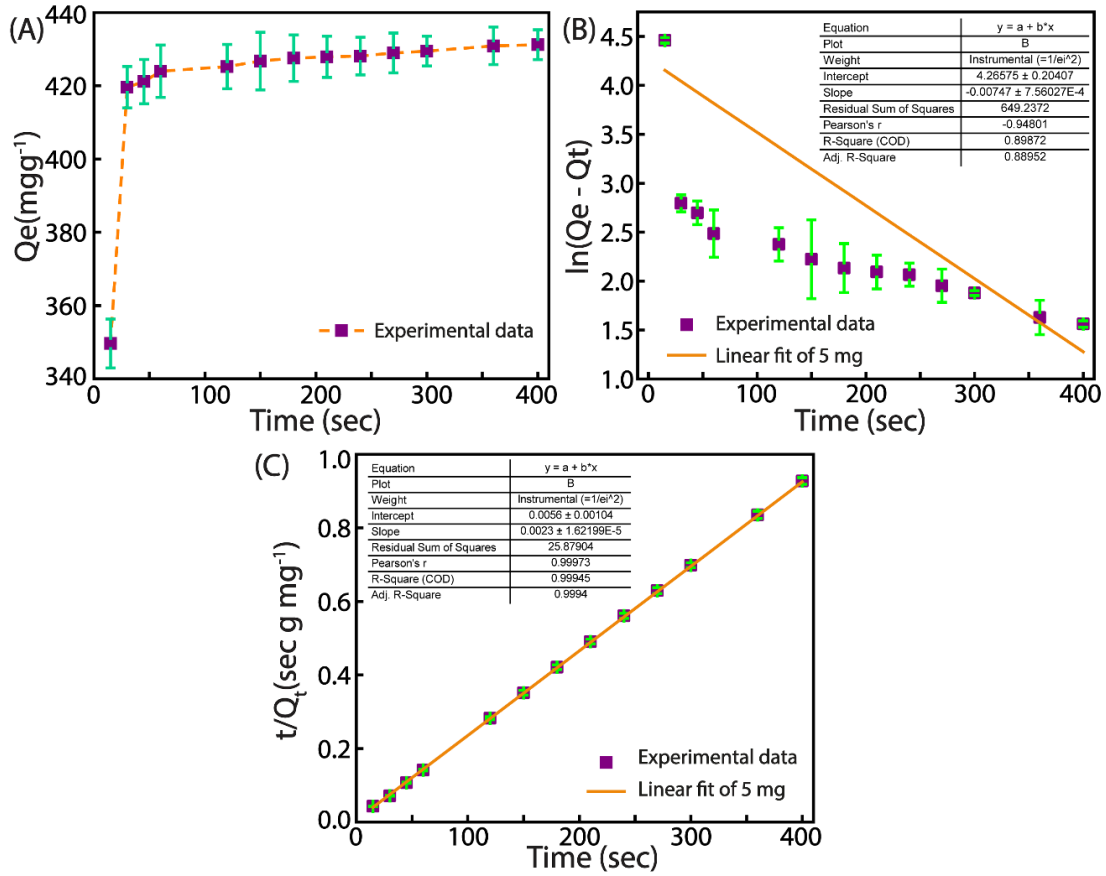

Figure A4.14. Time-dependent adsorption isotherm of arsenate by **IC-CON** (5 mg) at pH 7 under room temperature(A), the time-dependent arsenate adsorption efficiency of **IC-CON** fitted with the first order (B) and second order kinetics (C) models.

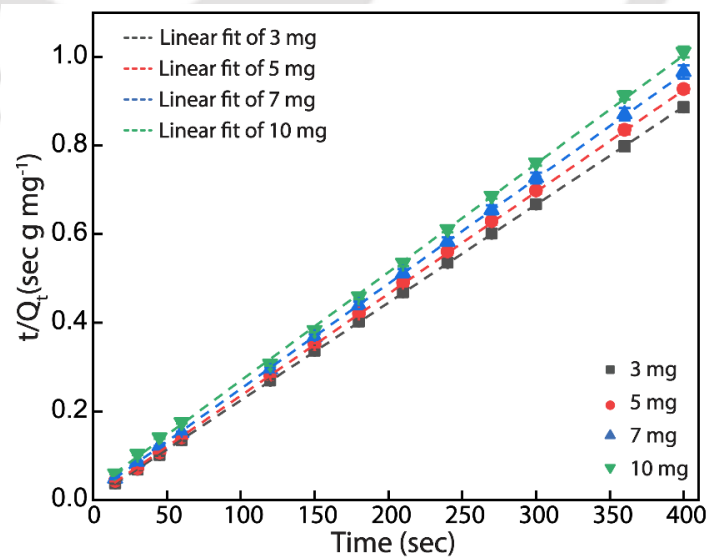

Figure A4.15. Pseudo-second-order kinetics curves of arsenate adsorption on **IC-CON** (3-10 mg) at pH 7.0 under room temperature.

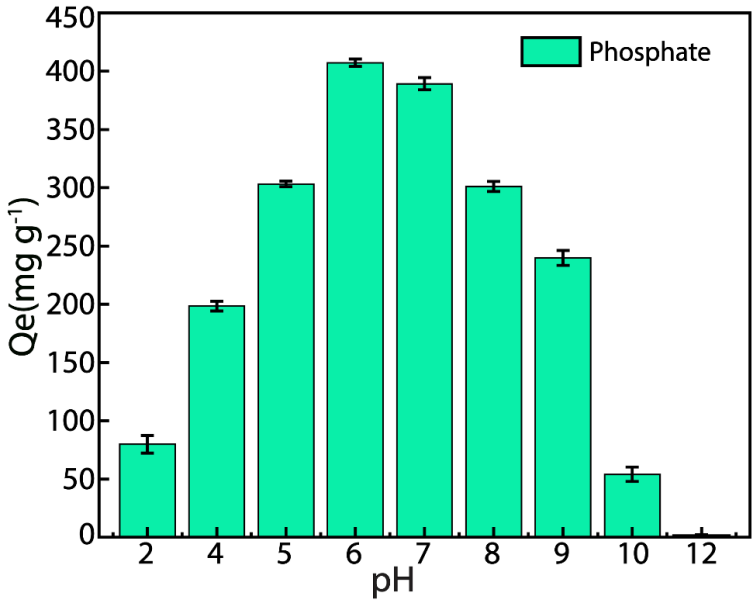

Figure A4.16. The pH-dependent phosphate ion adsorption efficiency of IC-CON.

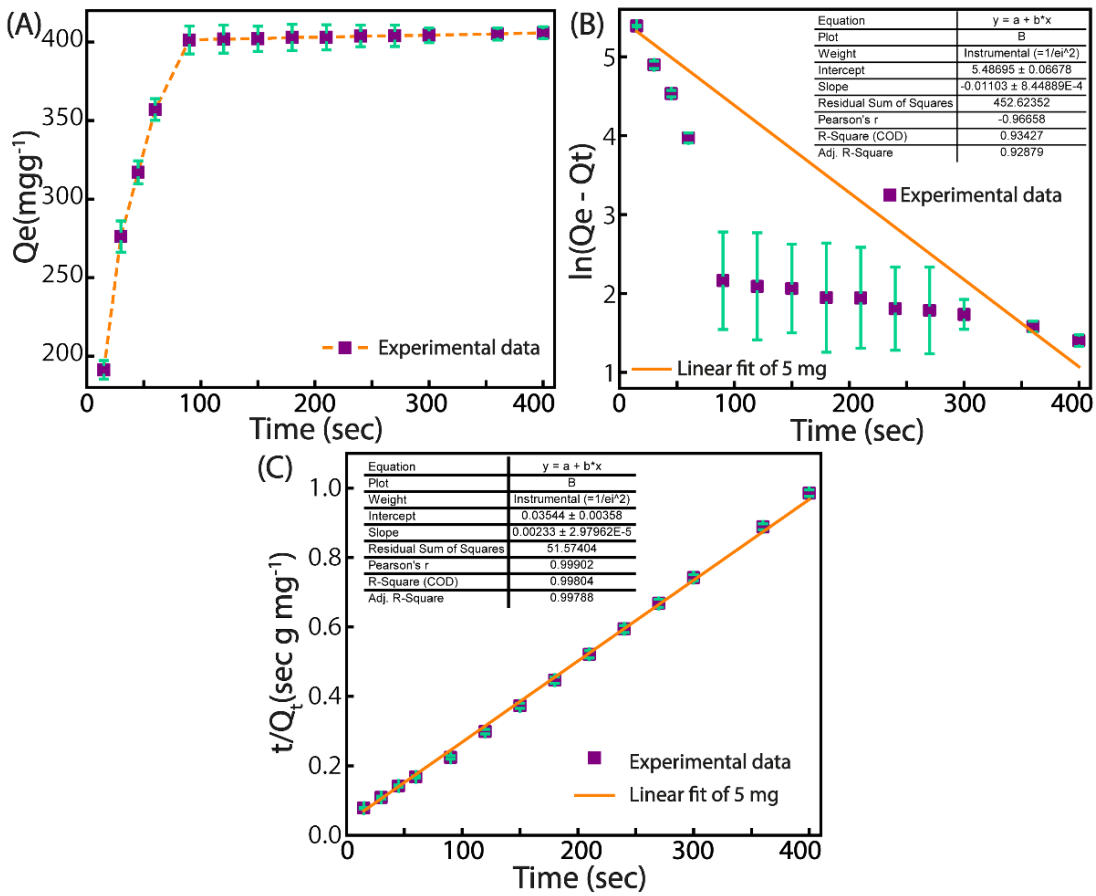

Figure A4.17. Time-dependent adsorption isotherm of phosphate by **IC-CON** (5 mg) at pH 7 under room temperature(A), time-dependent phosphate adsorption efficiency of **IC-CON** fitted with the first order (B) and second order kinetics (C) models.

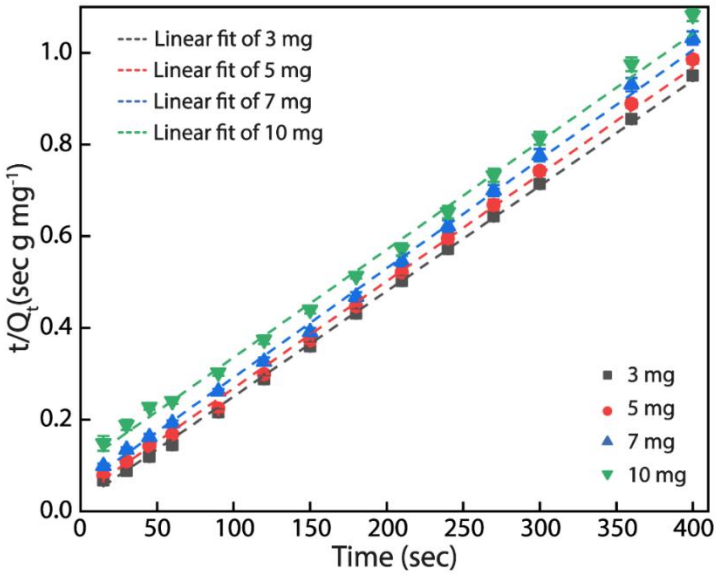

Figure A4.18. Pseudo-second-order kinetics curves of phosphate adsorption on **IC-CON** (3-10 mg) at pH 7.0 under room temperature.

4.4.4.5. Effect of temperature on arsenate and phosphate adsorption:

To examine the effect of temperature on arsenate adsorption, four batches of 5 mL arsenate solution (500 ppm) were individually mixed with 5 mg of the IC-CON polymer and agitated for 3 hours at different temperatures (298 K, 313 K, 328 K, and 343 K) at pH 7. Following adsorption, the polymer was separated via centrifugation, and the arsenate concentration in the solution before and after treatment with IC-CON was quantified using ICP-MS. A similar investigation was conducted for phosphate ions, with their concentrations measured before and after adsorption using IC.

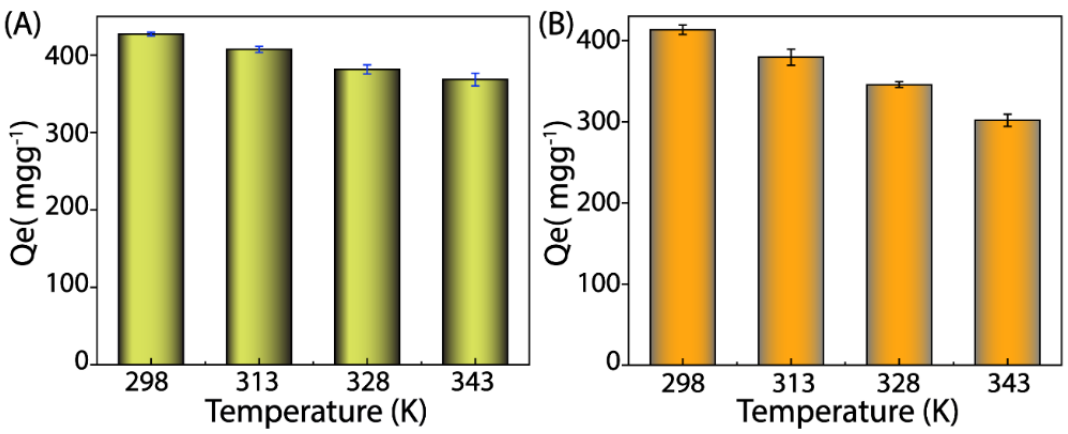

Figure A4.19. The equilibrium adsorption capacity of arsenate (A) and phosphate (B) by **IC-CON** at different temperatures.

4.4.4.6. Effect of counter ions on arsenate and phosphate adsorption:

To investigate the influence of competing anions, including Cl^-, F^-, NO_3^-, SO_4^{2-}, and CO_3^{2-}, on the adsorption of arsenate and phosphate, binary stock solutions were prepared using sodium salts of the aforementioned anions in Milli-Q water. These solutions were formulated at varying molar ratios of arsenate or phosphate to competing anions (1:1, 1:10, 1:50, and 1:100) to systematically evaluate their impact on adsorption efficiency. The concentrations of arsenate and phosphate ions in the stock solution were set at 20 ppm, while the concentrations of other ions were adjusted relative to these ions.

Subsequently, 5 mg of the IC-CON polymer was introduced into 5 mL of each stock solution and agitated for 3 hours. The adsorption efficacy of IC-CON for arsenate and phosphate in the presence of competing anions was then assessed.

The results indicate that Cl^- ions exert a negligible influence on the adsorption of arsenate and phosphate by the IC-CON polymer. Consequently, to evaluate the effect of metal cations on arsenate and phosphate adsorption, stock solutions were prepared using different chloride salts following the previously described procedure. Due to the solubility constraints of various metal arsenates and phosphates, metal chloride salts of Na^+, K^+, Rb^+, Cs^+, Mg^{2+}, and Al^{3+} were selectively employed for this investigation. These experiments were conducted following the same protocol as outlined above.

Two binary stock solutions were prepared to evaluate the adsorption efficacy of IC-CON towards arsenate (As) in the presence of chromate (Cr) and rhenate (Re). One stock solution contained a mixture of 20 ppm arsenate and chromate ions (Sodium chromate), while the other consisted of 20 ppm arsenate and rhenate ions (sodium perrhenate). A 5 mg portion of IC-CON was treated with 5 mL of each stock solution separately and agitated for 6 h at 180 rpm in an orbital shaker under ambient conditions. Following incubation, the polymer was separated from the solution via centrifugation at 8000 rpm for 5 minutes, followed by filtration using 0.45 µm syringe filters (Axiva). The filtered supernatants were subsequently diluted 20-fold to ensure arsenate ion concentrations remained below 1 ppm. The relative removal percentage of arsenate ions was then calculated using equation 2.1.

A similar experimental procedure was employed to assess the adsorption capacity of IC-CON for phosphate (P) in the presence of chromate and rhenate ions.

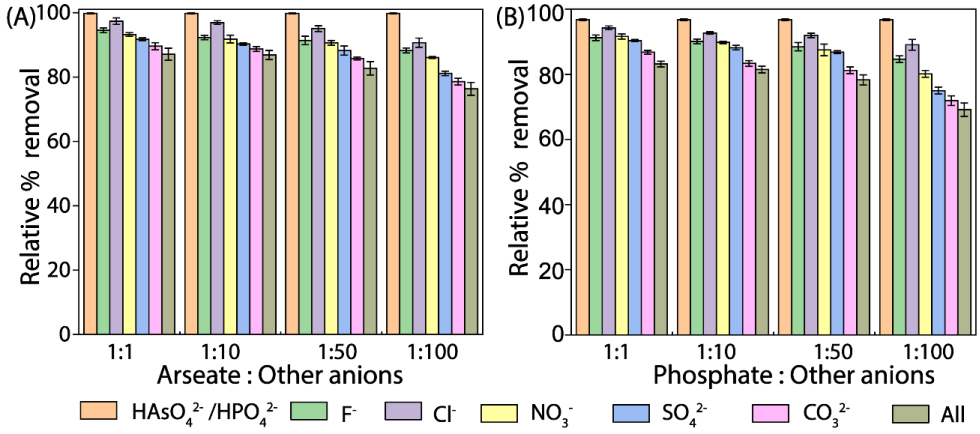

Figure A4.20. Arsenate (A) and phosphate (B) removal efficiency of **IC-CON** polymer in the presence of different ratios of Cl^-, F^-, NO_3^-, SO_4^{2-}, and CO_3^{2-} anions.

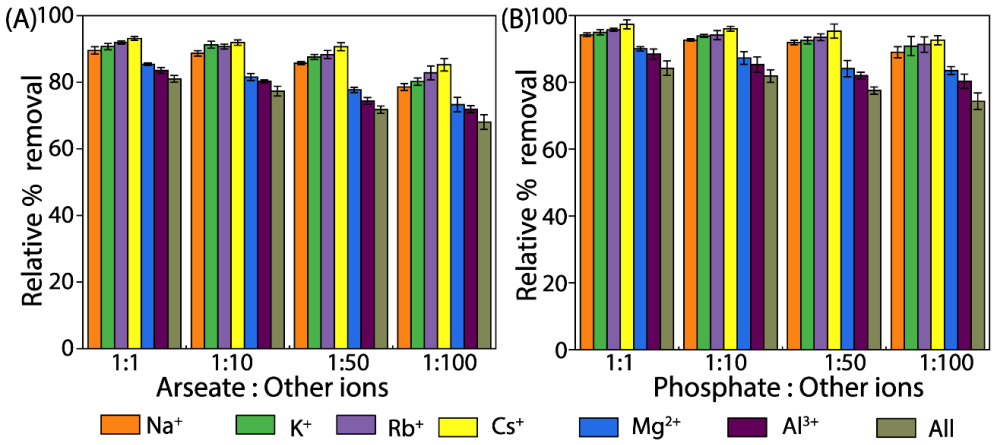

Figure A4.21. Arsenate (A) and phosphate (B) removal efficiency of **IC-CON** polymer in the presence of different ratios of Na^+, K^+, Rb^+, Cs^+, Mg^{2+}, and Al^{3+} ions.

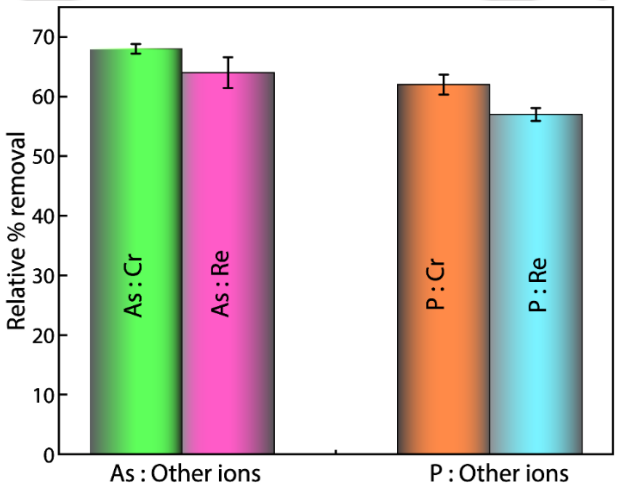

Figure 4.22. Arsenate (As) and phosphate (P) removal efficiency of **IC-CON** polymer in the presence of Cr and Re ions.

4.4.4.7. Adsorption performance of IC-CON for arsenate and phosphate from equimolar binary solutions at varying concentrations:

To evaluate the selective adsorption efficacy of IC-CON for arsenate and phosphate ions from a 1:1 arsenate-to-phosphate binary solution, five stock solutions with equimolar arsenate and phosphate concentrations ranging from 0.5 ppm to 100 ppm were prepared. Subsequently, 5 mg of the IC-CON polymer was introduced into 5 mL of each stock solution and subjected to agitation for 3 hours. Following adsorption, the polymer was separated via centrifugation, and the residual concentrations of arsenate and phosphate ions in the supernatant were quantified to assess the adsorption performance of IC-CON.

4.4.4.8. Regeneration analyses of IC-CON:

The reusability of the polymer was systematically assessed through a series of batch experiments involving cyclic adsorption and desorption of phosphate and arsenate ions. In each adsorption cycle, 5 mg of IC-CON was incubated individually with 5 mL of a 500-ppm aqueous solution containing arsenate and phosphate ions. The mixture was subjected to orbital shaking at 180 rpm for 1 hour at room temperature to facilitate adsorption. Subsequently, the polymer was separated from the solution through centrifugation and filtration, effectively isolating the adsorbent loaded with arsenate and/or phosphate ions. The unadsorbed arsenate and phosphate ion concentrations in the supernatant were then quantified.

Desorption of the adsorbed arsenate and phosphate ions was conducted by immersing the loaded IC-CON in 5 mL of a 0.5 N NaOH solution (pH ~13) at room temperature for 2 hours. The desorbed solution was collected and analysed to determine the amount of arsenate and phosphate ions released from the polymer. Following desorption, the IC-CON polymer was subjected to a regeneration process involving thorough washing with a 0.1 N NaBr solution to convert the polymer from the OH^- form to the Br^- form. Subsequently, extensive rinsing with Milli-Q water was performed to eliminate residual contaminants and restore the adsorption capacity of the polymer. The polymer was then recovered via centrifugation and filtration, followed by drying in a microwave oven at 70 °C for 6 hours before the next adsorption cycle.

This adsorption-desorption process was repeated for 15 consecutive cycles, with each adsorption cycle utilizing a fresh 500 ppm stock solution of arsenate and phosphate ions to evaluate the long-term reusability of the polymer.

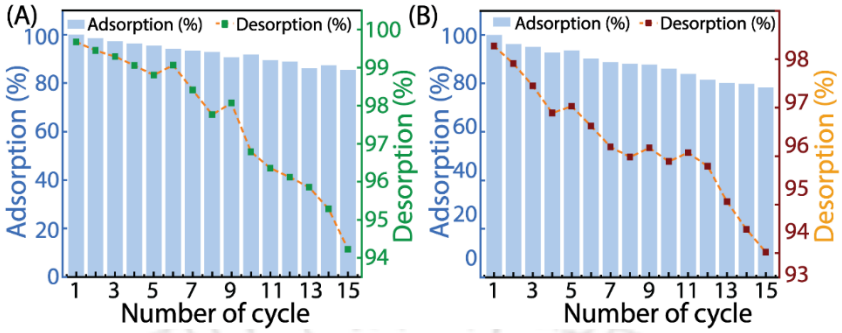

Figure A4.23. Arsenate (A) and Phosphate (B) ion adsorption and desorption efficiency of IC-CON after different cycles.

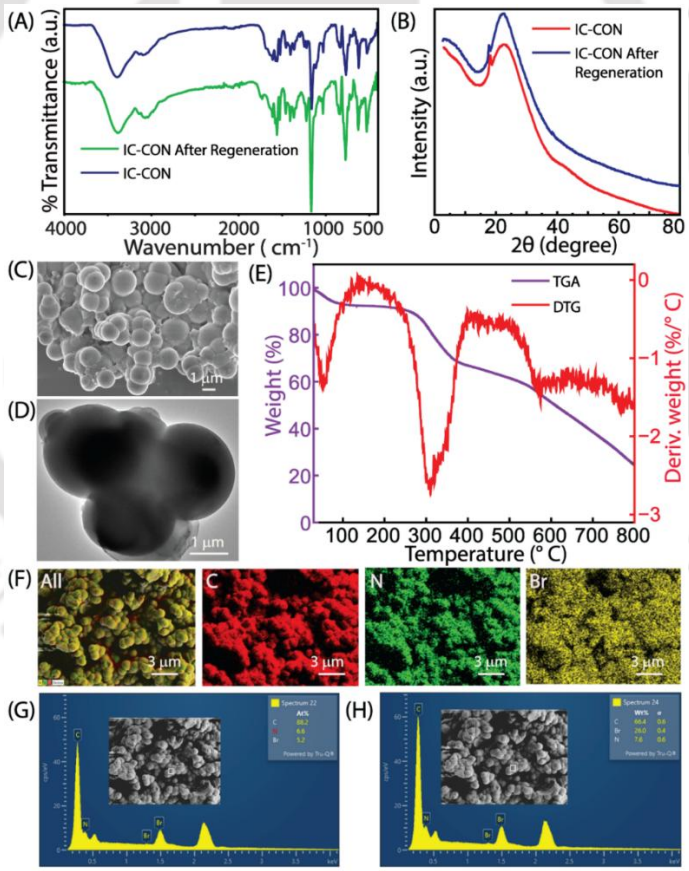

Figure A4.24. FT-IR (A), PXRD (B), FESEM image (C), TEM image (D), TGA-DTG analysis (E), FESEM mapping (F) and elemental analysis in atomic % (G) and weight % (H) of **IC-CON** polymer after undergoing 15 cycles of adsorption and desorption of arsenate.

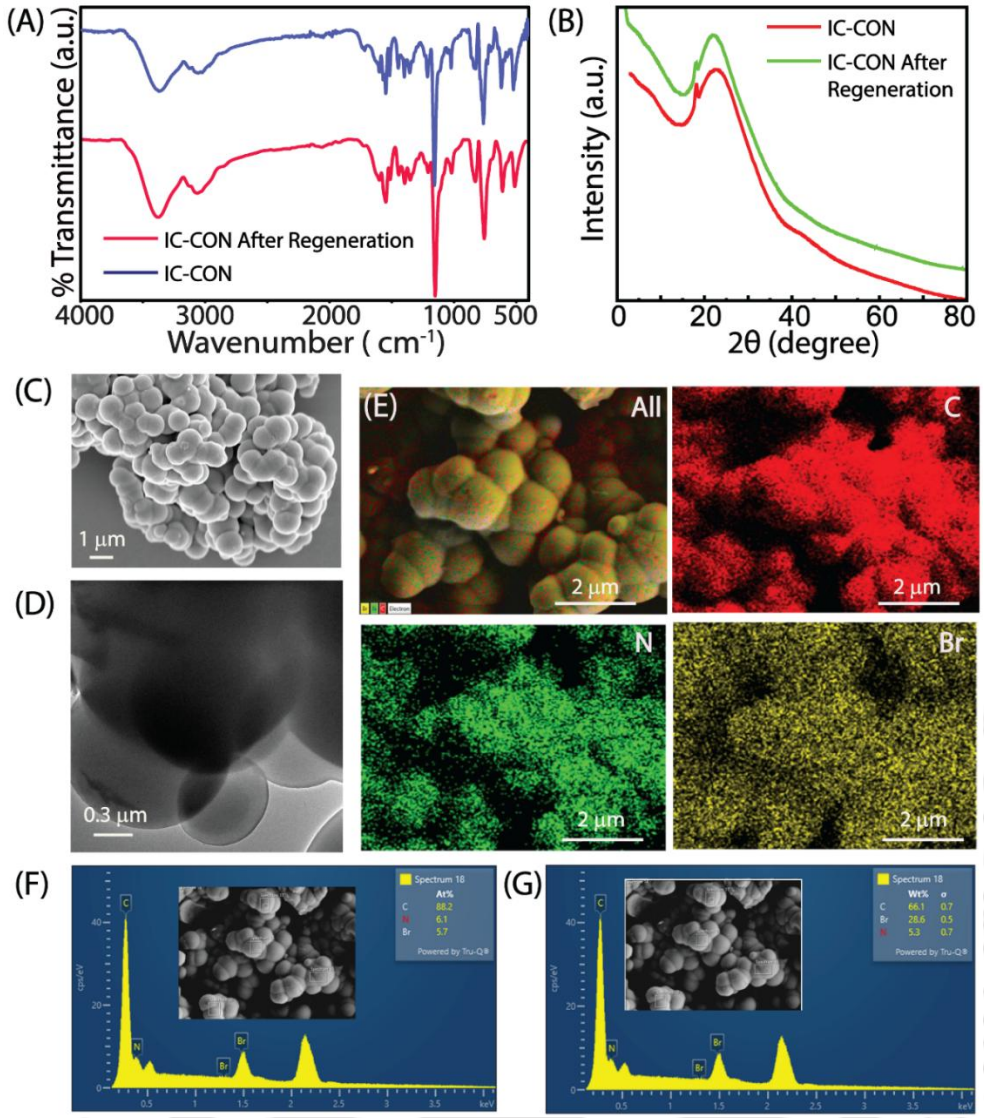

Figure A4.25. FT-IR (A), PXRD (B), FESEM image (C), TEM image (D), FESEM mapping (F) and elemental analysis in atomic % (G) and weight % (H) of **IC-CON** polymer after undergoing 15 cycles of adsorption and desorption of phosphate.

4.4.4.9. Arsenate and phosphate desorption kinetics study –

To investigate the desorption kinetics of arsenate and phosphate from the IC-CON polymer, 5 mg of arsenate- and phosphate-loaded polymers were individually mixed with 5 mL of 0.5 N NaOH solution. The suspensions were subjected to continuous agitation using an orbital shaker incubator (LabTech) set at 180 rpm and maintained at 25°C. At predetermined time intervals (ranging from 2 to 60 min), aliquots were collected, and the polymer was separated via centrifugation followed by filtration.

The filtrate containing arsenate was subsequently diluted by a factor of 500 to ensure an arsenate concentration of ≤1 ppm, followed by quantification using ICP-MS. Similarly, the filtrate containing phosphate was diluted by a factor of 25 to maintain a phosphate concentration of ≤20 ppm, with subsequent analysis conducted using IC.

The desorption kinetic data were analysed by plotting them using the linear forms of the pseudo-first-order and pseudo-second-order models. The results confirmed that both desorption processes followed the pseudo-second-order model. Arsenate desorption exhibited a rate constant of 0.000634 mg g^{-1} min^{-1} with a correlation coefficient (R^2) of 0.988, while phosphate desorption showed a rate constant of 0.000172 mg g^{-1} min^{-1} with an R^2 of 0.947.

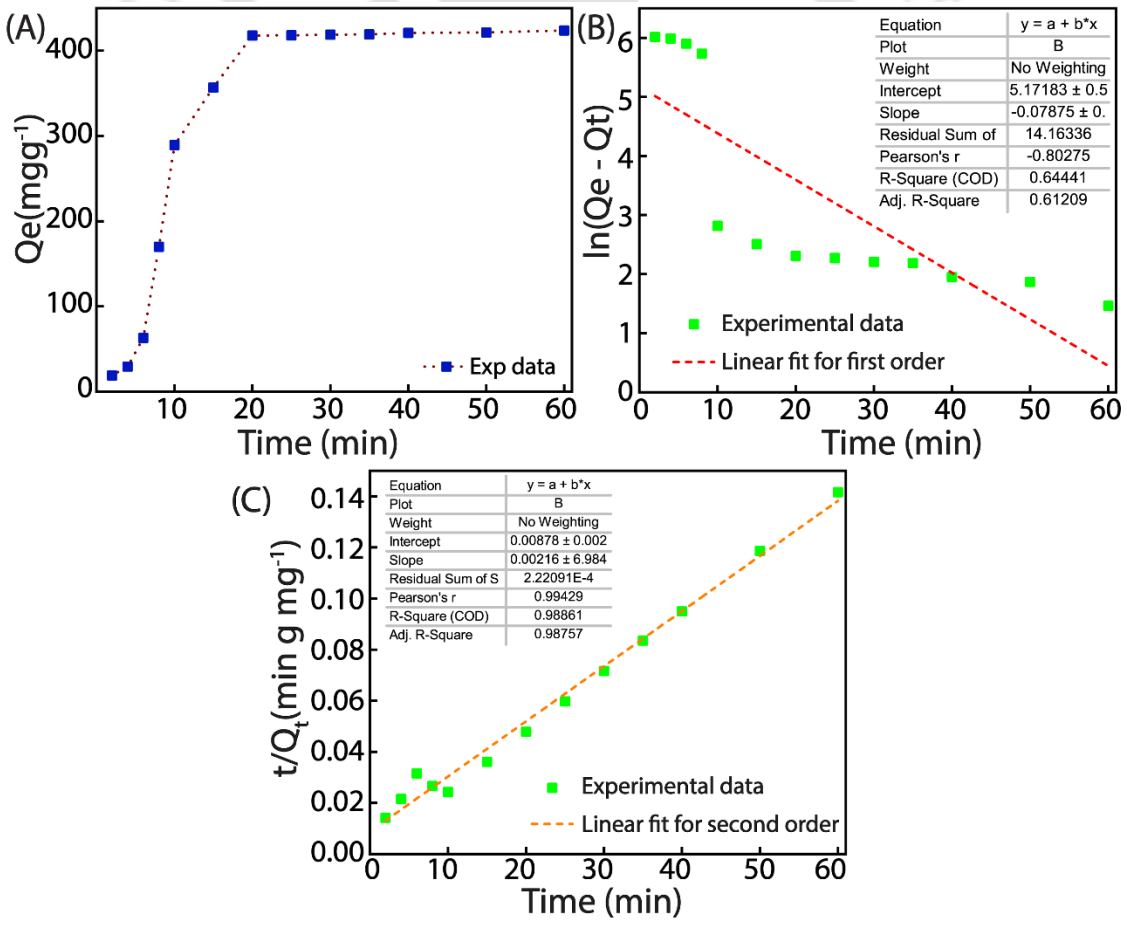

Figure A4.26. Time-dependent desorption isotherm of arsenate by **IC-CON** (5mg) under room temperature (A), time-dependent desorption efficiency of **IC-CON** fitted with the first order (B) and second order (C) kinetics models.

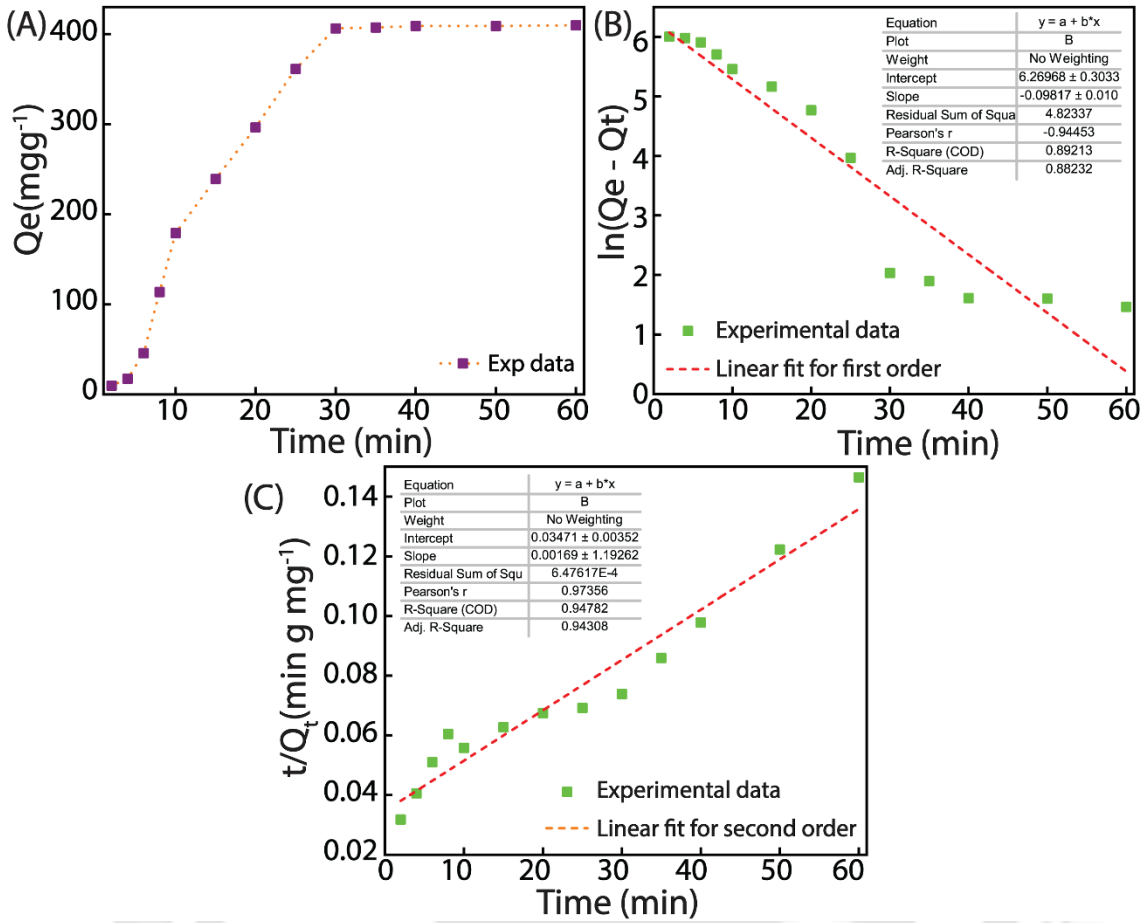

Figure A4.27. Time-dependent desorption isotherm of phosphate by **IC-CON** (5mg) under room temperature (A), time-dependent desorption efficiency of **IC-CON** fitted with the first order (B) and second order (C) kinetics models.

4.4.4.10. Morphological analysis after arsenate and phosphate ions adsorption:

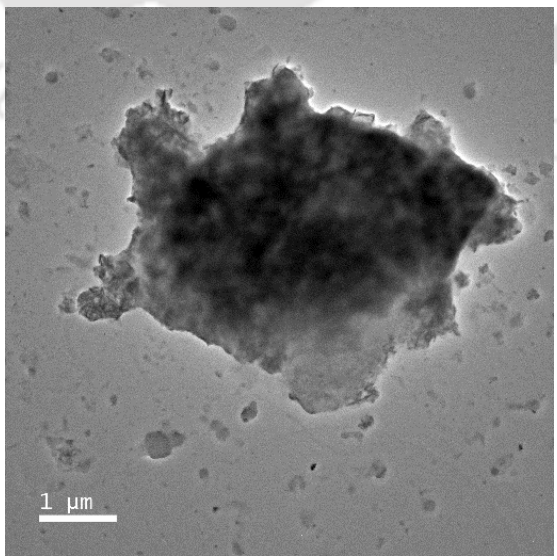

Figure A4.28. FETEM Image after arsenate adsorption.

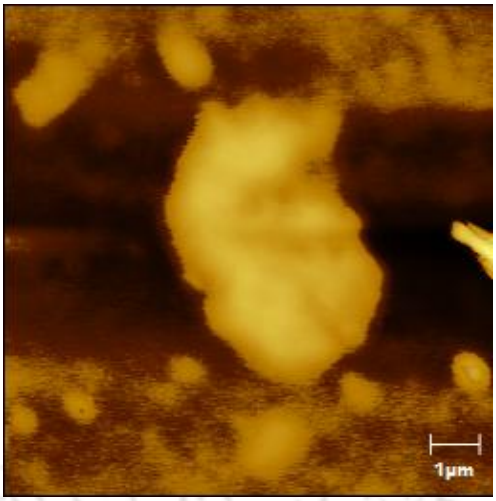

Figure A4.29. AFM Image after arsenate adsorption.

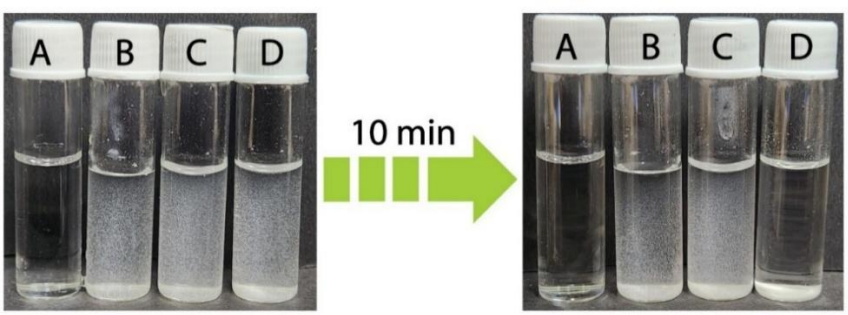

Figure A4.30. Visual observation experiment of different adsorption patterns of arsenate and phosphate. Here, A represents blank Milli-Q water, B is IC-CON treated with phosphate, C is untreated IC-CON, and D is IC-CON treated with arsenate.

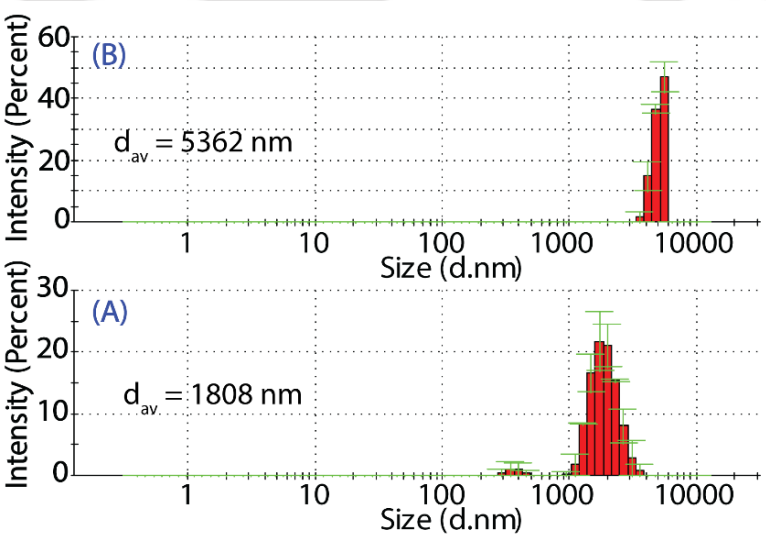

Figure A4.31. DLS measurements of IC-CON polymer after treated with phosphate (A) and arsenate (B).

4.4.4.11. Mechanism for arsenate and phosphate adsorption:

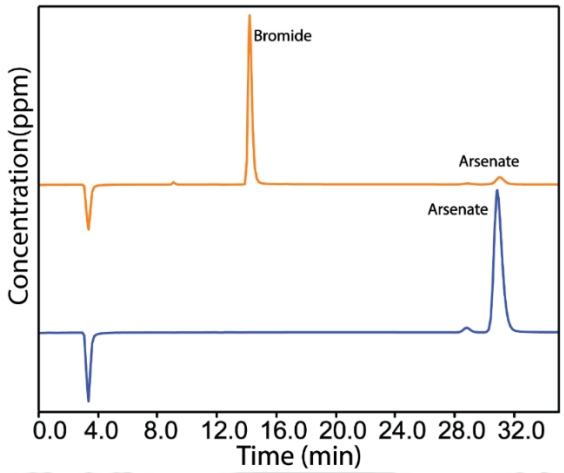

Figure A4.32. IC spectra of arsenate solution before (blue) and after the treatment (orange) of **IC-CON**.

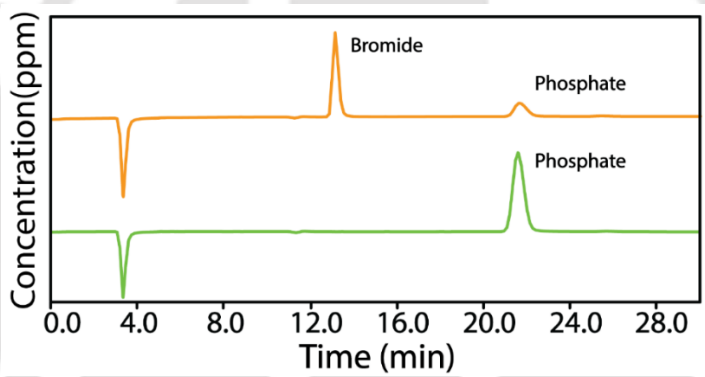

Figure A4.33. IC spectra of phosphate solution before (green) and after the treatment (orange) of **IC-CON**.

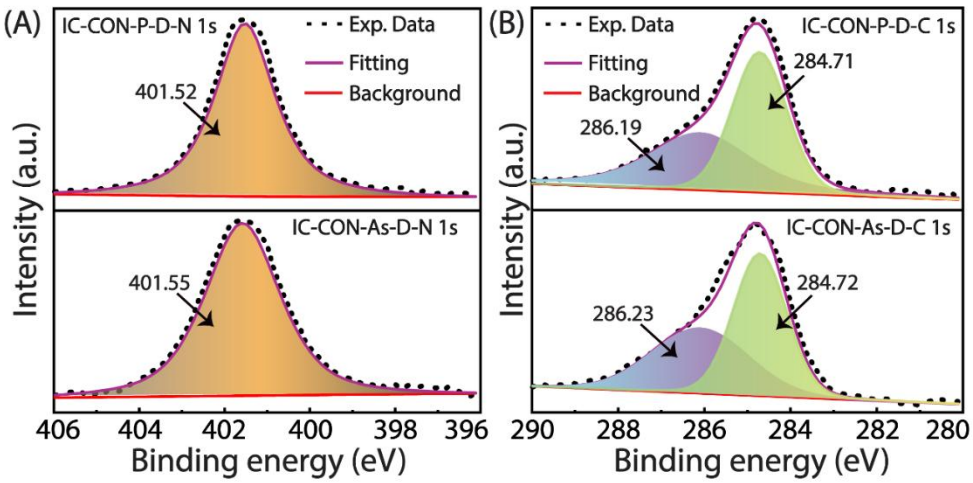

Figure A4.34. Deconvoluted XPS spectra for the N 1s (A) and the C 1s (B) of IC-CON after the desorption of arsenate and phosphate ions.

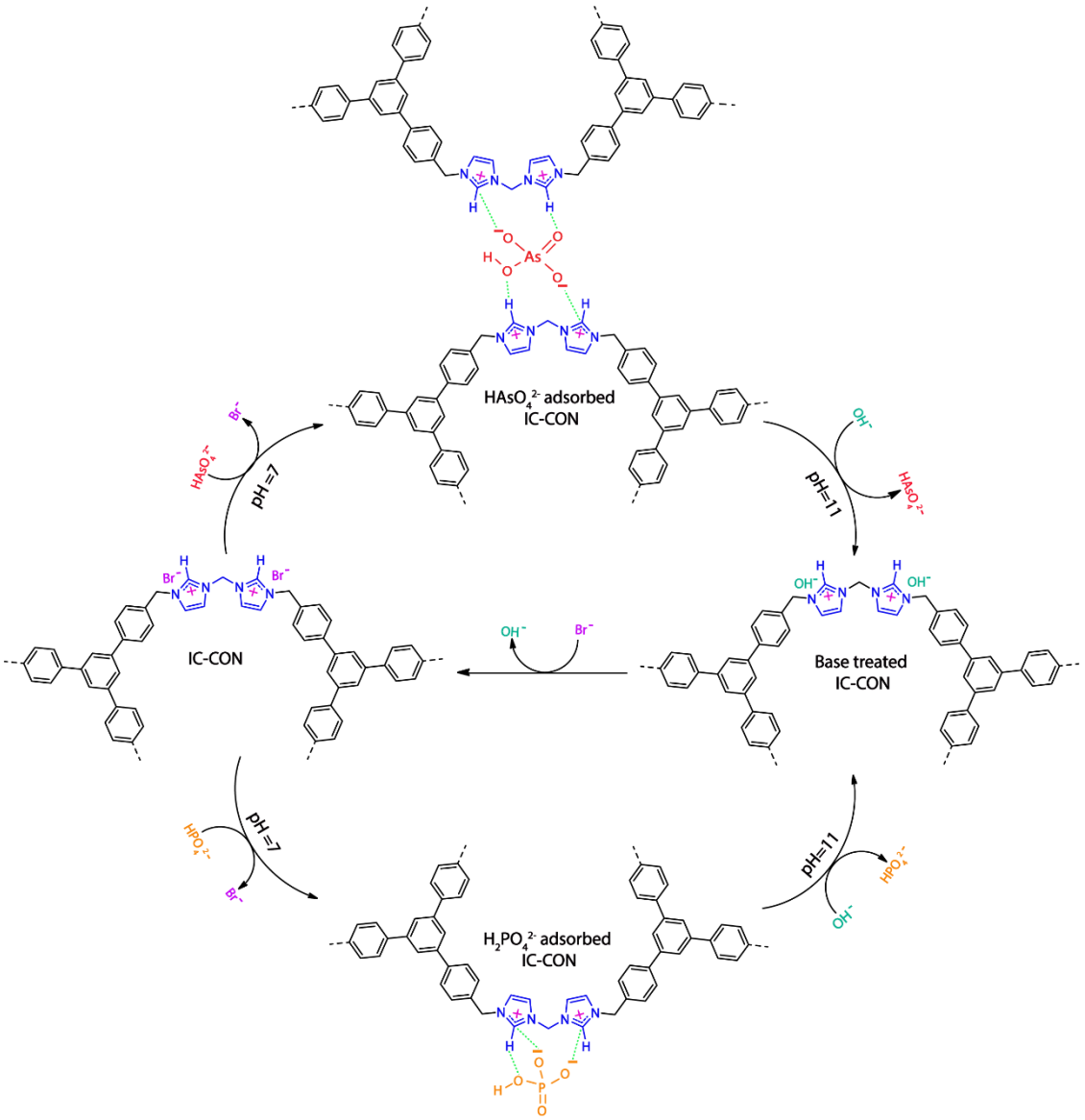

Figure A4.35. Possible mechanistic pathways for adsorption and desorption process of arsenate and phosphate ions by **IC-CON** polymer.

4.4.4.12. Dynamic adsorption column experiment:

A glass column with an internal diameter of approximately 0.5 cm was employed for adsorption studies. The column was packed with 50 mg of IC-CON polymer and 3 g of sand, forming a bed of about 5 cm in length. Prior to conducting adsorption experiments, the column was preconditioned by passing 50 mL of ultrapure Milli-Q water to remove any trapped air.

The initial investigation focused on arsenate removal. A 0.5 ppm arsenate solution (500 mL), containing a ten-fold excess of competing anions (F^-, Cl^-, NO_3^-, CO_3^{2-}, and SO_4^{2-}), was introduced into the column in 10 mL batch at a flow rate of

~0.5 mL/min, with an equilibration time of 30 seconds. The eluates were collected in 10 fractions of 50 mL batch, and arsenate concentrations in each batch were analysed. The results showed that arsenate concentrations in the effluent remained below the World Health Organization (WHO) limit of 10 ppb for up to 350 mL of processed solution in the first cycle. To regenerate the column, 100 mL of 0.5N NaOH solution, followed by 50 mL of a 0.1 N NaBr solution was passed through, achieving over 96% desorption efficiency. The adsorption-desorption cycle was repeated five cycles, consistently yielding effluent arsenate concentrations below the WHO limit within 300 – 350 mL of treated solution in each cycle. The IC-CON polymer exhibited over 90% adsorbed arsenate removal efficiency per cycle, demonstrating its practical applicability.

Encouraged by the arsenate adsorption results, a similar methodology was applied for phosphate adsorption. A 50-ppm phosphate solution (500 mL), containing a ten-fold excess of competing anions (F^-, Cl^-, NO_3^-, CO_3^{2-}, and SO_4^{2-}), was passed through the column in 50 mL batch at a flow rate of ~0.5 mL/min, with an equilibration time of 1 minute. Analysis of the eluates showed that phosphate concentrations remained below the WHO threshold for up to 350 mL of treated solution. The column was then regenerated using 0.5 N NaOH, followed by 0.1 N NaBr as mentioned above, achieving over 94% phosphate desorption efficiency. The experiment was repeated for five cycles, with effluent phosphate concentrations consistently below the WHO limit within 250 – 350 mL of processed solution. The IC-CON polymer demonstrated over 87% phosphate removal efficiency per cycle.

To visually confirm the phosphate adsorption, two conical flasks containing 10 mL of ammonium molybdate tetrahydrate and concentrated nitric acid solution were taken. Two columns were set up: one containing IC-CON polymer and sand, and another with only sand. Equal volumes of a 50-ppm phosphate solution were passed through both columns, each with an equilibration time of 1 min. The effluent from the sand-packed column underwent a noticeable colour change from colourless to yellow, indicating the presence of phosphate ions. In contrast, the effluent from the IC-CON polymer-packed column exhibited no colour change, signifying effective phosphate retention within the column.

The findings indicate that the IC-CON effectively removes arsenate and phosphate from aqueous solutions, even in the presence of competing anions. The

polymer exhibited high adsorption efficiency over multiple cycles, with effective desorption during column regeneration. The visual detection tests further confirmed the adsorption capabilities of the polymer, highlighting its potential for real-world water treatment applications.

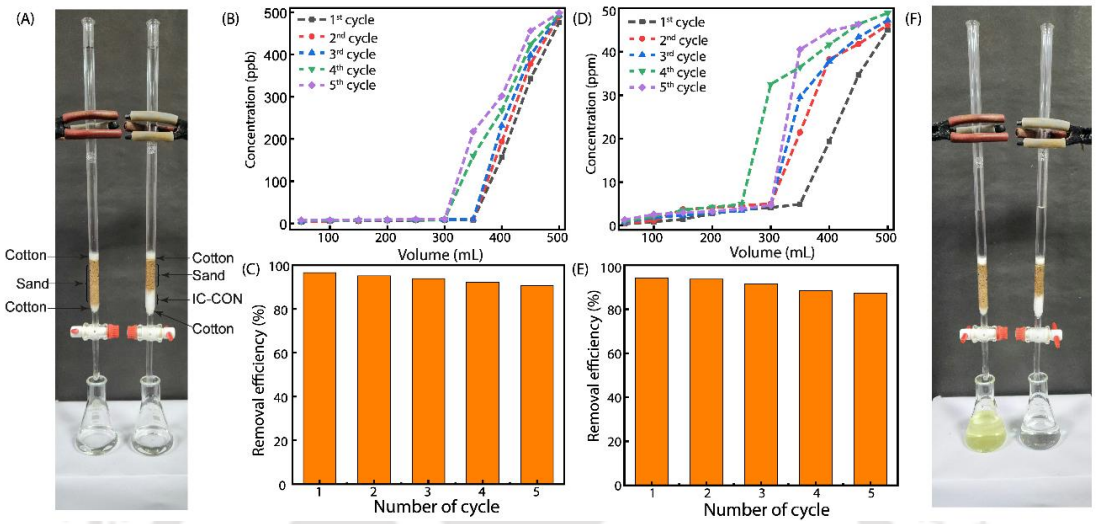

Figure A4.36. Digital image for dynamic adsorption column experiment (A). Arsenate adsorption (B) and desorption (C) efficacy through the dynamic adsorption column experiment. Phosphate adsorption (D) and desorption (E) efficacy through the dynamic adsorption column experiment. Visual observation test for phosphate adsorption through the dynamic adsorption column experiment (F).

4.4.5. ^{1}H and ^{13}C NMR spectra of synthesized compounds:

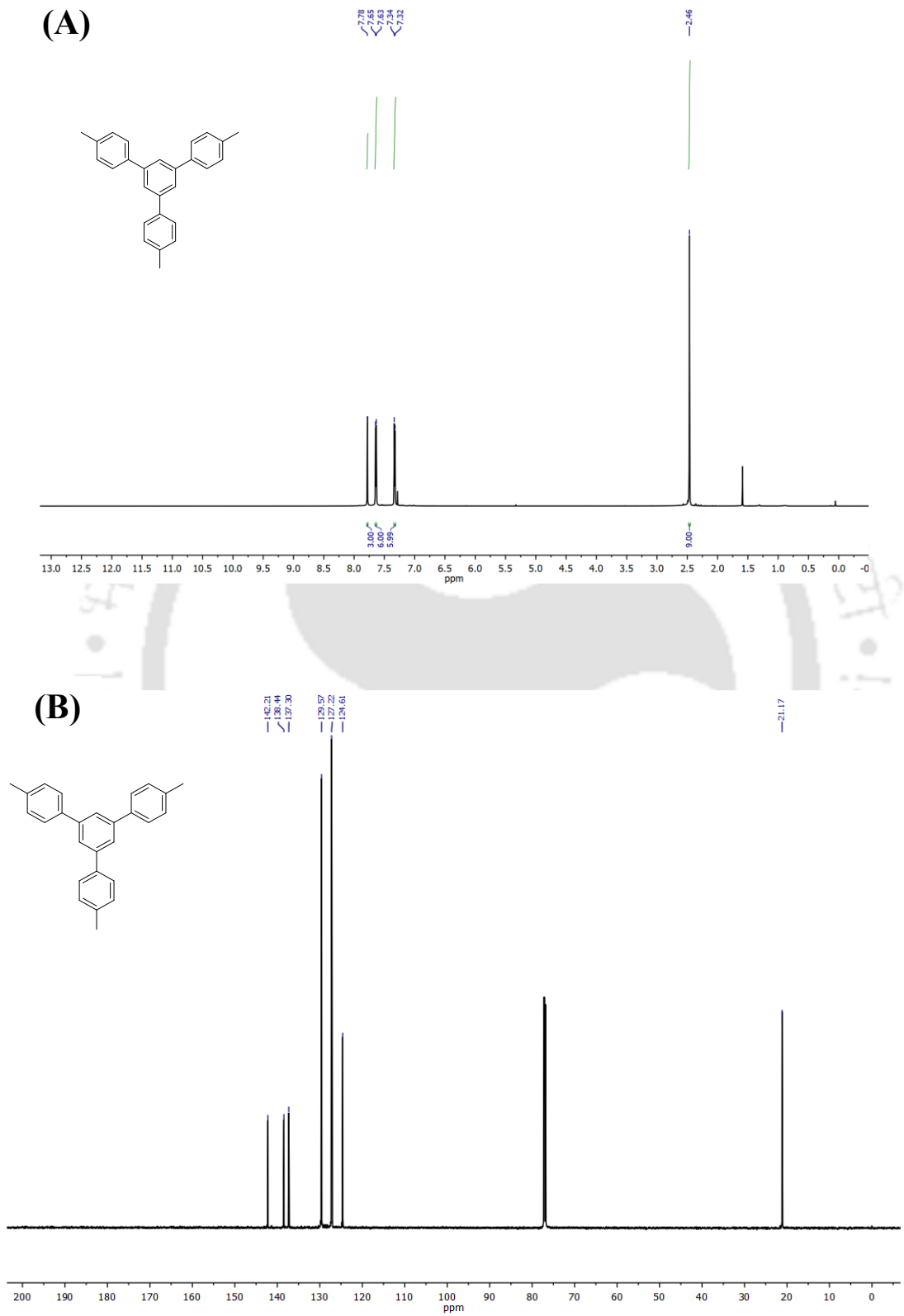

Figure A4.37. ^{1}H (A) and ^{13}C (B) NMR spectra of 4,4′′-dimethyl-5′-(p-tolyl)-1,1′:3′,1′′-terphenyl.

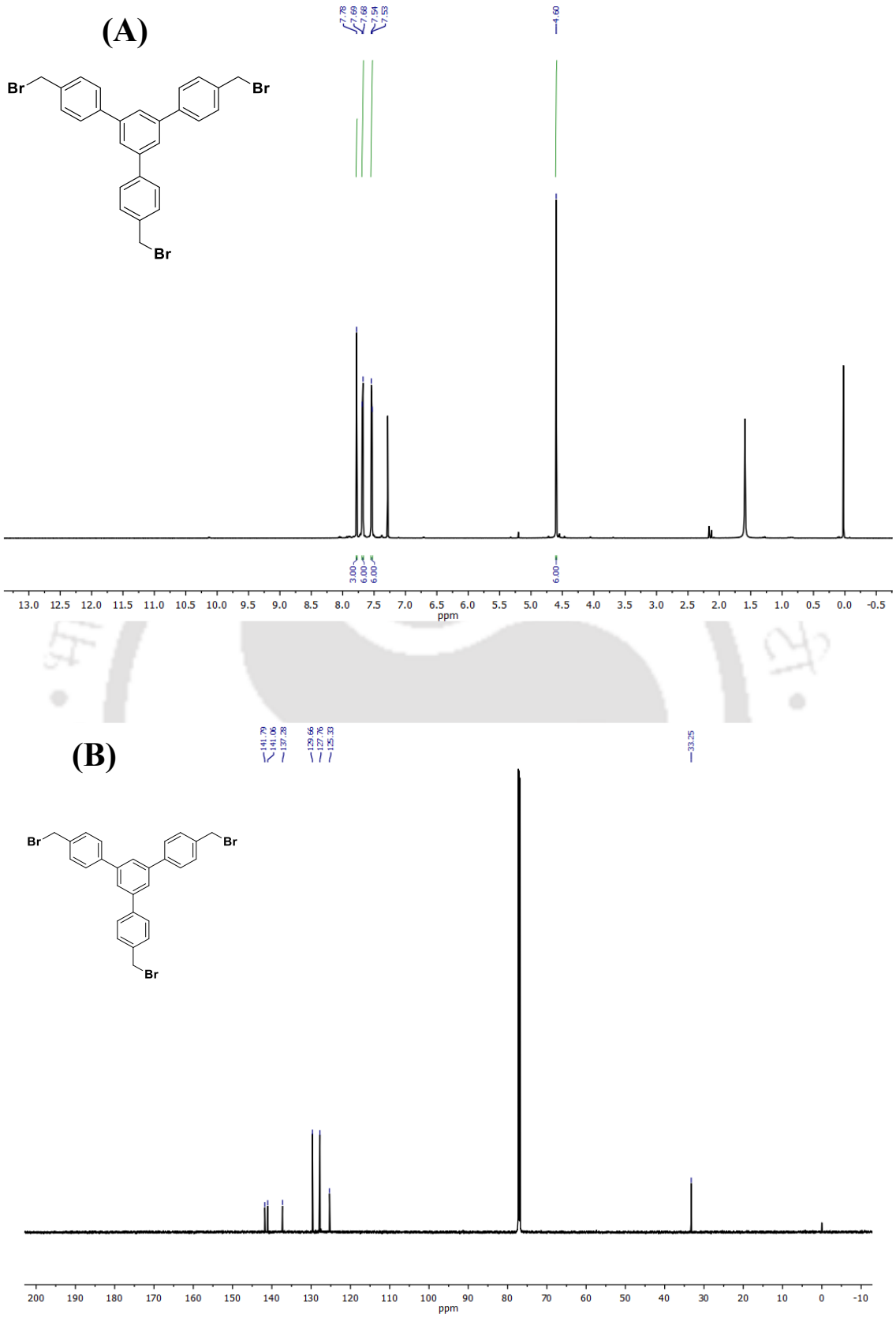

Figure A4.38. ^{1}H (A) and ^{13}C (B) NMR spectra of 4,4′′-bis(bromomethyl)-5′-(4-(bromomethyl) phenyl)-1,1′.

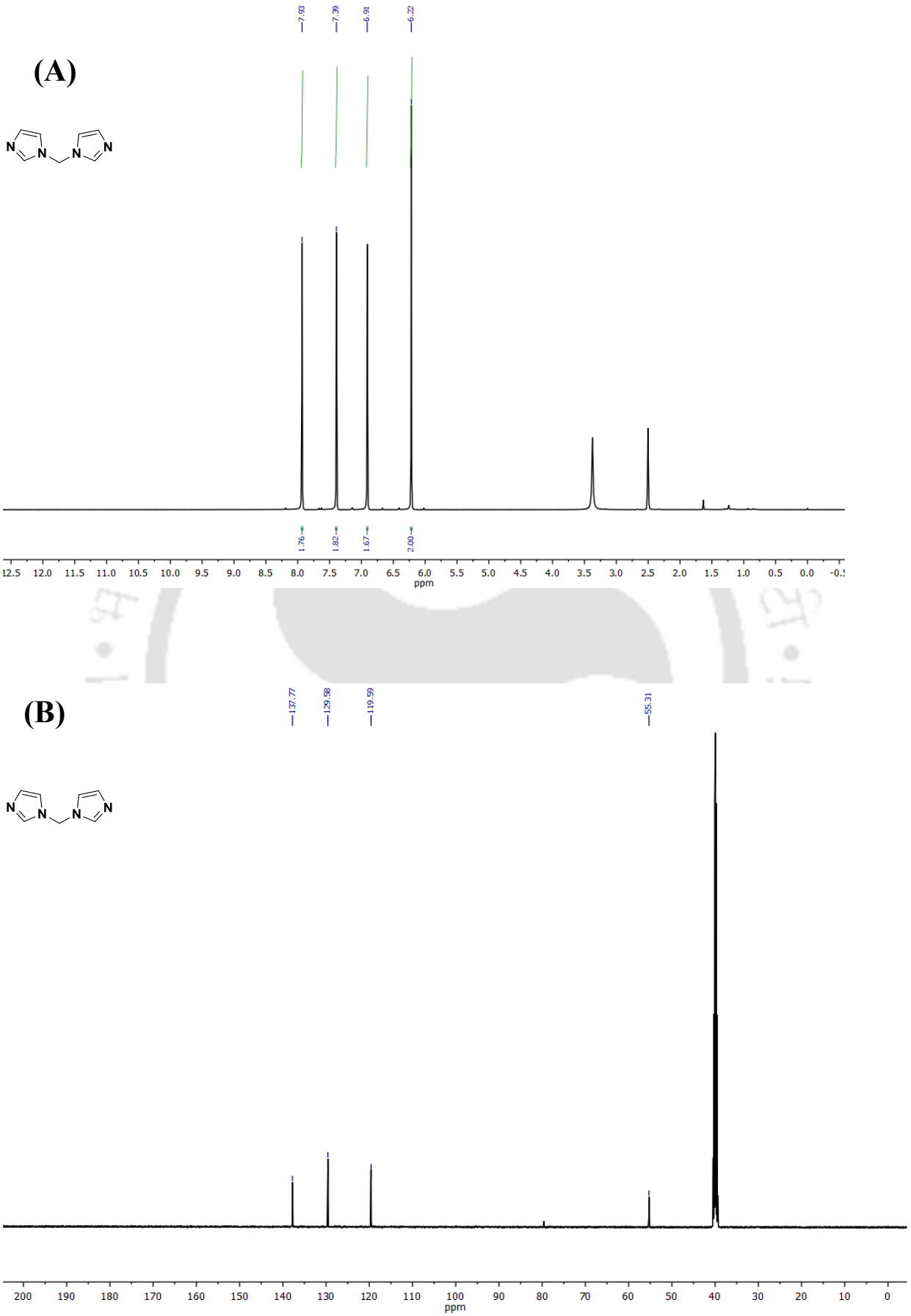

Figure A4.39. ^{1}H (A) and ^{13}C (B) NMR spectra of di(1*H*-imidazol-1-yl) methane.

4.5. References

1. Uliana, A. A.; Pezoulas, E. R.; Zakaria, N. I.; Johnson, A. S.; Smith, A.; Lu, Y.; Shaidu, Y.; Velasquez, E. O.; Jackson, M. N.; Blum, M., Removal of chromium and arsenic from water using polyol-functionalized porous aromatic frameworks. *J. Am. Chem. Soc.* **2024,** *146* (34), 23831-23841.
2. Meharg, A. A.; Hartley-Whitaker, J., Arsenic uptake and metabolism in arsenic resistant and nonresistant plant species. *New Phytol.* **2002,** *154* (1), 29-43.
3. Hasegawa, H.; Sohrin, Y.; Seki, K.; Sato, M.; Norisuye, K.; Naito, K.; Matsui, M., Biosynthesis and release of methylarsenic compounds during the growth of freshwater algae. *Chemosphere* **2001,** *43* (3), 265-272.
4. Guillem-Navajas, A.; Martín-Illán, J. Á.; Salagre, E.; Michel, E. G.; Rodriguez-San-Miguel, D.; Zamora, F.; Interfaces, Iron oxyhydroxide-covalent organic framework nanocomposite for efficient as (III) removal in water. *ACS Appl. Mater. Interfaces,* **2022,** *14* (44), 50163-50170.
5. Ravenscroft, P.; Brammer, H.; Richards, K., *Arsenic pollution: a global synthesis*. John Wiley & Sons: 2011.
6. Huang, Y.; Yang, J.-K.; Keller, A. A., Removal of arsenic and phosphate from aqueous solution by metal (hydr-) oxide coated sand. *ACS Sustain. Chem. Eng.* **2014,** *2* (5), 1128-1138.
7. Smedley, P. L.; Kinniburgh, D. G., A review of the source, behaviour and distribution of arsenic in natural waters. *Appl. Geochem.* **2002,** *17* (5), 517-568.
8. Weerasundara, L.; Ok, Y.-S.; Bundschuh, J., Selective removal of arsenic in water: A critical review. *Environ. Pollut.* **2021,** *268*, 115668.
9. Basu, A.; Saha, D.; Saha, R.; Ghosh, T.; Saha, B., A review on sources, toxicity and remediation technologies for removing arsenic from drinking water. *Res. Chem. Intermed.* **2014,** *40*, 447-485.
10. Kobielska, P. A.; Howarth, A. J.; Farha, O. K.; Nayak, S., Metal–organic frameworks for heavy metal removal from water. *Coord. Chem. Rev.* **2018,** *358*, 92-107.
11. Bolisetty, S.; Peydayesh, M.; Mezzenga, R., Sustainable technologies for water purification from heavy metals: review and analysis. *Chem. Soc. Rev.* **2019,** *48* (2), 463-487.
12. Hestekin, J.; Bachas, L.; Bhattacharyya, D., Poly (amino acid)-functionalized cellulosic membranes: Metal sorption mechanisms and results. *Ind. Eng. Chem. Res.* **2001,** *40* (12), 2668-2678.
13. Werber, J. R.; Osuji, C. O.; Elimelech, M., Materials for next-generation desalination and water purification membranes. *Nat. Rev. Mater.* **2016,** *1* (5), 1-15.
14. Shannon, M. A.; Bohn, P. W.; Elimelech, M.; Georgiadis, J. G.; Mariñas, B. J.; Mayes, A. M., Science and technology for water purification in the coming decades. *Nature* **2008,** *452* (7185), 301-310.
15. Hazarika, G.; Das, S.; Das, N. M.; Manna, D., A pH-responsive covalent organic network: Morphology change leads to capture and removal of phosphate ions from water. *J. Mater. Chem. A* **2024,** *12* (30), 19559-19566.
16. Hazarika, G.; Das, S.; Patel, A.; Manna, D., Guanidine-modified cellulose enhances capturing and recovery of phosphates from wastewater. *Water Res. Technol.* **2025,** 11 (3), 691-701.
17. Huang, W.; Zhu, Y.; Tang, J.; Yu, X.; Wang, X.; Li, D.; Zhang, Y., Lanthanum-doped ordered mesoporous hollow silica spheres as novel adsorbents for efficient phosphate removal. *J. Mater. Chem. A* **2014,** *2* (23), 8839-8848.

18. Hao, L.; Liu, M.; Wang, N.; Li, G., A critical review on arsenic removal from water using iron-based adsorbents. *RSC Adv.* **2018,** *8* (69), 39545-39560.
19. Mohan, D.; Pittman Jr, C. U., Arsenic removal from water/wastewater using adsorbents—a critical review. *J. Hazard. Mater.* **2007,** *142* (1-2), 1-53.
20. Majumder, A.; Ramrakhiani, L.; Mukherjee, D.; Mishra, U.; Halder, A.; Mandal, A. K.; Ghosh, S., Green synthesis of iron oxide nanoparticles for arsenic remediation in water and sludge utilization. *Clean Technol. Environ. Policy* **2019,** *21*, 795-813.
21. Kanel, S. R.; Manning, B.; Charlet, L.; Choi, H., Removal of arsenic (III) from groundwater by nanoscale zero-valent iron. *Environ. Sci. Technol.* **2005,** *39* (5), 1291-1298.
22. Swami, S., Next-Generation Arsenic Sensors: Advances in Zero-Dimensional (0D) Carbon Quantum Dots. *J. Clust. Sci.* **2025,** *36* (2), 53.
23. Nagaraj, K.; Shetty, A. N.; Trivedi, D. R., Colorimetric chemosensors for the selective detection of arsenite over arsenate anions in aqueous medium: Application in environmental water samples and DFT studies. *Anal. Chim. Acta.* **2023,** *1265*, 341355.
24. Galiano, F.; Mancuso, R.; Guazzelli, L.; Pomelli, C. S.; Bundschuh, J.; Rinklebe, J.; Wang, S.-L.; Apollaro, C.; Palumbo, F.; Chiappe, C., Arsenic water decontamination by a bioinspired As-sequestering porous membrane. *Nat. Water* **2024,** *2 (4)*, 350-359.
25. Dakova, I.; Karadjova, I., Ionic Liquid Modified Polymer Gel for Arsenic Speciation. *Molecules* **2024,** *29* (4), 898.
26. Lin, X. H.; Wong, M. J.; Li, S. F. Y., Highly Selective Arsenite Sensor Based on Gold Nanoparticles and Ionic Liquids. *Chemosensors* **2023,** *11* (5), 302.
27. AbhijnaKrishna, R.; Valoor, A.; Velmathi, S., Environmentally Sustainable Detection of Arsenic using Convolutional Neural Networks and Imidazole-Based Organic Probes: Application in Food Samples and Arsenic Album. *Chem. Res. Toxicol.* **2024,** *37* (12), 1934-1943.
28. Ahmed, N.; Shirinfar, B.; Geronimo, I.; Kim, K. S., Fluorescent imidazolium-based cyclophane for detection of guanosine-5′-triphosphate and I–in aqueous solution of physiological pH. *Org. Lett.* **2011,** *13* (20), 5476-5479.
29. Sen, A.; Dutta, S.; Dam, G. K.; Samanta, P.; Let, S.; Sharma, S.; Shirolkar, M. M.; Ghosh, S. K., Imidazolium-functionalized chemically robust ionic porous organic polymers (iPOPs) toward toxic oxo-pollutants capture from water. *Chem. Eur. J.* **2021,** *27* (53), 13442-13449.
30. Mondal, B.; Bishal Kashyap, A.; Das, G., Unveiling the Potential of Thiophene-Functionalized Porous Organic Polymers for Bromine Adsorption and Selective Separation from Iodine. *Chem. Eur. J.* **2025**, *31*, e202404177.
31. Bozorgi, M.; Mahinroosta, M.; Allahverdi, A., Purification of arsenic-contaminated drinking water by Fe-Al-CO3 layered double hydroxide derived from secondary aluminum dross: adsorption and stabilization studies. *Sci. Rep.* **2025,** *15* (1), 1856.
32. Dey, S.; Das, S.; Patel, A.; Raj, K. V.; Vanka, K.; Manna, D., Antimicrobial two-dimensional covalent organic nanosheets (2D-CONs) for the fast and highly efficient capture and recovery of phosphate ions from water. *J. Mater. Chem. A* **2022,** *10* (9), 4585-4593.
33. Razavi, S. A. A.; Habibzadeh, E.; Morsali, A., High Capacity Arsenate Removal from Real Samples Using Dihydrotetrazine Decorated Zirconium-Based Metal–Organic Frameworks. *ACS Appl. Mater. Interfaces* **2024,** *16* (10), 12573-12585.

Chapter 5

Thesis Conclusion and Future Prospects

5.1. Conclusion

This thesis presents the design, synthesis, and application of three distinct polymeric adsorbents to remove and recover phosphate and arsenate ions from water selectively. These materials also demonstrate superior adsorption capacities and selectivity, but exceptional thermal and chemical stability under harsh conditions and during real wastewater treatment applications.

A comprehensive overview of current literature, highlighting the limitations of existing adsorbents in selectivity, stability, and regeneration, was provided in Chapter 1. This chapter also highlighted the need to develop advanced materials to remove and recover phosphate and arsenate ions from wastewater.

Chapter 2 presents the design and synthesis of a zinc-coordinated 1-aminoguanidine functionalized cellulose-based biopolymer (Zn-gCP). This material showed a high binding affinity for phosphate ions, due to the synergistic interactions between the Zn(II) ion and the guanidine moieties. The Zn-gCP exhibited a maximum adsorption capacity of 310 $mg \cdot g^{-1}$ at neutral pH and maintained stable performance over multiple adsorption–desorption cycles, enabled by simple pH adjustment for regeneration. The material outperformed previously published biopolymeric systems in terms of adsorption capacity, reusability, and additional antimicrobial functionality, despite exhibiting comparatively slower adsorption kinetics (Table 5.1). These combined characteristics highlight its possibilities as a multifunctional sorbent for effective and environmentally friendly wastewater treatment uses.

To overcome the relatively slow adsorption kinetics of Zn-gCP, Chapter 3 focused on the development of a tris-aminoguanidine-functionalized 2D covalent organic framework (ag-CON). This advanced polymer exhibited significantly enhanced adsorption kinetics and a superior phosphate uptake capacity of 719 $mg \cdot g^{-1}$ at pH 6, outperforming Zn-gCP in both rate and efficiency. The improved performance of Zn-gCP could be due to the presence of multiple hydrogen bonding and salt-bridge-forming sites provided by the tris-aminoguanidine moieties, which facilitated strong and selective interactions with phosphate ions. Additionally, ag-CON demonstrated excellent chemical stability across a wide pH range and could be readily regenerated through simple pH adjustments, retaining its performance over multiple adsorption-desorption cycles. Notably, ag-CON exhibited dynamic morphological transitions–shifting between spherical and sheet-like configurations

in response to phosphate binding and release, which adds a unique and functional characteristic to the material. These features highlight ag-CON as a promising, high-performance, and reusable sorbent for phosphate remediation and recovery, particularly under harsh environmental conditions.

To extend the scope of remediation to arsenate alongside phosphate, Chapter 4 presented the synthesis of a bis-imidazolium-based cationic covalent organic framework (IC-CON). This polymer demonstrated high adsorption capacity, rapid kinetics, and strong selectivity for both arsenate and phosphate, with a marked preference for arsenate in equimolar systems. Mechanistic investigations revealed that electrostatic interactions, hydrogen bonding, and anion exchange were the primary forces driving adsorption. IC-CON exhibited excellent recyclability, maintaining its performance over 15 adsorption–desorption cycles**,** and could be efficiently regenerated using a mild alkaline salt treatment (0.5 N NaOH followed by 0.1 N NaBr). Furthermore, the polymer showed strong potential for continuous flow applications via column chromatography, making it suitable for scalable water treatment processes. A distinctive feature of IC-CON is its ion-responsive morphological reversibility**,** particularly during arsenate adsorption, transitioning between spherical and sheet-like structures – a property not observed during phosphate binding. These characteristics position IC-CON as a versatile and robust adsorbent for the selective removal and recovery of hazardous oxoanions from contaminated water sources.

Overall, by offering insightful analysis of the logical design of multifunctional, robust, and regenerable polymeric adsorbents for environmental remediation, the findings of this thesis contribute significantly to the field of water purification. The synthesized materials demonstrated outstanding adsorption performance, high selectivity, excellent reusability, and structural stability under harsh conditions, effectively targeting hazardous and valuable oxoanions such as phosphate and arsenate, outperforming most previously reported adsorbent materials (Table 5.2 and 5.3). The research results highlight the practical applications of these polymeric frameworks while establishing a solid basis for advancing next-generation sorbents that feature adjustable structures and improved functionalities. Collectively, this work offers a promising direction toward sustainable remediation technologies and resource recovery strategies for addressing water contamination challenges.

Table 5.1. Comparison of phosphate adsorption capacity by recently reported biomaterial-based adsorbents.

Sl No.	Compound	Adsorption capacity (mg/g)	Equilibrium time	Recycling conditions	Ref.
1	Zn-gCP	310	20 min	0.5 N NaOH	Chapter 1
2	PAN$_A$F–Cl	15.49	5 min	0.3 mol L^{-1} HCl	[1]
3	CMKGM-La microspheres	16.06	10 h	0.001 M NaOH	[2]
4	PAN-NH_2-Ce	17 mmol/g	24 h	0.1 M KNO_3, 0.1 M KOH	[3]
5	MALZ	80.8	180 min	0.5 M NaOH	[4]
6	La/GTB	109 ± 4	30 min	0.1 NaOH	[5]
7	MB	14.33 mg/m^2	120 min	NA	[6]
8	CTS-Fe	15.7	48 h	0.5 M NaOH	[7]
9	Zirconium-modified zeolite	10.2	24 h	NA	[8]
10	PMSB800	25.19	24 h	NA	[9]
11	Zr/Al-pillared montmorillonite	17.2	6 h	NA	[10]
12	Zr-loaded orange waste gel	57	15 h	95 % (0.2 M NaOH)	[11]
13	Zr-loaded wheat straw	31.9	10 h	98.2 % (5 wt % NaOH + 5 wt % NaCl)	[12]

14	ZrO_2-loaded amine crosslinked shaddock Peel	59.89	4 h	NA	[13]
15	Zr-modified activated sludge	27.55	270 min	0.1 mol L^{-1} NaOH	[14]
16	ZrO_2-loaded lignocellulose butanol residue	8.75	712 min	NA	[15]
17	La/C	48.8	NA	1 M NaOH	[16]

NA = Not Available.

Table 5.2. Comparison of phosphate adsorption capacity by recently reported advanced adsorbent materials.

Sl No.	**Compound**	**Adsorption capacity (mg/g)**	**pH**	**Equilibrium time**	**Recycling conditions**	**Ref.**
1	**ag-CON**	719	6.0	<1 min	1 N NaOH	Chapter 3
2	**IC-CON**					Chapter 4
3	gCON	398	7.0	20 min	0.5 M NaOH	[17]
4	UiO-66	85	NA	2 h	0.01 M NaOH	[18]
5	UiO-66-NH_2	92	NA	2 h	0.01 M NaOH	[18]
6	UiO-66	415	7.0	5 min	Dilute HNO3	[19]
7	Zr-loaded MIL-101	20.83	6.5	6 h	0.003 M NaOH	[20]

8	Fe3O4@ZrO2	69.44	5.0	16 h	1 M NaOH	[21]
9	Zr-loaded collagen fiber	33.8	6.0	3 h	NA	
10	Zirconium sulfateloaded polymer	110	7.0	2 h	NA	[22]
11	ZrO2-loaded D-201	47.9	6.5	6 h	5 % NaOH + 5 % NaCl	[23]
12	ZrO2-loaded IRA-400	91.74	NA	NA	NA	[24]

NA = Not Available.

Table 5.3. Comparison of arsenate adsorption capacity by recently reported advanced adsorbent materials.

Sl No.	**Compound**	**Adsorption capacity (mg/g)**	**pH**	**Equilibrium time**	**Recycling conditions**	**Ref.**
1	**IC-CON**	698	7.0	1 min	0.5 N NaOH/NaBr	Chapter 4
2	PAF-1-NMDG	94.2	4.0	NA	1 M HCl and 1M NaOH	[25]
3	PAF-1-NMDG	85.5	7.0	<10 s	1 M HCl and 1M NaOH	[25]
4	IRA743 Resin	46.7	7.0	4 h	1 M HCl and 1M NaOH	[25]

5	Fe_2O_3 and MnO on Honeycomb Briquette Cinders	1.5	7.0	12 h	NA	[26]
6	MOF-808	24.8	4.0	50 min	0.5 M Na_2SO_4	[27]
7	UiO-66	147.7	7.0	48 h	NA	[28]
8	Fe-BTC	12.3	4.0	10 min	NA	[29]
9	MIL-53 (Al)	106.5	8.0	50 h	NA	[30]
10	Crosslinked NMDG and Poly (vinylbenzene chloride)	16.4	6.0	10 h	NA	[31]
11	Fe-treated Cellulose	33.2	7.0	10 h	8% alkaline solution	[32]
12	Fe-modified Activated Charcoal	51.3	6.0	24 h	NA	[33]
13	Fe (0) Nanoparticles on Chitosan	119	7.0	3 h	0.1 M NaOH	[34]
14	Molybdate Chitosan Derivatives	230	2.0 - 3.0	24 h	Sodium phosphate	[35]
15	H-MFI-90 Synthetic Zeolite	34.8	6.5	100 min	HCl (0.1 N) and NaOH (0.1 N)	[36]
16	H-MFI-24 Synthetic Zeolite	35.8	6.5	100 min	HCl (0.1 N) and NaOH (0.1 N)	[36]
17	Ultrafine Fe_2O_3 Nanoparticles	47	7.0	2 h	NA	[37]

18	Poly (glycidyl methacrylate-*N*-methyl-D-glucamine)	45.9	3.0	NA	NA	[38]

NA = Not Available.

5.2. Future prospects

COFs are emerging as one of the most promising classes of porous materials for advanced water purification due to their highly ordered crystalline structures, tunable pore sizes, exceptional thermal and chemical stability, and the ability to introduce specific functional groups into their framework. Significant progress is anticipated in several key directions to expand the practical applicability of COFs in removing a broad spectrum of water pollutants. One of the foremost areas of interest lies in the rational design and post-synthetic functionalization of COFs with task-specific moieties – such as guanidinium, quaternary ammonium, sulfonic acid, or redox-active groups – to enhance their selectivity and affinity toward oxoanions (e.g., phosphate, arsenate, and chromate), heavy metal ions (e.g., Pb^{2+}, Cd^{2+}, and Hg^{2+}), and organic micropollutants (e.g., pharmaceuticals, dyes, and endocrine-disrupting compounds). Furthermore, the integration of COFs with photocatalytic or electroactive materials is expected to facilitate the development of multifunctional hybrid systems. This integration offers a more effective approach to addressing persistent and non-biodegradable contaminants by promoting the adsorption and in-situ degradation or transformation of pollutants when subjected to light or electrical stimuli.

Overcoming the constraints of batch adsorption systems, the fabrication of COF–based membranes that may operate under continuous flow conditions presents an exciting path for practical application. Because of their inherent porosity and chemical tunability, COFs provide high water permeability and selective pollution retention on these membranes. Innovations such as mixed – matrix membranes (MMMs), layer–by–layer assemblies, and in situ COF growth on polymeric or ceramic substrates will be pivotal in scaling their application. Moreover, it will be crucial for ensuring sustained operational stability and antifouling effectiveness of COF in real – world water matrices. Strategies such as surface grafting with hydrophilic or antimicrobial polymers, incorporating metal nanoparticles, or photoactive sites to

enable self–cleaning under visible light are expected to improve membrane longevity and reusability.

The economic and ecological sustainability of COF-based technologies depends on the development of scalable and ecologically friendly synthesis techniques in addition to improvements in materials. This includes low-temperature crystallization methods, microwave-assisted polymerization, and aqueous or solvent-free synthetic approaches. These methods work well to reduce the amount of energy used and the amount of harmful byproducts produced. Also, it is expected that the use of computational methods, such as molecular simulations and machine learning algorithms, will be very important in the predictive design of COFs. This approach will enable the quick identification of the most effective building blocks, topologies, and functional groups designed for the selective capture of pollutants. To sum up, even though covalent organic frameworks (COFs) have proven to be very effective in highly controlled laboratory conditions, thorough pilot-scale tests in real-world environments are necessary before they can be used in real-world applications. Durability, regeneration efficiency, cost per treatment volume, and environmental safety are some of the important factors that should be taken into account in this evaluation. To establish covalent organic frameworks (COFs) as a next-generation material platform in environmental remediation and water purification, interdisciplinary challenges must be addressed.

5.3. References

1. Zheng, W.; Wu, Q.; Xu, W.; Xiong, Q.; Kalkhajeh, Y. K.; Zhang, C.; Xu, G.; Zhang, W.; Ye, X.; Gao, H., Efficient capture of phosphate from wastewater by a recyclable ionic liquid functionalized polyacrylonitrile fiber: a typical “release and catch” mechanism. *Environ. Sci. Water Res. Technol.* **2022,** *8* (3), 607-618.

2. Zhang, X.; Lin, X.; He, Y.; Chen, Y.; Zhou, J.; Luo, X., Adsorption of phosphorus from slaughterhouse wastewater by carboxymethyl konjac glucomannan loaded with lanthanum. *Int. J. Biol. Macromol.* **2018,** *119*, 105-115.

3. Ko, Y. G.; Do, T.; Chun, Y.; Kim, C. H.; Choi, U. S.; Kim, J.-Y., CeO2-covered nanofiber for highly efficient removal of phosphorus from aqueous solution. *J. Hazard. Mater. Adv.* **2016,** *307*, 91-98.

4. Shi, W.; Fu, Y.; Jiang, W.; Ye, Y.; Kang, J.; Liu, D.; Ren, Y.; Li, D.; Luo, C.; Xu, Z., Enhanced phosphate removal by zeolite loaded with Mg–Al–La ternary (hydr) oxides from aqueous solutions: performance and mechanism. *Chem. Eng. J.* **2019,** *357*, 33-44.

5. Huang, Y.; Lee, X.; Grattieri, M.; Yuan, M.; Cai, R.; Macazo, F. C.; Minteer, S. D., Modified biochar for phosphate adsorption in environmentally relevant conditions. *Chem. Eng. J.* **2020,** *380*, 122375.

6. El Bouraie, M.; Masoud, A. A., Adsorption of phosphate ions from aqueous solution by modified bentonite with magnesium hydroxide Mg (OH) 2. *Appl. Clay Sci.* **2017,** *140*, 157-164.

7. Zhang, B.; Chen, N.; Feng, C.; Zhang, Z., Adsorption for phosphate by crosslinked/non-crosslinked-chitosan-Fe (III) complex sorbents: Characteristic and mechanism. *Chem. Eng. J.* **2018,** *353*, 361-372.

8. Yang, M.; Lin, J.; Zhan, Y.; Zhu, Z.; Zhang, H., Immobilization of phosphorus from water and sediment using zirconium-modified zeolites. *Environ. Sci. Pollut. Res.* **2015,** *22*, 3606-3619.

9. Zhang, M.; Lin, K.; Li, X.; Wu, L.; Yu, J.; Cao, S.; Zhang, D.; Xu, L.; Parikh, S. J.; Ok, Y. S., Removal of phosphate from water by paper mill sludge biochar. *Environ. Pollut.* **2022,** *293*, 118521.

10. Chen, J.; Yan, L.-g.; Yu, H.-q.; Li, S.; Qin, L.-l.; Liu, G.-q.; Li, Y.-f.; Du, B., Efficient removal of phosphate by facile prepared magnetic diatomite and illite clay from aqueous solution. *Appl. Clay. Sci.* **2016,** *287*, 162-172.

11. Biswas, B. K.; Inoue, K.; Ghimire, K. N.; Harada, H.; Ohto, K.; Kawakita, H., Removal and recovery of phosphorus from water by means of adsorption onto orange waste gel loaded with zirconium. *Bioresource Technol.* **2008,** *99* (18), 8685-8690.

12. Qiu, H.; Liang, C.; Yu, J.; Zhang, Q.; Song, M.; Chen, F., Preferable phosphate sequestration by nano-La (III)(hydr) oxides modified wheat straw with excellent properties in regeneration. *Chem. Eng. J.* **2017,** *315*, 345-354.

13. Duan, P.; Xu, X.; Shang, Y.; Gao, B.; Li, F., Amine-crosslinked Shaddock Peel embedded with hydrous zirconium oxide nano-particles for selective phosphate removal in competitive condition. *Taiwan Inst. Chem. E* **2017,** *80*, 650-662.

14. Wang, J.; Tong, X.; Wang, S., Zirconium-modified activated sludge as a low-cost adsorbent for phosphate removal in aqueous solution. *Water Air Soil Pollut.* **2018,** *229*, 1-10.

15. Zong, E.; Liu, X.; Jiang, J.; Fu, S.; Chu, F., Preparation and characterization of zirconia-loaded lignocellulosic butanol residue as a biosorbent for phosphate removal from aqueous solution. *Appl. Surf. Sci.* **2016,** *387*, 419-430.

16. Xia, W.-J.; Guo, L.-X.; Yu, L.-Q.; Zhang, Q.; Xiong, J.-R.; Zhu, X.-Y.; Wang, X.-C.; Huang, B.-C.; Jin, R.-C., Phosphorus removal from diluted wastewaters using a La/C nanocomposite-doped membrane with adsorption-filtration dual functions. *Chem. Eng. J.* **2021,** *405*, 126924.

17. Dey, S.; Das, S.; Patel, A.; Raj, K. V.; Vanka, K.; Manna, D., Antimicrobial two-dimensional covalent organic nanosheets (2D-CONs) for the fast and highly efficient capture and recovery of phosphate ions from water. *J. Mater. Chem. A* **2022,** *10* (9), 4585-4593.

18. Lin, K.-Y. A.; Chen, S.-Y.; Jochems, A. P., Zirconium-based metal organic frameworks: Highly selective adsorbents for removal of phosphate from water and urine. *Mater. Chem. Phys.* **2015,** *160*, 168-176.

19. Gu, Y.; Xie, D.; Ma, Y.; Qin, W.; Zhang, H.; Wang, G.; Zhang, Y.; Zhao, H., Size modulation of zirconium-based metal organic frameworks for highly efficient phosphate remediation. *ACS Appl. Mater. Interfaces* **2017,** *9* (37), 32151-32160.

20. Liu, T.; Feng, J.; Wan, Y.; Zheng, S.; Yang, L., ZrO2 nanoparticles confined in metal organic frameworks for highly effective adsorption of phosphate. *Chemosphere* **2018,** *210*, 907-916.

21. Wang, Z.; Xing, M.; Fang, W.; Wu, D., One-step synthesis of magnetite core/zirconia shell nanocomposite for high efficiency removal of phosphate from water. *Appl. Surf. Sci.* **2016,** *366*, 67-77.

22. Pitakteeratham, N.; Hafuka, A.; Satoh, H.; Watanabe, Y., High efficiency removal of phosphate from water by zirconium sulfate-surfactant micelle mesostructure immobilized on polymer matrix. *Water Res.* **2013,** *47* (11), 3583-3590.

23. Chen, L.; Zhao, X.; Pan, B.; Zhang, W.; Hua, M.; Lv, L.; Zhang, W., Preferable removal of phosphate from water using hydrous zirconium oxide-based nanocomposite of high stability. *J. Hazard. Mater.* **2015,** *284*, 35-42.

24. Acelas, N. Y.; Martin, B. D.; López, D.; Jefferson, B., Selective removal of phosphate from wastewater using hydrated metal oxides dispersed within anionic exchange media. *Chemosphere* **2015,** *119*, 1353-1360.

25. Uliana, A. A.; Pezoulas, E. R.; Zakaria, N. I.; Johnson, A. S.; Smith, A.; Lu, Y.; Shaidu, Y.; Velasquez, E. O.; Jackson, M. N.; Blum, M., Removal of chromium and arsenic from water using polyol-functionalized porous aromatic frameworks. *J. Am. Chem. Soc.* **2024,** *146* (34), 23831-23841.

26. Zhu, J.; Baig, S. A.; Sheng, T.; Lou, Z.; Wang, Z.; Xu, X., Fe3O4 and MnO2 assembled on honeycomb briquette cinders (HBC) for arsenic removal from aqueous solutions. *J. Hazard. Mater.* **2015,** *286*, 220-228.

27. Li, Z.-Q.; Yang, J.-C.; Sui, K.-W.; Yin, N., Facile synthesis of metal-organic framework MOF-808 for arsenic removal. *Mater. Lett.* **2015,** *160*, 412-414.

28. Wang, C.; Liu, X.; Chen, J. P.; Li, K., Superior removal of arsenic from water with zirconium metal-organic framework UiO-66. *Sci. Rep.* **2015,** *5* (1), 16613.

29. Zhu, B.-J.; Yu, X.-Y.; Jia, Y.; Peng, F.-M.; Sun, B.; Zhang, M.-Y.; Luo, T.; Liu, J.-H.; Huang, X.-J., Iron and 1, 3, 5-benzenetricarboxylic metal–organic coordination polymers prepared by solvothermal method and their application in efficient As (V) removal from aqueous solutions. *J. Phys. Chem.* **2012,** *116* (15), 8601-8607.

30. Li, J.; Wu, Y.-n.; Li, Z.; Zhu, M.; Li, F., Characteristics of arsenate removal from water by metal-organic frameworks (MOFs). *Water Sci. Technol* **2014,** *70* (8), 1391-1397.

31. Dambies, L.; Salinaro, R.; Alexandratos, S. D., Immobilized N-methyl-D-glucamine as an arsenate-selective resin. *Environ. Sci. Technol.* **2004,** *38* (22), 6139-6146.

32. Guo, X.; Chen, F., Removal of arsenic by bead cellulose loaded with iron oxyhydroxide from groundwater. *Environ. Sci. Technol.* **2005,** *39* (17), 6808-6818.

33. Chen, W.; Parette, R.; Zou, J.; Cannon, F. S.; Dempsey, B. A., Arsenic removal by iron-modified activated carbon. *Water Res.* **2007,** *41* (9), 1851-1858.

34. Gupta, A.; Yunus, M.; Sankararamakrishnan, N., Zerovalent iron encapsulated chitosan nanospheres–A novel adsorbent for the removal of total inorganic Arsenic from aqueous systems. *Chemosphere* **2012,** *86* (2), 150-155.

35. Dambies, L.; Vincent, T.; Guibal, E., Treatment of arsenic-containing solutions using chitosan derivatives: uptake mechanism and sorption performances. *Water Res.* **2002,** *36* (15), 3699-3710.

36. Chutia, P.; Kato, S.; Kojima, T.; Satokawa, S., Arsenic adsorption from aqueous solution on synthetic zeolites. *J. Hazard. Mater.* **2009,** *162* (1), 440-447.

37. Tang, W.; Li, Q.; Gao, S.; Shang, J. K., Arsenic (III, V) removal from aqueous solution by ultrafine α-Fe2O3 nanoparticles synthesized from solvent thermal method. *J. Hazard. Mater.* **2011,** *192* (1), 131-138.

38. Toledo, L.; Rivas, B. L.; Urbano, B. F.; Sánchez, J., Novel N-methyl-D-glucamine-based water-soluble polymer and its potential application in the removal of arsenic. *Sep. Purif. Technol.* **2013,** *103*, 1-7.

CCC Marketplace

Order Date	11-Aug-2025	Type of Use	Republish in a thesis/dissertation
Order License ID	1639647-1	Publisher	R S C Publications
ISSN	2053-1419	Portion	Chapter/article

LICENSED CONTENT

Publication Title	Environmental Science : Water Research & Technology	Publication Type	e-Journal
Article Title	Guanidine-modified cellulose enhances capturing and recovery of phosphates from wastewater †	Start Page	691
		End Page	701
		Issue	3
Author / Editor	Royal Society of Chemistry (Great Britain),	Volume	11
Date	01/01/2015	URL	http://pubs.rsc.org/en/journals/journaliss...
Language	English		
Country	United Kingdom of Great Britain and Northern Ireland		
Rightsholder	Royal Society of Chemistry		

REQUEST DETAILS

Portion Type	Chapter/article	Rights Requested	Main product
Page Range(s)	691-701	Distribution	Worldwide
Total Number of Pages	11	Translation	Original language of publication
Format (select all that apply)	Print, Electronic	Copies for the Disabled?	No
Who Will Republish the Content?	Author of requested content	Minor Editing Privileges?	Yes
Duration of Use	Life of current edition	Incidental Promotional Use?	No
Lifetime Unit Quantity	Up to 499	Currency	USD

NEW WORK DETAILS

Title	Design and Development of Advanced Porous Organic Polymeric Adsorbents for the Efficient and Selective Removal and Recovery of Phosphate and Arsenate from Water	Institution Name	Indian Institute of Technology Guwahati
		Expected Presentation Date	2025-10-01
Instructor Name	Prof. Debasis Manna		

ADDITIONAL DETAILS

Order Reference Number	N/A	The Requesting Person / Organization to Appear on the License	Mr. Gunanka Hazarika

REQUESTED CONTENT DETAILS

Title, Description or Numeric Reference of the Portion(s)	Design and Development of Advanced Porous Organic Polymeric Adsorbents for the Efficient and Selective Removal and Recovery of Phosphate and Arsenate from Water	Title of the Article / Chapter the Portion Is From	Guanidine-modified cellulose enhances capturing and recovery of phosphates from wastewater †
		Author of Portion(s)	Hazarika, Gunanka; Das, Sribash; Patel, Anjali; Manna, Debasis
Editor of Portion(s)	Hazarika, Gunanka; Das, Sribash; Patel, Anjali; Manna, Debasis	Issue, if Republishing an Article From a Serial	3
Volume / Edition	11	Publication Date of Portion	2025-02-27
Page or Page Range of Portion	691-701		

भारतीय प्रौद्योगिकी संस्थान गुवाहाटी
Indian Institute of Technology Guwahati

CCC Marketplace

This is a License Agreement between Mr. Gunanka Hazarika ("User") and Copyright Clearance Center, Inc. ("CCC") on behalf of the Rightsholder identified in the order details below. The license consists of the order details, the Marketplace Permissions General Terms and Conditions below, and any Rightsholder Terms and Conditions which are included below.

All payments must be made in full to CCC in accordance with the Marketplace Permissions General Terms and Conditions below.

Order Date	11-Aug-2025	Type of Use	Republish in a thesis/dissertation
Order License ID	1639646-1	Publisher	Royal Society of Chemistry
ISSN	2050-7496	Portion	Chapter/article

LICENSED CONTENT

Publication Title	Journal of materials chemistry. A, Materials for energy and sustainability	Publication Type	e-Journal
Article Title	A pH-responsive covalent organic network: morphology change leads to capture and removal of phosphate ions from water †	Start Page	19559
		End Page	19566
		Issue	30
Author / Editor	Royal Society of Chemistry (Great Britain)	Volume	12
Date	01/01/2013	URL	http://pubs.rsc.org/en/journals/journaliss...
Language	English		
Country	United Kingdom of Great Britain and Northern Ireland		
Rightsholder	Royal Society of Chemistry		

REQUEST DETAILS

Portion Type	Chapter/article	Rights Requested	Main product
Page Range(s)	19559-19566	Distribution	Worldwide
Total Number of Pages	8	Translation	Original language of publication
Format (select all that apply)	Print, Electronic	Copies for the Disabled?	No
Who Will Republish the Content?	Author of requested content	Minor Editing Privileges?	Yes
Duration of Use	Life of current edition	Incidental Promotional Use?	No
Lifetime Unit Quantity	Up to 499	Currency	USD

NEW WORK DETAILS

Title	Design and Development of Advanced Porous Organic Polymeric Adsorbents for the Efficient and Selective Removal and Recovery of Phosphate and Arsenate from Water	Institution Name	Indian Institute of Technology Guwahati
		Expected Presentation Date	2025-10-01
Instructor Name	Prof. Debasis Manna		

ADDITIONAL DETAILS

Order Reference Number	N/A	The Requesting Person / Organization to Appear on the License	Mr. Gunanka Hazarika

REQUESTED CONTENT DETAILS

Title, Description or Numeric Reference of the Portion(s)	Design and Development of Advanced Porous Organic Polymeric Adsorbents for the Efficient and Selective Removal and Recovery of Phosphate and Arsenate from Water	Title of the Article / Chapter the Portion Is From	A pH-responsive covalent organic network: morphology change leads to capture and removal of phosphate ions from water †
		Author of Portion(s)	Hazarika, Gunanka; Das, Sribash; Das, Niku Moni; Manna, Debasis
Editor of Portion(s)	Hazarika, Gunanka; Das, Sribash; Das, Niku Moni; Manna, Debasis	Issue, if Republishing an Article From a Serial	30
Volume / Edition	12	Publication Date of Portion	2024-07-30
Page or Page Range of Portion	19559-19566		

भारतीय प्रौद्योगिकी संस्थान गुवाहाटी
Indian Institute of Technology Guwahati

CCC Marketplace

This is a License Agreement between Mr. Gunanka Hazarika ("User") and Copyright Clearance Center, Inc. ("CCC") on behalf of the Rightsholder identified in the order details below. The license consists of the order details, the Marketplace Permissions General Terms and Conditions below, and any Rightsholder Terms and Conditions which are included below.

All payments must be made in full to CCC in accordance with the Marketplace Permissions General Terms and Conditions below.

Order Date	11-Aug-2025	Type of Use	Republish in a thesis/dissertation
Order License ID	1639648-1	Publisher	Royal Society of Chemistry
ISSN	2050-7496	Portion	Chapter/article

LICENSED CONTENT

Publication Title	Journal of materials chemistry. A, Materials for energy and sustainability	Publication Type	e-Journal
		Start Page	19695
Article Title	Bis-imidazolium linked covalent organic network effectively removes arsenate from water and wastewater containing phosphates †	End Page	19704
		Issue	25
		Volume	13
Author / Editor	Royal Society of Chemistry (Great Britain)	URL	http://pubs.rsc.org/en/journals/journaliss...
Date	01/01/2013		
Language	English		
Country	United Kingdom of Great Britain and Northern Ireland		
Rightsholder	Royal Society of Chemistry		

REQUEST DETAILS

Portion Type	Chapter/article	Rights Requested	Main product
Page Range(s)	19695-19704	Distribution	Worldwide
Total Number of Pages	10	Translation	Original language of publication
Format (select all that apply)	Print, Electronic	Copies for the Disabled?	No
Who Will Republish the Content?	Author of requested content	Minor Editing Privileges?	Yes
Duration of Use	Life of current edition	Incidental Promotional Use?	No
Lifetime Unit Quantity	Up to 499	Currency	USD

NEW WORK DETAILS

Title	Design and Development of Advanced Porous Organic Polymeric Adsorbents for the Efficient and Selective Removal and Recovery of Phosphate and Arsenate from Water	Institution Name	Indian Institute of Technology Guwahati
		Expected Presentation Date	2025-10-01
Instructor Name	Prof. Debasis Manna		

ADDITIONAL DETAILS

Order Reference Number	N/A	The Requesting Person / Organization to Appear on the License	Mr. Gunanka Hazarika

REQUESTED CONTENT DETAILS

Title, Description or Numeric Reference of the Portion(s)	Design and Development of Advanced Porous Organic Polymeric Adsorbents for the Efficient and Selective Removal and Recovery of Phosphate and Arsenate from Water	Title of the Article / Chapter the Portion Is From	Bis-imidazolium linked covalent organic network effectively removes arsenate from water and wastewater containing phosphates †
		Author of Portion(s)	Hazarika, Gunanka; Manna, Debasis
Editor of Portion(s)	Hazarika, Gunanka; Manna, Debasis	Issue, if Republishing an Article From a Serial	25
Volume / Edition	13		
Page or Page Range of Portion	19695-19704	Publication Date of Portion	2025-06-25

भारतीय प्रौद्योगिकी संस्थान गुवाहाटी
Indian Institute of Technology Guwahati

Publications

1. **Hazarika, G.**; Manna, D., Bis-imidazolium linked covalent organic network effectively removes arsenate from water and wastewater containing phosphates. *J. Mater. Chem. A* **2025,** *13*, 19695-19704.
2. **Hazarika, G.**; Das, S.; Patel, A.; Manna, D., Guanidine-modified cellulose enhances capturing and recovery of phosphates from wastewater. *Environ. Sci.: Water Res. Technol.* **2025,** *11* (3), 691-701.
3. **Hazarika, G.**; Das, S.; Das, N. M.; Manna, D., A pH-responsive covalent organic network: Morphology change leads to capture and removal of phosphate ions from water. *J. Mater. Chem. A* **2024,** *12* (30), 19559-19566.
4. Das, N. M.; Prusty, B. M.; Sahoo, A.; Mazumder, P.; Chauhan, S.; **Hazarika, G.**; Kumar, S.; Dhabal, D.; Manna, D., Photoresponsive prodrug for regulated inhibition of indoleamine 2, 3-dioxygenase 1 enzyme activity. *RSC Med. Chem.* **2025,** 16, 3240-3250.
5. Borah, R.; Mattaparthi, V. S. K.; **Hazarika, G.**, Assessment of the Comparative Interactions of Cuminaldehyde with Bovine Serum Albumin and Human Serum Albumin through Spectroscopic and Molecular Docking Investigation. *J. Solution Chem.* **2024,** 53 (8), 1130–1148.
6. Patel, A.; Goswami, S.; **Hazarika, G.**; Sivaprakasam, S.; Bhattacharjee, S.; Manna, D., Sulfonium-Cross-Linked Hyaluronic Acid-Based Self-Healing Hydrogel: Stimuli-Responsive Drug Carrier with Inherent Antibacterial Activity to Counteract Antibiotic-Resistant Bacteria. *Adv. Healthc. Mater.* **2023,** 2302790.
7. Dey, S.; Patel, A.; Haloi, N.; Srimayee, S.; Paul, S.; Barik, G. K.; Akhtar, N.; Shaw, D.; **Hazarika, G.**; Prusty, B. M. , Quinoline thiourea-based zinc ionophores with antibacterial activity. *J. Med. Chem.* **2023,** 66 (16), 11078-11093.
8. Das, S.; **Hazarika, G.**; Manna, D. , Guanidine-Functionalized Fluorescent sp^2 Carbon-Conjugated Covalent Organic Framework for Sensing and Capture of Pd (II) and Cr (VI) Ions. *Chem. Eur. J.* **2023,** 29 (15), e202203595.